89

07304

U·M·I

MICROFILMED 1989

INFORMATION TO USERS

The most advanced technology has been used to photograph and reproduce this manuscript from the microfilm master. UMI films the text directly from the original or copy submitted. Thus, some thesis and dissertation copies are in typewriter face, while others may be from any type of computer printer.

The quality of this reproduction is dependent upon the quality of the copy submitted. Broken or indistinct print, colored or poor quality illustrations and photographs, print bleedthrough, substandard margins, and improper alignment can adversely affect reproduction.

In the unlikely event that the author did not send UMI a complete manuscript and there are missing pages, these will be noted. Also, if unauthorized copyright material had to be removed, a note will indicate the deletion.

Oversize materials (e.g., maps, drawings, charts) are reproduced by sectioning the original, beginning at the upper left-hand corner and continuing from left to right in equal sections with small overlaps. Each original is also photographed in one exposure and is included in reduced form at the back of the book. These are also available as one exposure on a standard 35mm slide or as a 17" x 23" black and white photographic print for an additional charge.

Photographs included in the original manuscript have been reproduced xerographically in this copy. Higher quality 6" x 9" black and white photographic prints are available for any photographs or illustrations appearing in this copy for an additional charge. Contact UMI directly to order.

U·M·I

University Microfilms International
A Bell & Howell Information Company
300 North Zeeb Road, Ann Arbor, MI 48106-1346 USA
313/761-4700 800/521-0600

Order Number 8907304

Resolution of kinematic redundancy through local and global optimization

Shiao, Cheng-Mu, Ph.D.

The Ohio State University, 1988

U·M·I
300 N. Zeeb Rd.
Ann Arbor, MI 48106

RESOLUTION OF KINEMATIC REDUNDANCY THROUGH LOCAL AND GLOBAL OPTIMIZATION

A Dissertation

Presented in Partial Fulfillment of the Requirements for

the Degree Doctor of Philosophy in the

Graduate School of the Ohio State University

by

Cheng-Mu Shiao, B.S.E.E, M.S.E.E.

* * * * *

The Ohio State University

1988

Dissertation Committee:

Said H. Koozekanani

Charles A. Klein

David E. Orin

Approved by:

S. H. Koozekanani

Adviser
Department of Electrical
Engineering

To my parents

ACKNOWLEDGMENTS

I would like to thank my advisor, Professor Said H. Koozekanani, for his advice, encouragement and support throughout this work. I sincerely appreciate Professors Charles A. Klein for the many hours he has devoted to consultations and the review of this dissertation. In addition, I would like to thank Professor David E. Orin for his valuable comments and careful review of this dissertation.

I would like to thank the numerous friends and classmates who, over the many years of my graduate study, have been a source of encouragement, support, and inspiration. Especially, I am indebted to Dr. Anthony A. Maciejewski and Mr. Chin-Cheng Kau for many valuable discussions.

I would also like to thank Dr. David Rathke and the members in Lake Erie Area Research Center for their constant friendship and support.

Finally, I would like to thank my entire family for their support, and especially my parents without their love and support this work would not have been possible.

This research was supported by the National Science Foundation under grant DMC - 8421321.

VITA

November 23, 1950	Born Hsin-Chu, Taiwan, R.O.C.
June, 1972	B.S.E.E. National Cheng-Kung University Tainan, Taiwan R.O.C.
June, 1975	M.S.E.E. National Cheng-Kung University Tainan, Taiwan R.O.C.
1977 - 1981	Assistent Researcher Telecommunication Laboratories Chung-Li, Taiwan R.O.C.
1983 - 1988	Graduate Research Associate Center of Lake Erie Research The Ohio State University Columbus, Ohio
1987 - 1988	Graduate Research Associate Department of Electrical Engineering The Ohio State University Columbus, Ohio

FIELDS OF STUDY

Major Field: Electrical Engineering

Studies in Computer Engineering:	Professors K. J. Breeding, C. A. Klein, S. H. Koozekanani, R. B. McGhee, K. W. Olson, D. E. Orin, F. Özgüner
Studies in Computer and Information Science:	Professors M. T. Liu, T. W. Lai, B. W. Weide
Studies in Control Engineering:	Professors R. Fenton, H. Hemami R.J. Mayhan, Ü. Özgüner
Studies in Statics:	Professors R. Bartoszynski, J. Klein

TABLE OF CONTENTS

ACKNOWLEDGMENTS iii

VITA iv

LIST OF FIGURES x

LIST OF TABLES xxii

I. INTRODUCTION 1

II. PSEUDOINVERSE METHOD FOR KINEMATIC REDUNDANCY RESOLUTION 8

2.1 Resolution of the Kinematic Redundancy 10

2.1.1 Resolution of Kinematic Redundancy at the Velocity Level 12

2.1.2 Resolution of the Kinematic Redundancy at the Acceleration Level 14

2.2 Generation of the Locus of Joint Configurations for Some End Effector's Position 15

2.2.1 Analytic Method for Generating the Locus of Joint Configurations for Some End Effector's Position 15

2.2.2 Geometrical Method for Generating the Locus of Joint Configurations for Some End Effector's Position 16

2.3 Projection of the Locus of Joint Configurations for Some End Effector's Position on a Plane Spanned by Joint Angle Coordinates 21

2.3.1 The Projection of the Locus of Joint Configurations for Some End Effector's Position on a Plane Spanned by θ_2 and θ_3 24

2.3.2 The Projection of Locus of Joint Configurations for Some End Effector's Position on the Plane Spanned by θ_1 and θ_2 25

2.3.3 The Projection of the Locus of Joint Configurations for Some End Effector's on the Plane Spanned by θ_1 and θ_3 28

2.4 Summary 34

III. COMPARISON OF THE REDUNDANCY RESOLUTION AT THE VELOCITY AND AT THE ACCELERATION LEVELS 35

3.1 The Utilization of Null Space 36

3.2 Euler-Lagrange Equation 39

3.3 Physical Interpretation 41

3.4 Computer Simulations 42

3.4.1 Effects of Changing Initial Posture 49

3.4.2 Effects of Changing Initial Joint Rate 63

3.4.3 Effects of Changing Base Location 68

3.5 Conclusions 81

IV. RESOLVING THE REDUNDANCY AT THE HIGHER ORDER LEVELS 82

4.1 Derivation of the Formulas for Resolving Redundancy at the Higher Order Derivative Levels 84

4.2 The Relationship between Methods of Resolving the Redundancy at Different Order of Derivative Levels 87
4.3 Computer Simulations 89
4.4 Conclusion 90

V. LOCAL TORQUE OPTIMIZATION TECHNIQUE 95
5.1 Kinematics and Dynamics of a Manipulator 96
5.2 Review of the Local Torque Optimization Technique 98
5.3 Analysis of the Algorithm 101
5.3.1 Two Types of Singularity 103
5.3.2 Interpretation of the Algorithm's Instability 106
5.4 Damped Least-squares Method 111
5.4.1 Choice of the Damping Factor α 118
5.5 Choice of a Proper Initial State 128
5.5.1 A Proper Initial Configuration 128
5.5.2 A Proper Initial Joint Rate for Some Specific Initial Posture 147
5.5.3 Effects of the Base Location 155
5.6 Summary 155

VI. RESOLUTION OF KINEMATIC REDUNDANCY THROUGH GLOBAL OPTIMIZATION 168
6.1 Review of Global Optimization Methods 170
6.1.1 Nakamura and Hanafusa Method 170
6.1.2 Hollerbach and Suh Method 171
6.2 Derivation of the Formulas for Resolving Redundancy Globally at the Velocity Level 174

6.2.1 Redundancy Resolution through Global Joint Rate Square Optimization 174
6.2.2 Resolving Kinematic Redundancy through Global Kinematic Energy Optimization 176
6.3 Derivation of the Formulas for Resolving Redundancy Globally at the Acceleration Level 178
6.3.1 Redundancy Resolution through Global Joint Acceleration Square Optimization 178
6.3.2 Redundancy Resolution through Global Optimization of Joint Torques 180
6.4 Summary 186

VII. CONCLUSION AND SUGGESTION OF FUTURE WORK 187
7.1 Conclusion 187
7.2 Extended Research 189

A. FORMULAS FOR CALCULATING TORQUES FOR A 3-LINK PLANAR MANIPULATOR 190
A.1 Coordinate Transformation 190
A.2 Derivation of Recursive Equations for Calculating the Required Torques for a 3–link Manipulator 193

B. CALCULATION OF THE JACOBIAN AND ITS DERIVATIVES FOR A 3-LINK PLANAR MANIPULATOR 206

BIBLIOGRAPHY 209

LIST OF FIGURES

1 Generation of the locus of joint configurations for some end effector's position by the geometric method 18

2 A n–link planar manipulator 22

3 The projection of the locus of joint configurations for some end effector's position on the plane spanned by θ_2 and θ_3 with a fixed α ($\alpha = 0$) and a varied r ($0 \leq r \leq 3l$) [5] 26

4 Cases for deriving the projection of the locus of joint configurations for some end effector's position on the planes spanned by the coordinates θ_1 and θ_2, θ_2 and θ_3 and θ_3 and θ_1 27

5 The projection of the locus of joint configurations for some end effector's position on the plane spanned by θ_1 and θ_2 with a fixed r ($r = 2.0$) and a varied α ($-90° \leq \alpha \leq 90°$) 29

6 The projection of the locus of joint configurations for some end effector's position on the plane spanned by θ_1 and θ_2 with a fixed α ($\alpha = 0$) and a varied r ($0 \leq r \leq 3l$) 30

7 The projection of the locus of joint configurations for some end effector's position on the plane spanned by θ_1 and θ_3 with a fixed r ($r = 2.0$) and a varied α ($-90° \leq \alpha \leq 90°$) 32

8 The projection of the locus of joint configurations for some end effector's position on the plane spanned by θ_1 and θ_3 with a fixed α ($\alpha = 0$) and a varied r ($0 \leq r \leq 3l$) 33

9 The cartesian space position, velocity, acceleration as functions of time for a straight line trajectory shown in Table 2 with $\alpha = 1.0$ and initial posture $(75°, -120°, 150°)$ 45

10 The cartesian space position, velocity, acceleration as functions of time for a circular trajectory shown in Table 1 with $a = 0.5$ and initial posture $(76.7°, 29.9°, 92.6°)$ 46

11 Trajectories of curve line ($\alpha \geq 1$) shown in Table 2 for the computer simulations 47

12 Trajectories of curve line ($\alpha \leq 1$) shown in Table 2 for the computer simulations 48

13 The 3−link manipulator and the circular task for computer simulation of comparing the velocity control and the acceleration control schemes 50

14 The joint configurations of the starting end effector's position at $(-1.0, 1.6)$ and the base located at (0.0,0.0) 52

15 Performance measure $\int_{t_0}^{t_f} \dot{\theta}^T \dot{\theta} dt$ as a function of initial configurations for starting end effector's position at (-1.0 1.6) and base at (0.0 0.0) with velocity and acceleration control 53

16 The projection of joint angle space curve on $\theta_1 = 0$ plane for 5 different starting postures with end effector at (-1.0 1.6) and base at (0.0 0.0) by using velocity control 54

17 The projection of joint angle space curve on $\theta_1 = 0$ plane for 5 different starting postures with end effector at (-1.0 1.6) and base at (0.0 0.0) by using acceleration control 55

18 The joint angles and the manipulator geometry as a function of time, tracing a circle ($a = 0.5$) with the starting posture (S_2) which is conservative for velocity control 57

19 The joint angles and the manipulator geometry as a function of time, tracing a circle ($a = 0.5$) with the starting posture (S_2) which is conservative for acceleration control 58

20 The joint angles and the manipulator geometry as a function of time, tracing a circle ($a = 0.5$) with the starting posture (S_1) which is not conservative for velocity control 59

21 The joint angles and the manipulator geometry as a function of time, tracing a circle ($a = 0.5$) with the starting posture (S_1) which is not conservative for acceleration control 60

22 The joint rates as a function of time for the starting posture (S_2) which is conservative for acceleration control 61

23 The joint rates as a function of time for the starting posture (S_1) which is not conservative for acceleration control 62

24 The projections of joint angle space curves on $\theta_1 = 0$ plane for 8 different initial joint rates as shown in Table 5 having the same initial posture ($172.5°, -39.4°, -85.4°$) to trace a circular trajectory with acceleration control 65

25 The projection of joint-angle space curve on $\theta_1 = 0$ plane for 5 different initial postures with proper initial joint rate as shown in Table 6 to achieve minimum drift for the acceleration control . . . 67

26 The projection of joint-angle space curve on $\theta_1 = 0$ plane for 4 different initial postures with the base located at (1.07,0.46) and end effector position at (-1.0, 2.0) corresponding to trajectories in Table 7 which trace a straight line trajectory with acceleration control 70

27 The projection of joint-angle space curve on $\theta_1 = 0$ plane for 4 different initial postures with the base located at (0.0,0.0) and end effector position at (-1.0, 2.0) corresponding to trajectories in Table 8 which trace a straight line trajectory with acceleration control . 71

28 The projection of joint-angle space curve on $\theta_1 = 0$ plane for 4 different initial postures with the base located at (-0.8,0.9) and end effector position at (-1.0, 2.0) corresponding to trajectories in Table 9 which trace a straight line trajectory with acceleration control . 72

29 The plot of performance measure $I_{\dot{\theta}}$ among possible configurations for base located at (1.07,0.46) and end effector position at (-1.0, 2.0) corresponding to trajectories in Table 7 which trace a straight line trajectory for both velocity and acceleration control 73

30 The plot of performance measure $I_{\dot{\theta}}$ among possible configurations for base located at (0.0,0.4) and end effector position at (-1.0, 2.0) corresponding to trajectories in Table 8 which trace a straight line trajectory for both velocity and acceleration control 74

31 The plot of performance measure $I_{\dot{\theta}}$ among possible configurations for located at (-0.8,0.9) and end effector position at (-1.0, 2.0) corresponding to trajectories in Table 9 which trace a straight line trajectory for both velocity and acceleration control 75

32 Joint angles and manipulator geometries as functions of time for the best configuration with base located at (1.07,0.46) and end effector position at (-1.0, 2.0) corresponding to trajectory 4 in Table 7 which traces a straight line trajectory with acceleration control 76

33 Joint angles and manipulator geometries as functions of time for the best configuration with the base located at (0.0,0.4) and end effector position at (-1.0, 2.0) corresponding to trajectory 4 in Table 8 which traces a straight line trajectory with acceleration control 77

34 Joint angles and manipulator geometries as functions of time for the best configuration with the base located at (-0.8,0.9) and end effector position at (-1.0, 2.0) corresponding to trajectory 4 in Table 9 which traces a straight line trajectory with acceleration control . 78

35 The plot of performance measure $I_{\dot{\theta}}$ for the all possible base locations with end effector position at (-1.0, 2.0), lower extremity of the straight line trajectory at 45° with acceleration control and symbols 0 to f designate values 0.18 to 2.95 80

36 The performance measure $I_{\dot{\theta}}$ for four different kinematic redundancy resolution strategies through minimization of the norm of joint rate, joint acceleration, the 3rd and 4th derivatives of joint angles respectively to trace a circular trajectory with end effector at (-1.0 1.6) and base at (0.0,0.0) 91

37 The projection of the joint angle space curve on the $\theta_1 = 0$ plane for 5 starting postures corresponding to trajectories in Table 6 Chapter 3 for the control strategy which minimizes the norm of the 3rd order derivative to trace a circular trajectory with base located at (0.0,0.0) 92

38 The projection of the joint angle space curve on the $\theta_1 = 0$ plane for 5 starting postures corresponding to trajectories in Table 6 Chapter 6 for the control strategy which minimizes the norm of the 4th order derivative to trace a circular trajectory with base located at (0.0,0.0) 93

39 Relative singular values of the matrix $H[I - J^+J]$ on the plane spanned by the coordinates θ_2 and θ_3, with $-180° \leq \theta_2 \leq 180°$, $-180° \leq \theta_2 \leq 180°$ and symbols 0 to f designate values from 0.41 to 16.0. 102

40 The joint angles and geometries as functions of time for a 3-link planar manipulator to pass through a singular state: joint angles $(113.24°, -28.75°, -48.42°)$ and joint rates (-4.58,9.92,-7.92), with initial posture $(130°, -120°, 120°)$ and base located at (0.0,0.0) . . 112

41 Joint torques as functions of time for a 3-link planar manipulator to go through a singular state: joint angles $(113.24°, -28.75°, -48.42°)$ and joint rates (-4.58,9.92,-7.92) 113

42 Each singular value of the inertia matrix H times the inner product of its corresponding input vector and the output vector of null-space matrix $[(I - J^+J)]$ together with the singular value of the matrix $H[I - J^+J]$ in the vicinity of dynamic singularity for minimum torque method. 114

43 Projections of the joint angle space trajectories on the $\theta_1 = 0$ plane for damped least-squares algorithm to trace a straight line at 45° with damping factor changing from 0 to 1 and with initial posture $(130°, -120°, 120°)$ and base located at (0.0,0.0) 117

44 Projections of the joint angle space trajectories on the $\theta_1 = 0$ plane for minimum torque, minimum acceleration and damped least-squares algorithms to trace a straight line at 45° with initial posture (130°, −120°, 120°) and base located at (0.0,0.0) 120

45 Projections of the joint angle space trajectories on the $\theta_1 = 0$ plane for damped least-squares algorithms with damping factor changing from 0 to 1 to trace a straight line at 45° with initial posture (−45°, 135°, −135°) and base located at (0.0,0.0) 121

46 Projections of the joint angle space trajectories on the $\theta_1 = 0$ plane for damped least-squares algorithm with damping factor changing from 0 to 1 to trace a straight line at 45° with initial posture (75°, −120°, 150°) and base located at (0.0,0.0) 122

47 Projections of the joint angle space trajectories on the $\theta_1 = 0$ plane for minimum torque, minimum acceleration and damped least-squares algorithms to trace a straight line at 45° with initial posture (−45°, 135°, −135°) and base located at (0.0,0.0) 125

48 Projections of the joint angle space trajectories on the $\theta_1 = 0$ plane for minimum torque, minimum acceleration and damped least-squares algorithms to trace a straight line at 45° with initial posture (75°, −120°, 150°) and base located at (0.0,0.0) 126

49 The joint angles and geometries of the manipulator for tracing a straight line at 45° with starting posture (130°, −120°, 120°) and base located at (0.0,0,0) for damped least-squares method 129

50 The norm of torques for tracing a straight line at 45° with starting posture (130°, −120°, 120°) and base located at (0.0,0.0) for minimum torque and damped least-squares methods 130

51 The singular value of $H(I - J^+J)$ for a straight line at 45° with starting posture (130°, −120°, 120°) and base located at (0.0,0.0) for minimum torque and damped least-squares methods 131

52 The product of the singular value of $H(I - J^+J)$ and $\| - \tau_p \|$ for a straight line at 45° with starting posture (130°, −120°, 120°) and base located at (0.0,0.0) for minimum torque and damped least-squares methods 132

53 The damping factors for tracing a straight line at 45° with starting posture (130°, −120°, 120°) and base located at (0.0,0,0) for damped least-squares method 133

54 The projections of joint angle space trajectories on $\theta_1 = 0$ plane for a straight line at 45° with initial postures given in Table 16, trajectories 3 and 7 pass through the small singular value region shown in Fig. 38 134

55 The homogeneous configurations of the starting end effector's position (1.414, −0.414) with base located at (0.0,0.0) 138

56 The initial joint rates in the null space for an given initial posture (−45.0°, 135.0°, −135.0°) and base located at (0.0,0.0) 139

57 The performance measure, I_τ, for minimum norm of torque and damped least-squares methods to trace a straight line at 45° with base located at (0.0,0.0) and $t_f = 1.9$ sec as a function of initial postures corresponding to homogeneous configurations of the end effector position (1.414, −0.414) 140

58 The performance measure, I_T, for minimum norm of joint acceleration and damped least-squares methods to trace a straight line at 45° with base located at (0.0,0.0) and $t_f = 1.9$ sec as a function of initial postures corresponding to homogeneous configurations of the end effector position $(1.414, -0.414)$ 141

59 The joint angles and geometries as functions of time, tracing a straight line trajectory with initial posture $(-75.32°, 50.82°, 99.97°)$ corresponding to trajectory no. 3 (T=1.822 sec) in Table 16 142

60 The joint torques and the norm of the torque as functions of time, tracing a straight line trajectory (T=1.822 sec) with initial posture $(-75.32°, 50.82°, 99.97°)$ corresponding to trajectory no. 3 in Table 16 143

61 The joint angles and geometries as functions of time, tracing a straight line trajectory with initial posture $(-25.32°, 102.04°, -150.42°)$ corresponding to trajectory no. 8 (T=1.822 sec) in Table 16 144

62 The joint torques and the norm of the torque as functions of time, tracing a straight line trajectory (T=1.822 sec) with initial posture $(-25.32°, 102.04°, -150.42°)$ corresponding to trajectory no. 8 in Table 16 145

63 The projection of the joint angle space trajectories on the $\theta_1 = 0$ plane for minimum norm of torque control tracing a circle trajectory with zero initial joint rates and different initial postures as given in Table 19, trajectories 2 and 6 pass through the small singular value region shown in Fig. 38 146

64 The joint angles and geometries as functions of time, tracing a circle trajectory with initial posture (129.0°, 48.6°, −126.4°) corresponding to trajectory no. 4 in Table 19 148

65 The joint torques and the norm of the torque as functions of time, tracing a circle trajectory with initial posture (129.0°, 48.6°, −126.4°) corresponding to trajectory no. 4 in Table 19 149

66 The joint angles and geometries as functions of time, tracing a circle trajectory with initial posture (73.8°, 35.3°, 88.7°) corresponding to the trajectory no. 1 in Table 19 150

67 The joint torques and the norm of the torque as functions of time, tracing a circle trajectory with initial posture (−73.8°, 35.3°, 88.7°) corresponding to trajectory no. 1 in Table 19 151

68 The projection of the joint angle space trajectories on the $\theta_1 = 0$ plane tracing a straight line with initial posture (−45°, 135°, −135°) and the initial joint rates as given in Table 20, trajectories 1, 6, 7 and 8 pass through small singular value region shown in Fig. 38 156

69 The joint angles and geometries as functions of time, tracing a straight line trajectory with initial posture (−45°, 135°, −135°) and initial joint rates (-0.74,0.74,0.74) corresponding to trajectory no. 7 (T=1.822 sec) in Table 20 157

70 The joint torques and the norm of joint torques along the straight line trajectory (T=1.822 sec) as functions of time with initial posture (−45°, 135°, −135°) and initial joint rates (-0.74,0.74,0.74) corresponding to trajectory no. 7 in Table 20 158

71 The joint angles and geometries as functions of time, tracing a straight line trajectory with initial posture $(-45°, 135°, -135°)$ and initial joint rates (0.74,-0.74,-0.74) corresponding to trajectory no. 3 (T=1.822 sec) in Table 20 159

72 The joint torques and the norm of joint torques along the straight line trajectory (T=1.822 sec) as functions of time with initial posture $(-45°, 135°, -135°)$ and initial joint rates (0.74,-0.74,-0.74) corresponding to trajectory 3 in Table 20 160

73 The projection of the joint angle space trajectories on $\theta_1 = 0$ plane to trace a circle trajectory with initial posture $(104.6°, 95.9°, -121.4°)$ for 8 different initial joint rates as given in Table 23, trajectories 1 and 6 pass through small singular value region shown in Fig. 38 . 161

74 The joint angles and geometries as functions of time, tracing a circle trajectory with initial posture $(104.6°, 95.9°, -121.4°)$ and initial joint rates (0.985,-1.481,-0.651) corresponding to trajectory 1 in Table 23 162

75 The joint torques and the norm of joint torques along a circle trajectory as a function of time with initial posture $(104.6°, 95.9°, -121.4°)$ and initial joint rates (0.985,-1.481,-0.651) corresponding to trajectory 1 in Table 23 163

76 The joint angles and geometries as functions of time, tracing a circle trajectory with initial posture $(104.6°, 95.9°, -121.4°)$ and initial joint rates (0.199,-0.299,-0.131) corresponding to trajectory no. 4 in Table 23 164

77 The joint torques and the norm of joint torques along a circle trajectory as a function of time with initial posture (104.6°, 95.9°, −121.4°) and initial joint rates (0.199,-0.299,-0.131) corresponding to trajectory 4 in Table 23 165

78 The relative performance measure I_τ for different base locations with symbols 0 to f designate values from 1.45 to 25.0 166

79 The Denavit-Hartenberg notation for a manipulator [31] 191

LIST OF TABLES

1 The formulas of position, velocity and acceleration in the cartesian space for a trajectory of circle with radius a, zero initial and zero final velocities 44

2 The formulas of position, velocity and acceleration in the cartesian space for the trajectories of curve lines with parameter α 49

3 Two initial configurations which are conservative and have the minimum performance measure, $I_{\dot{\theta}}$ for tracing a circular trajectory . . 51

4 Three other initial configurations which are non-conservative for tracing a circular trajectory. 56

5 The cost functions for different initial joint rate with initial posture $(172.5°, -39.4°, -85.4°)$ and base located at (0.0 0.0) to trace a circular trajectory with acceleration control 64

6 The required initial joint rates for achieving minimum drift for 5 different initial postures 66

7 The cost functions for different initial posture with end effector and base positions at (-1.0,2.0) and (1.07,0.46) respectively for a straight line trajectory and minimum norm of joint acceleration control . . 69

8 The cost functions for different initial posture with end effector and base positions at(-1.0,2.0) and (0.0,0.0) respectively for a straight line trajectory and minimum norm of joint acceleration control . . 69

9 The cost functions for different initial posture with end effector and base positions at (-1.0,2.0) and (-0.8,0.9) respectively for a straight line trajectory and minimum norm of joint acceleration control . . 79

10 The performance measures for three redundancy resolution methods to trace a straight line at 45° with initial posture (130°, −120°, 120°) and base located at (0.0,0.0) 119

11 Effects of damping factor on the performance measures for damped least-square torque optimization method to trace a straight line at 45° with initial posture (130°, −120°, 120°) and base located at (0.0,0.0) 123

12 The performance measures for three redundancy resolution methods to trace a straight line at 45° with initial posture (−45°, 135°, −135°) and base located at (0.0,0.0) 123

13 Effects of damping factor on the performance measures for damped least-squares torque optimization method to trace a straight line at 45° with initial posture (−45°, 135°, −135°) and base located at (0.0,0.0) 124

14 The performance measures for three redundancy resolution methods to trace a straight line at 45° with initial posture (75°, −120°, 150°) and base located at (0.0,0.0) 124

15 Effects of damping factor on the performance measures for damped least-squares torque optimization method to trace a straight line at 45° with initial posture (75°, −120°, 150°) and base located at (0.0,0.0) 127

16 The performance measures for minimum norm of torque control to trace a straight line at 45° with base located at (0.0,0.0) and $t_f = 1.822$ sec for 8 different starting postures 135

17 The performance measures for damped least-squares control to trace a straight line at 45° with base located at (0.0,0.0) and $t_f = 1.822$ sec for 8 different starting postures 136

18 The performance measures for minimum acceleration control to trace a straight line at 45° with base located at (0.0,0.0) and $t_f = 1.822$ sec for 8 different starting postures 136

19 The performance measures for minimum norm of torque control to trace a circular trajectory with base located at (0.0,0.0) and zero initial joint rate for 6 different initial postures 147

20 The performance measures for minimum norm of torque control to trace a straight line at 45° with initial posture $(-45°, 135°, -135°)$, base located at (0.0,0.0) and $t_f = 1.822$ sec for 8 different initial joint rates 153

21 The performance measures for damped least-squares torque optimization control to trace a straight line at 45° with initial posture $(-45°, 135°, -135°)$, base located at (0.0,0.0) and $t_f = 1.822$ sec for 8 different initial joint rates 153

22 The performance measures for minimum norm of acceleration control to trace a straight line at 45° with initial posture $(-45°, 135°, -135°)$, base located at (0.0,0.0) and $t_f = 1.822$ sec for 8 different initial joint rates 154

23 The performance measures for minimum norm of torques control to trace a circular trajectory with an initial posture $(104.6°, 95.9°, -121.4°)$, base located at (0.0,0.0) and $t_f = 2.0sec$ for 6 different initial joint rates 155

CHAPTER I

INTRODUCTION

The field of robotics is becoming more attractive to researchers since robots have the ability to accomplish jobs that most people are unable or unwilling to do, such as working with radioactive and dangerous material, doing repetitive and tedious jobs, carrying heavy objects, and performing fine-scale operations. In recent years, the development of robotics and advanced technologies has increased the demand for manipulators to operate in complex environments and perform delicate work. Advanced robots also have some ability to collect and process information from the surroundings, and have artificial intelligence to make decisions.

Unfortunately, manipulators sometimes may lose degrees of freedom due to kinematic singularities in the workspace [1]. A nonredundant manipulator could have difficulty in accomplishing some jobs. Owing to the limitations of nonredundant manipulators and the demand for having better performance and more sophisticated capability, a manipulator with some degree of redundancy becomes necessary and desirable.

The development of redundant manipulators is still in the simulation and experimental stage. Even though only a few redundant manipulators having been built [2], their potential capabilities and the strong demand among users make the research and development of the redundant manipulator attractive and important.

When redundancies are included, they enlarge and enhance the capability of

a manipulator. They enable a manipulator to do sophisticated work and perform better. On the other hand, when provided with redundancy, the structure of a manipulator becomes more complicated and the development of algorithms to control the redundant manipulator becomes difficult. In other words, advanced kinematic design and sophisticated control schemes become necessary when developing a redundant manipulator.

Many research topics on redundant robots have attracted researchers. These topics are generally divided into three categories: 1) developing methods to resolve the redundancy [3], 2) utilizing the redundancy to increase the capability of a manipulator [4,5] or optimizing the performance measures, and 3) using different control techniques to achieve the utilization of redundancy and overcome the difficulties introduced by having extra degrees of freedom [6,7]. In summary, the main objective of research in the area of redundant robotics is to find optimal algorithms for resolving the kinematic redundancy so that the performance of the manipulator can be improved and the difficulties introduced by the increasing degrees of freedom can be overcome.

Different criteria and performance measures such as dexterity [5,7,8], manipulability [8], condition number, minimum singular value or eigenvalue [5], flexibility [9,10] and the required efforts [11,12,13] have been proposed to be improved by redundancy utilization. Redundancy has been applied to improve the manipulator's dexterity, so that it avoids singularity [7,14] increases manipulability [8] and becomes isotropic [5]. Redundancy has also been used to enhance a manipulator's capability so that it avoids obstacles [6,15], achieves higher accuracy [10], becomes more adaptive to the environment [4] and has higher mobility and faster response time [9]. Finally redundancy has been used to optimize the required effort, that is, to minimize the energy consumed [11] and the torques and forces required [12,13].

Several different approaches such as pseudoinverse [16], linear and nonlinear programming [17], and artificial intelligence [18] have been used for resolving the kinematic redundancy of the redundant manipulator. Generally, the pseudoinverse method is the most favored technique of resolving the kinematic redundancy locally; it has many attractive properties [12] and has the advantage of possibly being used for real-time applications. The disadvantage of using the pseudoinverse method to resolve the kinematic redundancy is that there is no guarantee of achieving global optimality. Therefore, some other methods such as calculus of variation technique [13] or Pontryagin's maximum principle [19] have been proposed to achieve global optimization. Most research that has been done resolves the kinematic redundancy instantaneously or locally through the usage of the pseudoinverse [16]. Some researchers [13,19] considered global performance measures, but the optimization processes that have been used are tedious, time consuming and probably impractical. Therefore, simplifying the global optimization processes by utilizing the special properties of redundant manipulators or searching for a compromise local optimization algorithm to resolve the kinematic redundancy is the main purpose of this research.

Four parts are included in this research: first, methods of resolving the redundancy of manipulators by using the pseudoinverse are studied and compared with each other; second, the stability problem pointed out by Hollerbach and Suh [12] of the redundancy resolution through local torque optimization is investigated and solutions are proposed; third, global optimization together with best location of the base are determined; and finally, the relationship between the methods of resolving the redundancy through local optimization and global optimization are obtained.

In the first part of this research, the redundancies are resolved through mini-

mization of the norms of different order time derivatives of the joint angles. The study includes resolving the redundancy at the inverse kinematic level, the velocity level, the acceleration level, and the higher order derivative levels. Many control schemes such as position control [3,20], velocity control [11] and also acceleration control [21] have been developed for achieving the specific performance criteria. Most pseudoinverse methods used resolve the redundancy at the position [3,20] or at the velocity level [11]. In order to incorporate the dynamics the redundancy must be resolved at the acceleration level [21]. Due to the necessity of resolving the redundancy at the acceleration level, more properties of acceleration control need to be studied. A comparison of the results of using acceleration control and velocity control to trace a cartesian space trajectory is presented. Some superior properties for using acceleration control to achieve better performance are also discussed. Moreover, the redundancies are resolved through minimizing the norms of higher order time derivatives (such as the third and fourth) of the joint angles. Comparisons of the results are made and the relationships among them are also discussed.

The second part of this research investigates the problem which was pointed out by Hollerbach and Suh [12]. Several different methods, including singular value decomposition [22], contour map, and the vector analysis method, are used to analyze this problem. The effects of using null-space components are investigated. The results of this research indicate that the instability does not depend on how big the movement is, but on what the current states (joint angles and joint velocities) of the manipulator are. When the effort is made to achieve the instantaneous optimization of the required torques, there is a tendency to drive the manipulator into unstable states (very high joint rates). This unstable situation may be improved or avoided altogether by choosing a proper initial configuration or applying a suit-

able amount of homogeneous components, otherwise, an unacceptable amount of torque becomes required to compensate for it. The effect of initial state (initial configuration and initial joint rate) on the performance measure is demonstrated by the resolution of kinematic redundancy through torque optimization. Proper choice of an initial state makes the torque optimization algorithm effective and stable.

A suboptimal method using a modified pseudoinverse is proposed. This method minimizes the norm of the required torques and the norm of null-space components simultaneously; therefore, by using the modified pseudoinverse method and choosing a proper damping factor, the required torques are near locally minimized and the algorithm remains stable.

The third part of this study considers the location of the base as another degree of freedom and searches for an optimal base location as well as an initial configuration so that the best performance can be reached. Works already done on either local or global optimization schemes [12,13,19] assume that the base of a manipulator is fixed. A few [5] consider the optimization with respect to the location of the base while the performance measures are highly dependent on the base location with respect to jobs. The effect of base location on the performance measures is considered as having one more degree of freedom. As a result, the performance measure can be optimized over all possible base locations.

A 3–link redundant planar manipulator is used for the computer simulation. The reason for using this planar model is that a planar case is simple and easy to visualize. Moreover, since most of the researchers used the planar model to illustrate their results, comparing the simulation with those of others is made convenient. This simple model makes it easier to determine what postures and what amount of null space are to be used in part two of this study. It provides

useful insight for proper usage of redundancy without causing instability.

In the fourth part of this research, a general formula of resolving the redundancy through global optimization of torques is derived. Other important performance measures such as joint rates' norm, joint accelerations' norm and also the norm of higher order derivatives are considered, and a unified approach for resolving the kinematic redundancies through local and global optimizations of these performance measures is proposed. By using the principle of optimality global and local measures are related, so that the resolution of the redundancy through the optimization of a global performance measure can be obtained by the resolution of the redundancy through the optimization of a local performance measure with a proper value of initial state.

Two interesting results were obtained from this research that provide useful information for controlling the redundant manipulator. These are listed as follows: first, the norms of kinematic quantities such as joint rate, joint acceleration and the higher order derivatives, are globally optimized only if the joint rate's norm is globally optimized. As a result, only the search over the joint space trajectories which give global optimum norm of joint rate is needed. The optimal configuration obtained from the above search also gives the global minimum norm of joint acceleration and of other higher derivatives; second, the performance and stability of the local torque optimization algorithm depend on the initial state $(\theta, \dot{\theta})$ and the specified cartesian space trajectory. Therefore, for some sets of the initial configurations or some types of end effector's movement, the local torque optimization algorithm may not reach an acceptable performance measure. Proper modification is necessary for the local optimization algorithm to achieve a better global performance measure. For a given initial configuration, proper initial joint rate component in the null space can be chosen to improve the global performance.

Furthermore, the global minimum norm of torque can be obtained by proper choice of initial state $(\theta, \dot{\theta})$.

This dissertation includes seven chapters: this chapter gives a brief introduction, the statement of the problem and the organization of this dissertation. Chapter two introduces the pseudoinverse method for resolving the kinematic redundancy. Chapter three compares two generally used control techniques of a redundant manipulator: velocity control and acceleration control. In chapter four the techniques for kinematic redundancy resolution are extended to minimizing the higher order derivatives of joint angle space variables and comparisons are made. In chapter five the redundancy resolution through local optimization is discussed. Limitations and instability of the local optimization algorithms are investigated and solutions are proposed. Chapter six is a discussion of the global optimization techniques. Calculus of variation and principle of optimality are applied to the derivation of the required Euler-Lagrange equations and boundary conditions for resolving the redundancy through global optimization. The relationship between the resolution of redundancy through global optimization and local optimization is obtained. In the seventh chapter conclusions and suggestions for future research are contained.

CHAPTER II

PSEUDOINVERSE METHOD FOR KINEMATIC REDUNDANCY RESOLUTION

Redundancy can be achieved by a manipulator if there are more degrees of freedom than is required for its end effector to track the commanded trajectory. The introduction of redundancy allows the joints to move in the null space. The motion of the joints in the null space which contributes no movement to the end effector plays an important role in the control of a redundant manipulator by either increasing the flexibility or reducing the required effort.

Redundancies also play an important part in the control of robots. There are some advantages and disadvantages for a robot arm to have kinematical redundancy. The main advantage is that the redundancies provide the designer and controller more degrees of freedom to accomplish their secondary goals. These goals include avoiding obstacles, increasing manipulability, avoiding joint limits, providing flexibility for allocating force and torque on each joint, and getting optimal solutions under some criteria. These extra capabilities are useful and attractive either at the design, planning or control stage. On the other hand, there are some disadvantages in having redundancy; the requirement of extra joints to provide kinematic redundancy means additional weight for actuators, gear, etc.; all of these extra components increase the loading of the actuators. Moreover, the introduction of the extra degrees of freedom also complicates the control structures

and schemes.

Several different techniques, pseudoinverse [16], linear and nonlinear programming [17] and artificial intelligence [18] methods, have been applied to resolve the kinematic redundancy. The pseudoinverse method, due to having less complicated computations and easier representation of redundancy with null-space components, is a powerful tool for resolving the redundancy. The pseudoinverse method distinguishes the joints' motion as being composed of two components: minimum norm and null-space components. The minimum norm component is used for tracking the desired end effector's trajectory while the null-space component is usually used for achieving a secondary goal. Since the null-space components are responsible for accomplishing the secondary goal while the redundancy is resolved, more knowledge about their characteristics and usage is desirable. Therefore, algorithms to generate the locus of joint configurations for any specific end effector's position have been developed. Knowing the properties of these joint configurations, and also the performance measure for different redundancy resolution methods are required to facilitate effective use of the null space.

This chapter is divided into four sections: first, two methods generally used for resolving the kinematic redundancy are introduced. They resolve redundancy at the velocity and acceleration levels. Second, algorithms which generate the locus of joint configurations for some end effector position for a 3−link planar manipulator are discussed. This set of joint configurations construct a useful test space for evaluating the performance of different control schemes. Third, the projections of the locus of joint configurations for some end effector position on different pairs of joint angles' planes are described. These planar projections provide simpler means and clearer views for investigating the redundancy resolution problems.

2.1 Resolution of the Kinematic Redundancy

Particular solutions generated by the pseudoinverse method for resolving kinematic redundancy minimize the norm of some quantities in the joint angle space such as joint displacement, joint rate, or joint acceleration are considered. According to the kinematical quantities which are intended to be minimized, two methods generally used for resolving the redundancy are formulated. They resolve the kinematic redundancy at the velocity level and at the acceleration level. Special algorithms are necessary for finding the proper amount of null-space component to achieve the desired performance measure. The required null-space component together with the particular part of the solutions obtained from the minimum norm pseudoinverse are optimally distributed to drive the manipulators. Generally, these two methods used to find the particular solutions are also named velocity control and acceleration control.

Manipulators are usually commanded in the cartesian coordinates while the controller and the actuators are controlled and driven in the joint angle space. Being commanded and driven in two different coordinates, the coordinate transformations, kinematics and inverse kinematics, are required for controlling a manipulator. The procedure for obtaining the kinematic quantities, such as linear and angular displacement, velocity or acceleration, in the cartesian coordinates from the quantities in the joint angle space is called direct kinematics. On the other hand, the reverse procedure for finding quantities in the joint angle coordinates from those in the cartesian space is called the inverse kinematics.

A general expression specifying the manipulator's kinematic relationship between the position of the end effector and the configuration of the links, can be written as a set of vector equation:

$$\mathbf{x} = f(\theta) \tag{2.1}$$

where $\mathbf{x}$ is an m-dimensional vector in the cartesian space, θ is an n-dimensional vector in the joint angle space, and f is a vector function consisting of m scalar equations, with $m \leq n$. If the dimension of two vectors $\mathbf{x}$ and θ are equal, i.e., $m = n$, there is one-to-one correspondence between these two coordinates locally. Therefore, the manipulator has no redundancy. The characteristics and techniques for solving the kinematic and inverse kinematic problems of a nonredundant manipulator can be found in [1]. On the other hand, if the number of cartesian space variables is less than the number of joint angle space variables, i.e., $m < n$, then the manipulator has some degrees of redundancy. In other words, a set of under-determined nonlinear system equations need to be solved. Being under-determined, these equations may have infinite sets of solutions. It is allowed to add $n - m$ constraint equations for achieving some secondary goals and making this system fully determined.

Several formulations [7,15,20] have been developed to integrate the primary and the secondary goals in controlling the redundant manipulators, and several numerical methods were proposed by them for solving these resultant problems. Kee [10] also compared the two different numerical methods, hierarchical pseudoinverse and extended jacobian method, in several different ways.

When the redundancy is resolved and the kinematic relationship has become a fully determined set of system equations, many numerical methods which are available for solving the nonredundant inverse kinematic problems (for example, Gaussian elimination) can be used for obtaining the solution. A closed form solution which resolves the redundancy at the position level was proposed by Chang [20]. He used the Lagrange multiplier method to introduce the extra set of con-

straint equations for optimizing the specific sets of objective functions. An iteratively numerical solution by solving a set of fully specified kinematic equations was proposed to obtain the proper values of joint angles.

The disadvantage of resolving the redundancy by solving the inverse kinematic equations are: first, the computation is too complicated because it is necessary to solve a set of nonlinear system equations. Second, the variables contained in the objective functions are joint angles only. If a cost function contains higher order derivatives of joint angle space variables such as joint rates and joint accelerations, then other methods which resolve the redundancy at the higher level should be used.

2.1.1 Resolution of Kinematic Redundancy at the Velocity Level

Since the nonlinear mapping between the cartesian coordinate and the joint angle coordinate results in complicated computations for solving the inverse kinematic equations, the linearization process has been applied to develop two methods of resolving the redundancy at the velocity level and at the acceleration level. These two methods overcome the shortcomings of nonlinear transformation at the position level, and a set of piecewise linear transformations are obtained from series of linearization processes.

The kinematic equations Eq. (2.1) which relate the position of the end effector and the corresponding joint angles are highly nonlinear. By taking the time derivative of the above kinematic equations Eq. (2.1), the linear relationship between the joint rates and end effector velocities is obtained. The joint velocities are determined by solving a set of first order approximation equations. Numerical integration is used to obtain the corresponding joint angles. The constraint equation which expresses the linear transformation between joint rate and end effector's

velocity is as follows:

$$\dot{\mathbf{x}} = J\dot{\theta} \tag{2.2}$$

where J is called the jacobian matrix of the kinematic equation Eq. (2.1). The set of equations Eq. (2.2) is under-determined because the system has redundancy. The joint velocities can be solved from above equation by taking the pseudoinverse of the Jacobian matrix. The general solution obtained is as follows:

$$\dot{\theta} = J^{+}\dot{\mathbf{x}} + (I - J^{+}J)\dot{\psi} \tag{2.3}$$

where I is an identity matrix of order n, and $\dot{\psi}$ is any vector in the n dimensional joint rate space. The quantity $(I - J^{+}J)$ is called the projection operator. It projects an arbitrary vector $\dot{\psi}$ on the null space in which the motion does not contribute any movement to the end effector. In the case of $\dot{\psi} = 0$, i.e., the resultant motion has no null-space components, then the general solution, Eq. (2.3), becomes a minimum norm of joint rate solution:

$$\dot{\theta} = J^{+}\dot{\mathbf{x}}. \tag{2.4}$$

The null-space component $(I - J^{+}J)\dot{\psi}$ in the complete solution, Eq. (2.3), of joint rate $\dot{\theta}$ can be used for achieving a secondary goal. By using the joint rates obtained and the numerical integration techniques, the joint angles are updated. Due to the null-space components being added to the joint rates, this method resolves the kinematic redundancy at the velocity level. Because the joint velocities are computed by taking the pseudoinverse of the jacobian matrix J the joint rate pseudoinverse is also named the jacobian control.

The advantage of resolving the redundancy at the velocity level is that the relationship of the velocity between joint angle space and cartesian space is linear.

And also, many well developed and efficient computation methods for jacobian control techniques exist. The disadvantage is, because the jacobian matrix is a linear approximation relationship, some intrinsic inaccuracy will be introduced. Also since the pseudoinverse is not conservative, that is, it does not return to the starting configuration when the end effector goes through a closed path, the joint angles are obtained from numerical integration of joint rate, therefore, joint angles are also nonconservative [10,16].

2.1.2 Resolution of the Kinematic Redundancy at the Acceleration Level

The acceleration parameters are the highest order derivatives included in both kinematic and dynamic equations. The kinematic constraint equations should contain acceleration variables to incorporate with the dynamics. Differentiating Eq. (2.2) with respect to time, gives;

$$J\ddot{\theta} = \ddot{\mathbf{x}} - \dot{J}\dot{\theta}. \tag{2.5}$$

This is the kinematic constraint equation at the acceleration level which provides a linear relation for the acceleration between the cartesian space and the joint angle space. Being an under-determined system equation, Eq. (2.5) can be solved by using the pseudoinverse method and the redundancy is resolved at the acceleration level. The general solution is as follows:

$$\ddot{\theta} = J^{+}(\ddot{\mathbf{x}} - \dot{J}\dot{\theta}) + (I - J^{+}J)\ddot{\phi} \tag{2.6}$$

where I is an identity matrix of order n, $\ddot{\phi}$ is any vector in the n dimensional space. The null-space component $\ddot{\phi}$ is used for achieving some specific secondary goal. When $\ddot{\phi}$ equals 0, then (2.6) becomes a minimum acceleration norm solution, i.e.,

$$\ddot{\theta} = J^{+}(\ddot{x} - \dot{J}\dot{\theta}). \tag{2.7}$$

The other variables in the joint angle space such as joint angles and joint velocities can be obtained by using Runge-Kutta fourth-order numerical integration. Due to the null-space components included in the joint accelerations, the kinematic redundancy has been resolved at the acceleration level. The advantage of this method is that it incorporates the control with system dynamics. Furthermore, both initial posture and joint rate can be searched for achieving an optimum for an objective function. The disadvantage of joint acceleration control is that both joint angle and joint rate are not conservative, i.e., they do not return to the same joint configuration and joint rate after the end effector goes through a closed path. Moreover, the performance measures are more sensitive to the initial state (both θ_0 and $\dot{\theta}_0$). This property will be discussed in the next chapter.

2.2 Generation of the Locus of Joint Configurations for Some End Effector's Position

The locus of joint configurations which correspond to the same end effector's position are useful for evaluating the performance of different techniques when resolving the kinematic redundancy. Two methods will be discussed for generating these joint configurations, one is analytic and the other is geometric.

2.2.1 Analytic Method for Generating the Locus of Joint Configurations for Some End Effector's Position

The locus of joint configurations for some end effector position can be generated by moving the manipulator gradually in the null space. The differential displacement in the null-space direction which results with no movement of the end effector is determined by adding an extra row which is orthogonal to all the row vectors of the jacobian matrix. It can be obtained by taking the cross product

of two row vectors of the joint velocity jacobian [16] for a 3-link case. A 3-link planar manipulator is the simplest redundant manipulator. It provides a useful conceptual view which is essential for the understanding of more complicated manipulators. This planar manipulator model is used in the following sections for generating and illustrating some properties of these joint configurations.

The formula for determining the null-space direction of a 3−link planar manipulator to generate these joint configurations are as follows [5]:

$$\begin{bmatrix} J_x \\ J_y \\ J_x \times J_y \end{bmatrix} \begin{bmatrix} \dot{\theta}_1 \\ \dot{\theta}_2 \\ \dot{\theta}_3 \end{bmatrix} = \begin{bmatrix} 0 \\ 0 \\ \delta \end{bmatrix} \tag{2.8}$$

where J_x and J_y are two rows of the jacobian matrix J, and δ is a small displacement along the null-space direction which is orthogonal to the range space of the jacobian matrix. One simple solution is the cross product of J_x and J_y, $J_x \times J_y$. According to Eq. (2.8) the motion in the joint angle space results in no movement of the end effector. The configurations generated by moving the manipulator in null space have the same end effector position in cartesian space.

2.2.2 Geometrical Method for Generating the Locus of Joint Configurations for Some End Effector's Position

A comparison of the geometrical and numerical methods to generate the locus of points in the joint angle space which correspond to one end effector position is discussed in this section. The numerical method which uses the jacobian matrix has the disadvantages of introducing drift and inaccuracy [5]. Therefore, a more accurate set of joint configurations which have the same end effector's position can be determined by solving the nonlinear kinematic equations at the kinematic level. An algorithm derived from the basic geometrical theorem is simple and provides

precise joint configurations which have the same end effector's position for a 3-link planar manipulator. The derivation of this algorithm is described below:

From Fig. 1 and the basic geometrical formula, the following equations are obtained:

$$\begin{aligned} \beta &= \cos^{-1}\left(\frac{b^2 + l_2^2 - l_3^2}{2bl_2}\right) \\ \gamma &= \cos^{-1}\left(\frac{b^2 + l_1^2 - r^2}{2bl_1}\right) \end{aligned} \tag{2.9}$$

and

$$\begin{cases} \theta_2 = \pi - (\beta + \gamma) \\ \theta_3 = \beta + \delta \end{cases} \quad \text{if } \beta + \gamma \leq \pi$$

or

$$\begin{cases} \theta_2 = \pi - (\gamma - \beta) \\ \theta_3 = -(\beta + \delta) \end{cases} \quad \text{if } \beta + \gamma \leq \pi$$

where **r** and **b** are vectors from the base (the first joint) to the second joint and to the end effector respectively, while β is the angle between $\mathbf{l}_2$ and **b**, and γ is the angle between **b** and $\mathbf{l}_1$.

The geometrical structure of a 3–link manipulator, when the last two links stretch out, i.e., θ_3 equals zero, gives the bounds of θ_1 by using the geometrical theorem. The angle between **r**, the vector from the base to the end effector, and the vector of the first link is equal to α. By using the relationship, $\theta_{1_{max}} - \alpha = \alpha - \theta_{1_{min}}$, the extreme values of θ_1 are obtained.

$$\theta_{1_{max}} - \alpha = \alpha - \theta_{1_{min}} = \cos^{-1}\left(\frac{r^2 + l_1^2 - (l_2 + l_3)^2}{2rl_1}\right) \tag{2.10}$$

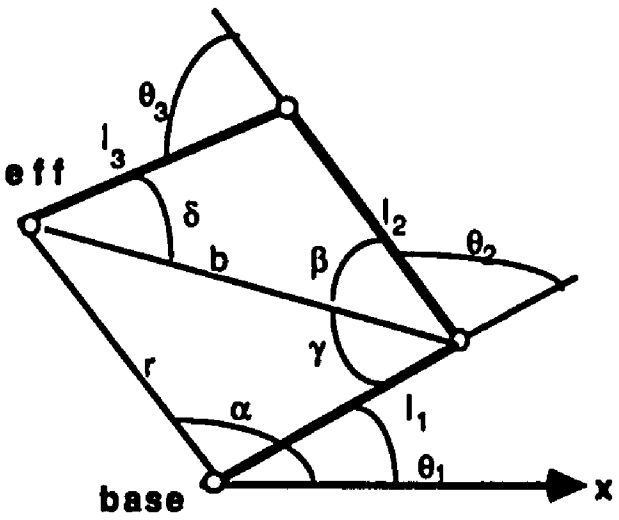

$$\theta_2 = \pi - (\beta + \gamma)$$
$$\theta_3 = \beta + \delta$$

(a). b is between l_1 and l_2

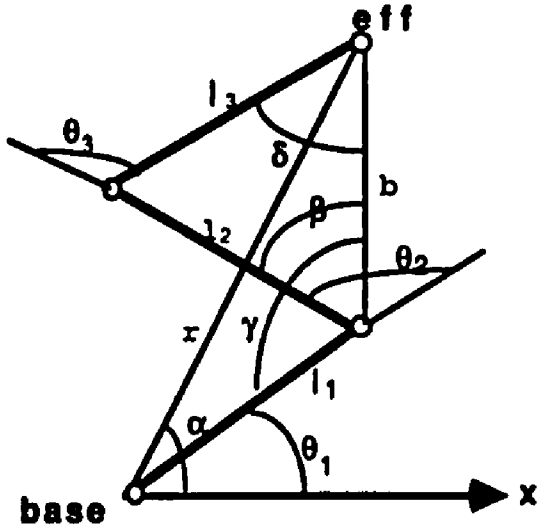

$$\theta_2 = \pi - (\gamma - \beta)$$
$$\theta_3 = -(\beta + \delta)$$

(b). l_1 is between l_2 and b

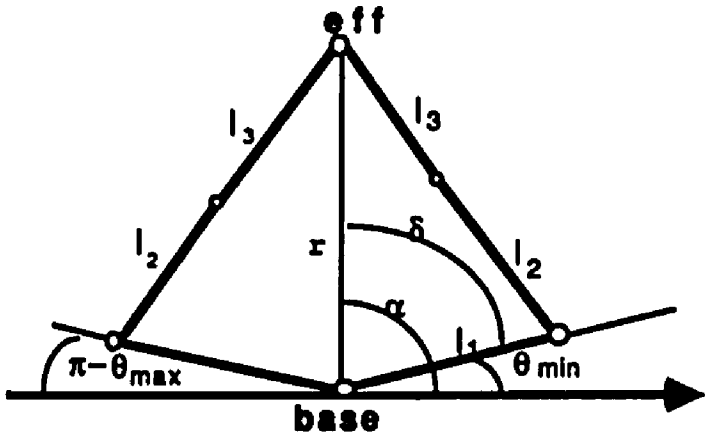

$$\theta_{max} = \alpha + \delta$$
$$\theta_{min} = \alpha - \delta$$

(c). upper and lower bound of θ_1

Figure 1: Generation of the locus of joint configurations for some end effector's position by the geometric method

where α is the angle between the vector **r** and the positive **x** axis. And the valid range of θ_1 can be found from Eq. (2.10), i.e.,

$$\begin{aligned} \theta_1 &\geq \alpha + \cos^{-1}\left(\frac{r^2 + l_1^2 - (l_2 + l_3)^2}{2rl_1}\right) = \theta_{1_{min}} \\ \theta_1 &\leq \alpha - \cos^{-1}\left(\frac{r^2 + l_1^2 - (l_2 + l_3)^2}{2rl_1}\right) = \theta_{1_{max}}. \end{aligned} \tag{2.11}$$

If, for simplicity, all the link lengths $l_i, i = 1,2,3$ are set equal to l, the formulation can be divided into three cases depending on the relative magnitude between link length l and the distance from manipulator's base to end effector $r(0 \leq r \leq 3l)$, that is, $0 \leq r < l$, $r = l$ and $l < r \leq 3l$. For the first and second cases, $r \leq l$, the range of θ_1 varies from $-\pi$ to π, while for the third case, the distance from base to end effector r, is greater than the link length l, i.e., $r > l$, the range of θ_1 becomes $\theta_{1_{min}} < \theta_1 < \theta_{1_{max}}$. Knowing the range of θ_1, the locus of joint configurations which correspond to the same end effector's location are generated by the following procedures [5]:

1. Start with $\theta_1 = \theta_{1_{min}}$.
2. The corresponding θ_2 and θ_3 are determined by using Eq. (2.10).
3. Increase θ_1 gradually by a small increment, for example 2° and use step 2 to determine θ_2 and θ_3.
4. If θ_1 reaches $\theta_{1_{max}}$, then stop.

By applying these procedures, the locus of joint configurations for some end effector's position can be generated.

- Case 1: $r > l$. The locus of joint configurations which have the same end effector's position for a 3−link manipulator with $r > l$ are:

$$\begin{cases} \theta_1 &= -\pi \leq \theta_1 \leq \pi \\ \theta_2 &= \pi - (\beta + \gamma) \quad \text{if } \beta + \gamma < \pi \\ \theta_3 &= \beta \end{cases}$$

or

$$\begin{cases} \theta_1 &= -\pi \leq \theta_1 \leq \pi \\ \theta_2 &= \pi - (\gamma - \beta) \quad \text{if } \beta + \gamma \geq \pi \\ \theta_3 &= -2\beta \end{cases} \tag{2.12}$$

- Case 2: $r = l$. In this case γ=β, therefore, the joint configurations which have the same end effector position (r, α) are:

$$\begin{cases} -\pi \leq \theta_1 \leq \pi \\ \theta_2 = \pm\pi \\ \theta_3 = -(\theta_1 + \alpha) \end{cases} \quad \text{or} \quad \begin{cases} \theta_1 = \alpha \\ -\pi \leq \theta_2 \leq \pi \\ \theta_3 = \pm\pi \end{cases} \tag{2.13}$$

- Case 3: $r > l$.

$$\begin{cases} \theta_{1_{min}} \leq \theta_1 \leq \theta_{1_{max}} \\ \theta_2 = \pi - (\beta + \gamma) \quad \text{if } \beta + \gamma < \pi \\ \theta_3 = 2\beta \end{cases}$$

or

$$\begin{cases} \theta_{1_{min}} \leq \theta_1 \leq \theta_{1_{max}} \\ \theta_2 = \pi - (\gamma - \beta) \quad \text{if } \beta + \gamma \geq \pi \\ \theta_3 = -2\beta \end{cases}$$

with

$$\begin{aligned} (\theta_1)_{min} &= \alpha + \cos^{-1}\left(\frac{r^2 + l_1^2 - (l_2 + l_3)^2}{2rl_1}\right) \\ (\theta_1)_{max} &= \alpha - \cos^{-1}\left(\frac{r^2 + l_1^2 - (l_2 + l_3)^2}{2rl_1}\right). \end{aligned} \tag{2.14}$$

The advantage of using the above technique is that precise locus of joint configuration corresponding to the same end effector's position are obtained because no approximation has been used in the computation process. Moreover, in the case of r is less than the link length (where r is the distance from the end effector to the base of the manipulator), this algorithm generates a complete set instead of just half of the locus [5]. Finally, no drift in either the cartesian or the joint angle space is introduced.

2.3 Projection of the Locus of Joint Configurations for Some End Effector's Position on a Plane Spanned by Joint Angle Coordinates

An n-link planar manipulator is shown in Fig. 2. The location of the end effector in x, y plane with cartesian space coordinates (x, y) is represented by the expression in joint angle space as follows:

$$\begin{aligned} x &= \sum_{i=1}^{3} l_i \cos(\sum_{j=1}^{i} \theta_j) \\ y &= \sum_{i=1}^{3} l_i \sin(\sum_{j=1}^{i} \theta_j). \end{aligned} \tag{2.15}$$

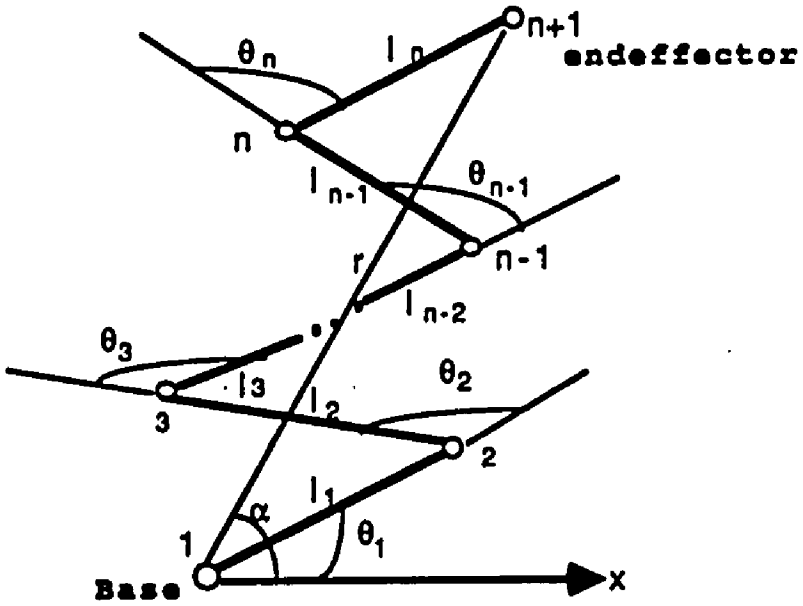

Figure 2: A $n-$link planar manipulator

Eqs. (2.15) are the kinematic relationship between the cartesian and the joint angle space coordinates for the planar 3-link manipulator. There are more variables in the joint angle space than in the cartesian space, that is, an infinite number of possible configurations in the joint angle space can reach the same specific end effector location. Some of these possible configurations can be chosen to optimize some performance measure.

Assuming that the base of a manipulator is located at the origin of the cartesian coordinate, a pair (r, α) in a cylindrical coordinate can be used to represent a point (x, y) in the cartesian space. The distance from the end effector (x, y) to the base $(0, 0)$ is r, and the angle between the line connecting the origin to the end effector and the positive x-axis is α. The quantities r and α can be expressed as a function of the variables in the joint angle space, that is,

$$\begin{aligned} r &= f(\theta_1, \theta_2, \theta_3, ..., \theta_n) \\ \alpha &= g(\theta_1, \theta_2, \theta_3, ..., \theta_n) \end{aligned} \tag{2.16}$$

where f and g are two real functions. The cylindrical coordinates (r, α) are computed directly from the joint angle space variables $(\theta_1, \theta_2, \theta_3, \ldots, \theta_n)$ by using Eq. (2.16). Similarly, for a given (r, α) the joint configurations are obtained by solving the same equation. For the 3-link redundant manipulator, there are only two linearly independent variables, therefore, one of the joint angle space variables can be eliminated and the projection on the two variable plane are obtained.

The projection of the locus of joint configurations on planes spanned by θ_1 and θ_2, θ_2 and θ_3 and θ_3 and θ_1 are derived and will also be discussed. These projections provide a simpler view for analyzing the effect of the null-space components on the motion of a redundant manipulator.

2.3.1 The Projection of the Locus of Joint Configurations for Some End Effector's Position on a Plane Spanned by θ_2 and θ_3

The distance from the end effector to the base can be computed from Eq. (2.15), that is:

$$\begin{aligned} r^2 &= x^2 + y^2 \\ &= l_1^2 + l_2^2 + l_3^2 + 2[l_1 l_2 cos\theta_2 + l_1 l_3 cos(\theta_2 + \theta_3) + l_2 l_3 cos\theta_3]. \end{aligned} \tag{2.17}$$

The above equation can be rearranged and becomes

$$l_1 l_2 cos\theta_2 + l_1 l_3 cos(\theta_2 + \theta_3) + l_2 l_3 cos\theta_3 = \frac{r^2 - (l_1^2 + l_2^2 + l_3^2)}{2}, \tag{2.18}$$

assuming that the length of each link is fixed and equal to l, then the parameter r becomes:

$$r^2 = l^2\{3 + 2[cos\theta_2 + cos(\theta_2 + \theta_3) + cos\theta_3]\}, \tag{2.19}$$

or

$$\frac{(r/l)^2 - 3}{2} = \cos\theta_2 + \cos(\theta_2 + \theta_3) + \cos\theta_3. \tag{2.20}$$

Eq. (2.20) depends only on the variables θ_2 and θ_3, in other words, r is independent of θ_1. This property is useful because a two-dimensional plot can be used to visualize the effect of the joint angle variables on some performance measures. If each link has unit length 1 then Eq. (2.20) becomes:

$$\frac{r^2 - 3}{2} = \cos\theta_2 + \cos(\theta_2 + \theta_3) + \cos\theta_3. \tag{2.21}$$

The projection of the locus of joint configurations for some end effector's position on the $\theta_1 = 0$ plane with a fixed α ($\alpha = 0$) and a varied r ($0 \leq r \leq 3l$) are given in Fig. 3 [5]. Each curve corresponds to a specified r. It is interesting to

notice that only the cartesian coordinate variable r appears in Eq. (2.21), and the other variable α does not. That is, points on a circle with radius r (independent of parameter α) have the same projection curve on the plane spanned by θ_2 and θ_3.

2.3.2 The Projection of Locus of Joint Configurations for Some End Effector's Position on the Plane Spanned by θ_1 and θ_2

Similarly, projection of the locus of joint configurations for some end effector's position on the planes spanned by θ_1 and θ_2 and by θ_1 and θ_3 are obtained as follows: By applying some geometric theorems to Fig. 4

$$\begin{aligned} a^2 &= l_1^2 + l_2^2 - 2l_1 l_2 \cos(\pi - \theta_2) \\ &= l_1^2 + l_2^2 + 2l_1 l_2 \cos\theta_2 \end{aligned} \tag{2.22}$$

and

$$\begin{aligned} \cos\zeta &= \frac{a^2 + l_1^2 - l_2^2}{2al_1} \\ \cos\delta &= \frac{r^2 + a^2 - l_3^2}{2ar} \end{aligned} \tag{2.23}$$

are obtained and from

$$\delta + \zeta = \theta_1 - \alpha \tag{2.24}$$

equations for θ_1 and θ_2 are obtained as follows:

Case 1: $\theta_1 > \alpha$.

Fig. 4 shows the relation $\zeta + \delta = \theta_1 - \alpha$, therefore:

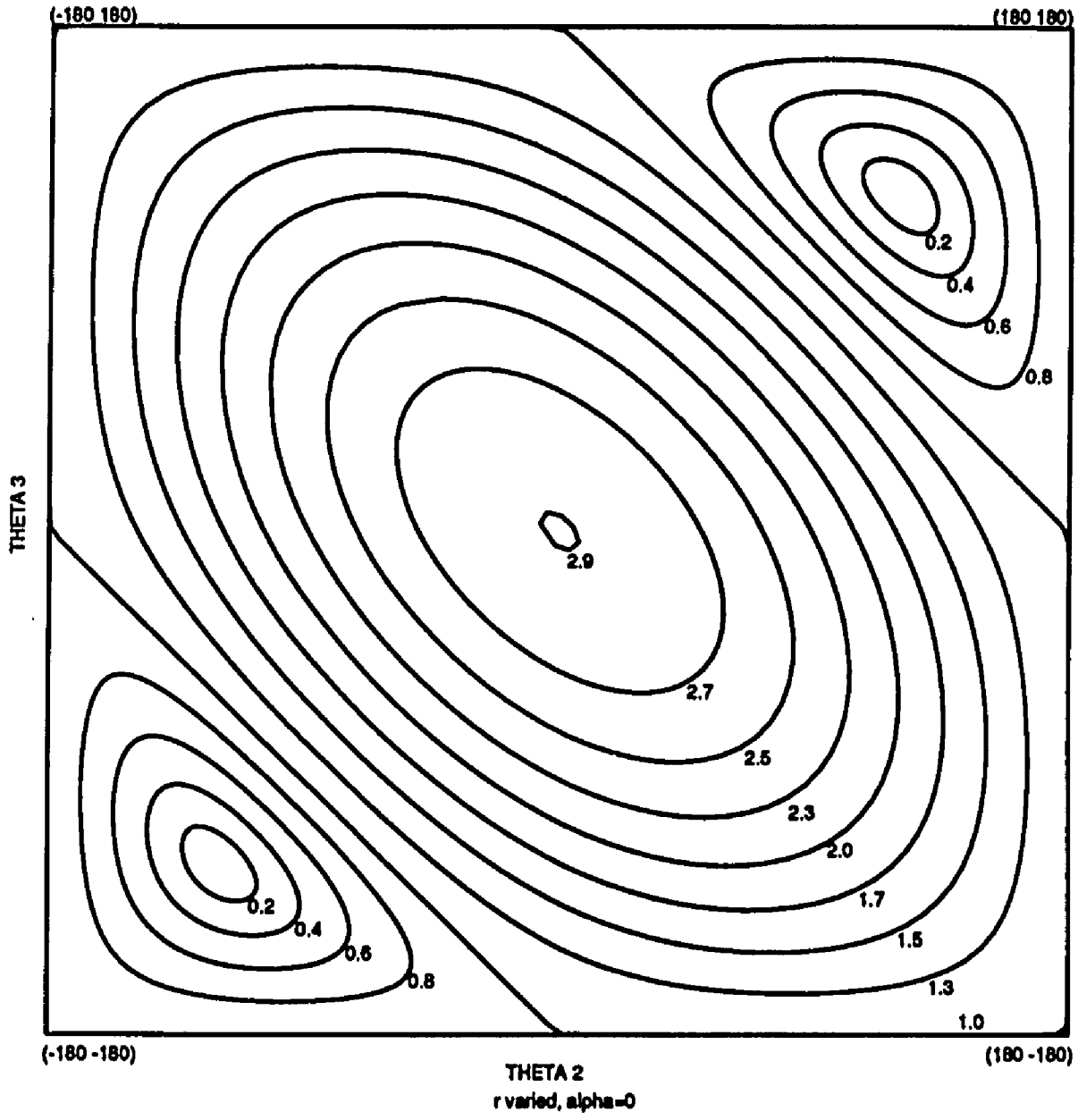

Figure 3: The projection of the locus of joint configurations for some end effector's position on the plane spanned by θ_2 and θ_3 with a fixed α ($\alpha = 0$) and a varied r ($0 \leq r \leq 3l$) [5]

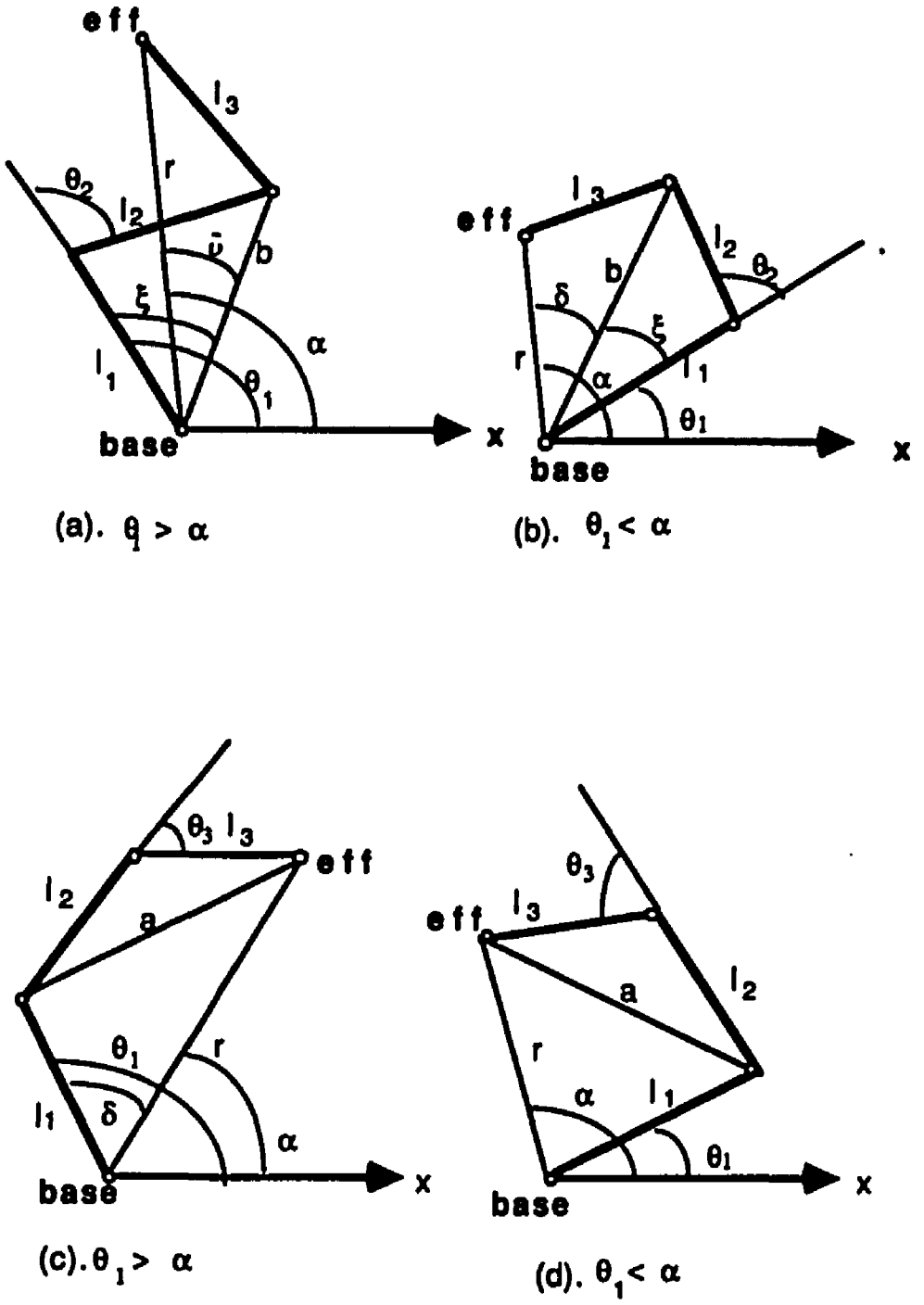

Figure 4: Cases for deriving the projection of the locus of joint configurations for some end effector's position on the planes spanned by the coordinates θ_1 and θ_2, θ_2 and θ_3 and θ_3 and θ_1

$$\cos^{-1}\left(\frac{(l_1 + l_2\cos\theta_2)}{\sqrt{l_1^2 + l_2^2 + 2l_1l_2\cos\theta_2}}\right) + \cos^{-1}\left(\frac{2l_1^2 + l_2^2 - l_3^2 + 2l_1l_2\cos\theta_2}{2r\sqrt{l_1^2 + l_2^2 + 2l_1l_2\cos\theta_2}}\right) \quad (2.25)$$

$$= \theta_1 - \alpha, \quad (2.26)$$

if the length of each link is l, then Eq. (2.26) becomes:

$$\cos^{-1}\left(\sqrt{\frac{1+\cos\theta_2}{2}}\right) + \cos^{-1}\left(\sqrt{\frac{(1+\cos\theta_2)l}{2r^2}}\right) = \theta_1 - \alpha. \quad (2.27)$$

Case 2: $\theta_1 < \alpha$.

In this case, Eq. (2.24) is $\delta + \zeta = \alpha - \theta_1$ instead of $\delta + \zeta = \theta_1 - \alpha$, therefore, the relation between joint angle θ_1 and θ_2 becomes:

$$\cos^{-1}\left(\frac{(l_1 + l_2\cos\theta_2)}{\sqrt{l_1^2 + l_2^2 + 2l_1l_2\cos\theta_2}}\right) + \cos^{-1}\left(\frac{2l_1^2 + l_2^2 - l_3^2 + 2l_1l_2\cos\theta_2)}{2r\sqrt{l_1^2 + l_2^2 + 2l_1l_2\cos\theta_2}}\right) \quad (2.28)$$

$$= \alpha - \theta_1. \quad (2.29)$$

If the length of each link is l, then (2.27) becomes:

$$\cos^{-1}\left(\sqrt{\frac{1+\cos\theta_2}{2}}\right) + \cos^{-1}\left(\sqrt{\frac{(1+\cos\theta_2)l}{2r^2}}\right) = \alpha - \theta_1. \quad (2.30)$$

The projection of the locus of joint configurations for some end effector's position on the $\theta_3 = 0$ plane with a fixed r ($r = 2.0$) and a varied α ($-90° \leq \alpha \leq 90°$) are given in Fig. 5. While the projection of these configurations on the plane spanned by θ_1 and θ_2 with a fixed α ($\alpha = 0$) and a varied r ($0 \leq r \leq 3l$) are shown in Fig. 6.

2.3.3 The Projection of the Locus of Joint Configurations for Some End Effector's on the Plane Spanned by θ_1 and θ_3

The relationship between joint angles θ_1 and θ_3 is derived as follows:

As seen in Fig. 4:

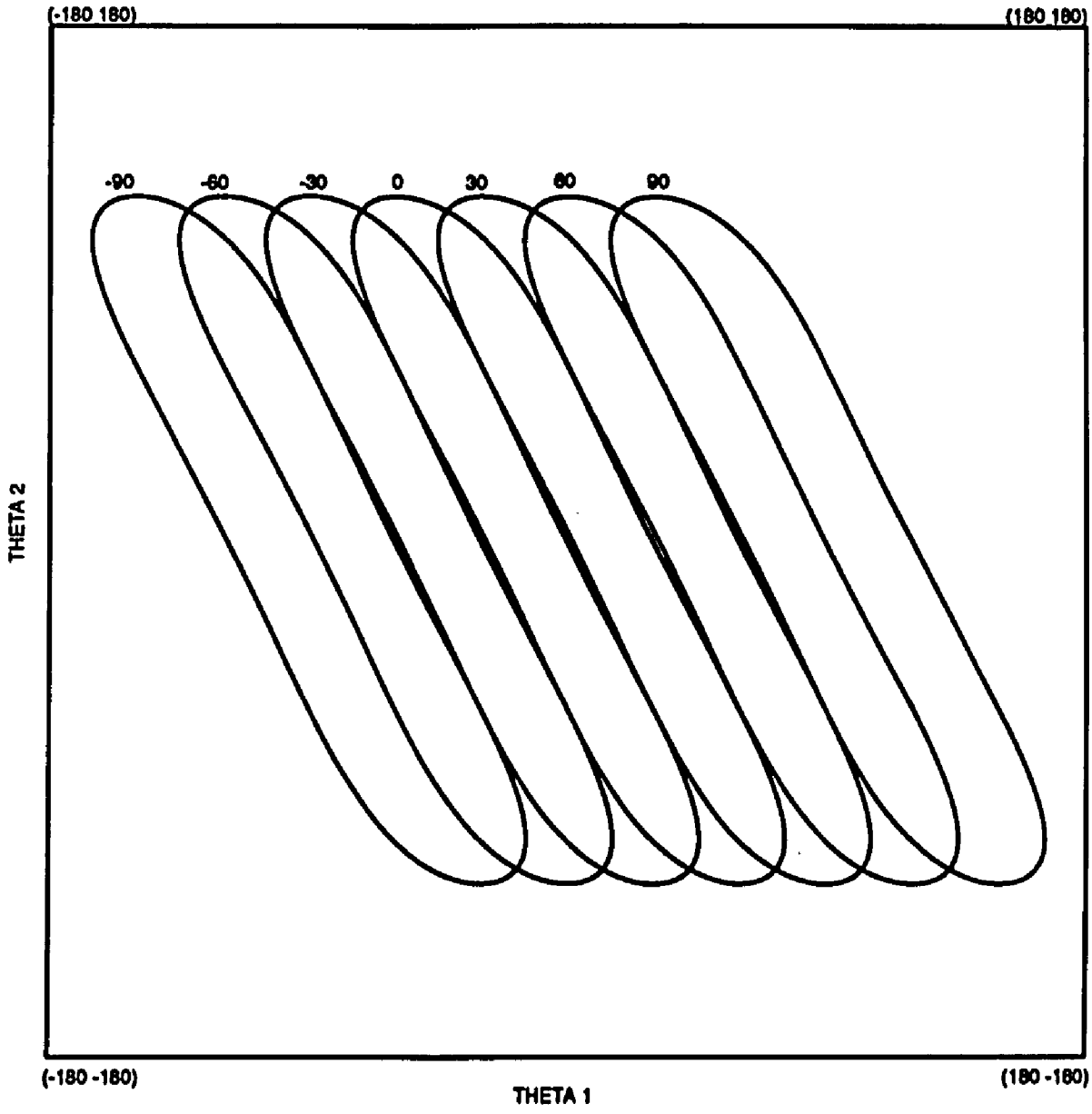

Figure 5: The projection of the locus of joint configurations for some end effector's position on the plane spanned by θ_1 and θ_2 with a fixed r ($r = 2.0$) and a varied α ($-90° \leq \alpha \leq 90°$)

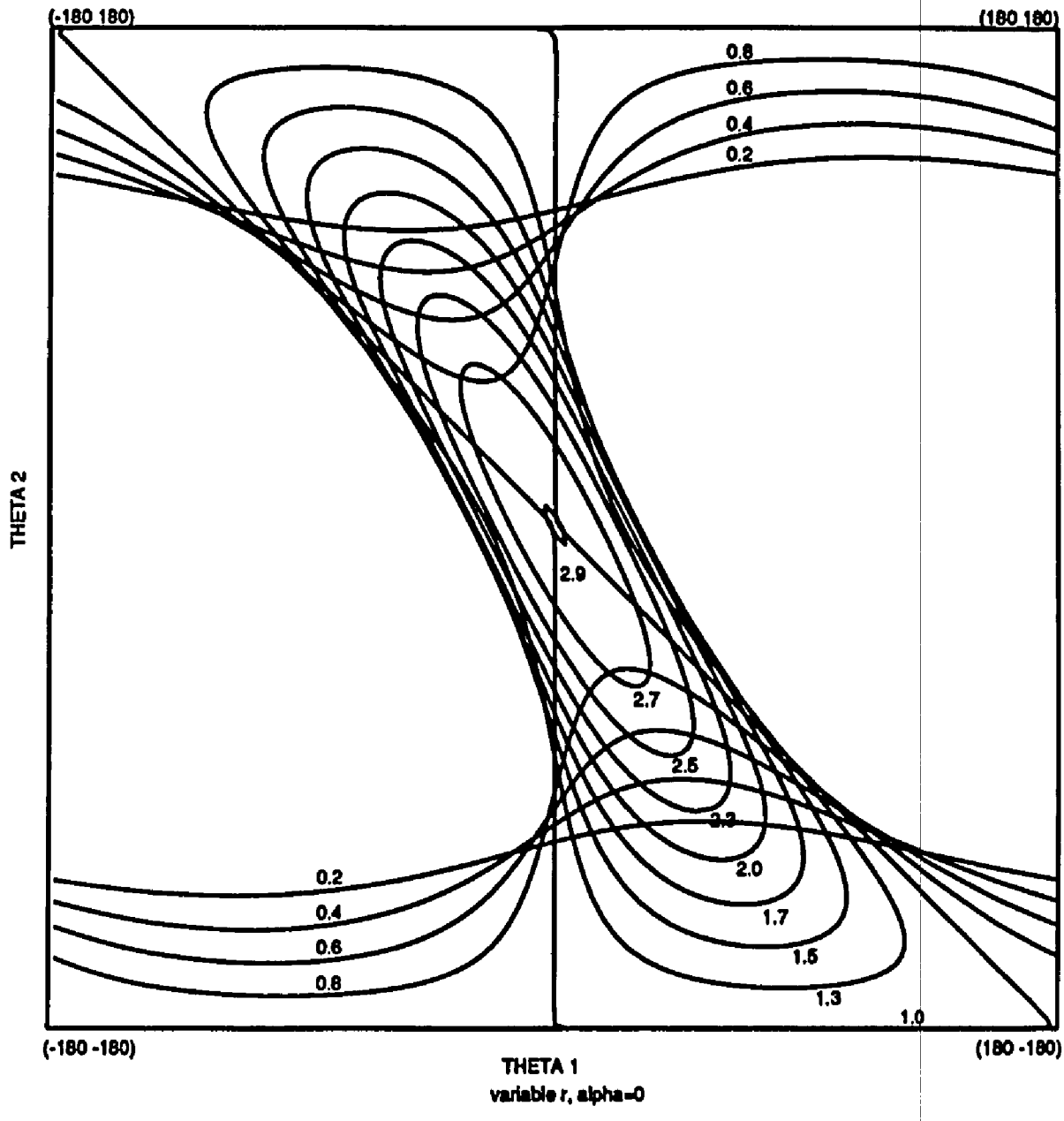

Figure 6: The projection of the locus of joint configurations for some end effector's position on the plane spanned by θ_1 and θ_2 with a fixed α ($\alpha = 0$) and a varied r ($0 \leq r \leq 3l$)

$$
\begin{aligned}
b^2 &= l_2^2 + l_3^2 - 2l_2l_3\cos(\pi - \theta_3) \\
\cos\delta &= \frac{l_1^2 + r^2 - b^2}{2l_1r}
\end{aligned}
\tag{2.31}
$$

where

$$
\delta = \begin{cases} \theta_1 - \alpha & \text{if } \theta_1 \geq \theta \\ \alpha - \theta_1 & \text{if } \theta_1 < \theta \end{cases} . \tag{2.32}
$$

Therefore, the relation between θ_1 and θ_3 is obtained, i.e.,

$$
\cos(\theta_1 - \alpha) = \frac{l_1^2 + r^2 - b^2}{2l_1r} \tag{2.33}
$$

that is,

$$
2\left[l_1r\cos(\theta_1 - \alpha) - l_2l_3\cos\theta_3\right] = r^2 + l_1^2 - l_2^2 - l_3^2. \tag{2.34}
$$

If all the links have the same length l, then the relation of θ_1 and θ_3 becomes:

$$
2\{l[r\cos(\theta_1 - \alpha) - l\cos\theta_3]\} = r^2 + l^2. \tag{2.35}
$$

The projection of the locus of joint configurations for some end effector position on the plane spanned by θ_1 and θ_3 with a fixed r ($r = 2.0$) and a varied α ($-90° \leq \alpha \leq 90°$) are given in Fig. fig:105. While the projection of these configurations on the plane spanned by θ_1 and θ_3 with a fixed α ($\alpha = 0$) and a varied r ($0 \leq r \leq 3l$) are shown in Fig. 8.

From the above discussion, the equations providing the relationship for projecting the locus of joint configurations, which have the same end effector location, on the planes spanned by the coordinates θ_1 and θ_2, θ_2 and θ_3 also θ_3 and θ_1 are derived. They provide three two-dimensional projections on the joint angles'

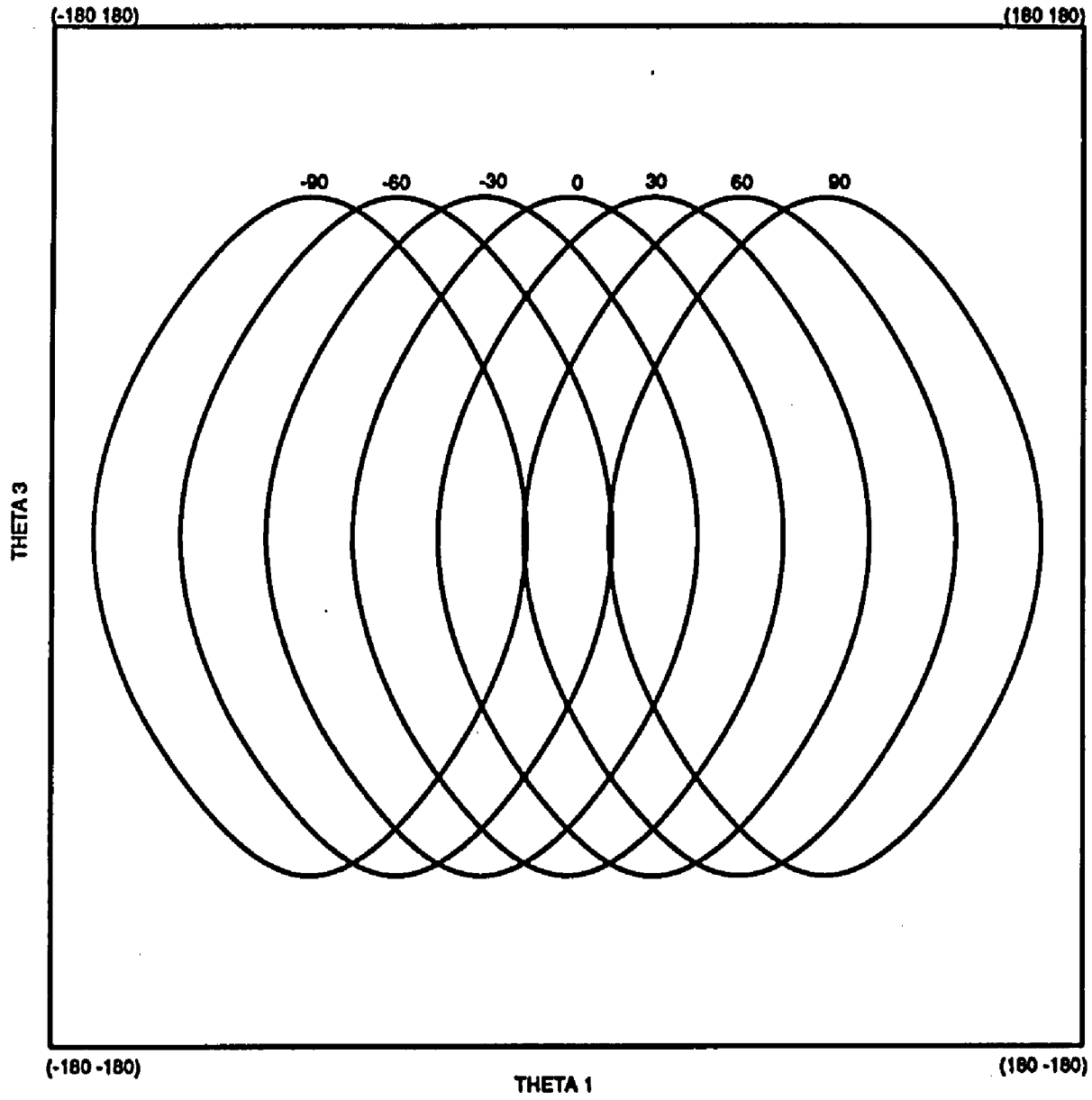

Figure 7: The projection of the locus of joint configurations for some end effector's position on the plane spanned by θ_1 and θ_3 with a fixed r ($r = 2.0$) and a varied α ($-90° \leq \alpha \leq 90°$)

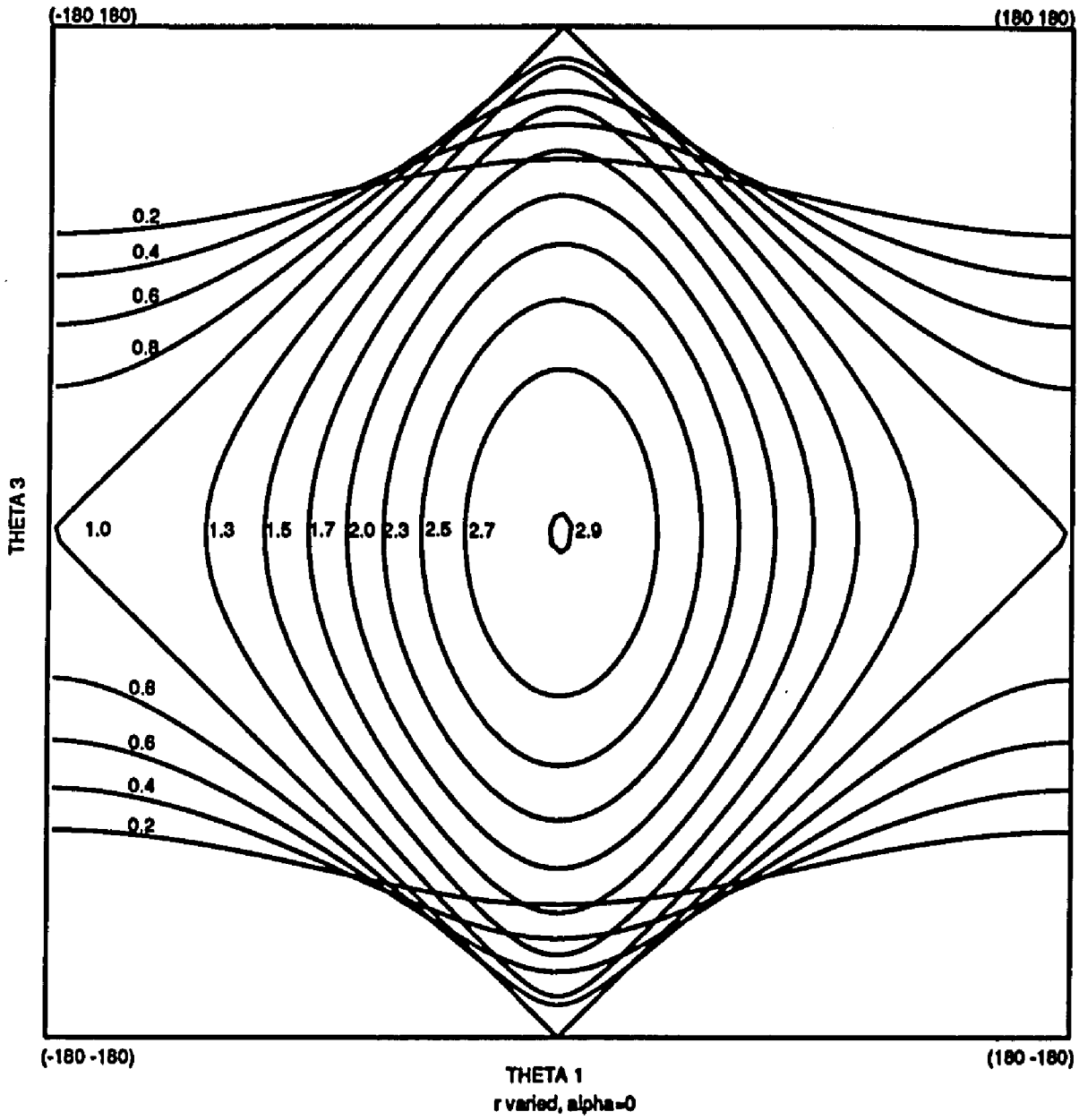

Figure 8: The projection of the locus of joint configurations for some end effector's position on the plane spanned by θ_1 and θ_3 with a fixed α ($\alpha = 0$) and a varied r ($0 \leq r \leq 3l$)

plane for those three-dimensional locus of joint configurations. These projections are helpful for visualizing the characteristics and patterns of a 3-dimensional locus of joint configurations.

2.4 Summary

In this chapter, first, resolution of the kinematic redundancy by using pseudoinverse method was discussed. The pseudoinverse method, having less complicated computations and easier representation of redundancy with null-space component, is a powerful tool for resolving the redundancy. Second, two methods for generating the locus of joint configurations which have the same end effector location were described. This set of joint configurations construct a useful test space for evaluating the performance of different control schemes. Third, the projection of the locus of joint configurations, which have the same end effector location, on each pair of joint-angle planes are derived. These projections are helpful for visualizing the characteristics and patterns of a 3-dimensional locus of joint configurations. Moreover, These planar projections provide simpler means and clearer views for investigating the redundancy resolution problems. They provide three two-dimensional projections on the joint angles' plane for those three-dimensional locus of joint configurations.

CHAPTER III

COMPARISON OF THE REDUNDANCY RESOLUTION AT THE VELOCITY AND AT THE ACCELERATION LEVELS

The joint angles of a manipulator in the joint space and the position of the end effector in the cartesian space are related by a set of nonlinear kinematic equations. However the instantaneous relationships between these two coordinates for both velocity and acceleration are linear. Moreover, in order to incorporate kinematics with dynamics, kinematic redundancy is more desirable to be resolved either at the velocity or at the acceleration level rather than at the position level. As a result, investigating resolutions of the redundancy at the velocity and at the acceleration level is essential in facilitating the control of redundant manipulators, so that a choice of proper control scheme for resolving the kinematic redundancy can be made, and the desired goal can be achieved.

The joint angle and velocity of each joint constitute a state which plays a very important role in the control of a manipulator. Joint rates as well as joint configurations are essential quantities which together with the trajectory specification of the end effector in the cartesian space (external inputs) determine the characteristics of a manipulator's system. The integration of the joint rates' square, $|\dot{\theta}|^2$, along the specified end effector's trajectory is a useful global performance measure,

$$I_{\dot{\theta}} = \int_{t_0}^{t_f} \dot{\theta}^T \dot{\theta} dt, \tag{3.1}$$

where t_0 and t_f are the initial and final times for the specified trajectory. Based on the measure $I_{\dot{\theta}}$, the performance of two generally used redundancy resolution schemes, minimum norm of joint rate and minimum norm of joint acceleration methods, is compared.

This chapter is divided into three sections. The first section compares two redundancy resolution methods, i.e., resolution at the velocity level and resolution at the acceleration level. The second section describes the relationship between them by using the calculus of variation method. The third section presents the computer simulation results, the effects of initial posture, and initial joint rates on the performance measure, Eq. (3.1), are also discussed.

3.1 The Utilization of Null Space

The kinematic constraints of a redundant manipulator at the velocity and at the acceleration levels can be obtained by differentiating the constraint equations relating the position of end effector in the cartesian space in terms of joint angles in the joint space, i.e., $\mathbf{x} = f(\theta)$,

$$\dot{\mathbf{x}} = J\dot{\theta} \tag{3.2}$$

and

$$\ddot{\mathbf{x}} = J\ddot{\theta} + \dot{J}\dot{\theta} \tag{3.3}$$

respectively. By using the pseudoinverse method, the kinematic redundancy can be resolved at the velocity level giving

$$\dot{\theta} = J^{+}\dot{\mathbf{x}} + (I - J^{+}J)\dot{\psi} \tag{3.4}$$

or at the acceleration level

$$\ddot{\theta} = J^{+}(\ddot{\mathbf{x}} - \dot{J}\dot{\theta}) + (I - J^{+}J)\ddot{\phi} \tag{3.5}$$

with $\dot{\psi}$ and $\ddot{\phi}$ as two arbitrary vectors in the $n-$dimensional joint velocity and joint acceleration spaces. The minimum norm solutions of joint rate and joint acceleration are achieved by setting the null-space components $\dot{\psi}$ and $\ddot{\phi}$ in Eqs. (3.4) and (3.5) equal to zero, that is, the minimum norm of joint rate solution becomes

$$\dot{\theta} = J^{+}\dot{\mathbf{x}} \tag{3.6}$$

and the minimum norm of joint acceleration solution is

$$\ddot{\theta} = J^{+}(\ddot{\mathbf{x}} - \dot{J}\dot{\theta}). \tag{3.7}$$

By taking the time derivative of Eq. (3.6), the required joint accelerations resulting from the resolution of redundancy at the velocity level can be expressed as:

$$\begin{aligned} \ddot{\theta} &= J^{+}(\ddot{\mathbf{x}} - \dot{J}\dot{\theta}) + J^{+}\dot{J}\dot{\theta} + \frac{d}{dt}(J^{+})\dot{\mathbf{x}} \\ &= J^{+}(\ddot{\mathbf{x}} - \dot{J}\dot{\theta}) + J^{+}\dot{J}J^{+}\dot{\mathbf{x}} + \frac{d}{dt}(J^{+})\dot{\mathbf{x}}. \end{aligned} \tag{3.8}$$

If the jacobian matrix J is of full column rank, i.e., the configuration is not singular, then the pseudoinverse of the jacobian matrix J can be computed from the following expression:

$$J^{+} = J^{T}(JJ^{T})^{-1}. \tag{3.9}$$

and $JJ^{+} = JJ^{T}(JJ^{T})^{-1} = I$, with I an identity matrix. By taking the time derivative of this equality, the following relationship is obtained:

$$\dot{J}J^{+} = -J\frac{d}{dt}(J^{+}). \tag{3.10}$$

In Eq. (3.8) substituting $\dot{J}J^{+}$ for $-J\frac{d}{dt}(J^{+})$ gives

$$\begin{aligned}\ddot{\theta} &= J^{+}(\ddot{\mathbf{x}} - \dot{J}\dot{\theta}) - J^{+}J\frac{d}{dt}(J^{+})\dot{\mathbf{x}} + \frac{d}{dt}(J^{+})\dot{\mathbf{x}} \\ &= J^{+}(\ddot{\mathbf{x}} - \dot{J}\dot{\theta}) + (I - J^{+}J)\frac{d}{dt}(J^{+})\dot{\mathbf{x}}. \end{aligned} \tag{3.11}$$

By comparing the joint acceleration $\ddot{\theta}$ of Eq. (3.7) for the minimum norm of acceleration method with that of the Eq. (3.11) which is the joint acceleration required for the minimum norm of joint rate method, it can be seen that the only difference between them is the null-space component. If the null-space component $(I - J^{+}J)\frac{d}{dt}(J^{+})\dot{\mathbf{x}}$ is added to the Eq. (3.7) then these two equations become equivalent.

From the above discussion, it is seen that resolving redundancy, through norm of joint rate minimization can be achieved by resolving the redundancy at the acceleration level with adding proper null-space components. In other words, the only difference between these two redundancy resolution schemes is the usage of the null space. Therefore, it is interesting to compare these two methods for resolving redundancy by looking at the variation of the null-space component $(I - J^{+}J)\frac{d}{dt}(J^{+})\dot{\mathbf{x}}$. This quantity gives the information of how much difference these two methods will have. A computer simulation has been carried out through all possible joint configurations which have the same end effector position in Cartesian space. These joint configurations were used as an initial posture to start the job. Some properties related to these two redundancy resolution schemes for the optimization of the objective function, Eq. (3.1), will be discussed in later sections.

3.2 Euler-Lagrange Equation

Calculus of variation is another useful technique which can be used to obtain the optimal trajectory for the optimization of a global performance measure. The Euler-Lagrange equation and the associated boundary conditions required for optimizing the performance measure, Eq. (3.1), are discussed in this section. The objective function $I_{\dot{\theta}}$ of Eq. (3.1) is

$$I_{\dot{\theta}} = \int_{t_0}^{t_f} \dot{\theta}^T \dot{\theta} dt \tag{3.12}$$

combining the performance measure $I_{\dot{\theta}}$ with the kinematic constraint equation gives the augmented objective function, i.e.,

$$I^* = \int_{t_0}^{t_f} g_a(\theta, \dot{\theta}, \mathbf{x}, \dot{\mathbf{x}}, \ddot{\mathbf{x}}, t) dt \tag{3.13}$$

with

$$g_a = \dot{\theta}^T \dot{\theta} + \boldsymbol{\lambda}^T h(\mathbf{x}, \theta) \tag{3.14}$$

where $\boldsymbol{\lambda}$ is the Lagrange multiplier and $h(\mathbf{x}, \theta) = \mathbf{x} - f(\theta)$ is the kinematic constraint equation. From calculus of variation, the corresponding Euler-Lagrange equation

$$\frac{\partial g_a}{\partial \theta} - \frac{d}{dt}\frac{\partial g_a}{\partial \dot{\theta}} = 0 \tag{3.15}$$

gives

$$\ddot{\theta} = J^+(\ddot{\mathbf{x}} - \dot{J}\dot{\theta}) \tag{3.16}$$

which is the minimum norm of joint acceleration solution. The boundary conditions which need to be satisfied are

$$\dot{\theta}(b) = J^{+}\dot{\mathbf{x}}(b) \tag{3.17}$$

where $b = t_0$ or $b = t_f$. It can be seen that the optimum trajectory is obtained by first starting with minimum joint rate solution then following with the minimum acceleration solutions and finally also ending with minimum joint rate solution. The Euler-Lagrange equation, Eq. (3.16), and the associated boundary conditions, Eq. (3.17) are the necessary conditions required to minimize the objective function $I_{\dot{\theta}}$ in Eq. (3.1). It is interesting that two of these local minima remain the same, shown in the following section Fig. 15, no matter which updating scheme, minimum norm of joint rate or minimum norm of joint acceleration, is used. The computer simulation results shown in the next section, Figs. 18 and 19, show that starting at these initial postures the joint space trajectories generated by the two control strategies are the same. This property can be interpreted as follows:

The joint space trajectories starting with these special initial configurations give the same local minimum of the performance measure, Eq. (3.1), for both control schemes. These joint space trajectories satisfy both the Euler-Lagrange equation and the required initial and final boundary conditions. That is, they start from one homogeneous surface and also end at another homogeneous surface orthogonally and follow the Euler-Lagrange equation in between.

For the extreme case, as the trajectory becomes smaller and smaller, then the initial and the final points almost coincide. Therefore, minimizing the global measure is the same as minimizing the local measure, i.e., the trajectories generated by two control strategies are the same. Let the length of the trajectory be subdivided into several pieces of smaller subtrajectories. In order to get the minimum measure of $\int_{t_0}^{t_f} \dot{\theta}^T \dot{\theta} dt$, each small piece of trajectory starts from one homogeneous surface and ends at another orthogonally. It can be seen that if the divisions are

small enough, then each point on the trajectory which gives the minimum global measure is orthogonal to the homogeneous surface, i.e., the minimum norm of joint rate solution. In other words, the trajectory which gives the local minimum of the global measure of $\int_{t_0}^{t_f} \dot{\theta}^T \dot{\theta} dt$ becomes the minimum joint rate solution. Therefore, if the proper initial posture has been chosen, then the optimal performance can be achieved by either velocity or acceleration control scheme.

In the previous section, it was shown that the difference between minimum norm of joint rate and minimum norm of joint acceleration solutions is the null-space component, $(I - J^+J)\frac{d}{dt}(J^+)\dot{\mathbf{x}}$. If this component becomes very small i.e., approaches zero, then these two schemes will have almost the same trajectory. Also the objective function $\int_{t_0}^{t_f} \dot{\theta}^T \dot{\theta} dt$ is optimized.

3.3 Physical Interpretation

In this section the physical meanings of joint velocity control and joint acceleration control are discussed and comparison between them is made. Physically, the joint rate pseudoinverse method minimizes the norm of joint rate at any instant. In other words, this method makes the manipulator always move its links so that they travel in the direction which minimizes the total changes of joint angles. On the other hand, the minimum joint acceleration strategy minimizes the norm of joint acceleration. That is, it tries to keep the instantaneous changes of joint rates as small as possible. Because different strategies are used, these two control schemes will result in having different joint angle space trajectories.

In the homogeneous space, the minimum norm of joint rate method always goes to the nearest point on the next homogeneous configuration surface, while the minimum norm of joint acceleration method chooses a path which gives the minimal norm of the change of joint rates, i.e., it will keep the joint movements

in the directions that are as close as possible to the current ones, and the speed changes as small as possible, that is, preserving the current velocity.

According to the above discussion, the joint rate pseudoinverse is less constrained than joint acceleration pseudoinverse. The next instant of joint velocity does not depend on the current joint rate. The only constraint is to pick up the next destination from those points on the homogeneous surface that track the specified trajectory in the cartesian space. While in the joint acceleration method both current configuration and current joint rate must be considered. This property sometimes makes the manipulator give up the shortest path and maintain its current direction and speed. This explains why, for most of the initial starting configurations, the joint rate pseudoinverse method results in having smaller cost function than those of the joint acceleration method. The computer simulation will be shown in the next section Fig. 18. On the other hand, there exist a few initial configurations which the minimum joint acceleration method may have better performance measures than those of the minimum joint rate method. This is because the homogeneous surfaces are not equally spaced, the minimum norm of joint acceleration method, which keeps least changes of the current motion may drive the end effector into a small spacing region on the joint angle space, while joint rate pseudoinverse follows the minimum change of joint angle may eventually drive the end effector into large spacing region. Therefore, in this case, a small joint angle displacement may be required for the joint acceleration method.

3.4 Computer Simulations

Due to the highly nonlinear equations for the inverse kinematics for a redundant manipulator, finding a closed form to express the manipulator's motion is complicated if not impossible. As a result, numerical techniques are required for

the computer control of a redundant manipulator.

Computer simulation is effective and useful for investigating problems for which it is hard to get a closed-form expression. Several computationally efficient techniques i.e., recursive formulas [23,24] have been developed for computer simulation. By using the recursive formulas in [12,23] the equations used for the simulation in this research are derived. Eq. (3.1) is used as the performance measure for the comparison of the two generally used redundancy resolution schemes. These two control strategies give different trajectories in the joint angle space as well as the performance measure while both satisfying the kinematic requirements in the cartesian space. However, the difference and similarity of these two methods are interesting and need to be investigated.

The simulation results show that the initial state, both configuration and joint rate, plays an important role in determining the characteristics of the two redundancy resolution schemes. Moreover, it provides information for the motion planner to decide which method is more suitable for performing a given job.

Two kinds of trajectories in the cartesian space, open curve (straight or curve lines) shown in Figs. 11 and 12 and closed curves (circle or square) shown in Fig. 13, are used for the computer simulation. The specification of these curves in cartesian space are given in Tables 1 and 2. Among other complicated trajectories straight line is the simplest. The characteristics of redundancy resolution can be demonstrated best by going through a straight line, rather than the more complicated trajectories. The closed curve trajectories (circle or square) are essential due to their property of returning to the starting point after finishing their jobs. It is a useful test case for the joint angle space drift which results from the nonconservative property of the pseudoinverse method. Figs. 9 and 10 show the position, velocity and acceleration in the cartesian space as functions of time for the straight

Table 1: The formulas of position, velocity and acceleration in the cartesian space for a trajectory of circle with radius a, zero initial and zero final velocities

	$0 \leq t \leq 1$	$1 \leq t \leq 2$
x	$a\cos\pi t^2$	$a\cos\pi(2-t)^2$
y	$a\sin\pi t^2$	$-a\sin\pi(2-t)^2$
$\dot{x}$	$-2a\pi t\sin\pi t^2$	$-2a\pi(2-t)\sin\pi(2-t)^2$
$\dot{y}$	$2a\pi t\cos\pi t^2$	$2a\pi(2-t)\cos\pi(2-t)^2$
$\ddot{x}$	$-a(2\pi t)^2\cos\pi t^2 - 2a\pi\sin\pi t^2$	$-a(2\pi(2-t))^2\cos\pi(2-t)^2$ $-2a\pi\sin\pi(2-t)^2$
$\ddot{y}$	$-a(2\pi t)^2\sin\pi t^2 + 2a\pi\cos\pi t^2$	$-a(2\pi(2-t))^2\sin\pi(2-t)^2$ $-2a\pi\cos\pi(2-t)^2$

line and circle respectively. The physical dimensions for the 3−link manipulator used in the computer simulations of this research are: $l_1 = l_2 = l_3 = 1.0m$, $m_1 = m_2 = m_3 = 1.0kg$ with mass uniformly distributed on each link.

Three factors which affect the performance measure are studied in the computer simulation. These are initial state (configuration and joint rate), control scheme (velocity control or acceleration control) and external constraint (requirements in the cartesian space). In the first part of the simulation, a manipulator is driven either by velocity control or acceleration control scheme to track the specific end effector's trajectory with its initial joint rates fixed at 0. The initial posture is allowed to vary about all the possible homogeneous configurations for some specific end effector starting position; in the second part of simulation, the initial posture is fixed but the initial joint rate is allowed to change in the null-space direction.

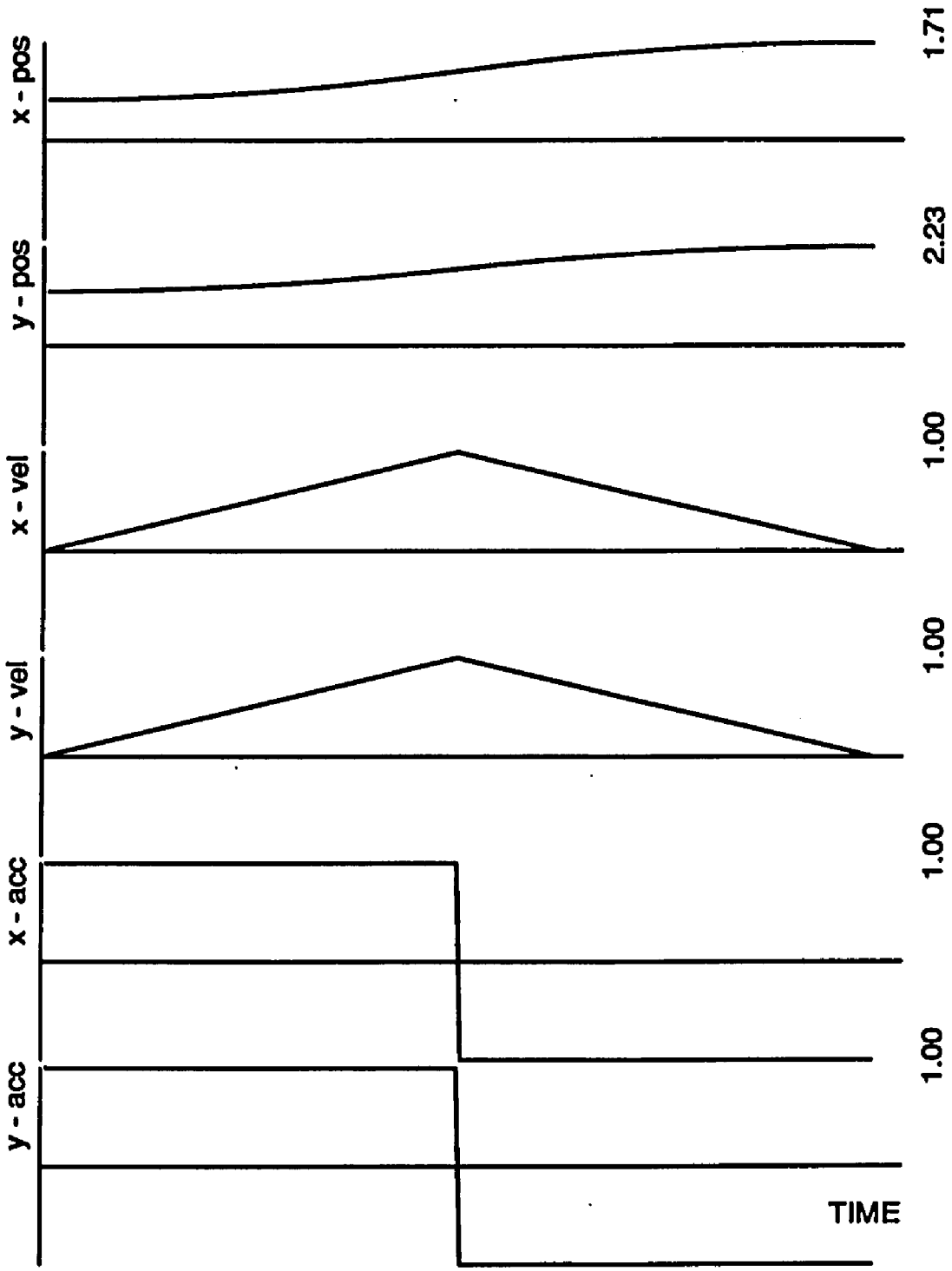

Figure 9: The cartesian space position, velocity, acceleration as functions of time for a straight line trajectory shown in Table 2 with $\alpha = 1.0$ and initial posture $(75°, -120°, 150°)$

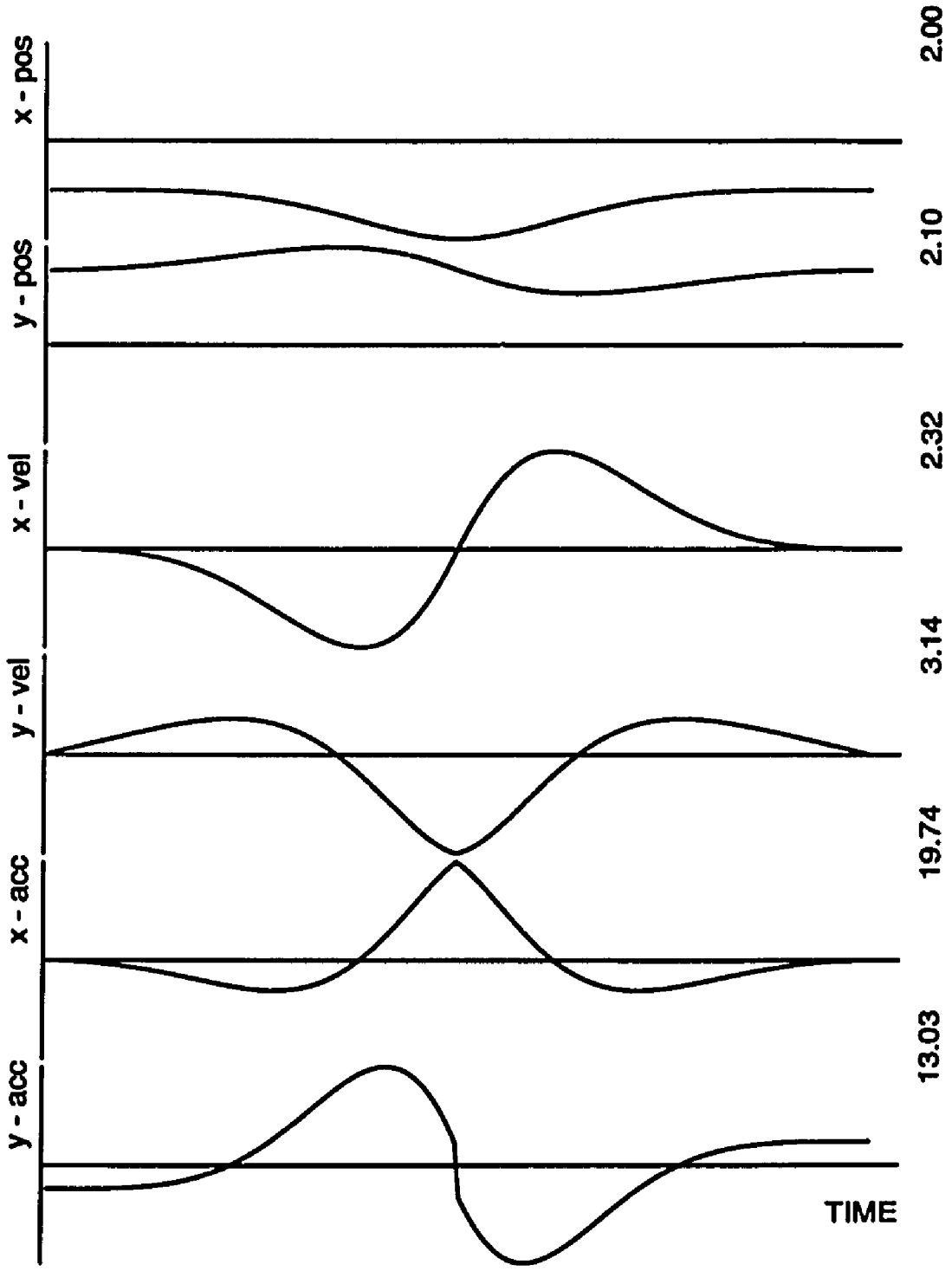

Figure 10: The cartesian space position, velocity, acceleration as functions of time for a circular trajectory shown in Table 1 with $a = 0.5$ and initial posture $(76.7°, 29.9°, 92.6°)$

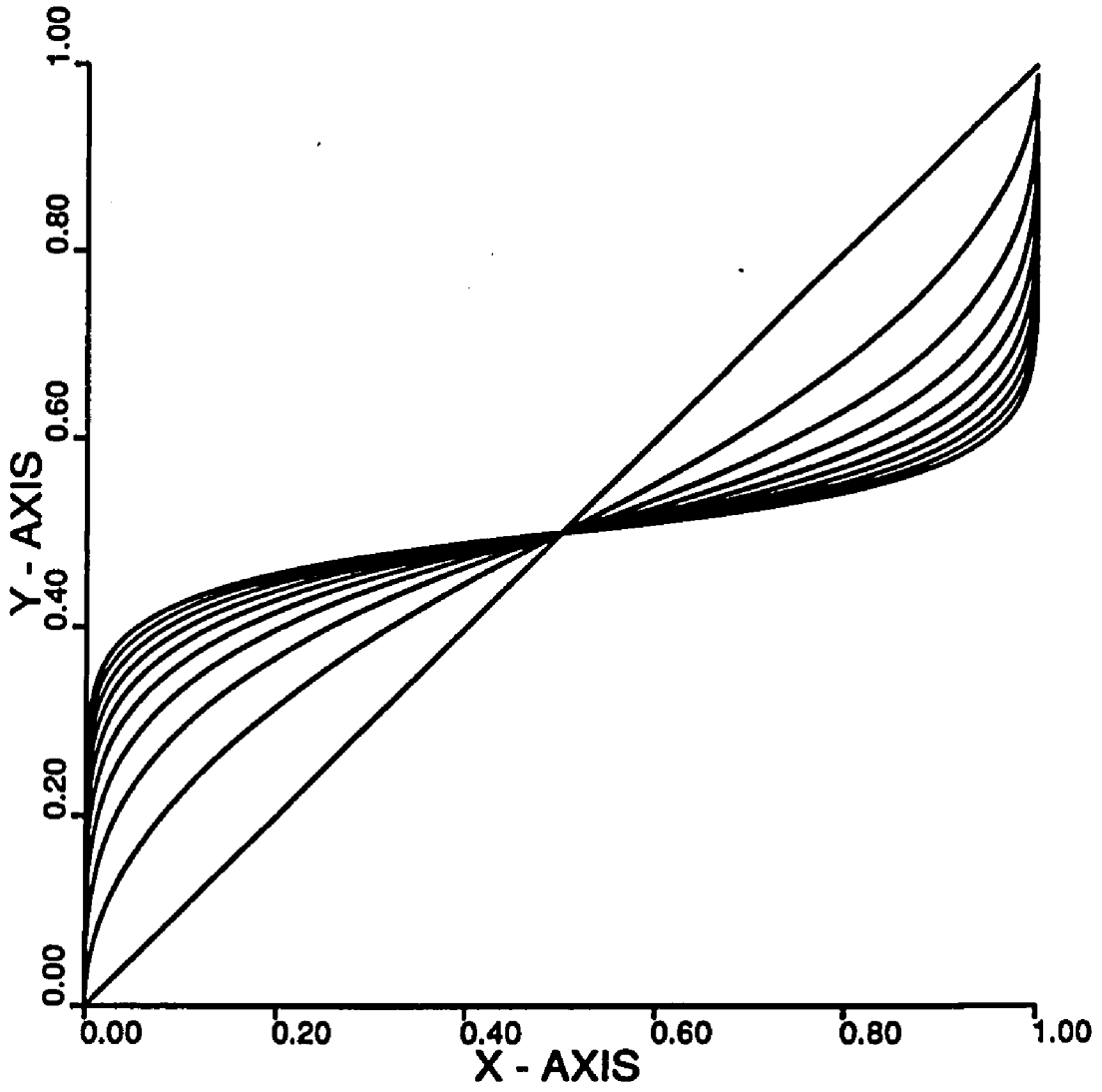

Figure 11: Trajectories of curve line ($\alpha \geq 1$) shown in Table 2 for the computer simulations

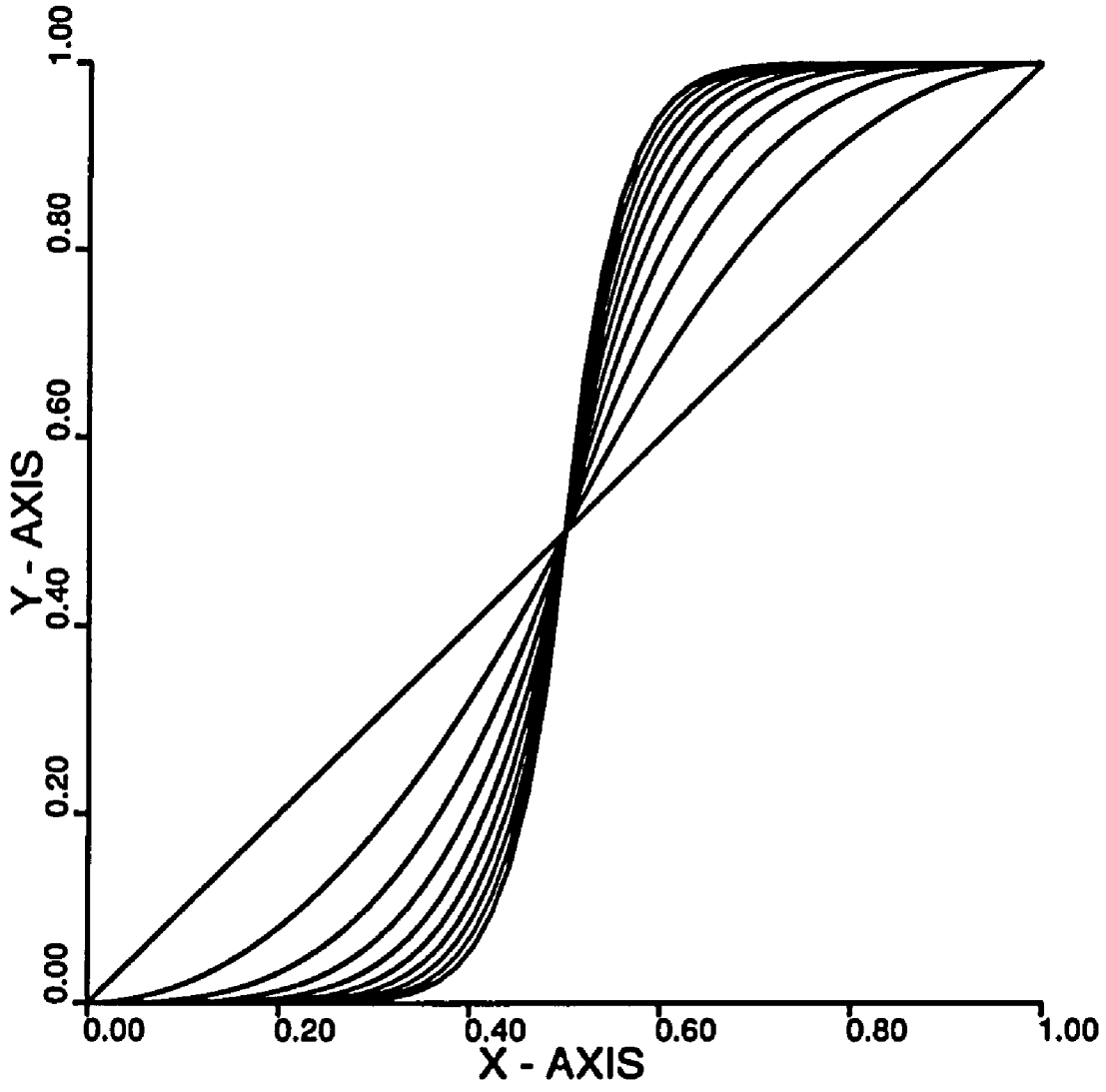

Figure 12: Trajectories of curve line ($\alpha \leq 1$) shown in Table 2 for the computer simulations

Table 2: The formulas of position, velocity and acceleration in the cartesian space for the trajectories of curve lines with parameter α

	$0 \leq t \leq 1$	$1 \leq t \leq 2$
x	$\frac{1}{2}t^2$	$\frac{1}{2}(1-t)^2$
y	$\frac{1}{2}t^{2\alpha}$	$\frac{1}{2}(1-t)^{2\alpha}$
$\dot{x}$	t	$1-t$
$\dot{y}$	$\alpha t^{2\alpha-1}$	$\alpha(1-t)^{2\alpha-1}$
$\ddot{x}$	1	-1
$\ddot{y}$	$\alpha(2\alpha-1)t^{2(\alpha-1)}$	$\alpha(2\alpha-1)(1-t)^{2(\alpha-1)}$

3.4.1 Effects of Changing Initial Posture

The cost function $I_{\dot{\theta}}$ in Eq. (3.1) was calculated over all possible initial joint angles $\theta_0 = \theta(t = t_0)$, the homogeneous surface for the same end effector position. The base of the manipulator was fixed at $x = 0, y = 0$ (the effect of changing the base location will be discussed later) and the starting position of the end effector is at point $B(-1.0, 1.6)$ as shown in Fig. 13. The task consisted of tracing the circle once counter-clockwise starting from the point B and returning back to the same point.

Fig. 14 gives the set of all the possible starting joint angles, $\theta_i(t = t_0)$, $i = 1, 2, 3$. These angles correspond to the self motion of the linkages in the joint space which keeps the base and the end effector B of the manipulator fixed. In Fig. 14, the vertical coordinate gives the possible initial postures, $\theta_i(t = t_0)$, $i = 1, 2, 3$ while the horizontal coordinate is divided into a set of 143 possible joint angles of

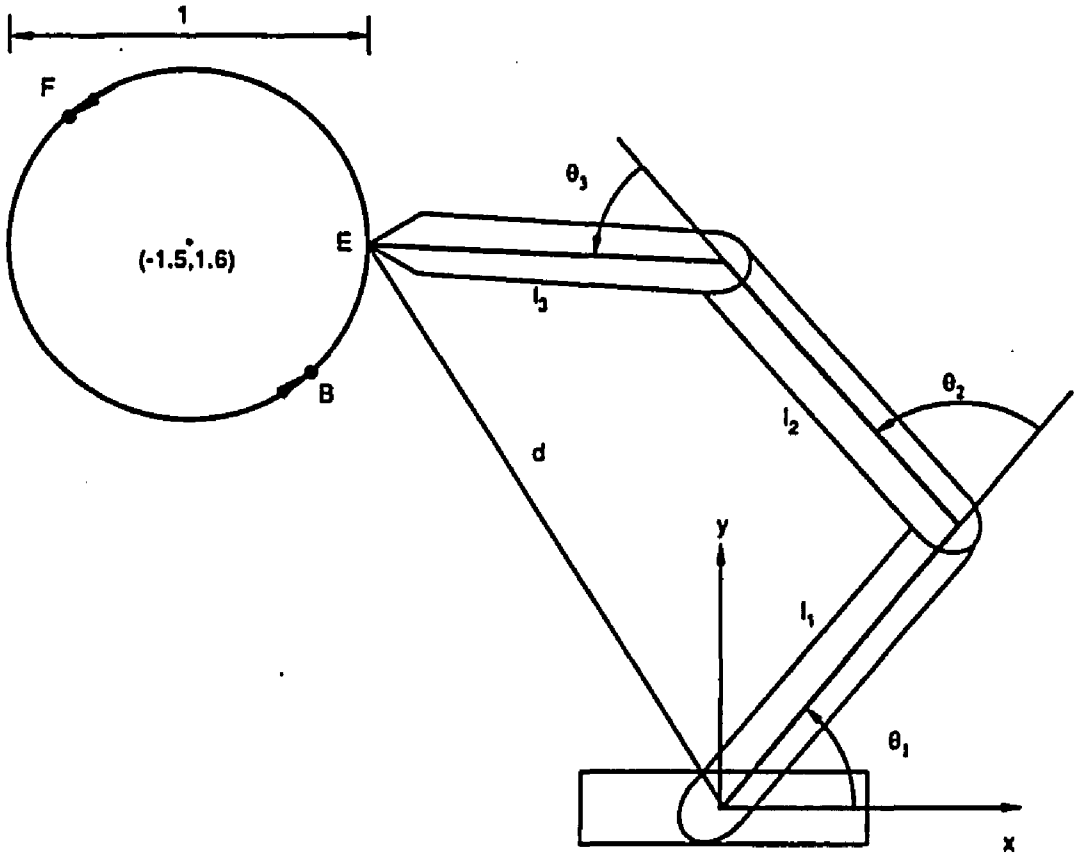

Figure 13: The 3–link manipulator and the circular task for computer simulation for comparing the velocity control and the acceleration control schemes

Table 3: Two initial configurations which are conservative and have the minimum performance measure, $I_{\dot{\theta}}$ for tracing a circular trajectory

Configuration	θ_1	θ_2	θ_3
$S_2(112)$	76.7°	29.9°	92.6°
$S_4(42)$	172.5°	−39.4°	−85.4°

$\theta_1(t = t_0)$, $\theta_2(t = t_0)$ and $\theta_3(t = t_0)$.

Fig. 15 gives the values of the cost function $I_{\dot{\theta}}$ tracing the circle, as a function of the 143 possible sets of starting angles given in Fig. 14. The two minima S_2 and S_4 in Fig. 15 correspond to the sets in Fig. 14 which have the starting values shown in Table 3.

It is seen that the starting posture has a great effect on the value of the cost function. These effects can best be visualized when viewed in the joint angle space of the manipulator. Figs. 16 and 17 are the projection of the three-dimensional joint angle space trajectories on the $\theta_1 = 0$ plane. Any point $E(x, y)$ in the two-dimensional xy plane at a distance d_1 from the origin would be uniquely represented by a three-dimensional curve $E_1(\theta_1, \theta_2, \theta_3)$ in the joint angle space. A segment $\delta\mathbf{r}$ in xy plane joining the point $E(x + \delta x, y + \delta y)$ to $E(x, y)$ would correspond to $\delta\theta$ in the joint plane jointing a point on the curve $E_1(\theta_1, \theta_2, \theta_3)$ to the curve $E_1(\theta_1 + \delta\theta_1, \theta_2 + \delta\theta_2, \theta_3 + \delta\theta_3)$. The choice of $\delta\theta$ is not unique. It depends where on $E_1(\theta)$ it starts and where on $E_1(\theta + \delta\theta)$ it ends. Although $\frac{\delta\mathbf{r}}{\delta t}$ in xy coordinate system may be small, $\frac{\delta\theta}{\delta t}$ may assume a large value.

In Figs. 16 and 17 the closed curve E_1, F_1 and B_1 correspond to the point E, F and B in Fig. 13. The closed curves E_1, F_1 and B_1 in the joint space are the homogeneous configurations that correspond to the same end effector's position

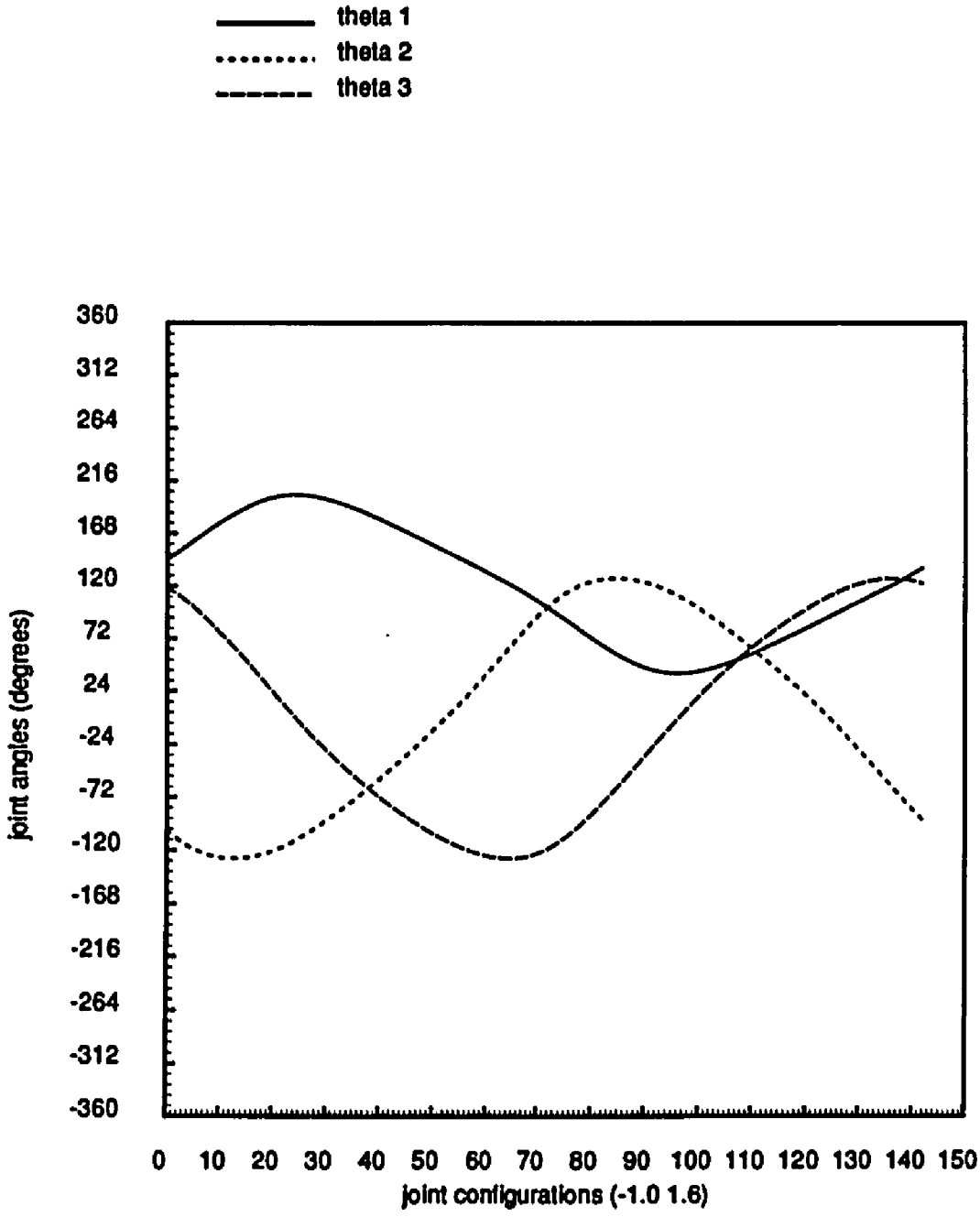

Figure 14: The joint configurations of the starting end effector's position at $(-1.0, 1.6)$ and the base located at (0.0,0.0)

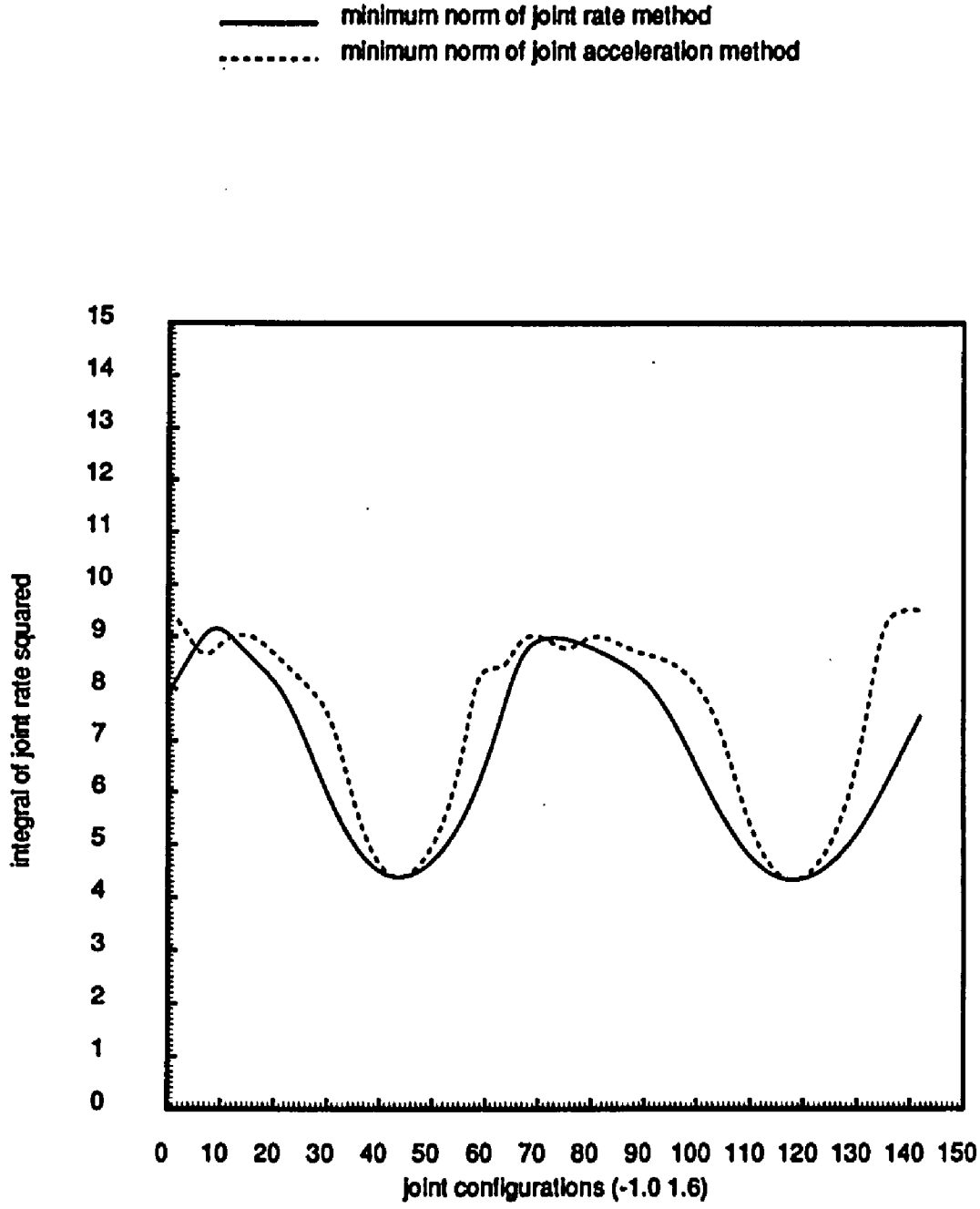

Figure 15: Performance measure $\int_{t_0}^{t_f} \dot{\theta}^T \dot{\theta} dt$ as a function of initial configurations for starting end effector's position at (-1.0 1.6) and base at (0.0 0.0) with velocity and acceleration control

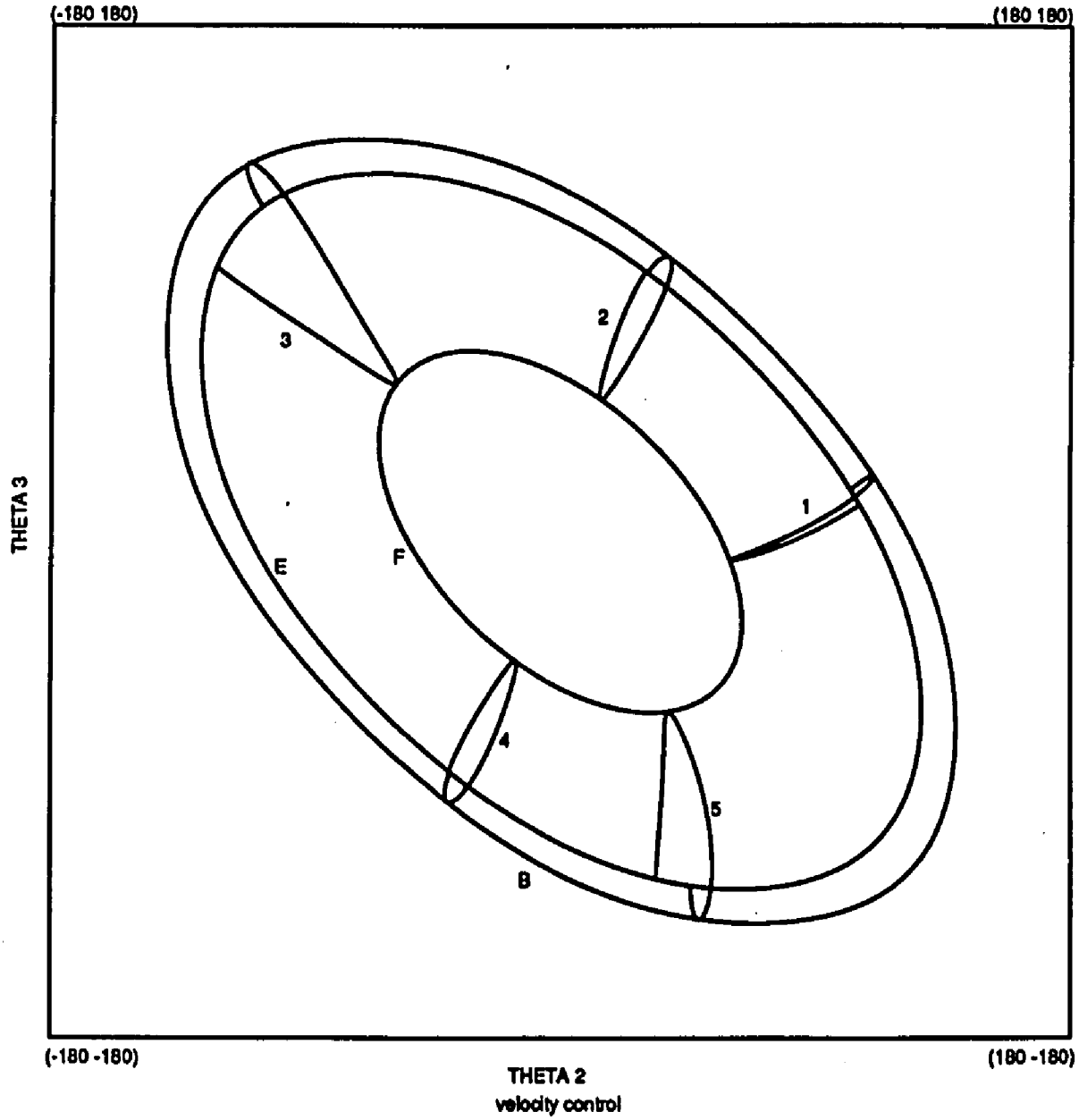

Figure 16: The projection of joint angle space curve on $\theta_1 = 0$ plane for 5 different starting postures with end effector at (-1.0 1.6) and base at (0.0 0.0) by using velocity control

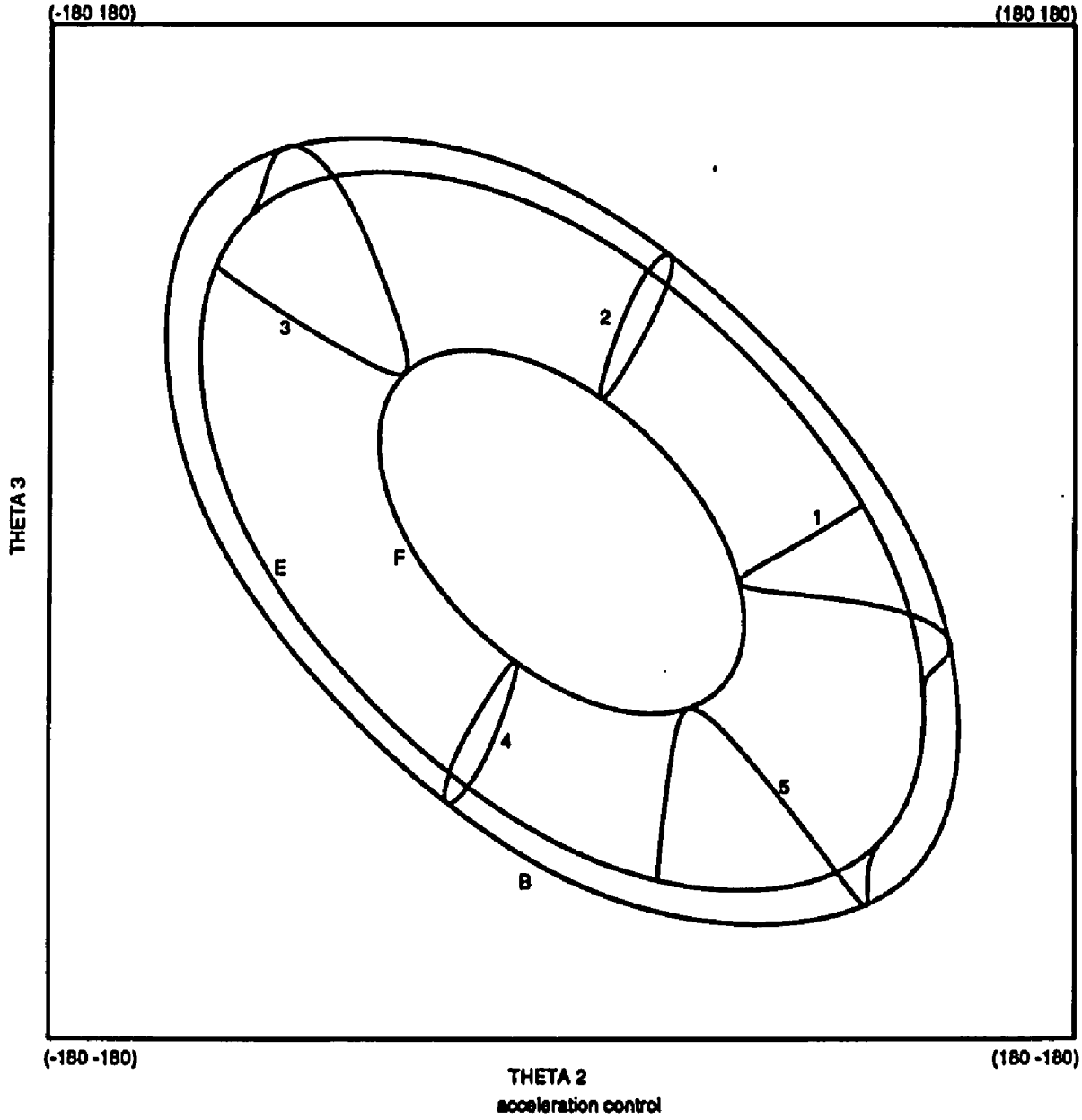

Figure 17: The projection of joint angle space curve on $\theta_1 = 0$ plane for 5 different starting postures with end effector at (-1.0 1.6) and base at (0.0 0.0) by using acceleration control

Table 4: Three other initial configurations which are non-conservative for tracing a circular trajectory.

Configuration	θ_1	θ_2	θ_3
$S_1(96)$	40.8°	105.8°	9.9°
$S_3(8)$	166.2°	−122.2°	94.2°
$S_5(60)$	135.4°	34.1°	−123.8°

(x, y) in the cartesian coordinates. In particular, the closed curve B_1 in Figs. 16 and 17 corresponds to the starting position of point B given in Fig. 13.

The path followed by the end effector in the joint space tracing the unit circle in the x-y plane starting from point B are shown in Figs. 16 and 17 by the numbered curves $1, 2, 3, 4$, and 5. The curves S_1, S_3, and S_5 have the starting postures shown in Table 4.

It can be seen for the two starting postures, S_2 and S_4, the path in the joint space is closed and the manipulator returns back to its starting configuration with no drift. On the other hand, there is drift for the starting postures S_1, S_3 and S_5, and the path is not closed. Figs. 18 and 20 give the values of θ_1, θ_2, and θ_3 as a function of time $(t_0 \leq t \leq t_f)$ and the manipulator geometry for the two starting configurations S_2 and S_1.

Now consider the resolution of the redundancy at the acceleration level. Once again the cost function $I_{\dot{\theta}}$ is calculated over all the 143 possible initial postures in the homogeneous joint space as shown in Fig. 14, except the redundancy was resolved at the acceleration level using the joint space acceleration equation

$$\ddot{\theta} = J^{+}(\ddot{x} - \dot{J}\dot{\theta}). \tag{3.18}$$

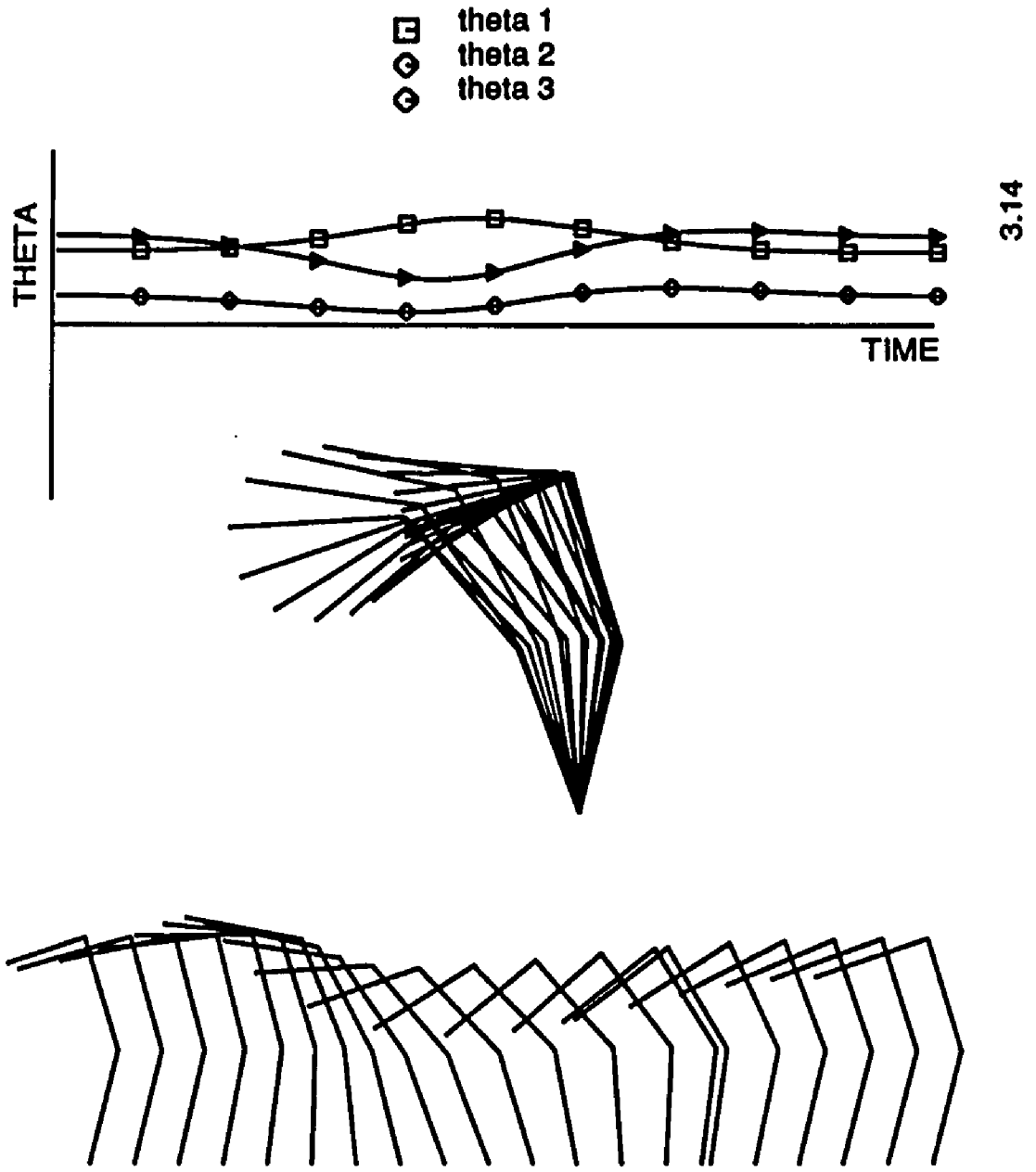

Figure 18: The joint angles and the manipulator geometry as a function of time, tracing a circle ($a = 0.5$) with the starting posture (S_2) which is conservative for velocity control

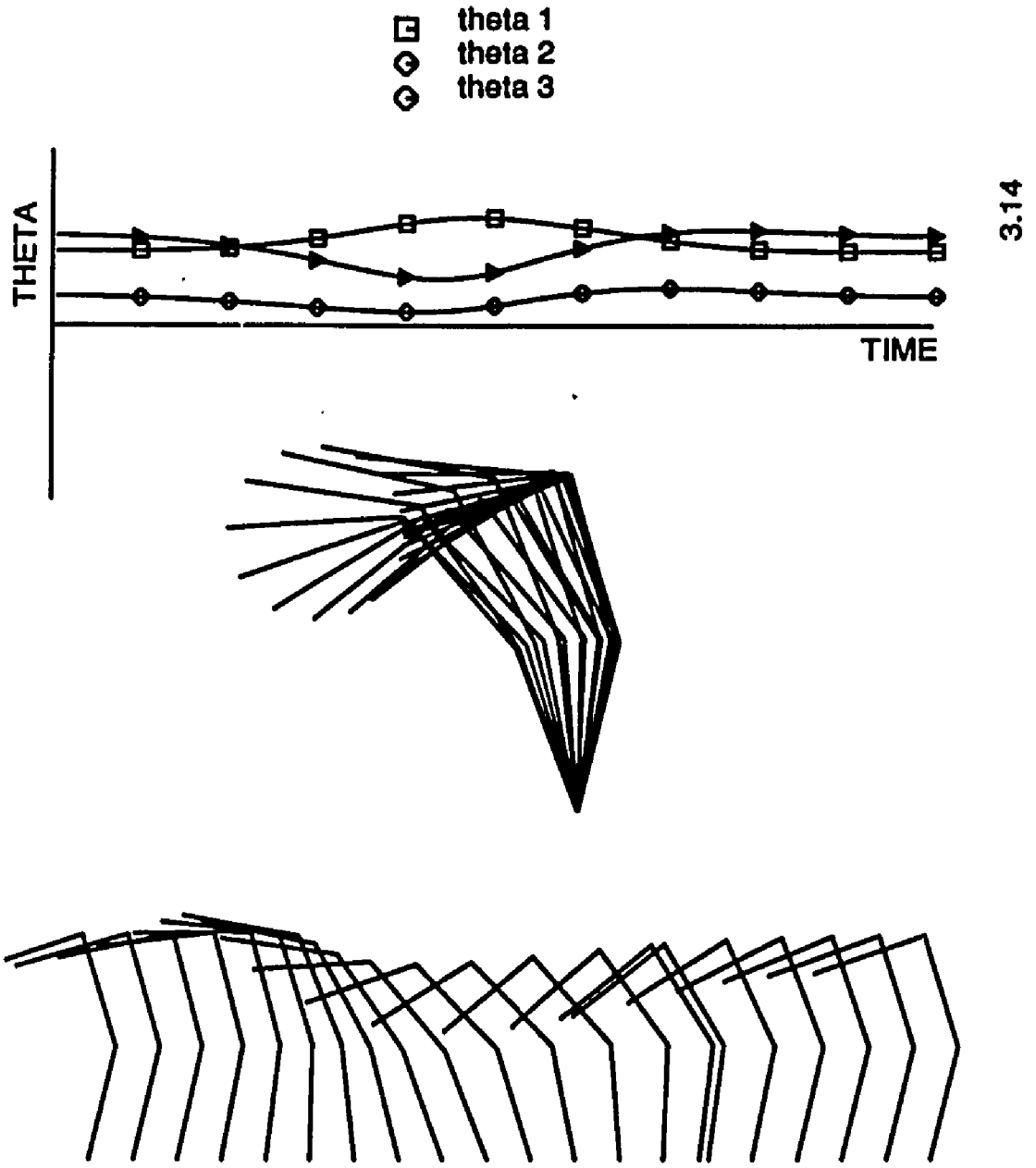

Figure 19: The joint angles and the manipulator geometry as a function of time, tracing a circle ($a = 0.5$) with the starting posture (S_2) which is conservative for acceleration control

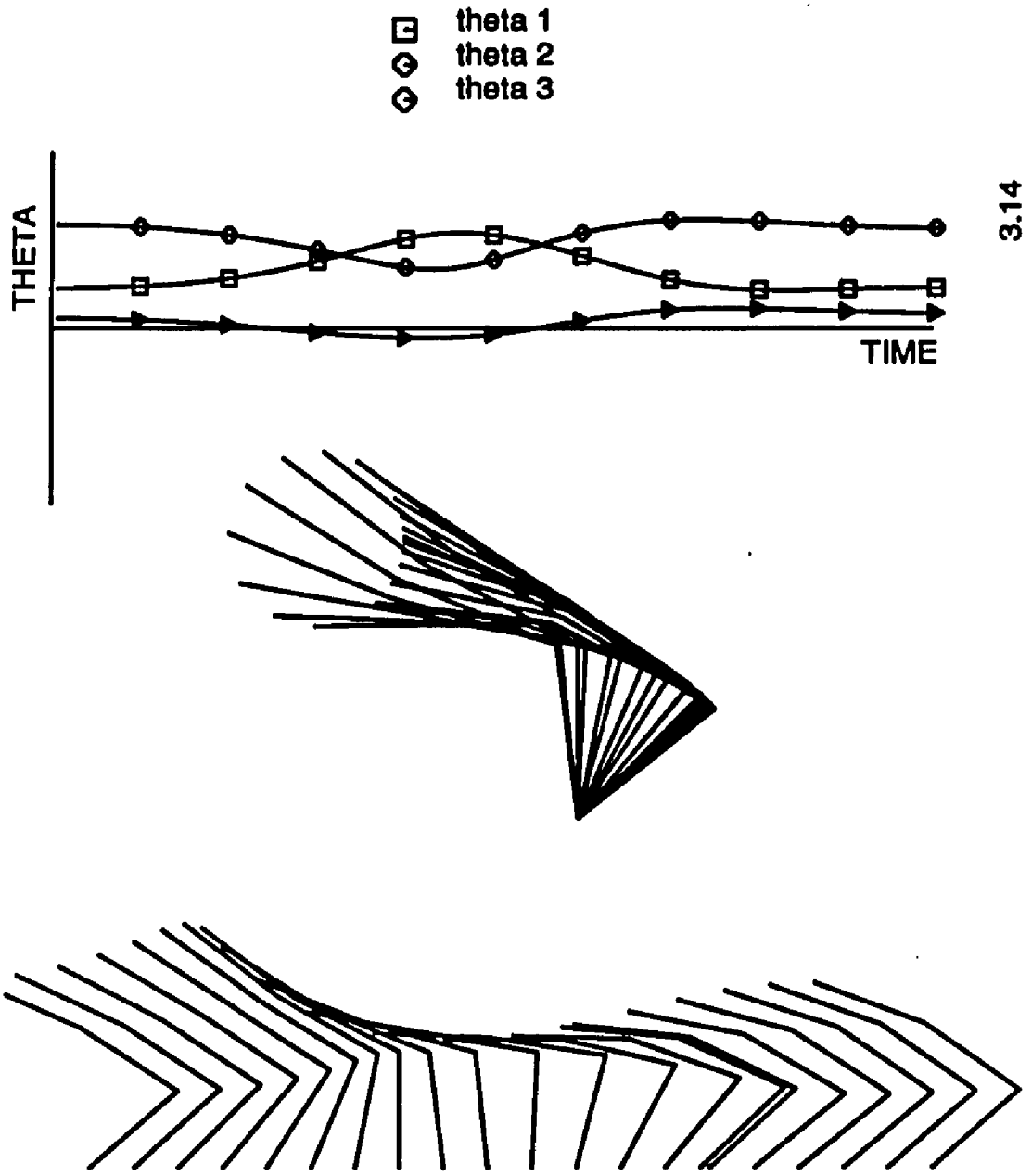

Figure 20: The joint angles and the manipulator geometry as a function of time, tracing a circle ($a = 0.5$) with the starting posture (S_1) which is not conservative for velocity control

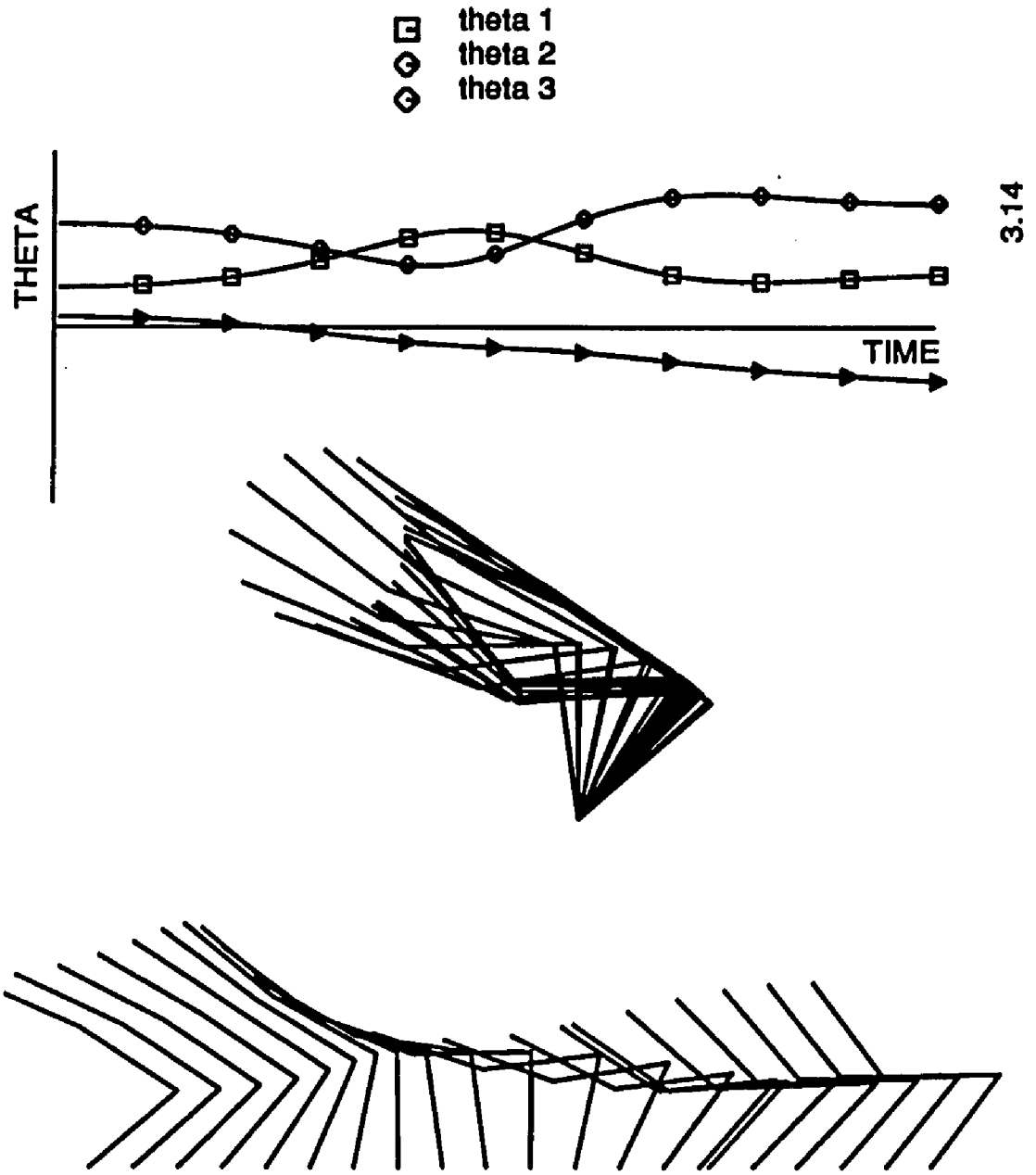

Figure 21: The joint angles and the manipulator geometry as a function of time, tracing a circle ($a = 0.5$) with the starting posture (S_1) which is not conservative for acceleration control

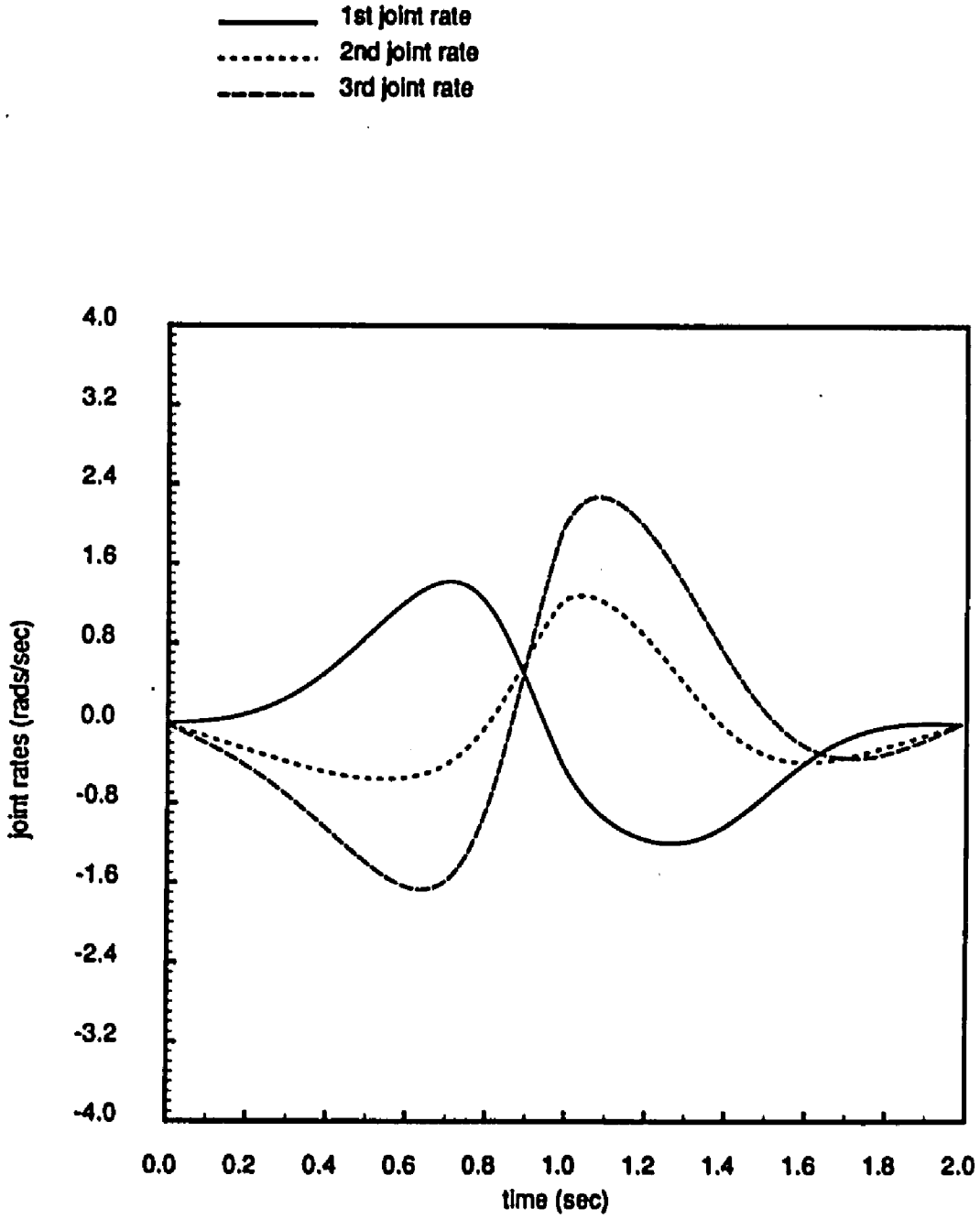

Figure 22: The joint rates as a function of time for the starting posture (S_2) which is conservative for acceleration control

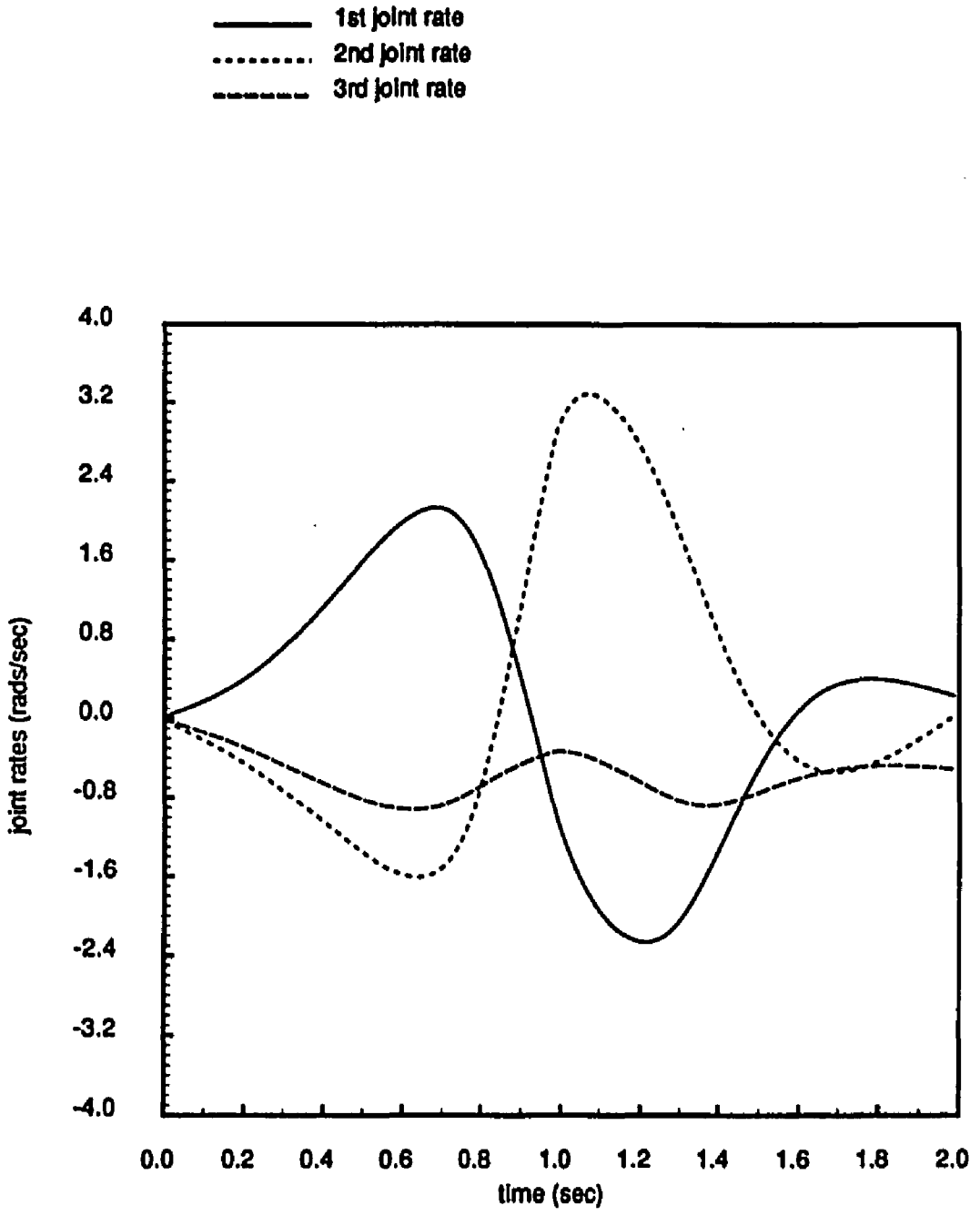

Figure 23: The joint rates as a function of time for the starting posture (S_1) which is not conservative for acceleration control

The values of $I_{\dot{\theta}}$ for acceleration control are superimposed on the same figure Fig. 15 for comparison. It is noted that there are two minima and these minima occur almost at the same starting postures, S_2 and S_4. Figs. 19 and 21 give the joint angles $\theta_i, i = 1,2,3$ and the manipulator geometries as functions of time for two initial postures, S_2 and S_1. Figs. 22 and 23 give their corresponding joint rates $\dot{\theta}_i, i = 1,2,3$. For paths with initial postures S_2 and S_4 the three joint angle rates $\dot{\theta}_1, \dot{\theta}_2$, and $\dot{\theta}_3$ are zero at $t = t_0$ and $t = t_f$, while for the paths S_1, S_3 and S_5 $\dot{\theta}_i = 0$ at $t = t_0$, but at $t = t_f$ $\dot{\theta}_i \neq 0$.

It is noticed that the paths of S_1, S_3 and S_5 that are generated by minimum norm of joint acceleration control strategy differ from the corresponding paths of Fig. 18 which result from the minimum norm of joint rate method. While the paths S_2 and S_4 corresponding to the local minima of the performance measure, $I_{\dot{\theta}}$ are the same for both methods.

3.4.2 Effects of Changing Initial Joint Rate

The initial joint rates in the null space have similar effects on the performance measures as the initial configurations do. Different joint angle space trajectories as well as the performance measures are obtained by starting with different initial joint rates along the null-space vector direction. Therefore, for a given initial posture, proper initial joint rate in the null space can be searched for achieving some specific goal.

The computer simulation results for applying minimum norm of joint acceleration control to trace a circular trajectory with the manipulator's base located at (0.0 0.0), the initial posture, $(172.5°, -39.4°, -85.4°)$, fixed, and 8 different initial joint rates as shown in Table 5. In this table, it gives the performance measures $I_{\dot{\theta}} = \int_{t_0}^{t_f} \dot{\theta}^T \dot{\theta} dt$, $I_{\ddot{\theta}} = \int_{t_0}^{t_f} \ddot{\theta}^T \ddot{\theta} dt$ and $I_\tau = \int_{t_0}^{t_f} \tau^T \tau dt$ for the 8 corresponding initial

Table 5: The cost functions for different initial joint rate with initial posture $(172.5°, -39.4°, -85.4°)$ and base located at (0.0 0.0) to trace a circular trajectory with acceleration control

Trajectory	Initial $\dot{\theta}$			Cost functions		
	$\dot{\theta}_{1_0}$	$\dot{\theta}_{2_0}$	$\dot{\theta}_{3_0}$	$\int_{t_0}^{tf} \dot{\theta}^T \dot{\theta} dt$	$\int_{t_0}^{tf} \ddot{\theta}^T \ddot{\theta} dt$	$\int_{t_0}^{tf} \tau^T \tau dt$
1	0.732	-1.335	1.069	13.78	141.24	396.92
2	0.488	-0.890	0.713	10.72	177.39	861.48
3	0.244	-0.445	0.356	6.621	140.24	1148.85
4	0.0	0.0	0.0	4.392	130.98	1420.16
5	-0.244	0.445	-0.356	6.301	138.93	1395.64
6	-0.488	0.890	-0.713	10.870	154.96	679.71
7	-0.732	1.335	-1.069	13.942	80.99	305.41
8	-0.976	1.780	-1.426	44.287	407.45	500.70

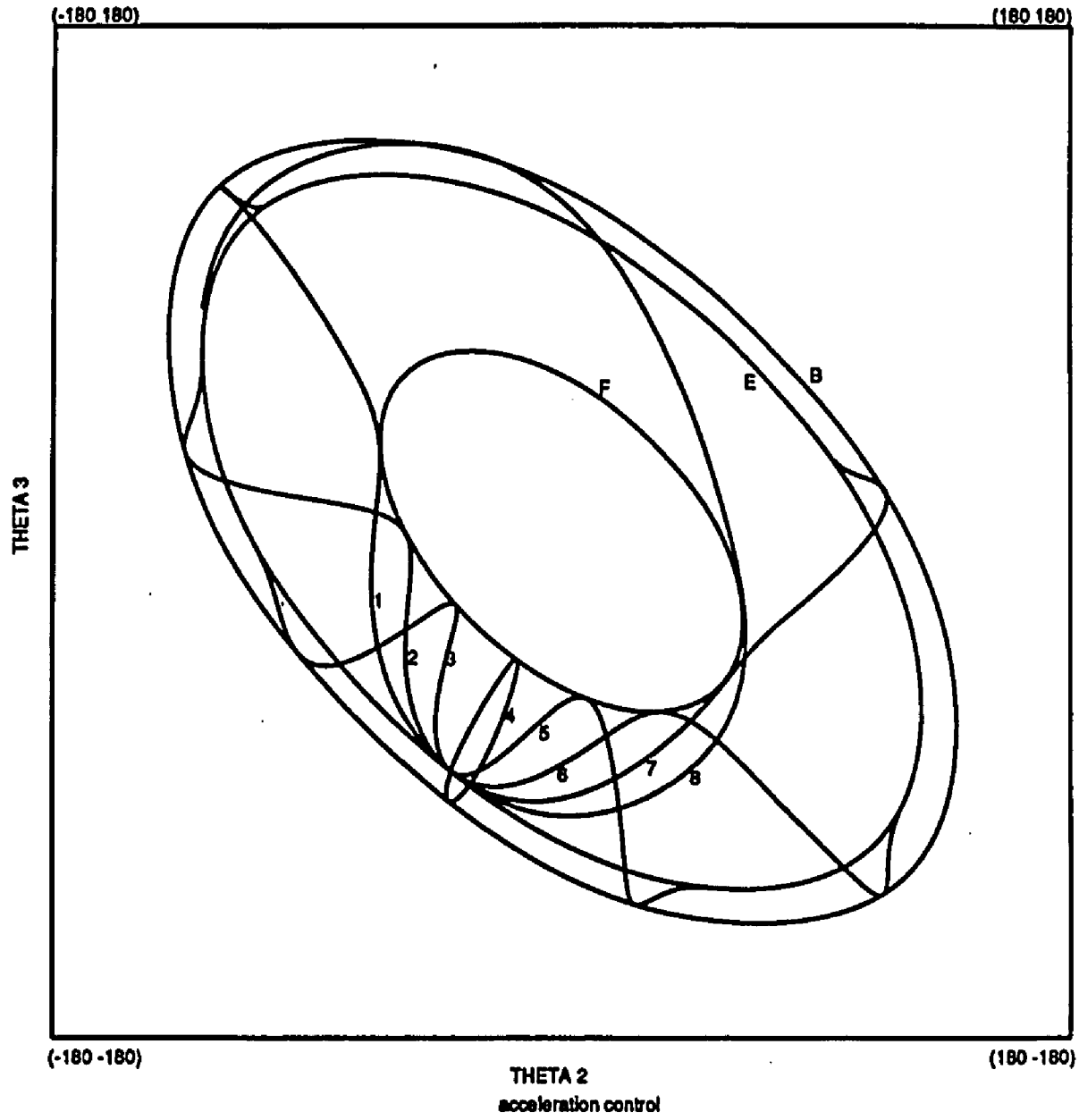

Figure 24: The projections of joint angle space curves on $\theta_1 = 0$ plane for 8 different initial joint rates as shown in Table 5 having the same initial posture $(172.5°, -39.4°, -85.4°)$ to trace a circular trajectory with acceleration control

Table 6: The required initial joint rates for achieving minimum drift for 5 different initial postures

Trajectory	Initial θ			Initial joint rate		
	θ_{1_0}	θ_{2_0}	θ_{3_0}	$\dot{\theta}_{1_0}$	$\dot{\theta}_{2_0}$	$\dot{\theta}_{3_0}$
S_1	40.8°	105.8°	9.9°	0.035	−0.215	0.373
S_2	76.7°	30.0°	92.7°	0.0	0.0	0.0
S_3	166.2°	−122.2°	94.2°	0.136	−0.072	−0.179
S_4	172.5°	−39.4°	−85.4°	0.0	0.0	0.0
S_5	135.4°	34.1°	−123.8°	0.190	−0.419	0.101

joint rates. Fig. 24 gives the projections of joint-angle space curves on the plane spanned by the coordinates θ_2 and θ_3. Fig. 24 and Table 5 show the effects of initial joint rates on the joint-angle space trajectories and performance measures. It is seen that proper initial joint rates are effective for achieving a better performance measure.

Fig. 25 gives the projections of the joint-angle space trajectories on the $\theta_1 = 0$ plane for 5 initial postures with the initial joint rate shown in Table 6. This figure shows that the proper initial joint rates as well as initial postures can be chosen to achieve minimum drift (zero) in the joint angle space. Table 6 gives the corresponding initial joint rates in the null space for 5 different initial postures required to achieve zero drift in joint-angle space for tracing a circular trajectory. The joint acceleration, $\ddot{\theta}$ which equals $J^{+}(\ddot{\mathbf{x}} - \dot{J}\dot{\theta})$ is the controlled variable in the acceleration control method. It depends on the present state $(\theta, \dot{\theta})$, the null-space components in the joint-acceleration space $(\ddot{\phi})$ and the cartesian space trajectory $(\ddot{\mathbf{x}})$. For a given trajectory, both the configuration (θ) and the joint rate $(\dot{\theta})$ are

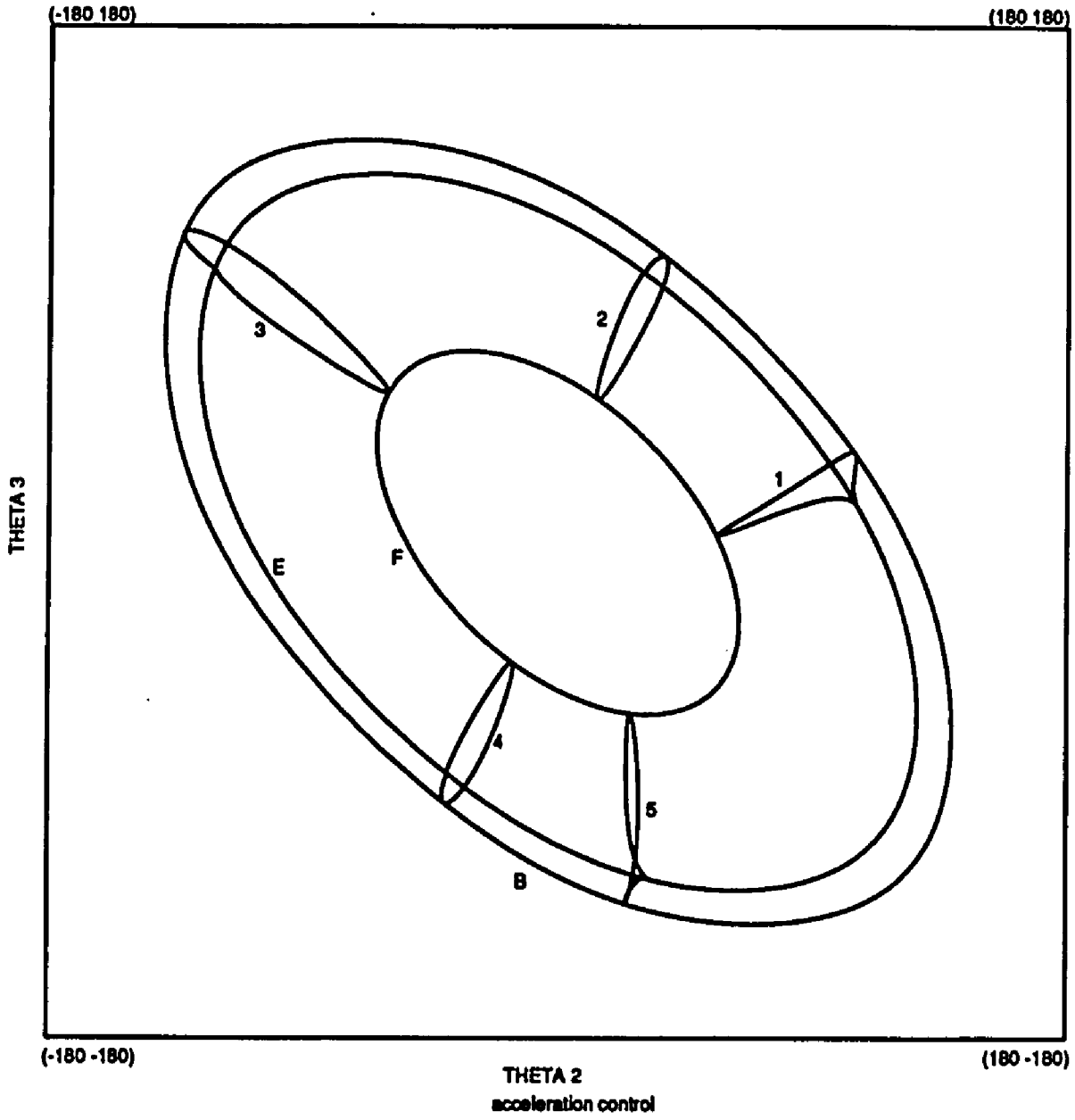

Figure 25: The projection of joint-angle space curve on $\theta_1 = 0$ plane for 5 different initial postures with proper initial joint rate as shown in Table 6 to achieve minimum drift for the acceleration control

effective for determining the next state. This gives the manipulator freedom to choose a proper initial state $(\theta, \dot{\theta})$ for starting a job and achieving some secondary goal.

On the other hand, the joint rate, $\dot{\theta}$, which equals $J^{+}\dot{x}$ is the controlled variable in the velocity control algorithm. It depends on the present configuration (θ), the null-space component in the joint-velocity space $(\dot{\theta})$ and the cartesian velocity $(\dot{x})$. The current joint rate does not affect the determination of the next state. Therefore, only the initial configuration (θ) can be chosen to optimize the specific objective function. In summary, the objective functions can be optimized by searching over the initial state $(\theta, \dot{\theta})$ if joint acceleration control is applied, while for velocity control method only initial configurations can be searched.

3.4.3 Effects of Changing Base Location

The effects on the performance measures by changing the base location are studied in this section. A 3-link planar manipulator and the minimum norm joint acceleration control strategy were used in the computer simulation to trace a straight line at 45° with constant acceleration in the first half of the path and constant deceleration in the second half. Tables 7 to 9 give the performance measures for different initial postures with the base of the manipulator located at 3 different positions. The data in these tables show that a proper base location is an important factor for redundant manipulators to achieve a good performance measure.

Figs. 29 to 31 give the performance measure, $I_{\dot{\theta}}$ as a function of initial postures for 3 different base locations. These figures show that proper choice of the base location is important for the manipulator to perform a task and can be searched to improve the performance.

Table 7: The cost functions for different initial posture with end effector and base positions at (-1.0,2.0) and (1.07,0.46) respectively for a straight line trajectory and minimum norm of joint acceleration control

Trajectory	Initial θ			Cost functions		
	θ_{1_0}	θ_{2_0}	θ_{3_0}	$\int_{t_0}^{tf} \dot{\theta}^T \dot{\theta} dt$	$\int_{t_0}^{tf} \ddot{\theta}^T \ddot{\theta} dt$	$\int_{t_0}^{tf} \tau^T \tau dt$
1	184.0	-75.4	29.87	0.50	2.11	33.6
2	168.0	-8.2	-61.3	0.35	1.39	52.9
3	127.0	60.9	-69.8	0.33	1.73	36.9
4	105.5	37.4	38.5	0.18	0.96	36.6

Table 8: The cost functions for different initial posture with end effector and base positions at(-1.0,2.0) and (0.0,0.0) respectively for a straight line trajectory and minimum norm of joint acceleration control

Trajectory	Initial θ			Cost functions		
	θ_{1_0}	θ_{2_0}	θ_{3_0}	$\int_{t_0}^{tf} \dot{\theta}^T \dot{\theta} dt$	$\int_{t_0}^{tf} \ddot{\theta}^T \ddot{\theta} dt$	$\int_{t_0}^{tf} \tau^T \tau dt$
1	-161.8	-123.8	34.3	1.51	4.81	23.28
2	155.0	-6.6	-107.7	0.82	2.60	50.14
3	86.7	116.3	-105.2	1.09	3.76	22.57
4	56.4	67.4	59.9	0.35	1.46	17.28

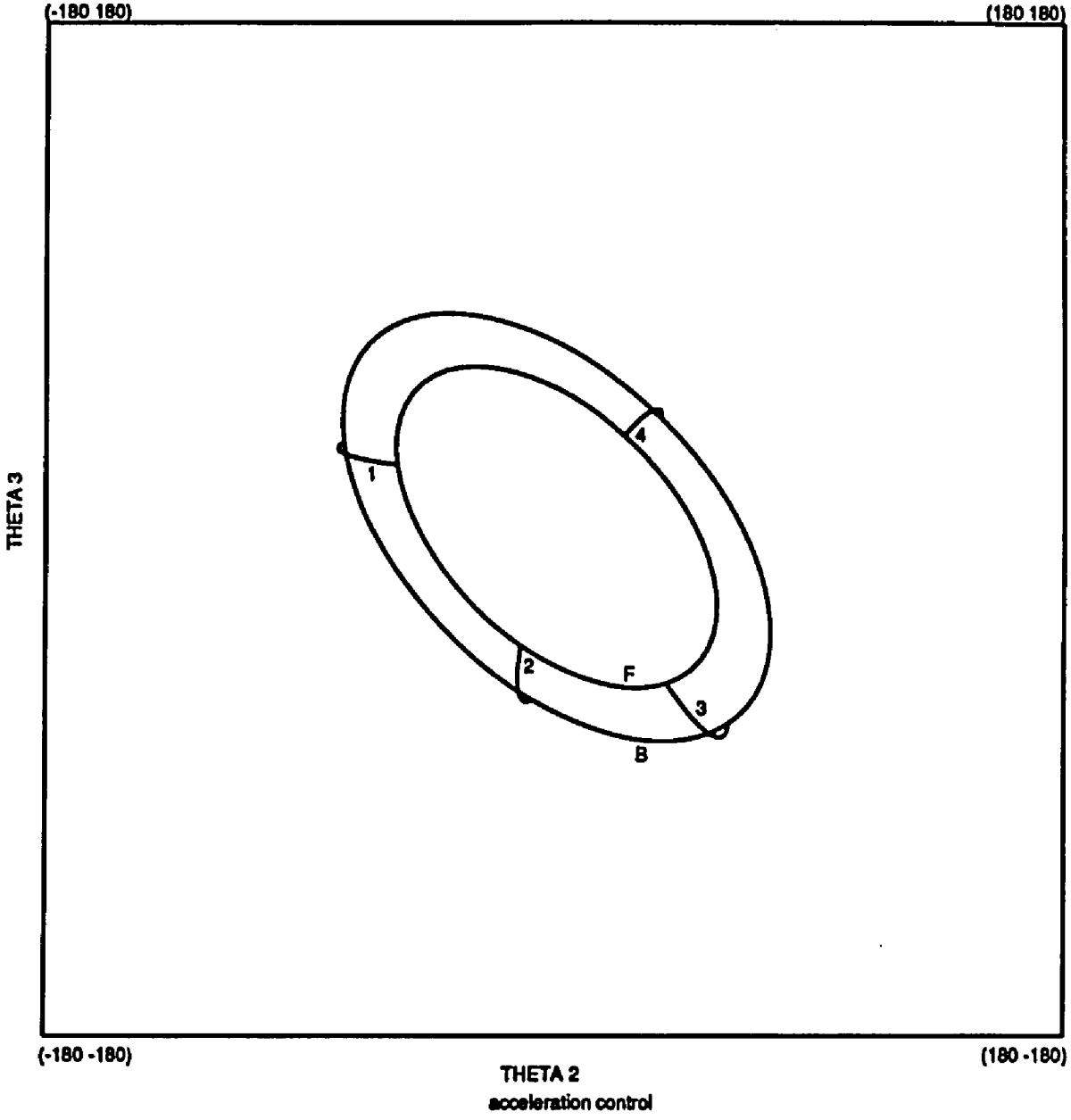

Figure 26: The projection of joint-angle space curve on $\theta_1 = 0$ plane for 4 different initial postures with the base located at (1.07,0.46) and end effector position at (-1.0, 2.0) corresponding to trajectories in Table 7 which trace a straight line trajectory with acceleration control

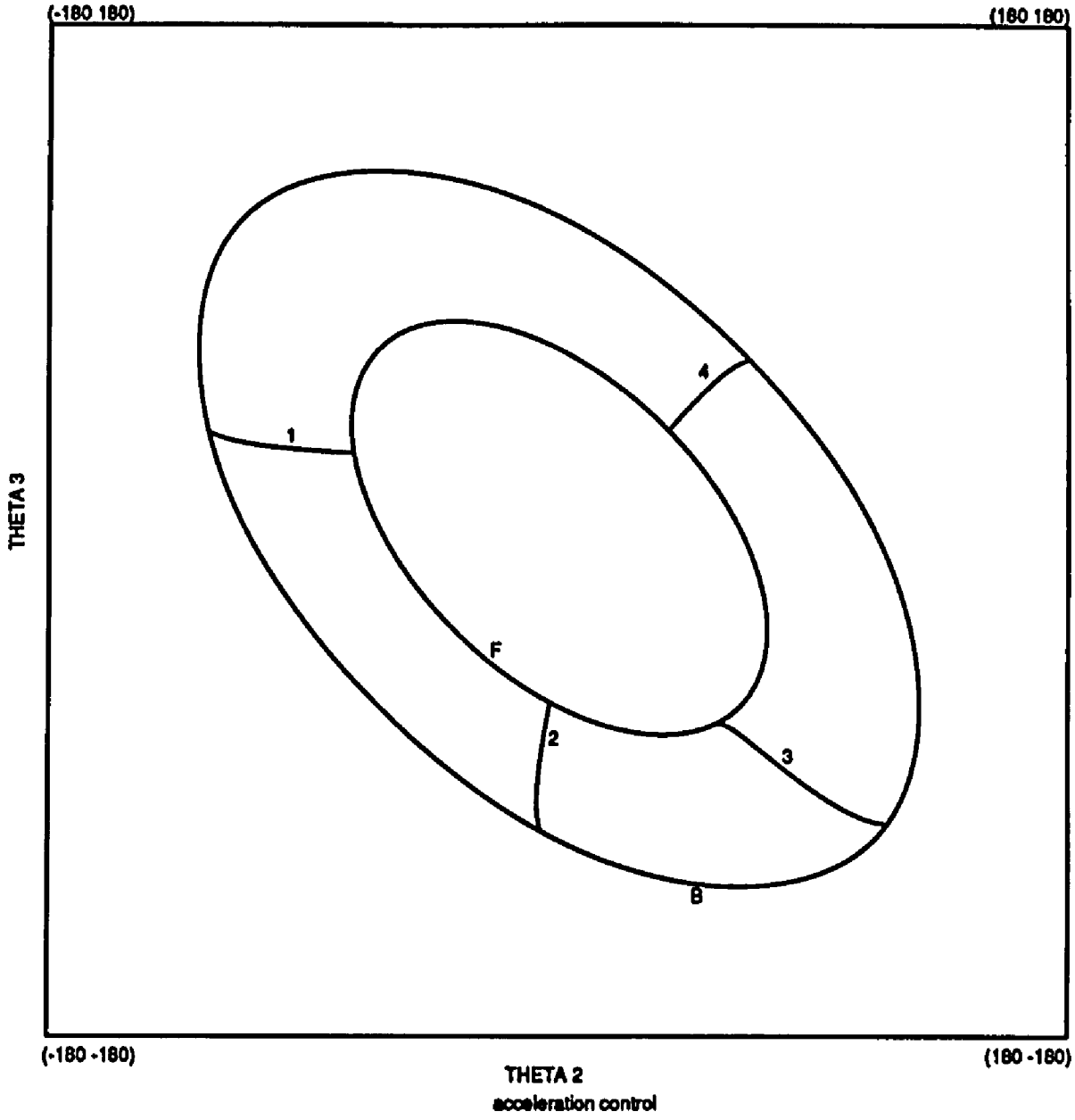

Figure 27: The projection of joint-angle space curve on $\theta_1 = 0$ plane for 4 different initial postures with the base located at (0.0,0.0) and end effector position at (-1.0, 2.0) corresponding to trajectories in Table 8 which trace a straight line trajectory with acceleration control

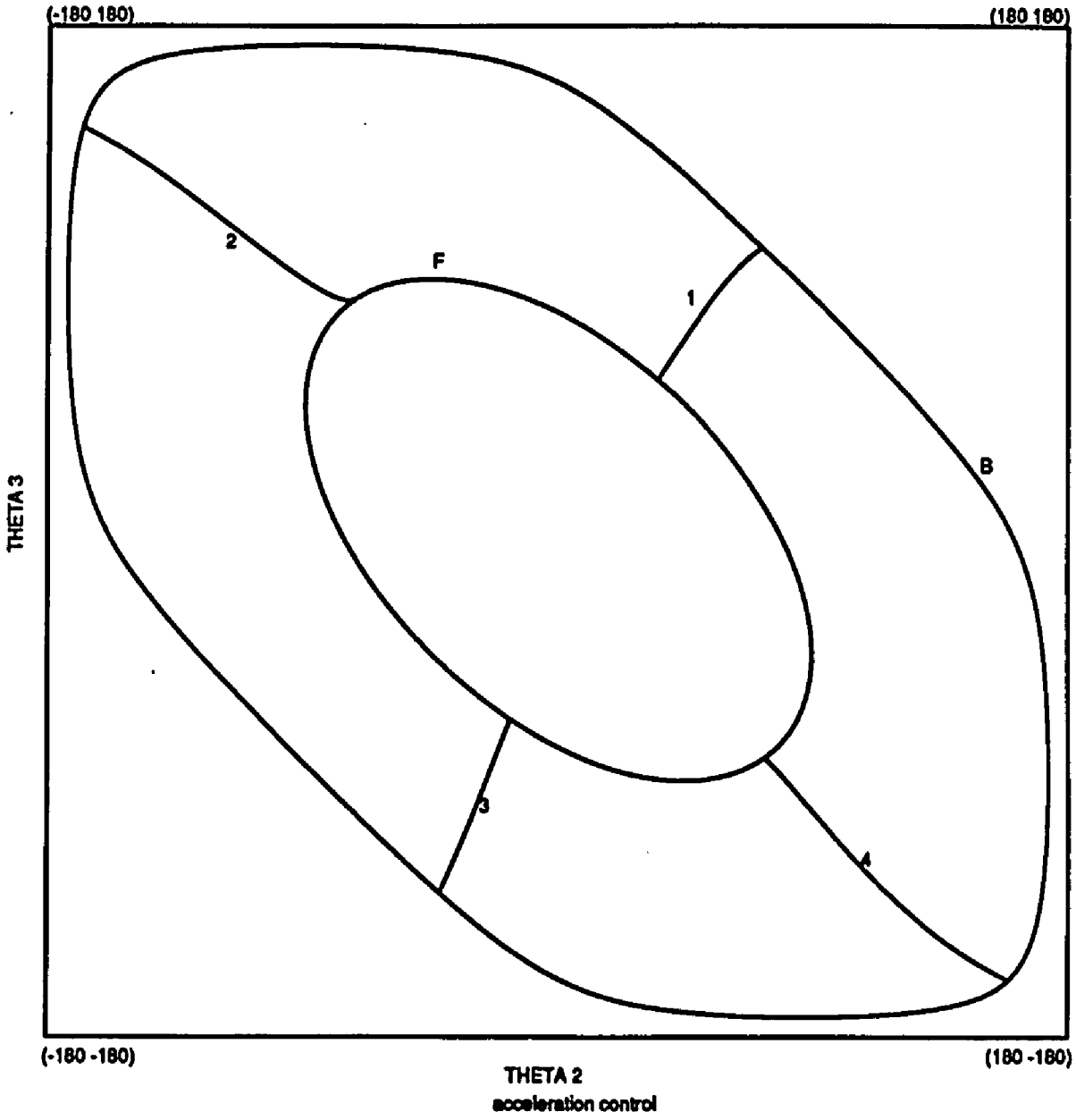

Figure 28: The projection of joint-angle space curve on $\theta_1 = 0$ plane for 4 different initial postures with the base located at (-0.8,0.9) and end effector position at (-1.0, 2.0) corresponding to trajectories in Table 9 which trace a straight line trajectory with acceleration control

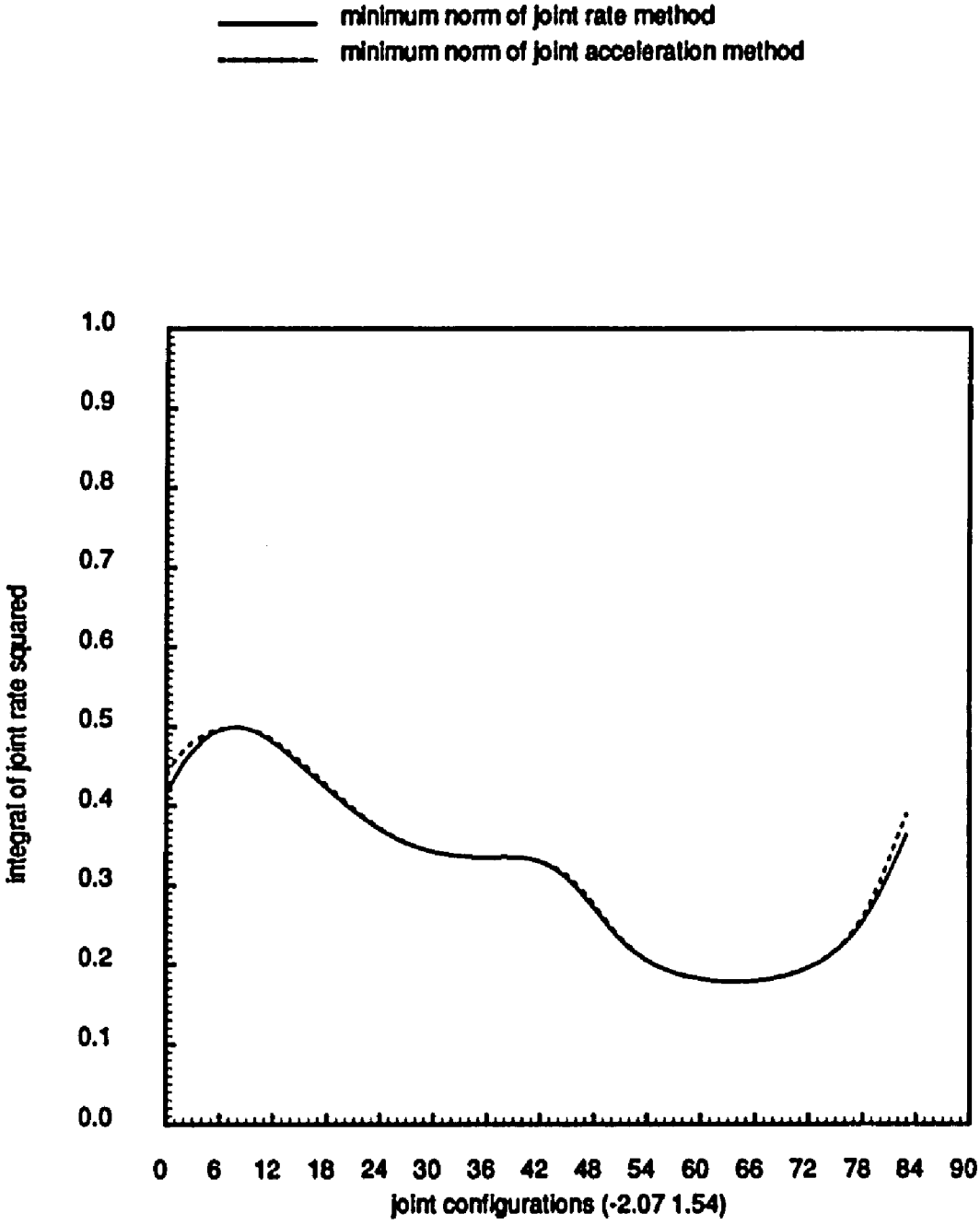

Figure 29: The plot of performance measure $I_{\dot{\theta}}$ among possible configurations for base located at (1.07,0.46) and end effector position at (-1.0, 2.0) corresponding to trajectories in Table 7 which trace a straight line trajectory for both velocity and acceleration control

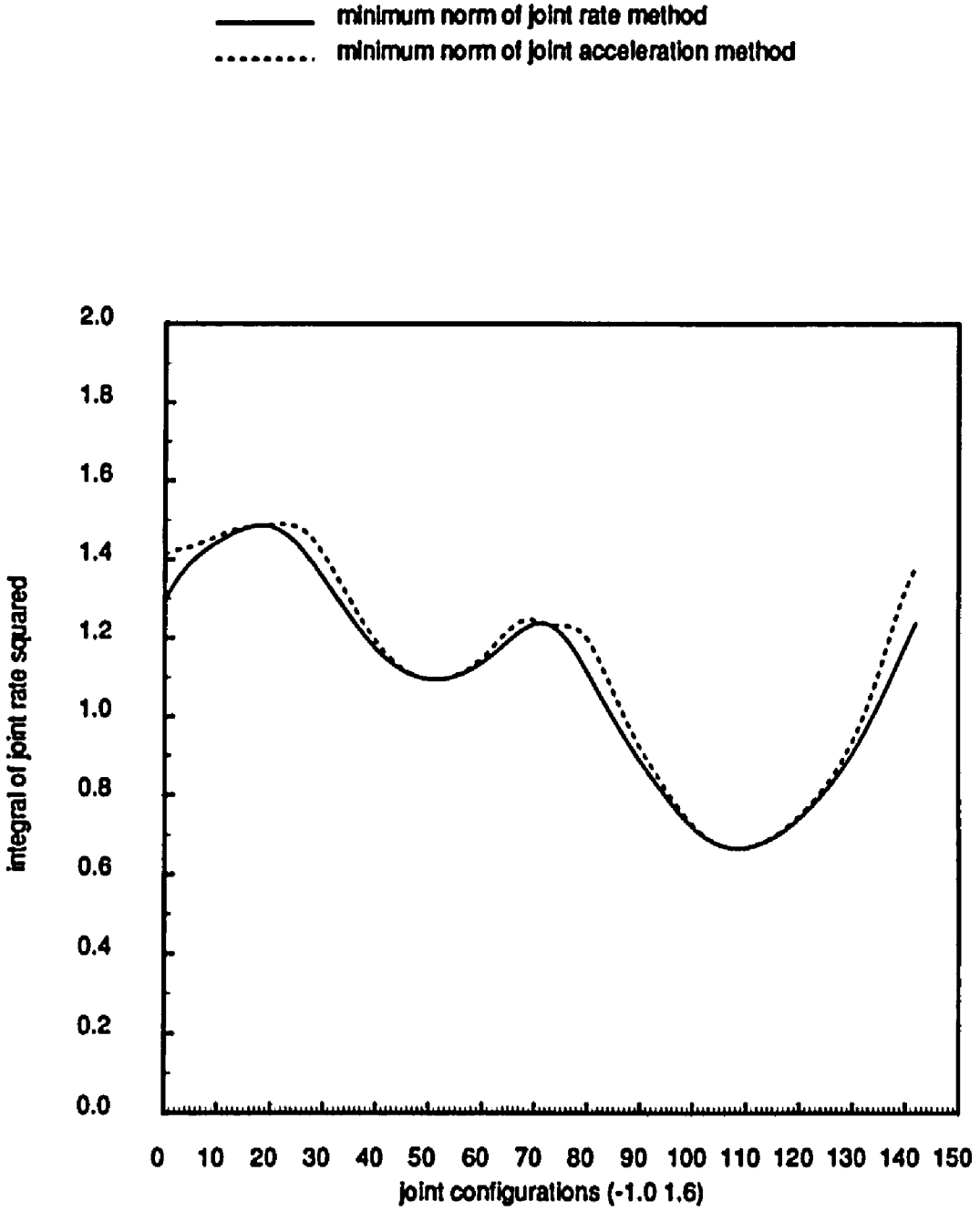

Figure 30: The plot of performance measure $I_{\dot{\theta}}$ among possible configurations for base located at (0.0,0.4) and end effector position at (-1.0, 2.0) corresponding to trajectories in Table 8 which trace a straight line trajectory for both velocity and acceleration control

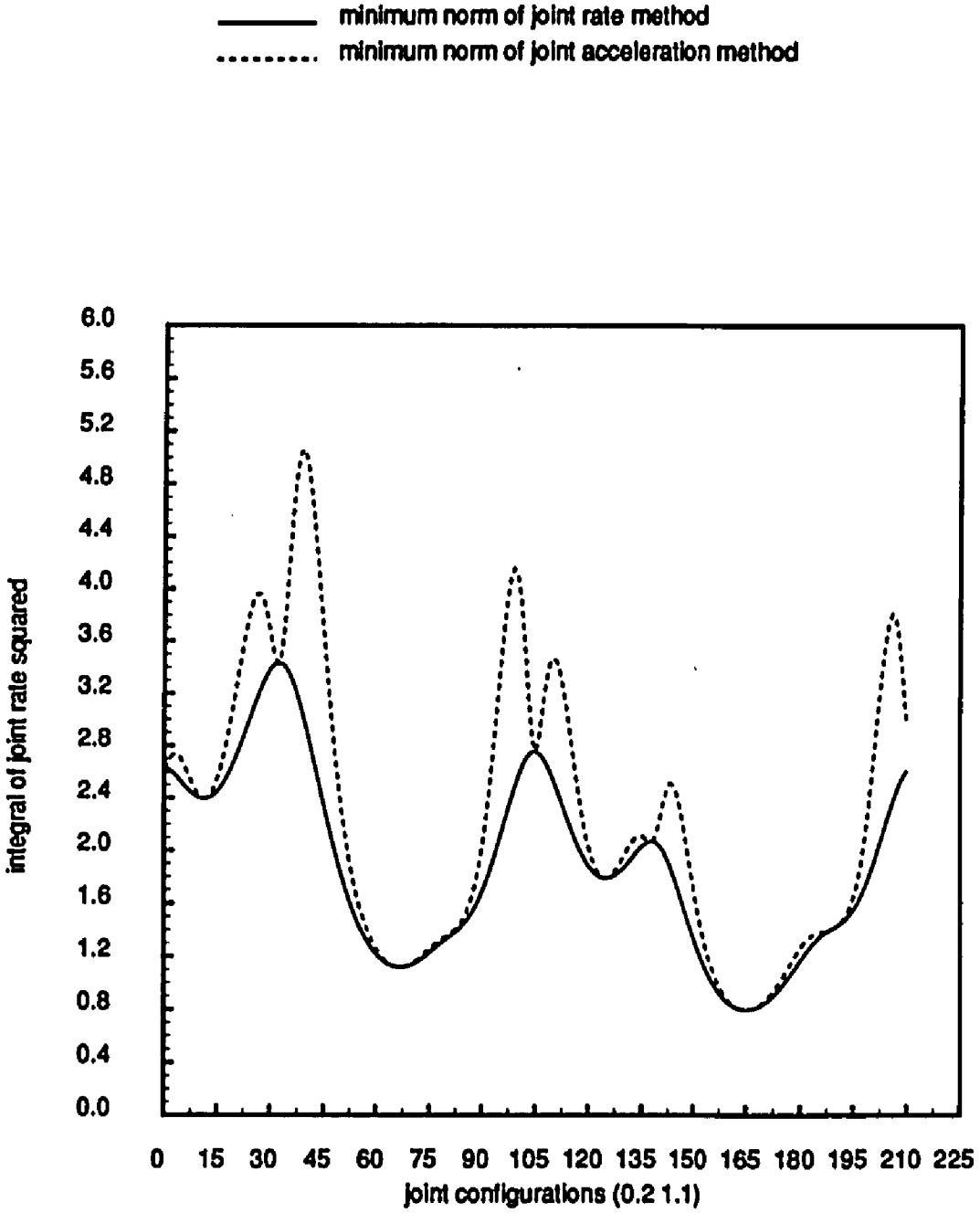

Figure 31: The plot of performance measure $I_{\dot{\theta}}$ among possible configurations for located at (-0.8,0.9) and end effector position at (-1.0, 2.0) corresponding to trajectories in Table 9 which trace a straight line trajectory for both velocity and acceleration control

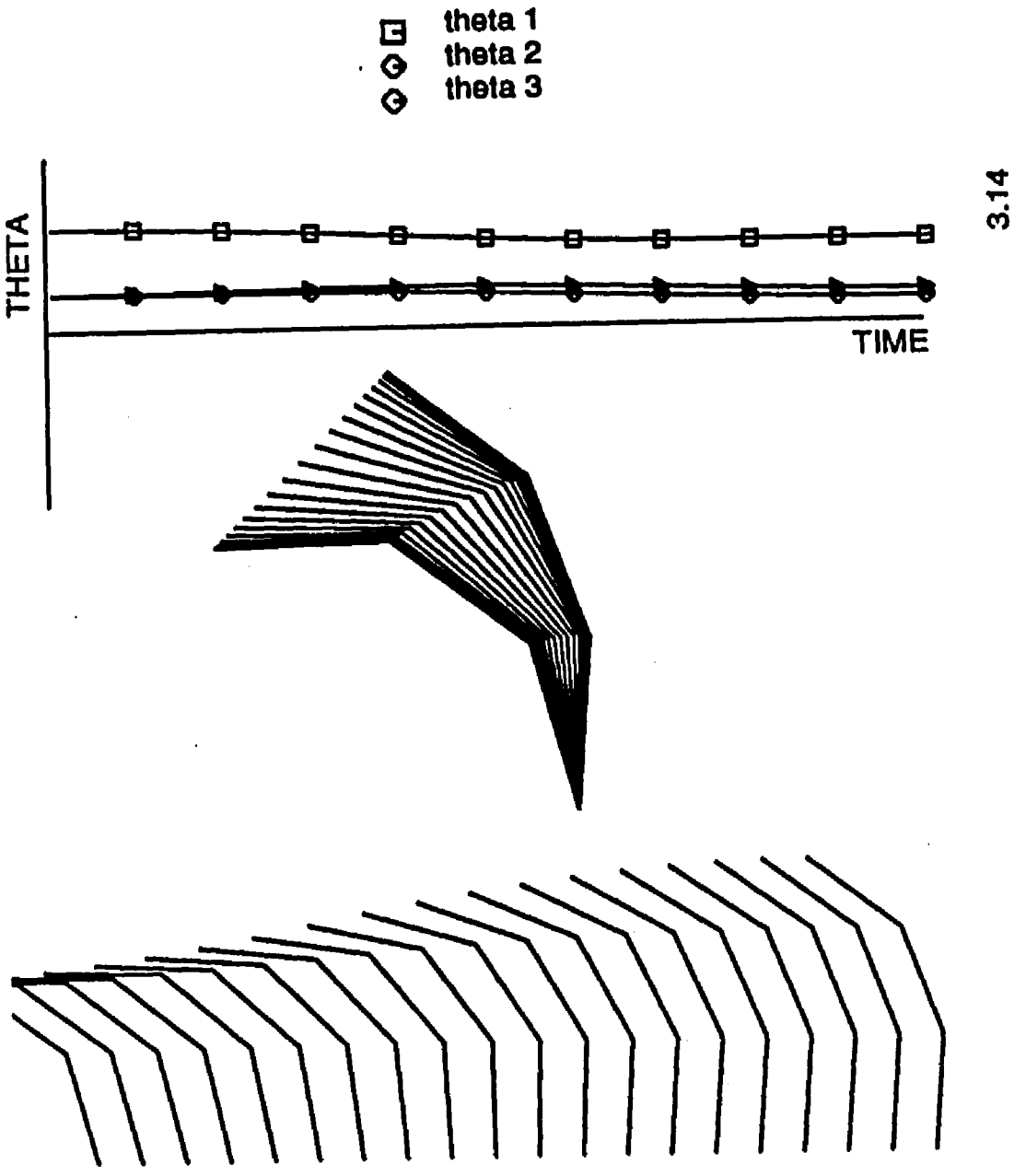

Figure 32: Joint angles and manipulator geometries as functions of time for the best configuration with base located at (1.07,0.46) and end effector position at (-1.0, 2.0) corresponding to trajectory 4 in Table 7 which traces a straight line trajectory with acceleration control

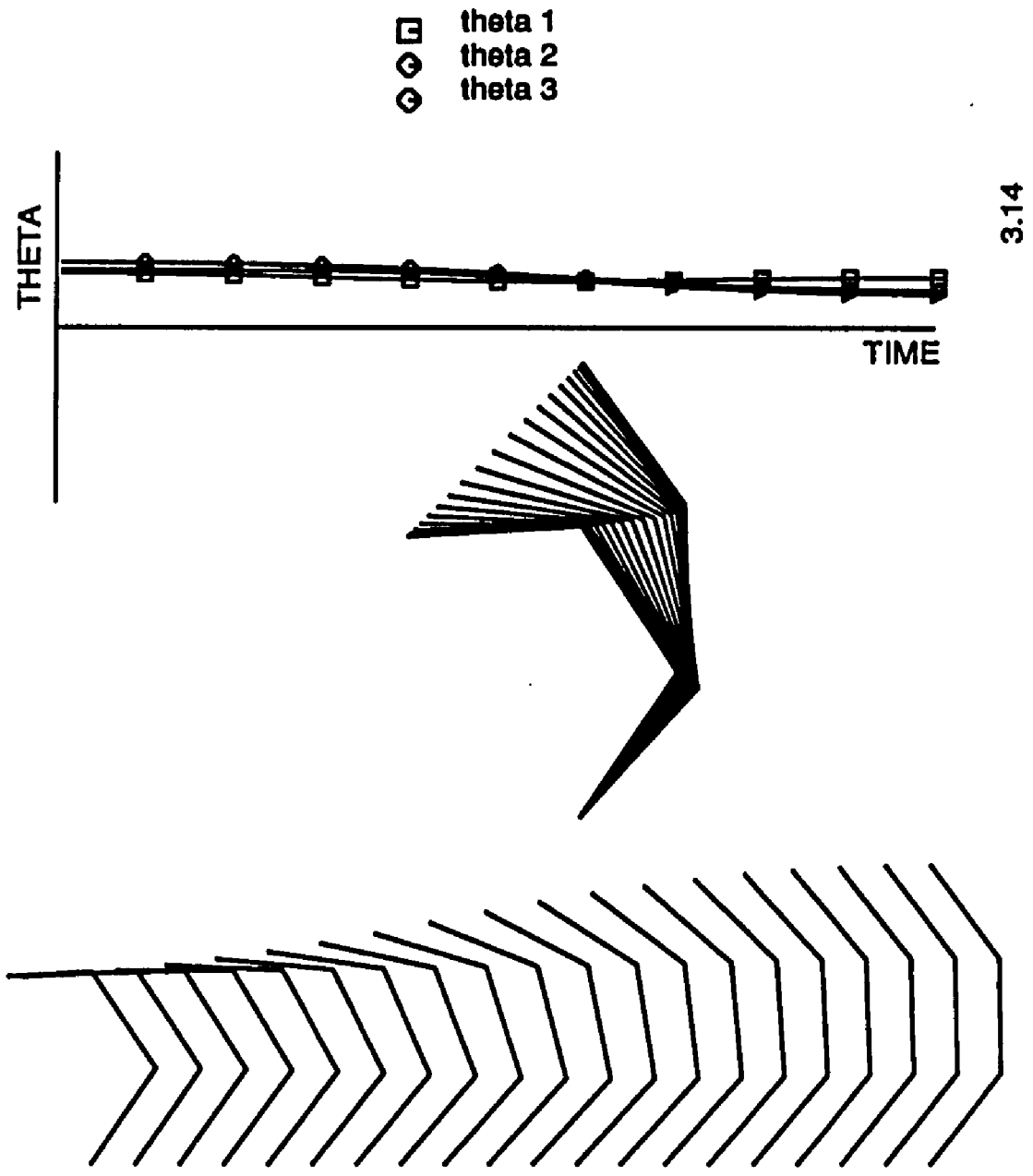

Figure 33: Joint angles and manipulator geometries as functions of time for the best configuration with the base located at (0.0,0.4) and end effector position at (-1.0, 2.0) corresponding to trajectory 4 in Table 8 which traces a straight line trajectory with acceleration control

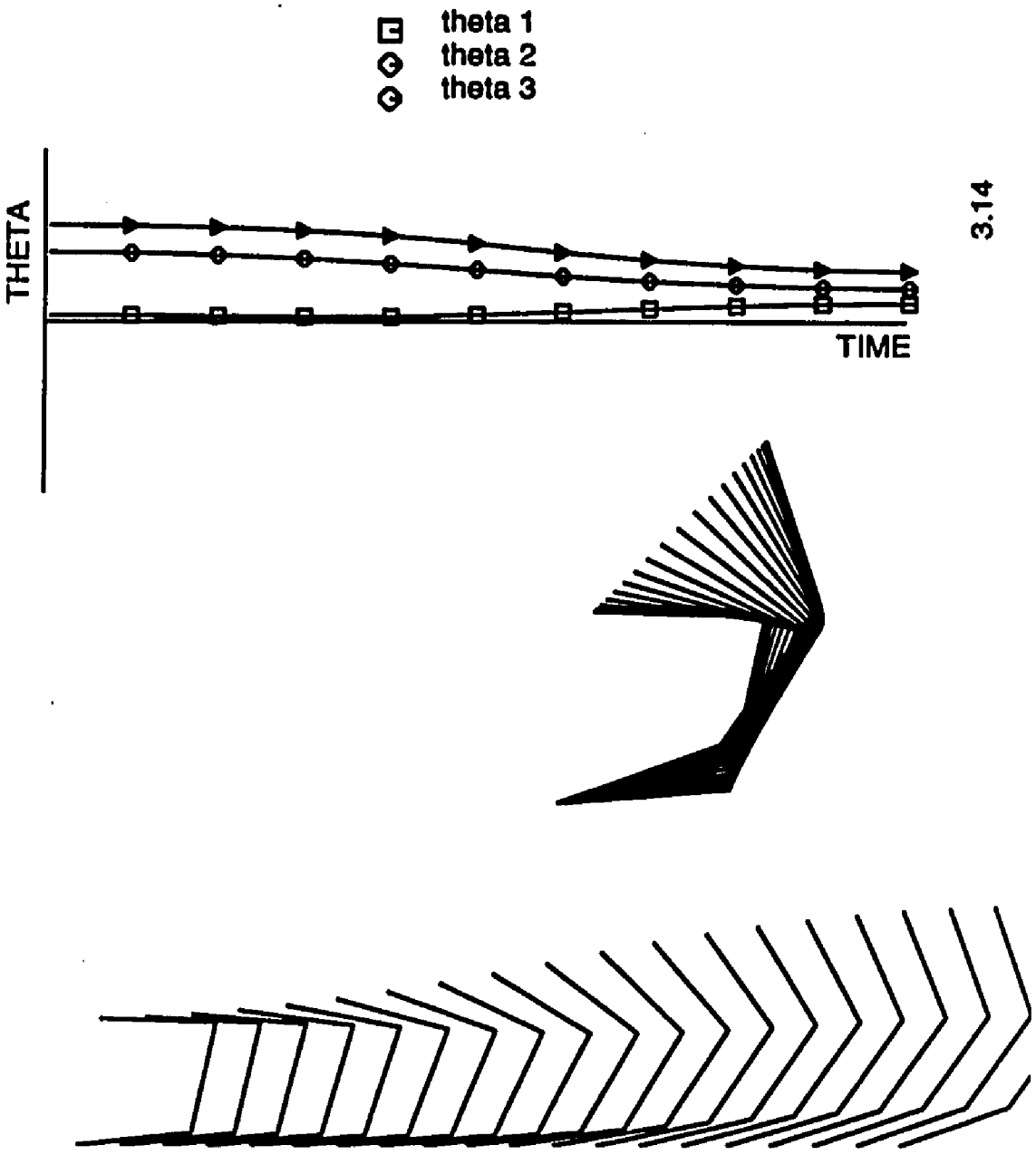

Figure 34: Joint angles and manipulator geometries as functions of time for the best configuration with the base located at (-0.8,0.9) and end effector position at (-1.0, 2.0) corresponding to trajectory 4 in Table 9 which traces a straight line trajectory with acceleration control

Table 9: The cost functions for different initial posture with end effector and base positions at (-1.0,2.0) and (-0.8,0.9) respectively for a straight line trajectory and minimum norm of joint acceleration control

Trajectory	Initial θ			Cost functions		
	θ_{1_0}	θ_{2_0}	θ_{3_0}	$\int_{t_0}^{t_f} \dot{\theta}^T \dot{\theta} dt$	$\int_{t_0}^{t_f} \ddot{\theta}^T \ddot{\theta} dt$	$\int_{t_0}^{t_f} \tau^T \tau dt$
1	6.1	72.2	100.6	0.80	2.64	6.20
2	113.5	-168.0	143.7	2.74	6.96	4.22
3	127.5	-42.0	-128.9	1.12	3.27	15.20
4	62.3	158.8	-160.1	2.76	8.24	10.10

Figs. 26 to 28 give the joint angle-space projections on the $\theta_1 = 0$ plane with different initial postures for 3 different base locations. They give two-dimensional views for comparing the performance measures. Figs. 32 to 34 show the joint angles and manipulator geometries for the 3 best joint space trajectories corresponding to initial postures of the 3 base locations as shown in Tables 7 to 9.

Fig. 35 shows the variation of performance measure, $\int_{t_0}^{t_f} \dot{\theta}^T \dot{\theta} dt$ for all the possible base locations. Simulation was carried out by updating the initial posture (θ_1, θ_2 and θ_3) by 10° each simulation. Comparison was made to find the smallest performance measure for each base location. The number shown in this figure was a relative value normalized by the absolute value of the difference between maximum (2.95) and minimum (0.18) of the performance measure, $I_{\dot{\theta}}$ for all possible base locations. These figures show the effects on the performance measures by changing manipulator's base in the work space. Computer simulations demonstrate that different base locations give different optimal joint-angle space trajectories and

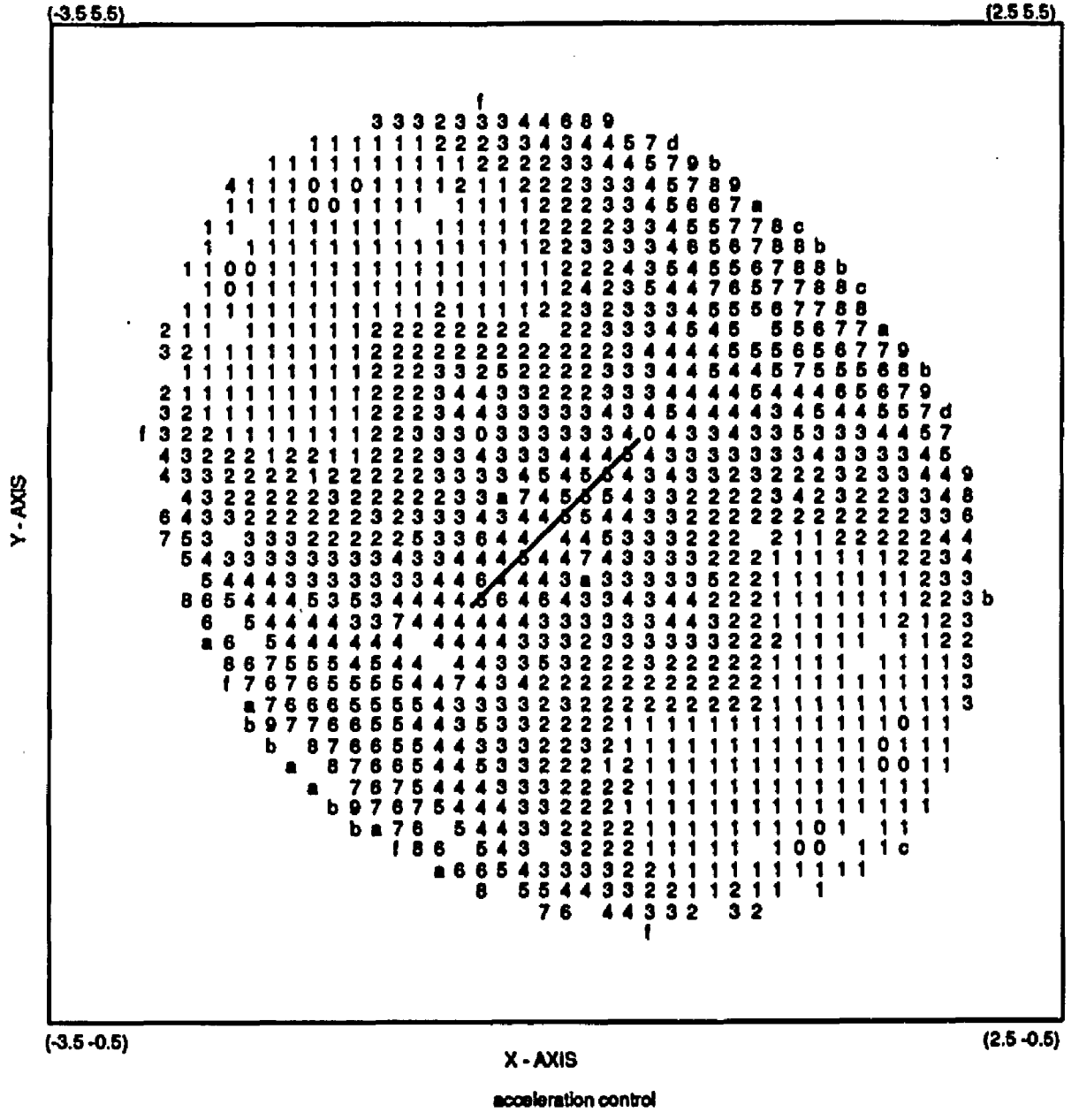

Figure 35: The plot of performance measure $I_{\dot{\theta}}$ for the all possible base locations with end effector position at (-1.0, 2.0), lower extremity of the straight line trajectory at 45° with acceleration control and symbols 0 to f designate values 0.18 to 2.95

performance curves with respect to all possible initial postures. It can be seen that the proper base location are effective for achieving a better performance measure.

3.5 Conclusions

Based on the performance measure, $I_{\dot{\theta}}$, two redundancy resolution methods, minimum norm of joint rate and minimum norm of acceleration, were compared. Their relationship has been described by using both null space utilization and calculus of variation methods. Computer simulation results illustrate the effects of initial posture, initial joint rates and base locations on the performance measure, Eq. (3.1). These simulation results can also be used for identifying the proper initial postures, joint rates and base locations to achieve a good performance for a redundant manipulator. Furthermore, there are some initial postures for which the performance measure, $I_{\dot{\theta}}$, becomes a minimum. For these initial postures the optimal trajectories are conservative and follow both minimum norm of joint rate and minimum norm of joint acceleration controls. Proper initial joint rates can also be chosen for a given initial posture to make the joint-angle space trajectory conservative. The choice of base location is effective for achieving a good performance measure. It has been shown that resolved acceleration technique is more flexible than resolved velocity method due to the possible choice of both initial postures and initial joint rates.

CHAPTER IV

RESOLVING THE REDUNDANCY AT THE HIGHER ORDER LEVELS

The kinematic redundancies of a robot manipulator are usually resolved at the velocity or at the acceleration level. There are no studies found in the literature where minimization of the norm of higher order derivatives used as a criterion for resolving the kinematic redundancies are investigated. Different responses and performance measures will result when different control schemes are applied to resolve the kinematic redundancy. The effect of resolving the redundancy through minimizing different order derivatives of joint-angle space variables will be discussed in this chapter.

The performance measure which integrates the joint rate squared along a specified trajectory has been used as an index for the comparison between velocity control and acceleration control schemes of a redundant manipulator in the previous chapter. From the previous discussion, it is known that resolving the redundancy at the velocity level is generally superior to the resolution of redundancy at the acceleration level as far as minimum norm of joints' movement or the algorithm's stability are concerned. On the other hand, due to the necessity of incorporating control with the dynamics of the system, the redundancy must be resolved at the acceleration level. Moreover, the acceleration control allows the initial joint rates as well as the initial postures to be chosen to achieve the

optimization of the specific cost function. As far as the utilization of the null-space components is concerned, the acceleration control is more flexible than the velocity control. Therefore, both techniques for resolving the redundancy at the velocity level and at the acceleration level are useful for the control of a redundant manipulator.

As the global performance optimization of a redundant manipulator is concerned, an optimal trajectory is not only required to satisfy the boundary conditions, but also to follow the corresponding Euler-Lagrange equation. In order to satisfy the Euler-Lagrange equation, the kinematic redundancy must be resolved at the higher derivative level. By continuously differentiating the kinematic equations which relate the joint angles in the joint coordinate with the position of the end effector in the cartesian space, the equations which give the relationship between the cartesian coordinate and the joint angle coordinate at the higher derivative levels are obtained.

The pseudoinverse method can be applied to derive the formulas which resolve kinematic redundancy through minimizing the norm of higher order derivatives of joint-angle space variables. Through the comparison of these equations, the effect of considering the higher order derivatives on the resolution of redundancies can be seen. The advantages and disadvantages of using the norm of higher derivatives as the criteria to resolve the redundancy are studied and computer simulation results are illustrated.

In this chapter, first, the formulas of resolving the redundancy at the higher levels are derived; second, the relationships between these two redundancy resolution schemes are studied; third, computer simulation was carried out and the results were compared; and finally, a conclusion and discussion is given in the last section.

4.1 Derivation of the Formulas for Resolving Redundancy at the Higher Order Derivative Levels

The formulas for resolving the redundancy at the higher order joint angle derivative levels are derived in this section. The derivation starts with the direct kinematic equations at the position level. Through continuously differentiating the kinematic equations at the position level, a series of kinematic equations which express the relationship of the variables between the cartesian coordinates and joint angle coordinates at the higher derivative's level are obtained. By taking the pseudoinverse of these direct kinematic equations, the corresponding minimum norm solutions are formulated.

The kinematic relationship between the position of the end effector in the cartesian coordinate and the joint configuration of each link in the joint angle space for a redundant robot manipulator can be expressed as follows:

$$\mathbf{x} = f(\boldsymbol{\theta}) \tag{4.1}$$

where $\mathbf{x}$ is the position vector of the end effector in the cartesian coordinate, $\boldsymbol{\theta}$ is the joint angle vector which specifies the configuration of the manipulator, and f is a vector function which gives the relationship for the end effector's position, vector $\mathbf{x}$ and the joint angle configuration, vector $\boldsymbol{\theta}$.

By differentiating Eq. (4.1), the kinematic equation which gives the relationship between the end effector's velocity ($\dot{\mathbf{x}}$) in the cartesian coordinate and the joint rate ($\dot{\boldsymbol{\theta}}$) in the joint angle space is obtained, i.e.,

$$\dot{\mathbf{x}} = J\dot{\boldsymbol{\theta}} \tag{4.2}$$

where J is the jacobian matrix with the elements $[J_{ij}] = \partial f_i / \partial \theta_j$.

By differentiating Eq. (4.2) again, the kinematic relationship between the end effector's acceleration in the cartesian coordinate ($\ddot{\mathbf{x}}$) and the joint acceleration ($\ddot{\theta}$) in the joint angle space is expressed as follows:

$$\ddot{\mathbf{x}} = J\ddot{\theta} + \dot{J}\,\dot{\theta}. \tag{4.3}$$

Differentiating Eq. (4.3) again, the kinematic relationship for the third order derivatives between the cartesian coordinate and the joint angle coordinate becomes:

$$\frac{d^3\mathbf{x}}{dt^3} = J\frac{d^3\theta}{dt^3} + 2\dot{J}\ddot{\theta} + \ddot{J}\dot{\theta}. \tag{4.4}$$

Differentiating Eq. (4.4) again, the kinematic relationship for the fourth order derivatives between the cartesian coordinate and the joint angle coordinate is obtained:

$$\frac{d^4\mathbf{x}}{dt^4} = J\frac{d^4\theta}{dt^4} + 3(\dot{J}\frac{d^3\theta}{dt^3} + \ddot{J}\ddot{\theta}) + \frac{d^3J}{dt^3}\dot{\theta}. \tag{4.5}$$

Differentiating Eq. (4.5) again, the kinematic relationship for the fifth order derivatives between the cartesian coordinate and the joint angle coordinate is given as:

$$\frac{d^5\mathbf{x}}{dt^5} = J\frac{d^5\theta}{dt^5} + 4\dot{J}\frac{d^4\theta}{dt^4} + 6\ddot{J}\frac{d^3\theta}{dt^3} + 4\frac{d^3J}{dt^3}\ddot{\theta} + \frac{d^4J}{dt^4}\dot{\theta}. \tag{4.6}$$

If more differentiation is taken, higher order derivatives relationships between these two coordinates can be obtained. Theoretically, this process may be continued indefinitely, but as physical meaning is concerned, the expansion to the 4th order derivative seems sufficient.

By applying the pseudoinverse technique to solve the above direct kinematic relations, a set of corresponding minimum norm solutions for resolving the kinematic redundancy at the different derivative levels are obtained as shown below:

- minimum norm solutions at the velocity level

$$\dot{\theta} = J^{+}\dot{\mathbf{x}} \tag{4.7}$$

- minimum norm solutions at the acceleration level

$$\ddot{\theta} = J^{+}(\ddot{\mathbf{x}} - \dot{J}\dot{\theta}) \tag{4.8}$$

- minimum norm solutions at the third order derivative's level

$$\frac{d^3\theta}{dt^3} = J^{+}(\frac{d^3\mathbf{x}}{dt^3} - 2\dot{J}\ddot{\theta} - \dddot{J}\dot{\theta}) \tag{4.9}$$

- minimum norm solutions at the fourth order derivative's level

$$\frac{d^4\theta}{dt^4} = J^{+}[\frac{d^4\mathbf{x}}{dt^4} - 3(\dot{J}\frac{d^3\theta}{dt^3} + \ddot{J}\ddot{\theta}) - \frac{d^3J}{dt^3}\dot{\theta}] \tag{4.10}$$

- minimum norm solutions at the fifth order derivative's level

$$\frac{d^5\theta}{dt^5} = J^{+}[\frac{d^5\mathbf{x}}{dt^5} - 4\dot{J}\frac{d^4\theta}{dt^4} - 6\ddot{J}\frac{d^3\theta}{dt^3} - 4\frac{d^3J}{dt^3}\ddot{\theta} - \frac{d^4J}{dt^4}\dot{\theta}]. \tag{4.11}$$

The pseudoinverse can be continuously carried on for resolving the kinematic redundancy through minimizing the norm of the higher order derivative joint space variables. As the order of the derivative gets higher, there are more initial values need to be decided, that is, it is more flexible to utilize the null-space component for achieving another goal by proper choice of initial conditions. On the other hand, the problem becomes more complicated and difficult to solve.

4.2 The Relationship between Methods of Resolving the Redundancy at Different Order of Derivative Levels

The kinematic relationships and their corresponding minimum norm solutions of a robot manipulator and the relations for resolving the redundancy at higher order derivative levels have been derived. By comparing the above equations, some relations between them can be obtained.

Let the subscript (i) for the following variables indicate the order of the joint angle derivative at which the norm is being minimized. Differentiating the Eq. (4.7) gives

$$\ddot{\theta}_{(1)} = J^{+}(\ddot{\mathbf{x}} - \dot{J}\dot{\theta}_{(2)}) + J^{+}\dot{J}\,\dot{\theta}_{(2)} + \frac{d(J^{+})}{dt}J\dot{\theta}_{(1)} \tag{4.12}$$

if $\dot{\theta}_{(1)} = \dot{\theta}_{(2)}$ then

$$J^{+}\dot{J}\dot{\theta}_{(2)} + \frac{d(J^{+})}{dt}J\dot{\theta}_{(1)} = \frac{d(J^{+}J)}{dt}\dot{\theta} \tag{4.13}$$

and if $\frac{d(J^{+}J)}{dt}\dot{\theta} = 0$ then

$$\begin{aligned} \ddot{\theta}_{(1)} &= J^{+}(\ddot{\mathbf{x}} - \dot{J}\dot{\theta}) + \frac{d(J^{+}J)}{dt}\,\dot{\theta} \qquad (4.14)\\ &= \ddot{\theta}_{(2)} + \frac{d(J^{+}J)}{dt}\dot{\theta} \\ &= \ddot{\theta}_{(2)} \end{aligned}$$

(4.15)

Differentiating Eq. (4.8) gives

$$\frac{d^3\theta_{(2)}}{dt^3} = J^+(\frac{d^3\mathbf{x}}{dt^3} - \dot{J}\ddot{\theta}_{(3)} - \ddot{J}\,\dot{\theta}_{(3)}) + \frac{d(J^+)}{dt}J\ddot{\theta}_{(2)} + J^+\dot{J}\ddot{\theta}_{(3)}$$
$$+J^+\dot{J}(\ddot{\theta}_{(3)} - \ddot{\theta}_{(2)}) + J^+\ddot{J}(\,\dot{\theta}_{(3)} - \dot{\theta}_{(2)})$$

$$\text{if} \begin{cases} \ddot{\theta}_{(3)} = \ddot{\theta}_{(2)} \\ \dot{\theta}_{(3)} = \dot{\theta}_{(2)} \end{cases} \text{ then}$$

$$\frac{d^3\theta_{(2)}}{dt^3} = J^+(\frac{d^3\mathbf{x}}{dt^3} - 2\dot{J}\ddot{\theta} - \ddot{J}\dot{\theta})\frac{d(J^+)}{dt}J\ddot{\theta} + J^+\dot{J}\ddot{\theta} \tag{4.16}$$
$$= \frac{d^3\theta_{(3)}}{dt^3} + \frac{d(J^+J)}{dt}\ddot{\theta}.$$

By the same token, Eq. (4.9) is differentiated and the following result is obtained:

$$\frac{d^4\theta_{(3)}}{dt^4} = J^+[\frac{d^4\mathbf{x}}{dt^4} - 3(\dot{J}\frac{d^3\theta}{dt^3} + \ddot{J}\dot{\theta}) - \frac{d^3J}{dt^3}\dot{\theta}]$$
$$+\frac{d(J^+)}{dt}J^+\frac{d^3\theta}{dt^3} + J^+\dot{J}\frac{d^3\theta}{dt^3} \tag{4.17}$$
$$= \frac{d^4\theta_{(4)}}{dt^4} + \frac{d(J^+J)}{dt}\frac{d^3\theta}{dt^3}.$$

Therefore, if

$$\frac{d(J^+J)}{dt}\dot{\theta} = 0 \tag{4.18}$$
$$\frac{d(J^+J)}{dt}\ddot{\theta} = 0$$
$$\frac{d(J^+J)}{dt}\frac{d^3\theta}{dt^3} = 0$$
$$\frac{d(J^+J)}{dt}\frac{d^4\theta}{dt^4} = 0$$

then

$$
\begin{aligned}
\dot{\theta}_{(1)} &= \dot{\theta}_{(2)} = \dot{\theta}_{(3)} = \dot{\theta}_{(4)} \cdots \\
\ddot{\theta}_{(1)} &= \ddot{\theta}_{(2)} = \ddot{\theta}_{(3)} = \ddot{\theta}_{(4)} \cdots \\
\frac{d^3\theta_{(1)}}{dt^3} &= \frac{d^3\theta_{(2)}}{dt^3} = \frac{d^3\theta_{(3)}}{dt^3} = \frac{d^3\theta_{(4)}}{dt^3} \cdots \\
\frac{d^4\theta_{(1)}}{dt^4} &= \frac{d^4\theta_{(2)}}{dt^4} = \frac{d^4\theta_{(3)}}{dt^4} = \frac{d^4\theta_{(4)}}{dt^4} \cdots .
\end{aligned}
\tag{4.19}
$$

From the above discussion, the conditions for minimizing the norm of different level of joint angles' derivatives, Eq. (4.19), mean that the joint rates, joint accelerations and higher derivatives of joint angles are orthogonal to the change of minimum norm space. If these conditions hold, then the same results will be obtained regardless of the level at which the redundancy is resolved. Moreover, all the norms are minimized. This property is very useful because a configuration which satisfies the above condition will give a conservative solution and also globally minimize the norm of each derivative.

4.3 Computer Simulations

In this section, four different criteria, minimum norms of joint rate, joint acceleration, the third order derivative and the fourth derivative of joint-angle space variables were used in computer simulations to resolve the kinematic redundancy. The trajectory used for the simulation is a circle of radius 0.5 whose specifications in cartesian space is given in Fig. 10 and Table 1 in Chapter 3. The performance measures are the integral of joint rate squared and joint acceleration squared along the specified trajectory. The simulation was carried out by applied the above updated schemes to trace the specified circular trajectory. Fig. 36 shows

the performance measure, $I_{\dot{\theta}}$, as a function of initial postures for four redundancy resolution methods. It can be seen that two initial postures which result at optimal trajectories are the same no matter the kinematic redundancy is resolved through the minimization of which order of the derivative's norm.

Fig. 37 gives the projections of the joint angle space curves on $\theta_1 = 0$ plane for 5 starting postures listed in Table 6 in Chapter 3 by using the control strategy which minimizes the norm of the 3rd order derivative. By the same token, the control strategy which minimizes the norm of the 4th order derivative of joint-angle space variables was used to obtain the results given in Fig. 38. By comparing these two figures, it can be seen that for both control methods the joint angle space trajectories are conservative at the two initial postures which $I_{\dot{\theta}}$ are minimum.

The calculations of the jacobian and its derivatives for a 3-link redundant manipulator which are required for the computer simulation is given in Appendix *B*.

4.4 Conclusion

Redundancy is useful for achieving certain desired goals. In this chapter, formulas for resolving kinematic redundancy through minimization of the higher order derivatives' norm in the joint-angle space have been derived. A comparison of the performance measure $I_{\dot{\theta}}$ by applying different control strategies was made. The comparison provides some insight of how the null-space components affect the resolution of the redundancy. Effects of considering the higher order derivatives of joint-angle space variables on the resolution of redundancies have also been studied.

The conditions, Eq. (4.19), for minimizing the norm of all orders of joint angles' derivatives, have been derived. When these conditions hold, the same

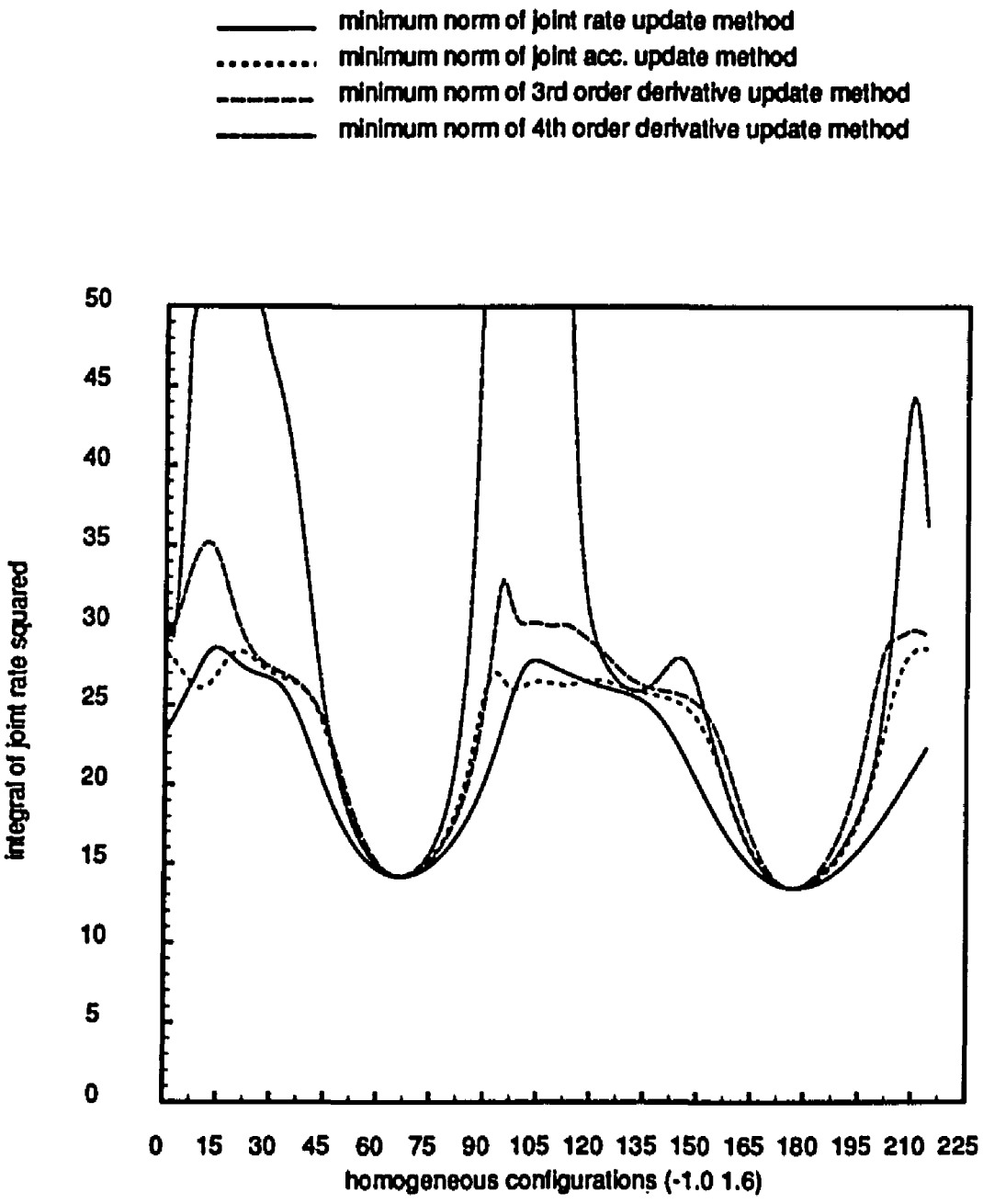

Figure 36: The performance measure $I_{\dot{\theta}}$ for four different kinematic redundancy resolution strategies through minimization of the norm of joint rate, joint acceleration, the 3rd and 4th derivatives of joint angles respectively to trace a circular trajectory with end effector at (-1.0 1.6) and base at (0.0,0.0)

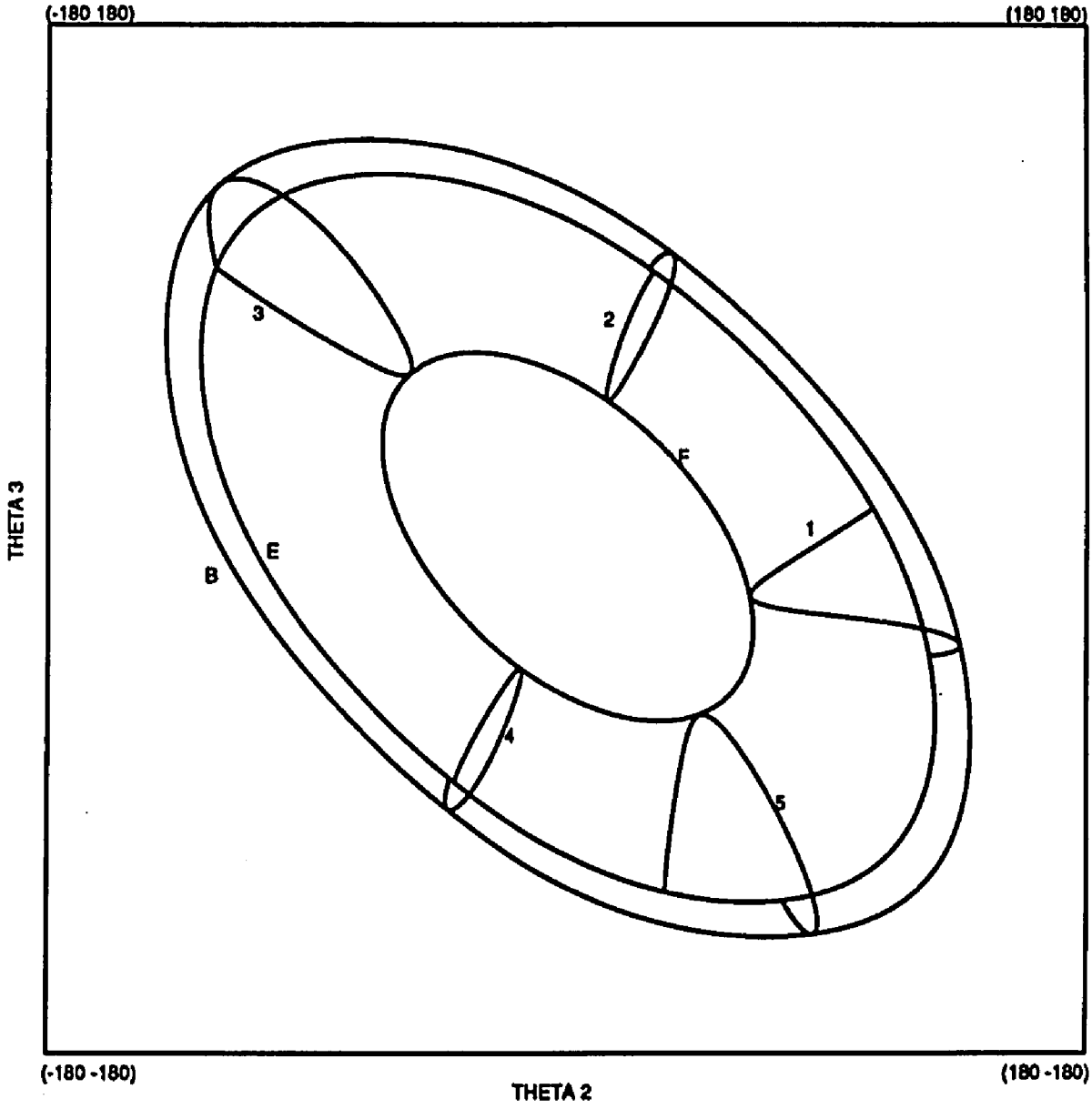

Figure 37: The projection of the joint angle space curve on the $\theta_1 = 0$ plane for 5 starting postures corresponding to trajectories in Table 6 Chapter 3 for the control strategy which minimizes the norm of the 3rd order derivative to trace a circular trajectory with base located at (0.0,0.0)

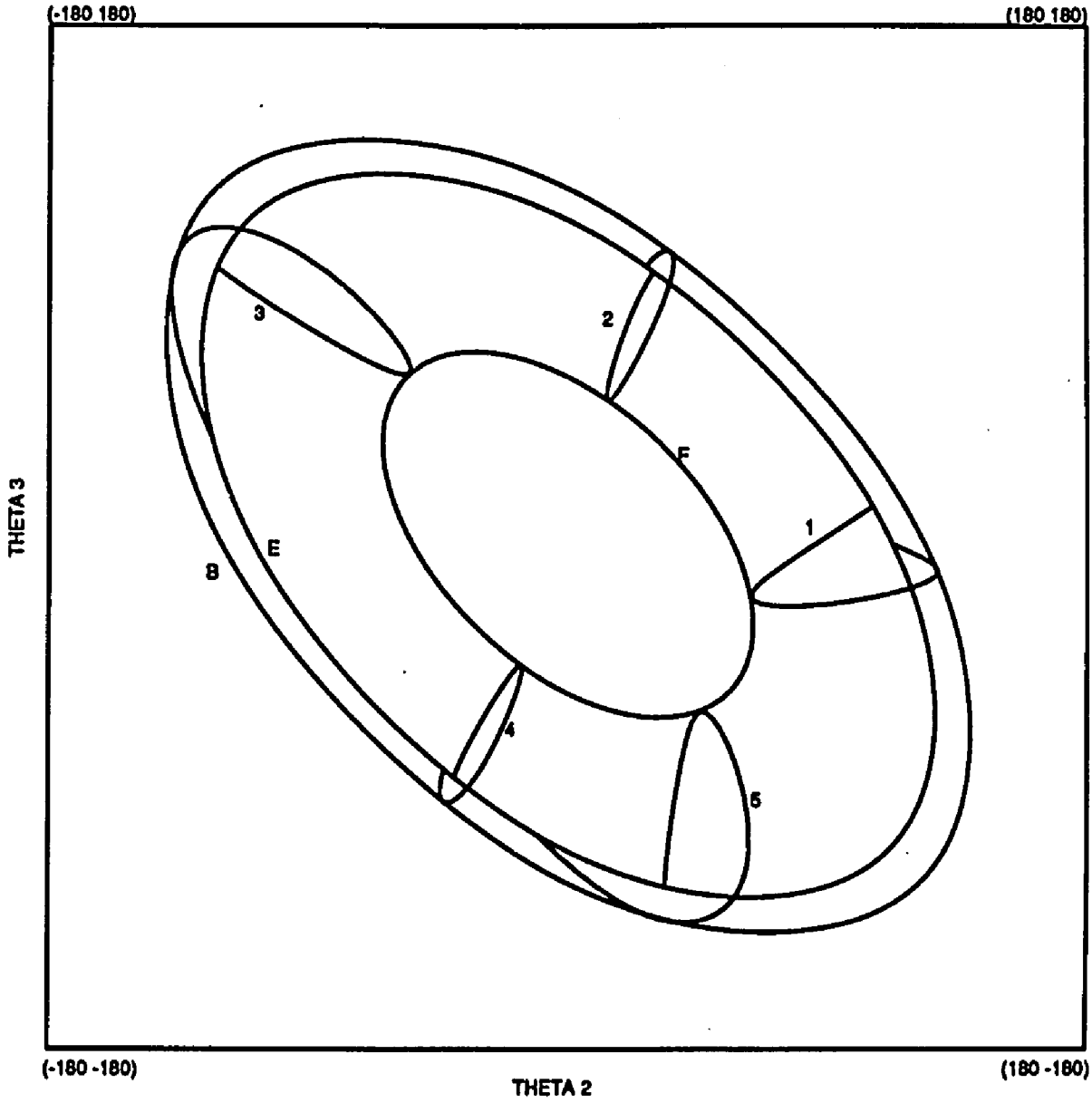

Figure 38: The projection of the joint angle space curve on the $\theta_1 = 0$ plane for 5 starting postures corresponding to trajectories in Table 6 Chapter 6 for the control strategy which minimizes the norm of the 4th order derivative to trace a circular trajectory with base located at (0.0,0.0)

performance measure $I_{\dot{\theta}}$ is obtained regardless of the level at which the redundancy is resolved. Moreover, a conservative solution and also global minimization of all order derivatives' norm is achieved. These results have been demonstrated by the computer simulations.

CHAPTER V

LOCAL TORQUE OPTIMIZATION TECHNIQUE

One important application of redundancy utilization is to optimize the required efforts, such as energy consumption [11], force, and torque requirement [12]. The actuators used for driving a manipulator, due to the limitation of the physical sizes, have finite power ratings. In order to achieve a better utilization of the actuators' driving capabilities, the required torques should be optimally distributed. Based on the limited driving force constraints, torque optimization is an important issue for resolving the redundancy.

Torque optimization is important for controlling a redundant manipulator. Due to the complexity of involving dynamics, only very few algorithms have been developed to achieve this goal [12]. Hollerbach and Suh [12] first proposed a performance measure of optimizing the norm of actuator's torques. They applied the pseudoinverse method to resolve kinematic redundancy and used null-space components to achieve the optimization of required torques. Their algorithm works well when the movement of end effector is small, but when the movement gets larger, a very large torque is required for the manipulator arm to pass through some specific configurations.

Two questions remain in this algorithm to be answered: first, why the system becomes unstable, and second, how to get rid of this instability. In other words, the sources causing the instability and the methods for preventing the manipulator

from reaching those undesirable situations need to be investigated. This study has shown that the local torque optimization algorithm becomes unstable when it passes through some undesirable states, that is, some configurations with large joint velocities.

There exist two possible solutions for keeping the manipulators from reaching those undesired situations: first, to apply a suitable amount of null-space component during the control process, or second, to choose a proper initial state for starting the job. For the first solution, a damped least-squares pseudoinverse method [25] can be applied to limit the amount of null-space components being used, so that a stable solution can be obtained. For the second solution, a proper initial state is searched and used for starting a job so that a torque optimization is achieved. Therefore, by choosing the best initial configuration (θ_0) and joint rate ($\dot{\theta}_0$), and utilizing the proper null-space components a stable local optimization algorithm can be found.

In this chapter, first, the kinematics and dynamics of the manipulator are introduced, and the recursive Newton-Euler dynamic equations for calculating the joint torques are derived. Second, the local torque optimization technique proposed by Hollerbach and Suh [12] is reviewed. Third, the sources that cause their algorithm's instability are investigated. Finally, two possible solutions are proposed.

5.1 Kinematics and Dynamics of a Manipulator

A manipulator is superior to other pick and place types of automation machinery because the manipulator is programable. The manipulator has the ability to adapt to various environments and jobs. In order to operate a manipulator, a task and the way to fulfill it, should be specified and designed, i.e., how the

manipulator is to be moved, and what the torques or forces required to accomplish the desired motions should be determined.

Kinematics and dynamics are the sciences which study how the objects move, and what causes them to move. Kinematics is the geometrical description of the motion of a physical system in time and in three-dimensional space. It can be described by the quantities such as position, displacement, velocity, acceleration and the higher-order derivatives of the position variables (with respect to time) and showing how objects move. Dynamics, on the other hand is the causal explanation of the motion as we observe it. The quantities which are used to describe dynamics are momentum, force, potential, torque, etc. Dynamics deal with the questions of why the objects move. That is, dynamics study the relationships between motion and force or torque which cause the motion.

The explicit relationship between kinematics and dynamics are Newton-Euler equations. Newton's equation relates the force with the acceleration through the masses of the system, while Euler's equation relates the torque and the angular acceleration through the system inertia. Newton's equation is

$$\mathbf{F} = m\dot{\mathbf{v}} \tag{5.1}$$

and Euler's equation is

$$\mathbf{N} = {}^{c}I\dot{\omega} + \omega \times {}^{c}I\omega \tag{5.2}$$

where $\mathbf{F}$ and $\mathbf{N}$ are the forces and torques applied from the outside world, $\mathbf{v}$ and ω are linear and angular velocity, and m and ${}^{c}I$ are mass and the inertia with respect to the center of mass. It can be seen that the kinematical quantities which relate the kinematics to the dynamics in these equations are accelerations.

5.2 Review of the Local Torque Optimization Technique

The local torque optimization technique proposed by Hollerbach and Suh [12] used the pseudoinverse technique and utilized the null-space component to minimize the norm of required torques instantaneously. A brief derivation of this local torque optimization algorithm is described as follows: The equation which provides the acceleration constraint equations between the end effector in the cartesian space and the joint angles in joint space is

$$J\ddot{\theta} = \ddot{\mathbf{x}} - \dot{J}\dot{\theta}. \tag{5.3}$$

Being a redundant manipulator, there are more degrees of freedom in joint angle space than those in the cartesian space. By solving the under-determined system equation Eq. (5.3), the kinematic redundancies are resolved at the acceleration level. Using the pseudoinverse method, a particular solution which minimizes the norm of the joint acceleration is obtained. Combining the particular solution with the null-space components, which have no effects on the end effector movement, a general solution of Eq. (5.3) is

$$\ddot{\theta} = J^{+}(\ddot{\mathbf{x}} - \dot{J}\dot{\theta}) + (I - J^{+}J)\ddot{\phi}. \tag{5.4}$$

where I is an identity matrix, $\ddot{\phi}$ is any $n-$dimensional space vector. The null-space components $(I - J^{+}J)\ddot{\phi}$ in Eq. (5.4) can be used for achieving a secondary goal, minimizing the norm of torque locally. According to this criterion an algorithm which instantaneously minimizes the required torques was derived [13].

Eq. (5.4) can be rewritten as

$$\ddot{\theta} = J^{+}(\ddot{\mathbf{x}} - \dot{J}\dot{\theta}) + (I - J^{+}J)\ddot{\phi} = \ddot{\theta}_p + \ddot{\theta}_h, \tag{5.5}$$

where $\ddot{\theta}_p$ is the particular part of the solution which minimizes the norm of joint acceleration, and $\ddot{\theta}_h$ is the homogeneous part of the solution, which has no effect on the end effector's movement. The closed form of the torques for a manipulator arm derived in [13] is

$$\tau = H(\theta)\ddot{\theta} + \dot{\theta}C(\theta,\dot{\theta})\dot{\theta} + \mathbf{g}(\theta), \tag{5.6}$$

where τ is the vector of joint torque, $H(\theta)$ represents the manipulator inertia, $C(\theta,\dot{\theta})$ corresponds to the centripetal and coriolis accelerations, and $\mathbf{g}(\theta)$ is the gravity term. The formulas of calculating the required torques for a 3–link planar manipulator with uniform mass distribution on each link are derived in Appendix *A*.

Substituting $\ddot{\theta}$ from Eq. (5.5) into Eq. (5.6)

$$\begin{aligned}
\tau &= H\ddot{\theta} + \dot{\theta}C\dot{\theta} + \mathbf{g} \\
&= H[J^{+}(\ddot{\mathbf{x}} - \dot{J}\dot{\theta}) + (I - J^{+}J)\ddot{\phi}] + \dot{\theta}C\dot{\theta} + \mathbf{g} \\
&= HJ^{+}(\ddot{\mathbf{x}} - \dot{J}\dot{\theta}) + \dot{\theta}C\dot{\theta} + \mathbf{g} + H(I - J^{+}J)\ddot{\phi} \\
&= \tau_p + \tau_h
\end{aligned}$$

is obtained, where

$$\tau_p = HJ^{+}(\ddot{\mathbf{x}} - \dot{J}\dot{\theta}) + \dot{\theta}C\dot{\theta} + \mathbf{g}. \tag{5.7}$$

and

$$\tau_h = H(I - J^{+}J)\ddot{\phi}. \tag{5.8}$$

Let α and β be the upper and lower bounds of the available torque, τ, that the actuators can provide. In order to provide a bigger safety margin, the actuators are

usually driven in a range which is closest to the middle of these two bounds, i.e., as close to $\frac{1}{2}(\alpha+\beta)$ as possible. That is, $\left\|\tau - \frac{\alpha+\beta}{2}\right\|^2$ is minimized. Let $\alpha' = \alpha - \tau_p$ and $\beta' = \beta - \tau_p$, then $\left\|\tau - \frac{\alpha+\beta}{2}\right\|^2$ becomes $\left\|H(I - J^+J)\ddot{\phi} - \frac{\alpha'+\beta'}{2}\right\|^2$. So, the required null-space component of joint acceleration $\ddot{\phi}$, to minimize the actuators' torque becomes:

$$\ddot{\phi} = [H(I - J^+J)]^+ \left(-\frac{\alpha' + \beta'}{2}\right). \tag{5.9}$$

and the corresponding joint acceleration

$$\begin{aligned} \ddot{\theta} &= J^+(\ddot{\mathbf{x}} - \dot{J}\dot{\theta}) + (I - J^+J)[H(I - J^+J)]^+ \left(-\frac{\alpha' + \beta'}{2}\right) \\ &= J^+(\ddot{\mathbf{x}} - \dot{J}\dot{\theta}) + [H(I - J^+J)]^+ \left(-\frac{\alpha' + \beta'}{2}\right). \end{aligned} \tag{5.10}$$

If the upper and lower limits are symmetrical with respect to zero, i.e., $\alpha+\beta = 0$, and $\frac{\alpha'+\beta'}{2} = \tau_p$, then $\ddot{\phi}$, the null-space component of joint acceleration that minimizes the norm of torques becomes

$$\ddot{\phi} = [H(I - J^+J)]^+ \left(-\tau_p\right). \tag{5.11}$$

The complete solution of $\ddot{\theta}$ for locally optimizing the required torques is obtained by substituting Eq. (5.11) into Eq. (5.4), that is:

$$\ddot{\theta} = J^+(\ddot{\mathbf{x}} - \dot{J}\dot{\theta}) + [H(I - J^+J)]^+ \left(-\tau_p\right). \tag{5.12}$$

Eq. (5.12) is the joint acceleration which gives at each instant the minimum norm of joint torque. Substituting $\ddot{\theta}$ from Eq. (5.12) back into Eq. (5.6) gives the corresponding torques for driving the actuators.

5.3 Analysis of the Algorithm

Hollerbach and Suh [12] applied the above algorithm to optimize the torques supplied by the actuators. Their algorithm works very well for small end effector movement, however stability problems are encountered when the movement gets larger. That is, there are some configurations that physically are not singular, but require very large torques to implement them. This problem has been investigated, and it has been found that these configurations and their associated velocities form a new type of singular state, and very large torques are required to pass through these states. Therefore, one should prevent the manipulator from falling into these singular states. The methods for preventing the manipulator from reaching these singular states are either by starting at a proper initial configuration and initial joint rate, or properly using the available null-space components.

The instability of the local torque optimization algorithm depends on the combination of configurations and their associated joint rates. In order to stabilize the system, another algorithm should be developed to keep track and prevent the manipulator from falling into those undesirable states. An explicit way for detecting these states is by checking the minimum singular value of the matrix $H[I - J^+J]$. If the singular value becomes small, and the associated joint rate is large then the manipulator is approaching the state of 'singularity'. A 3–link planar manipulator can be used as an example for investigating this problem. The matrix $H[I - J^+J]$ of a 3–link planar manipulator has rank 1. In other words, it has only one nonzero singular value. This singular value together with the corresponding joint rates can be used as an indicator of instability.

Fig. 39 shows the singular value of the matrix $H[I-J^+J]$ for a 3–link manipulator plotted with respect to the set of joint angles (θ_2, θ_3), where joint angles, θ_2

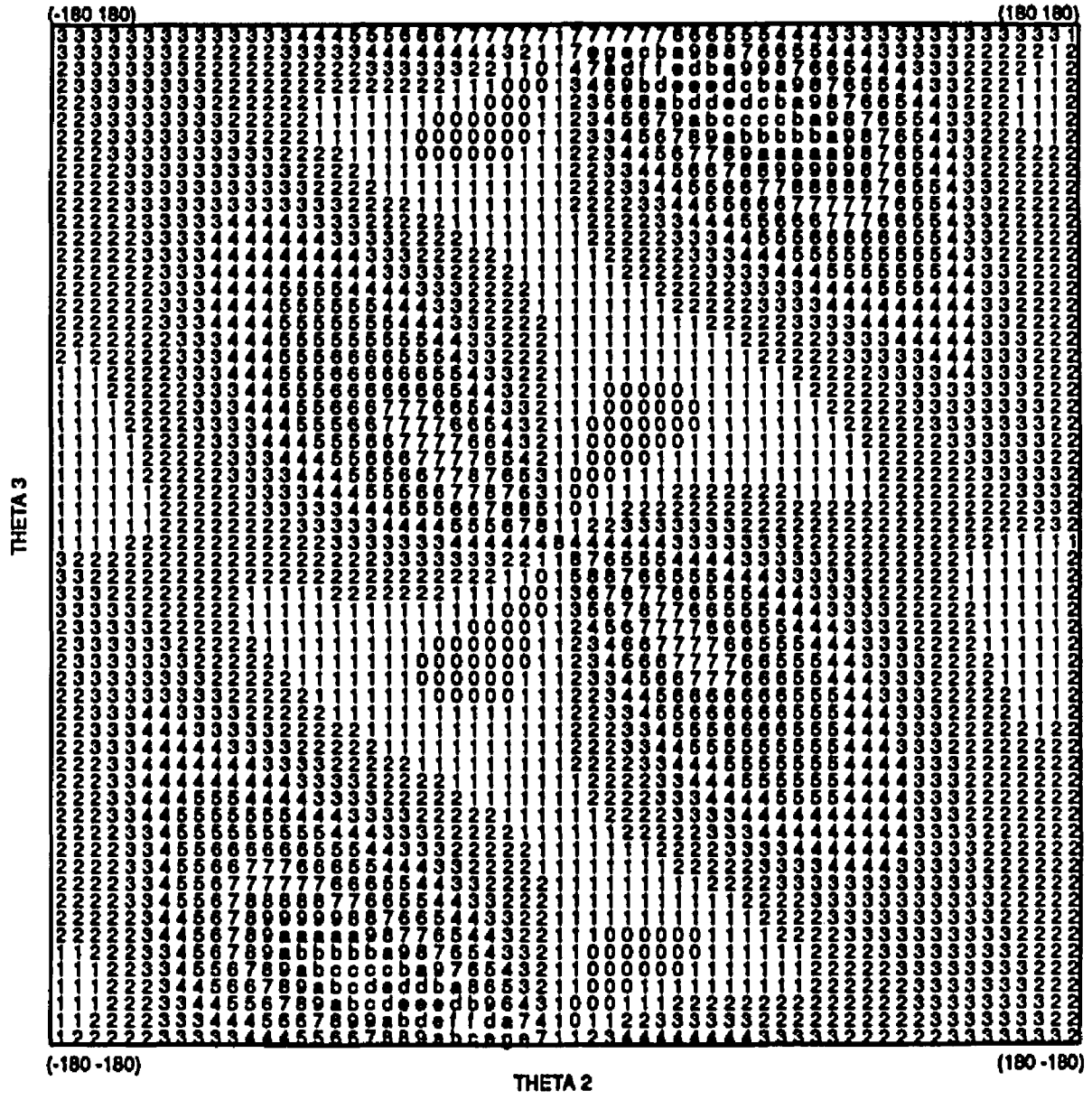

Figure 39: Relative singular values of the matrix $H[I - J^+J]$ on the plane spanned by the coordinates θ_2 and θ_3, with $-180° \leq \theta_2 \leq 180°$, $-180° \leq \theta_2 \leq 180°$ and symbols 0 to f designate values from 0.41 to 16.0.

and θ_3 range from $-\pi$ to π, while θ_1 is set to zero. The numbers which range from 0 to e represent the relative magnitude of that singular value, with 0 the smallest and e the largest value. This figure shows that there are some configurations which have very small singular values of the matrix $H(I-J^+J)$. If the manipulator goes through these configurations with relatively high joint rates, then very large torques are required. In order to stabilize the local torque optimization algorithm, it is important for the control of a redundant manipulator to avoid getting into these undesired states.

5.3.1 Two Types of Singularity

From the previous discussion, it is seen that singularities play a very important role on the stability of an algorithm. In this section, two types of singularities are studied and their effects on the stability of the instantaneous torque optimization technique are discussed.

One is a kinematic singularity and the other is a dynamic singularity. The former is encountered in the configurations when the manipulator loses some degree of freedom. The latter is seen in some state (joint angle and joint rate) when the manipulator requires much effort to move in a certain direction. It occurs because the local torque optimization algorithm was used. Both of these singularities are undesirable for the control of a redundant manipulator. Therefore, how to avoid these singularities is an important issue for controlling a manipulator.

The first kind of singularity is an inverse kinematic problem. Assume the manipulation variable in cartesian space is $\mathbf{r}$ and it has dimension m, and the control variable θ in joint angle space has dimension n. The relationship between the differential motion of the end effector and the differential motion of each joint satisfy the Jacobian equations $\dot{\mathbf{x}} = J\dot{\theta}$. If the manipulator is non-redundant and the con-

figuration is nonsingular, that is $m = n$ and $\det J(\theta) \neq 0$, then the differential joint motion $\delta\theta$ for the requested differential motion of the end effector $\delta\mathbf{r}$ can be solved by the inverse matrix as follows: $\delta\theta = J^{-1}(\theta)\delta\mathbf{r}$. When the manipulator moves to some configurations at which the determinant of the Jacobian J approaches zero, i.e., $\det J(\theta) \doteq 0$, then the configuration becomes singular. J^{-1} does not exist at these singular points. There are no solutions at these singular points, i.e., one cannot find a set of finite values $\delta\theta$ which satisfy the above Jacobian equation. It will need an infinite amount of effort to go through singular points.

If some position errors are allowed, that is, instead of using matrix inverse to find a set of exact solutions, the pseudoinverse technique is used to solve the problem, then a least-squares error solution is obtained. The pseudoinverse is defined even for a singular matrix. Using the pseudoinverse of the Jacobian matrix $J(\theta)$, the above equation can be solved by $\delta\theta = J^{+}(\theta)\delta\mathbf{r}$. This solution provides a least-squares solution with a minimum norm. i.e., $\delta\theta$ satisfies $\min_{\delta\theta} \|\delta\theta\|$ among all of $\delta\theta$ that fulfill the following condition: $\min_{\delta\theta} \|\delta\mathbf{r} - J(\theta)\delta\theta\|$, where $\|\mathbf{q}\|$ denotes the norm of $\mathbf{q}$.

The case where $m = n$, $\delta\theta$ which makes $\|\delta\mathbf{r} - J(\theta)\delta\theta\|$ equal to zero is uniquely determined for the nonsingular Jacobian matrix. Therefore the difference between $J^{-1}(\theta)$ and $J^{+}(\theta)$ is that $J^{-1}(\theta)$ is not defined at singular points, but $J^{+}(\theta)$ provides minimum norm and a least-squares error solution. In order to provide a feasible solution at the singular configurations, the pseudoinverse instead of the matrix inverse is used for finding the corresponding solution. But there is a discontinuous switching from an exact solution to an approximate solution at the singular points. Especially in the neighborhood of the singular point, the pseudoinverse of the Jacobian matrix has the tendency to find an exact solution; this may result in an infeasible solution. This problem is caused by regarding $\min_{\delta\theta} \|\delta\mathbf{r} - J(\theta)\delta\theta\|$

as more important than $\min_{\delta\theta} \|\delta\theta\|$. That is, where the pseudoinverse method is concerned, the exactness is always regarded as more important than the feasibility of a solution. The problem including matrix inverse around or near the kinematic singularity can be solved by using the robust inverse method [26], or damped least-squares method [25].

Another kind of singularity discussed here is that a state, which is a combination of configuration and joint rate, becomes singular or approaches a singularity. At these states, the manipulator has difficulty moving in some directions. It needs a large amount of effort to make the manipulator overcome this difficulty and move in the joint angle space to achieve the required end effector motion.

An example of a 'singular state' is as follows: the minimum torque algorithm is applied to drive a 3−link redundant manipulator with its base located at $(0.0, 0.0)$ and initial posture $(130°, -120°, 120°)$ such that the end effector is constantly accelerated during the first half, and decelerated during the second half of the motion along a straight line at 45°. Fig. 41 which will be shown later this section gives the required torques as functions of time for the manipulator to pass through the singular state: $\theta = (113.24°, -28.75°, -48.42°)$ and $\dot{\theta} = (-4.58, 9.92, -7.92) rad/sec.$ Being a redundant manipulator, the redundancy provides extra degrees of freedom for each joint to move in the null space. The extra motion in the null space resulted from the strategy to get the norm of torques minimized at every instant. This extra motion increases the joint accelerations and joint velocity for the latter motion. Continuing this process, a singular state which requires a very large torque may be reached. This kind of singularity is different from static singularity because it depends not only on the configuration, but also the joint velocity of the manipulator.

The cause of this problem is that the torque optimization algorithm has two

steps; first, it uses pseudoinverse to minimize the norm of joint accelerations; second, it uses another pseudoinverse to minimize the required torques. A minimum norm solution obtained by the first pseudoinverse tracks the end effector's trajectory, while a least-squares error solution reached by the second pseudoinverse tries to make the norm of the required torques as small as possible. This strategy works very well when the null-space component has more effect on decreasing the norm of required torques than increasing the joint rates. While a manipulator is approaching dynamic singularity, a very large null-space acceleration is needed for just reducing a little bit of torque. The result is that the joint rates get larger and larger, and eventually the whole system becomes unstable. So, it is very important to compromise by considering both effects at the same time, i.e., to optimize the norm of the torques and the norm of the null-space components simultaneously. It results with the first solution overcoming the 'instability' problem, that is, the usage of approximate pseudo- erse instead of regular pseudoinverse. The algorithm of using approximate pseudoinverse for solving the instability problem will be discussed later.

5.3.2 Interpretation of the Algorithm's Instability

Two aspects are considered for evaluating the local torque optimization algorithm, effectiveness and cost. In this section, the mechanism of torque optimization and the associated cost of increasing the joint rate are discussed.

The general formula of torques required to drive a manipulator is

$$\tau = H(I - J^{+}J)\ddot{\phi} + \tau_p, \tag{5.13}$$

with $\tau_p = HJ^{+}(\ddot{\mathbf{x}} - \dot{J}\dot{\theta}) + \dot{\theta}C\dot{\theta} + \mathbf{g}$ and $\ddot{\phi}$, any $n-$dimensional joint acceleration vector in joint angle space. Finding the minimal norm of τ is the same as finding the least-squares error solution for $\ddot{\phi}_h$ of the equation

$$H(I - J^+J)\ddot{\phi} = -\tau_p, \tag{5.14}$$

so that $\|H(I - J^+J)\ddot{\theta}_h - (-\tau_p)\|$ is minimized. As a result, Eq. (5.14) is solved, and the required $\ddot{\phi}$ for the torque optimization algorithm is found to be $[H(I - J^+J)]^+(-\tau_p)\|$ as shown in Eq. (5.11). Furthermore, the vector $-\tau_p$ can be decomposed into two orthogonal components, $[H(I-J^+J)][H(I-J^+J)]^+(-\tau_p)$ and $\{I - [H(I - J^+J)][H(I - J^+J)]^+\}(-\tau_p)$, that is,

$$\begin{aligned} -\tau_p &= [H(I - J^+J)][H(I - J^+J)]^+(-\tau_p) \\ &\quad +\{I - [H(I - J^+J)][H(I - J^+J)]^+\}(-\tau_p) \end{aligned} \tag{5.15}$$

is an orthogonal decomposition of vector $-\tau_p$ with

$$\begin{aligned} \|-\tau_p\|^2 &= \|[H(I - J^+J)][H(I - J^+J)]^+(-\tau_p)\|^2 \\ &\quad +\|\{I - [H(I - J^+J)][H(I - J^+J)]^+\}(-\tau_p)\|^2, \end{aligned} \tag{5.16}$$

where $[H(I-J^+J)][H(I-J^+J)]^+(-\tau_p)$ is the projection of vector $(-\tau_p)$ on to the column space of $[H(I-J^+J)]$, while the other component, $\{I-[H(I-J^+J)][H(I-J^+J)]^+\}(-\tau_p)$ is orthogonal to the column space of $[H(I - J^+J)]$. The former component is the negative of the torque that results from applying the null-space joint acceleration. This component cancels out part of the τ_p. Therefore, the latter component, that is, the remaining component of τ_p, becomes the torque required for the manipulator to achieve the specified motion. The norms' ratio of these two components is

$$\chi = \frac{\|[H(I - J^+J)][H(I - J^+J)]^+(-\tau_p)\|^2}{\|\{I - [H(I - J^+J)][H(I - J^+J)]^+\}(-\tau_p)\|^2}, \tag{5.17}$$

and it provides a measure of the inconsistency with the system equation, Eq. (5.14). In particular, $\chi = 0$ implies that $-\tau_p$ is orthogonal to the column space of $[H(I - J^+J)]$, whereas large values of χ imply that $-\tau_p$ is nearly contained in the column

space of $[H(I - J^+J)]$, that is, $\|\{I - [H(I - J^+J)][H(I - J^+J)]^+\}(-\tau_p)\|^2$ is relatively small. Physically, a large value of χ means the torque algorithm is effective at that configuration, whereas the algorithm is not effective if χ is small. As a result, the more inconsistent the system equation Eq. (5.14) is, that is χ is small, the less effective is the algorithm. In other words, the more $-\tau_p$ is orthogonal to the column space of $[H(I - J^+J)]$, the less effective this torque optimization algorithm becomes.

The effectiveness of the algorithm has been described in the previous paragraphs, and the associated cost paid for optimizing the torque is discussed in this section. Due to the utilization of the null-space component for torque optimization, the minimum torque algorithm requires a larger joint acceleration than the minimum acceleration algorithm does. The amount of the joint acceleration in null space required for minimizing the norm of joint torques is

$$\begin{aligned} \ddot{\theta}_h &= (I - J^+J)[H(I - J^+J)]^+(-\tau_p) \\ &= [H(I - J^+J)]^+(-\tau_p) \\ &= \ddot{\phi}_h. \end{aligned} \tag{5.18}$$

On the other hand, the joint acceleration for optimizing joint torques can also be decomposed into two orthogonal components, $\ddot{\theta}_p$ and $\ddot{\theta}_h$, where $\ddot{\theta}_p$ is the pseudoinverse solution of

$$J\ddot{\theta} = \ddot{\mathbf{x}} - \dot{J}\dot{\theta}, \tag{5.19}$$

and $\ddot{\theta}_h$ is the null-space component. Because Eq. (5.19) is consistent for all nonsingular configurations, $\ddot{\theta}_p$ is contained in the row space of the jacobian matrix J, and $\ddot{\theta}_h$ is orthogonal to the row space of J.

$$\ddot{\theta} = \ddot{\theta}_p + \ddot{\theta}_h \tag{5.20}$$

is the orthogonal decomposition of the joint acceleration $\ddot{\theta}$, with

$$\|\ddot{\theta}\|^2 = \|\ddot{\theta}_p\|^2 + \|\ddot{\theta}_h\|^2, \tag{5.21}$$

and the ratio

$$\rho = \frac{\|\ddot{\theta}_h\|}{\|\ddot{\theta}_p\|} \tag{5.22}$$

shows the relative amount of joint acceleration in null space needed for optimizing the joint torques' norm compared to the minimum norm joint acceleration required for tracking the specific trajectory. The value of ρ depends on both the configuration, and the associated joint rate. It shows how much price is needed to pay for the torque optimization.

The null-space component of joint acceleration needed for torque optimization is $\ddot{\theta}_h = [H(I - J^+J)]^+(-\tau_p)$. It depends on both the singular value of the matrix $H(I - J^+J)$ and the norm of $-\tau_p$. The singular value of some specific configuration with the value of $-\tau_p$. At that state $(\theta, \dot{\theta})$ gives how much homogeneous component should be applied for torque optimization.

The matrix $H[I - J^+J]$ has a rank of 1 and its singular value depends on both the inertia matrix H and null-space vector $[I - I^+J]$. Therefore, the matrix $H[I - J^+J]$ does not have the same singular value as matrix $[I - J^+J]$ which is always equal to 1. The singular value of the matrix $H[I - J^+J]$ is an important factor resulting in the algorithm's instability. The singular value decomposition of matrix $H[I - J^+J]$ can be expressed as:

$$\begin{aligned} H[I - J^+J] &= \sum_{i=1}^{r} s_i \, \mathbf{e}_i \, \mathbf{f}_i^T \\ &= (\sum_{i=1}^{r_h} s_{h_i} \, \mathbf{e}_{h_i} \, \mathbf{f}_{h_i}^T)(\sum_{i=1}^{r_n} s_{n_i} \, \mathbf{e}_{n_i} \, \mathbf{f}_{n_i}^T), \end{aligned} \tag{5.23}$$

where s is the singular value, e is the output vector and f is the input vector of the matrix with the subscripts h and n representing the inertial matrix H and null-space vector $[I - J^+J]$, respectively. The rank of inertial matrix H for a 3-link planar manipulator r_h is 3 and the rank of null space r_n, is 1 for one degree-of-redundancy system. Eq. (5.23) becomes

$$\begin{aligned} H[I - J^+J] &= (\sum_{i=1}^{r_h} s_{h_i}\, \mathbf{e}_{h_i}\, \mathbf{f}_{h_i}^T)(\mathbf{e}_n\, \mathbf{f}_n^T) \\ &= \sum_{i=1}^{r_h} [s_{h_i}\, (\mathbf{f}_{h_i}^T \mathbf{e}_n)\, \mathbf{e}_{h_i}] \mathbf{f}_n^T \\ &= s\, \mathbf{e}\, \mathbf{f}^T, \end{aligned} \tag{5.24}$$

with

$$s\,\mathbf{e} = \sum_{i=1}^{r_h} (s_{h_i}\, \mathbf{f}_{h_i}^T\, \mathbf{e}_n\, \mathbf{e}_{h_i}), \tag{5.25}$$

and

$$\mathbf{f} = \mathbf{f}_n. \tag{5.26}$$

It can be seen that the effect of multiplying the matrix H to the null-space vector $[I - J^+J]$, is the modification of the output vector e and singular value s. There is no modification of the resultant input vector f. The singular value of matrix $H(I - J^+J)$ depends on the configuration of the manipulator while the singular value of matrix $[I - J^+J]$ is a constant 1.

When this singular value is small, and τ_p is large, $\ddot{\theta}_h$ becomes very large and so does $\ddot{\theta}$. Therefore, the system may become unstable. The joint angles, manipulator's geometries and required torques as functions of time for a 3-link planar manipulator to track a straight line at 45° with minimum torque algorithm

are shown in Figs. 40 and 41. Each singular value of the inertia matrix H times the inner product of its corresponding input vector and the output vector of null-space matrix $[(I - J^+J)]$, together with the singular value of the matrix $H[I - J^+J]$ as functions of time are shown in Fig. 42. These figures show that the manipulator passes through a singular state which is kinematically non-singular. Furthermore, the input vector corresponding to the maximum singular value of inertia matrix H is almost orthogonal to the null-space output vector in the vicinity of this dynamic singularity. This feature results a large torque required to go through the singular state.

It can be seen that the local torque optimization algorithm becomes unstable when the manipulator reaches a configuration that has a small $H(I - J^+J)$ singular value and high joint rates. Two methods are proposed to prevent the manipulator from approaching these 'singularities'. The first method is to compromise the amount of null-space component usage and the degree of torque optimization achievement so that the null-space components are not overused. This compromised method is called damped least-squares [25] or approximate pseudoinverse [26]. The second method is to choose a proper initial state for starting the job. A better initial state guarantees that the end effector can reach as far as its physical limits and avoid unstable situations.

5.4 Damped Least-squares Method

In order to find the minimum torque solution, the equation

$$\tau = H\ddot{\theta}_h + \tau_p \tag{5.27}$$

is solved to give a least-squares effort solution. An overdetermined linear system

$$\mathbf{y} = A\mathbf{x} + \mathbf{b}, \tag{5.28}$$

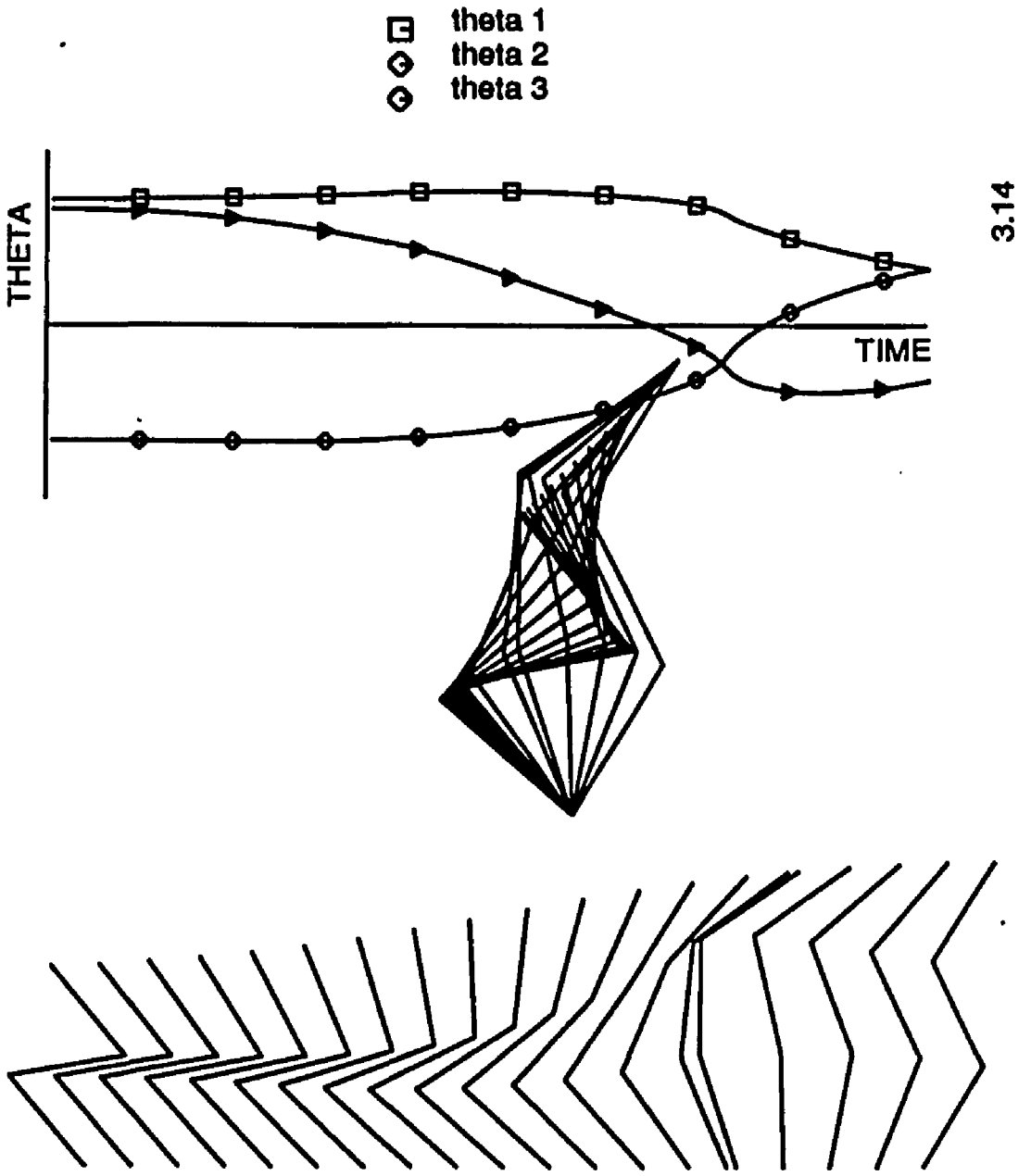

Figure 40: The joint angles and geometries as functions of time for a 3-link planar manipulator to pass through a singular state: joint angles $(113.24°, -28.75°, -48.42°)$ and joint rates (-4.58,9.92,-7.92), with initial posture $(130°, -120°, 120°)$ and base located at (0.0,0.0)

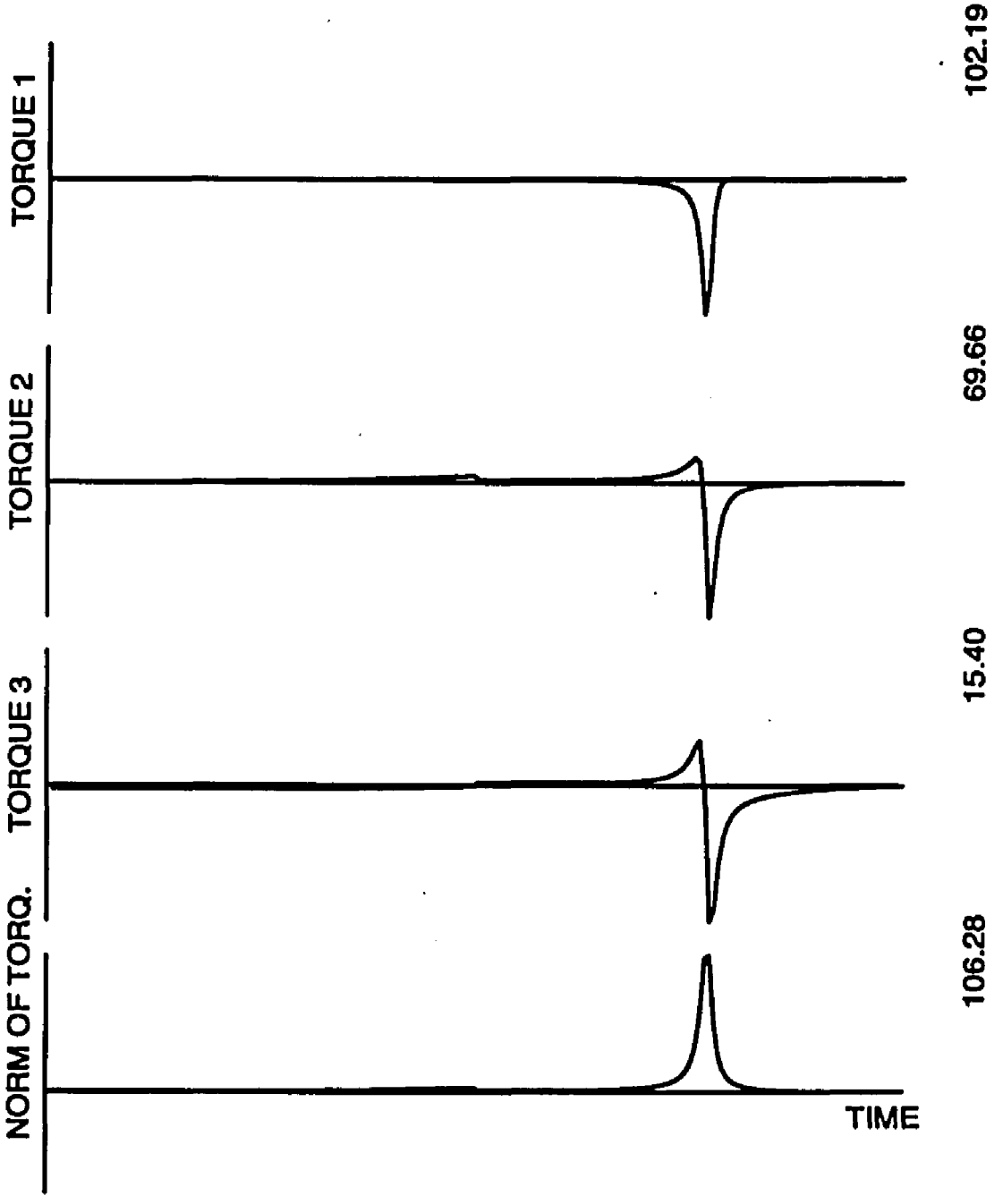

Figure 41: Joint torques as functions of time for a 3-link planar manipulator to go through a singular state: joint angles (113.24°, −28.75°, −48.42°) and joint rates (-4.58,9.92,-7.92)

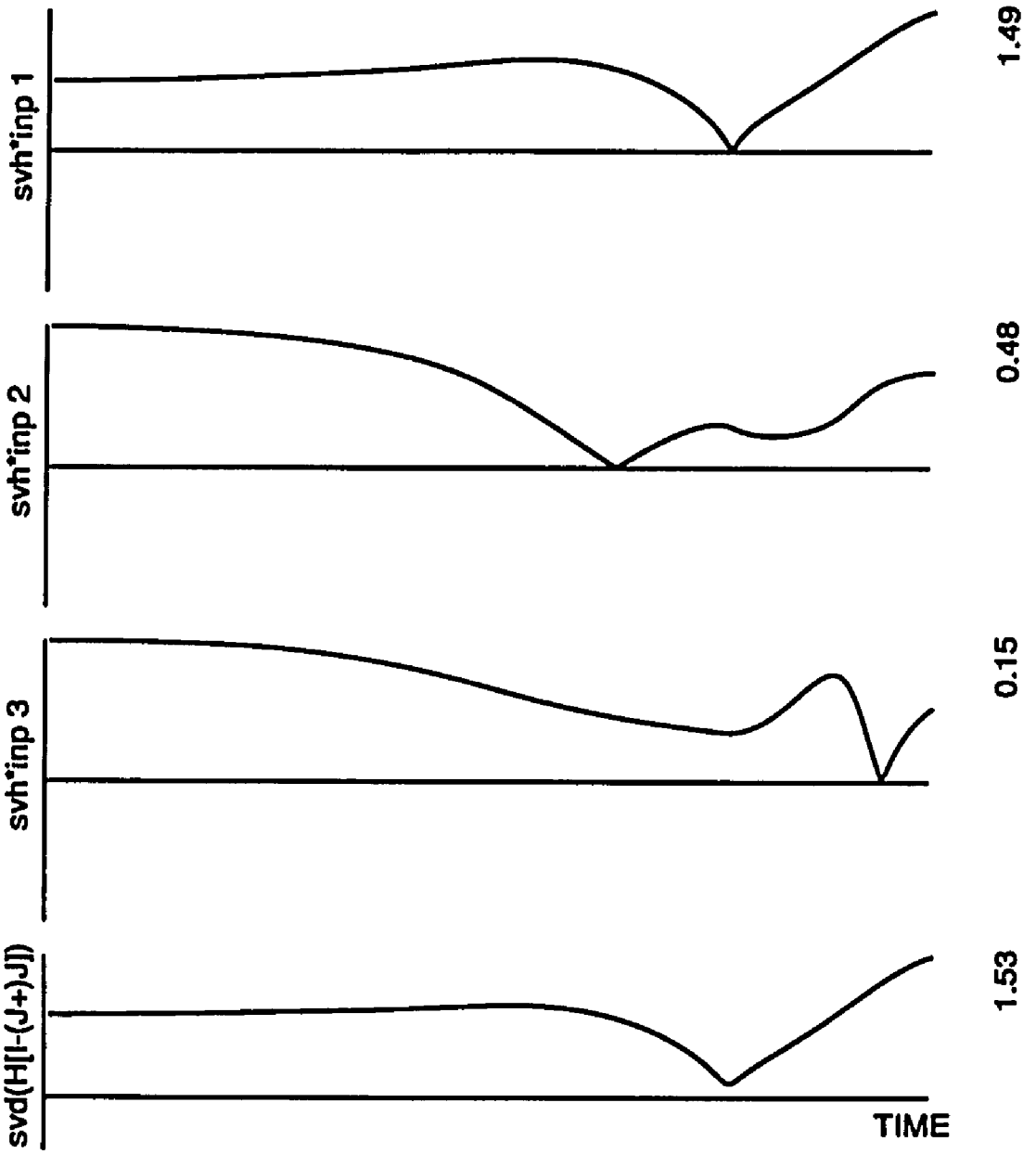

Figure 42: Each singular value of the inertia matrix H times the inner product of its corresponding input vector and the output vector of null-space matrix $[(I - J^{+}J)]$ together with the singular value of the matrix $H[I - J^{+}J]$ in the vicinity of dynamic singularity for minimum torque method.

Vector $\hat{\mathbf{x}} = A^{+}(-\mathbf{b})$, gives the minimum norm of the error vector $\hat{\mathbf{y}}$, i.e., minimum effort solution of $\mathbf{y}$. In other words, $\|\hat{\mathbf{y}}\| = \|A\hat{\mathbf{x}} + \mathbf{b}\| = \|(I - AA^{+})\mathbf{b}\|$ is minimized. It is an approximate solution of Eq. (5.28), that is, a least-squares error solution by setting the left side to 0. During this estimation process, the magnitude of $\mathbf{x}$ has not been considered. It functions very well if the system matrix is well conditioned, that is, no singular value of matrix A is very close to zero. If the matrix A has a singular value near zero, i.e., near singularity, the required $\mathbf{x}$ may become very large in order to minimize the norm of $\mathbf{y}$. This may give the possibility of the latter estimation of $\mathbf{y}$ to become very high. This is why the pseudoinverse method may become unstable for the local torque optimization.

From the previous section, it is seen that the algorithm becomes unstable due to either overusing the null space, or without considering the fast increase of the independent variable $\mathbf{x}$. In this section, an approximate pseudoinverse [25] will be introduced which considers the norms of $\mathbf{y}$ and $\mathbf{x}$ simultaneously. A damping factor α is determined to give proper weighting for each part. Proper choice of α prevent the local torque optimization algorithm from reaching an unstable state.

An approximate pseudoinverse is applied to solve the Eq. (5.28) and get a better estimation of $\mathbf{y}$ which will minimize the norms of both $\mathbf{y}$ and $\mathbf{x}$ by a weighting factor α. The derivation is as follows:

Let f be the function to be optimized, i.e.,

$$f = (1-\alpha)\|H(I - J^{+}J)\ddot{\phi} + \tau_p\|^2 + \alpha\|\ddot{\phi}\|^2. \tag{5.29}$$

Therefore, the sum of $(1-\alpha)\|H(I - J^{+}J)\ddot{\phi} + \tau_p\|$ and $\alpha\|\ddot{\phi}\|$ instead of $\|\tau\|$ $= \|H(I - J^{+}J)\ddot{\phi} + \tau_p\|$ will be optimized. Two extreme cases are: 1) $\alpha = 1$, the minimum norm of acceleration criterion; 2) $\alpha = 0$, minimum norm of torque criterion. Let $A = H(I - J^{+}J)$, $\mathbf{b} = \tau_p$ and $\mathbf{x} = \ddot{\phi}$, then Eq. (5.29) becomes

$$
\begin{aligned}
(1-\alpha)\|A\mathbf{x}+\mathbf{b}\|^2+\alpha\|\mathbf{x}\|^2 &= (1-\alpha)(A\mathbf{x}+\mathbf{b})^T(A\mathbf{x}+\mathbf{b})+\alpha\mathbf{x}^T\mathbf{x} \\
&= (1-\alpha)\left[\mathbf{x}^TA^TA\mathbf{x}+\mathbf{x}^TA^T\mathbf{b}+\mathbf{b}^TA\mathbf{x}+\mathbf{b}^T\mathbf{b}\right] \\
&\quad +\alpha\mathbf{x}^T\mathbf{x}. \qquad (5.30)
\end{aligned}
$$

By taking the derivative with respect to $\mathbf{x}$, $(1-\alpha)(A^TA\mathbf{x}+A^T\mathbf{b})+\alpha\mathbf{x}=0$ is obtained and if $\alpha \neq 1$ then

$$
\mathbf{x}=(\frac{\alpha}{1-\alpha}I+A^TA)^+A^T(-\mathbf{b}). \qquad (5.31)
$$

Therefore, the required $\ddot{\phi}$ to minimize the function f is

$$
\ddot{\phi}=(\frac{\alpha}{1-\alpha}I+A^TA)^+A^T(-\tau_p), \qquad (5.32)
$$

where $A=H(I-J^+J)$. Eq. (5.32) is the damped least-squares solution of (5.27), and can be used for local optimal torque control. The damping factor chosen for the damped least-squares method affects the performance measure $I_\tau=\int_{t_0}^{t_f}\tau^T\tau dt$.

Comparisons of the performance measures, I_τ, $\max\|\tau\|$ and $I_{\dot{\theta}}$ for damped least-squares methods for 8 different values of damping factors α to trace a straight line at 45° with initial posture $(130°,-120°,120°)$ and base located at $(0.0,0.0)$ are given in Table 11. The projections of corresponding joint angle space trajectories on $\theta_1=0$ plane are shown in Fig. 43. Those performance measures for initial postures $(-45°,135°,-135°)$ and $(75°,-120°,150°)$ are given in Tables 13 and 15 respectively. Their projections on the θ_1 plane are shown in Figs. 45 and 46. The simulation results show that damped least-squares algorithm functions as well as the local torque algorithm does and avoids the dynamic singularity if proper α is used.

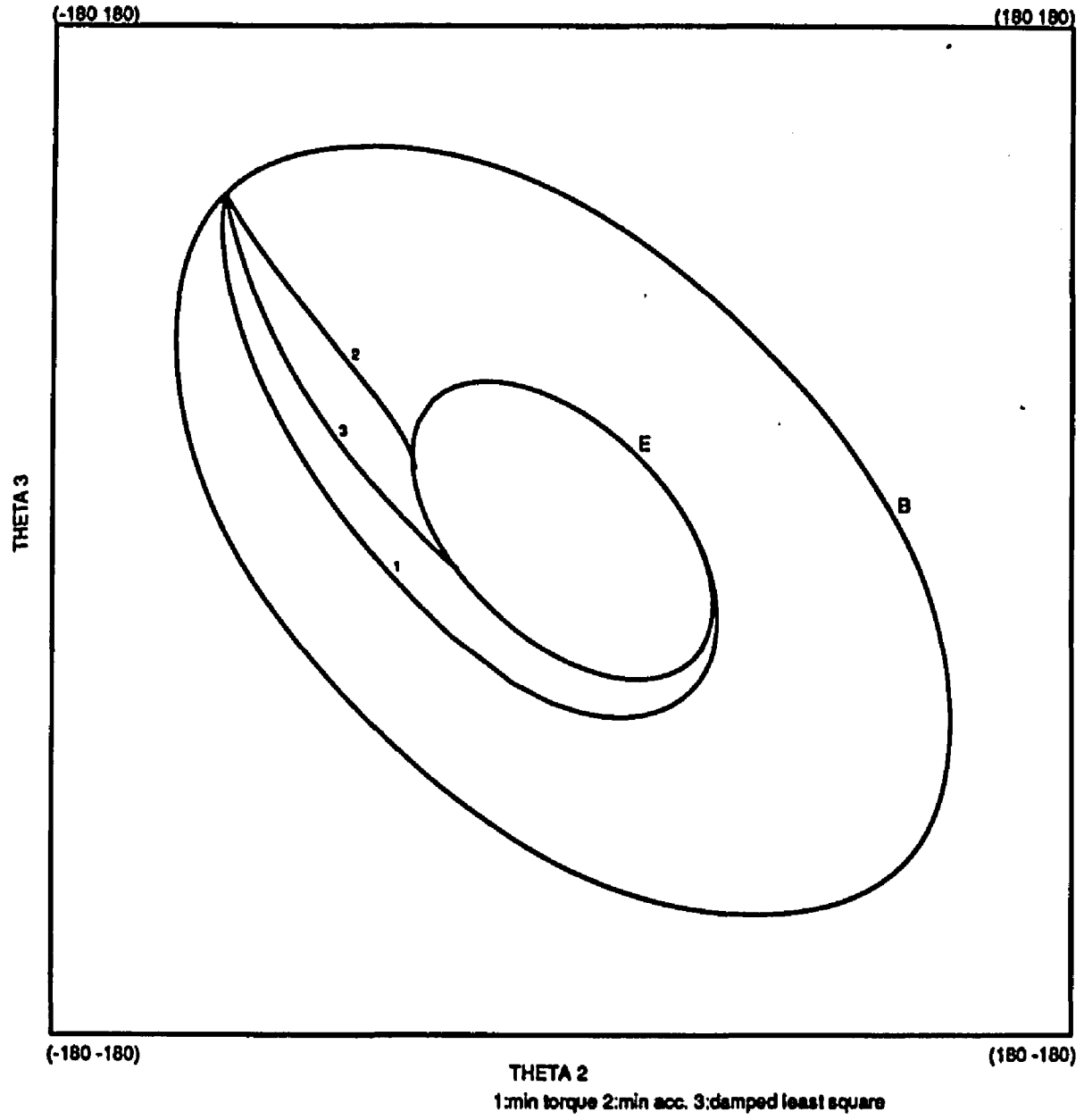

Figure 43: Projections of the joint angle space trajectories on the $\theta_1 = 0$ plane for damped least-squares algorithm to trace a straight line at 45° with damping factor changing from 0 to 1 and with initial posture $(130°, -120°, 120°)$ and base located at (0.0,0.0)

5.4.1 Choice of the Damping Factor α

A filtering or regulating algorithm is designed to adaptively regulate the parameter α so that the proper amount of null space is applied for the torque optimization. In other words, either the states with small singular value of $H[I-J^+J]$ are avoided, or very little null-space component is applied when the manipulator reaches these states. Maciejewski [25] applied the damped least-squares method with numerical filtering technique to go through the kinematic singularity. While the objective of this section is to obtain a regulating algorithm for determining the damping factor α to avoid the manipulator approaching kinetic singularity. The optimization of the required torques depends on both the configuration and the joint rate. Both kinematic and dynamic effects need to be considered during the optimization process. By considering the effectiveness and the cost of the algorithm at each instant, the damping factor α can be chosen as the ratio of effectiveness and cost. As a result, if the cost for achieving torque optimization can be maintained at a reasonable level then the algorithm remains stable. The damping factor used in the computer simulation is the ratio of $\|\ddot{\theta}_h\|$ over $\|[H(I-J^+J)][H(I-J^+J)]^+\tau_p\|$, where $\|\ddot{\theta}_h\|$, is the homogeneous part of joint acceleration and $\|[H(I-J^+J)][H(I-J^+J)]^+\tau_p\|$ is the projection of τ_p on the output vector of $H[I-(J^+J)]^+$. The numerator represents the effectiveness and the denominator is the cost paid for the algorithm at the specific instant.

Comparisons of performance measures, I_τ, $\max\|\tau\|$ and $I_{\dot{\theta}}$ for three redundancy resolution methods to trace a straight line at 45° with initial posture $(130°, -120°, 120°)$ and base located at $(0.0, 0.0)$ are given in Table 10. The projections of corresponding joint angle space trajectories on the $\theta_1 = 0$ plane are shown in Fig. 44. Those performance measures for initial postures $(-45°, 135°, -135°)$

Table 10: The performance measures for three redundancy resolution methods to trace a straight line at 45° with initial posture (130°, −120°, 120°) and base located at (0.0,0.0)

trajectory	control scheme	$\max \|\tau\|$	$\int_{t_0}^{t_f} \tau^T \tau dt$	$\int_{t_0}^{t_f} \dot{\theta}^T \dot{\theta} dt$
1	minimum torque	212.96	829.27	38.49
2	minimum acceleration	4.06	9.00	2.92
3	damped least squares	2.39	2.41	8.85

and (75°, −120°, 150°) are given in Tables 12 and 14 respectively. Their projections on the θ_1 plane are shown in Figs. 47 and 48.

The comparisons of norm of required torques, singular value of the matrix $H[I - J^+J]$, the product of the singular value of $H[I - J^+J]$ and norm of τ_p also the damping factor for two redundancy resolution methods, minimum norm of torque and damped least-squares algorithms, to trace a straight line trajectory are given in Figs. 50 to 53, respectively. The geometry of the manipulator as functions of time are given in Figs. 40 and 49. These figures show that how the damped least-squares method makes the manipulator avoid passing through the small singular value regions of the matrix $H[I - J^+J]$ and improves the performance measure I_τ.

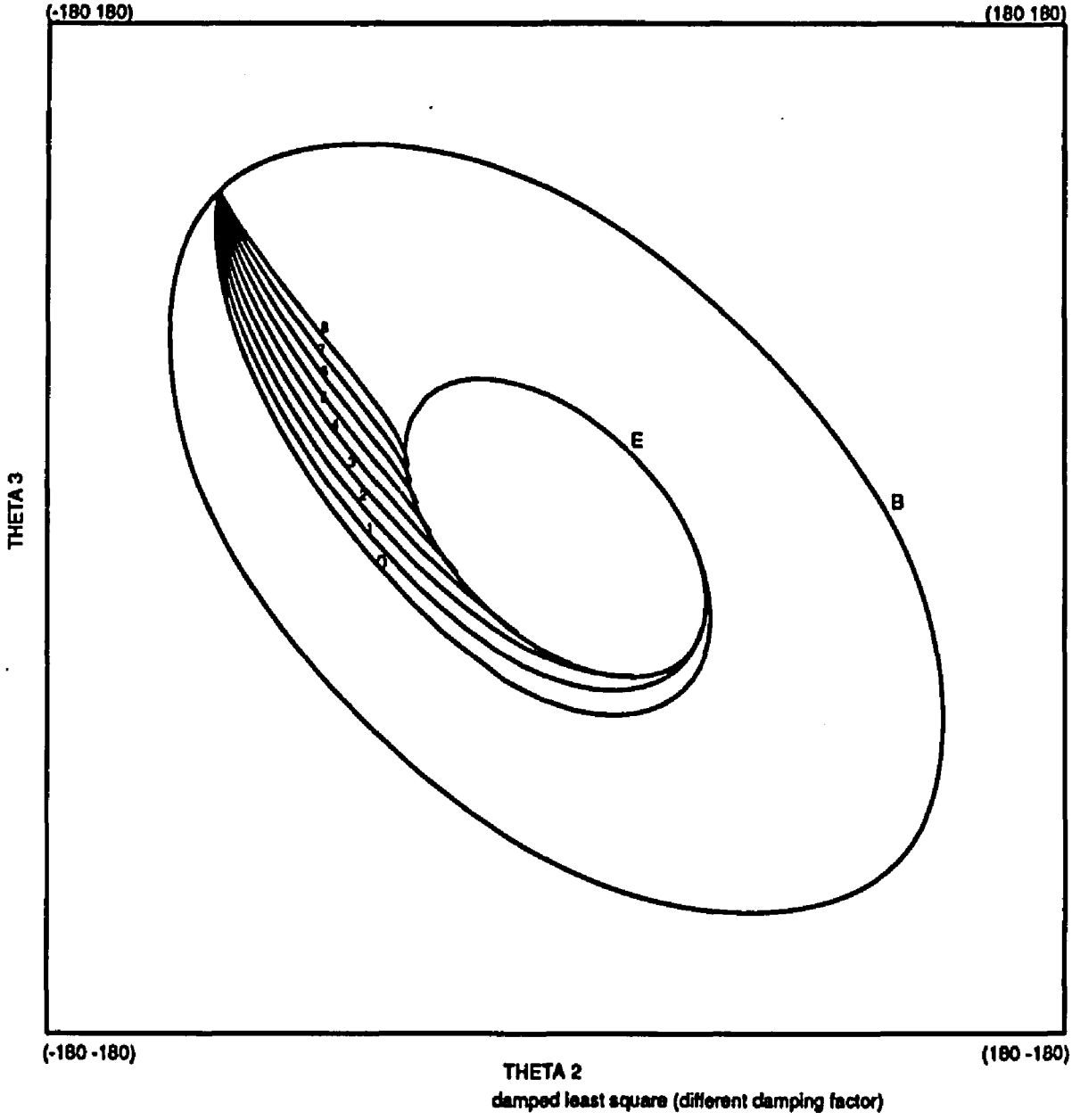

Figure 44: Projections of the joint angle space trajectories on the $\theta_1 = 0$ plane for minimum torque, minimum acceleration and damped least-squares algorithms to trace a straight line at 45° with initial posture $(130°, -120°, 120°)$ and base located at (0.0,0.0)

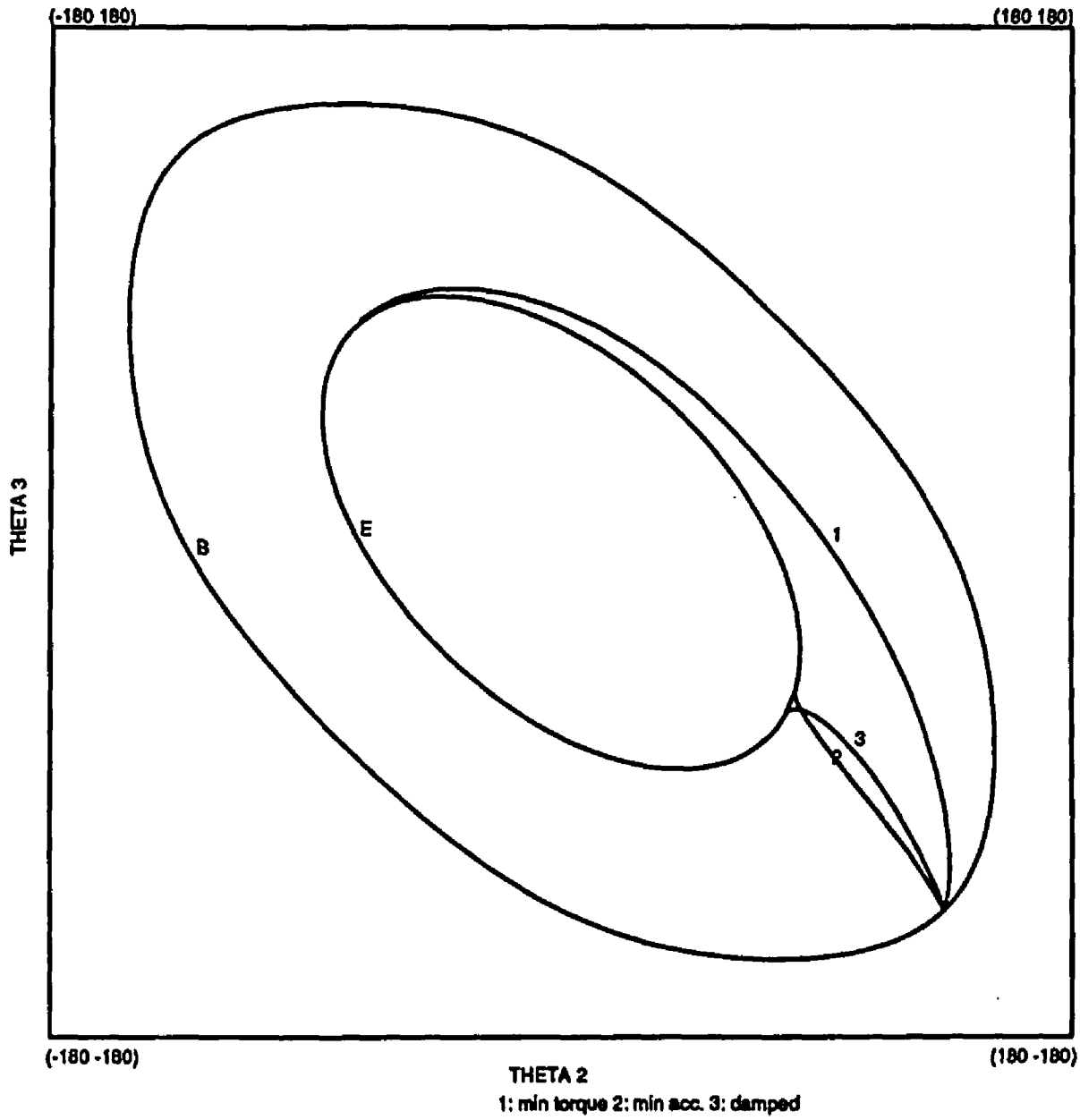

Figure 45: Projections of the joint angle space trajectories on the $\theta_1 = 0$ plane for damped least-squares algorithms with damping factor changing from 0 to 1 to trace a straight line at 45° with initial posture $(-45°, 135°, -135°)$ and base located at (0.0,0.0)

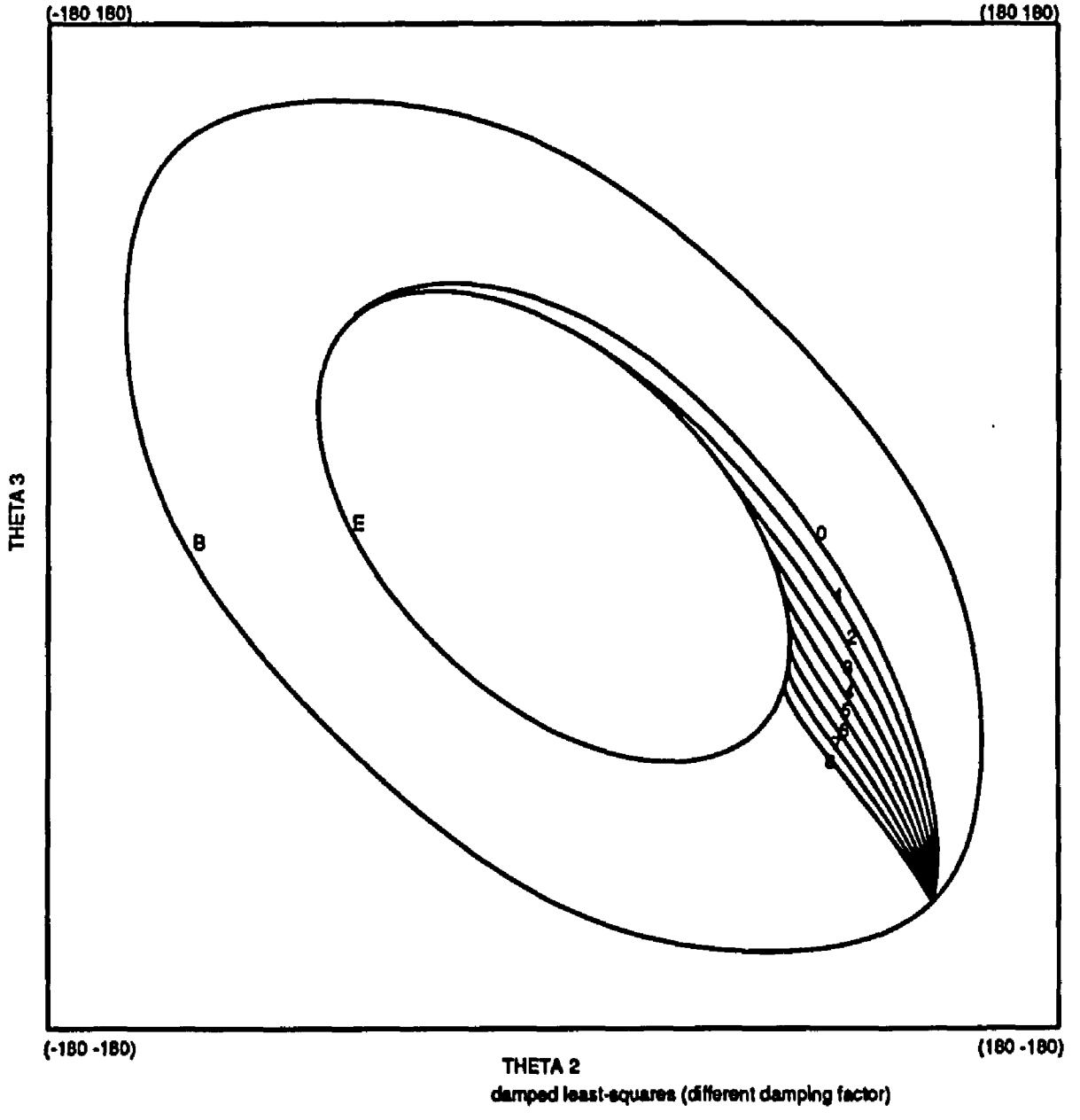

Figure 46: Projections of the joint angle space trajectories on the $\theta_1 = 0$ plane for damped least-squares algorithm with damping factor changing from 0 to 1 to trace a straight line at 45° with initial posture $(75°, -120°, 150°)$ and base located at (0.0,0.0)

Table 11: Effects of damping factor on the performance measures for damped least-square torque optimization method to trace a straight line at 45° with initial posture (130°, −120°, 120°) and base located at (0.0,0.0)

Trajectory	damping factor	max $\|\tau\|$	$\int_{t_0}^{t_f} \tau^T \tau dt$	$\int_{t_0}^{t_f} \dot{\theta}^T \dot{\theta} dt$
0	0.000	212.96	829.27	38.49
1	0.125	34.80	106.30	21.56
2	0.250	12.23	26.87	13.92
3	0.375	2.33	1.73	7.98
4	0.500	3.51	3.79	5.27
5	0.625	3.67	4.88	4.13
6	0.750	3.65	5.85	3.51
7	0.875	3.78	7.15	3.13
8	1.000	4.06	9.01	2.92

Table 12: The performance measures for three redundancy resolution methods to trace a straight line at 45° with initial posture (−45°, 135°, −135°) and base located at (0.0,0.0)

trajectory	control scheme	max $\|\tau\|$	$\int_{t_0}^{t_f} \tau^T \tau dt$	$\int_{t_0}^{t_f} \dot{\theta}^T \dot{\theta} dt$
1	minimum torque	53.75	166.67	33.38
2	minimum acceleration	2.25	5.49	1.92
3	damped least squares	1.47	2.07	2.16

Table 13: Effects of damping factor on the performance measures for damped least-squares torque optimization method to trace a straight line at 45° with initial posture $(-45°, 135°, -135°)$ and base located at (0.0,0.0)

trajectory	damping factor	max $\|\tau\|$	$\int_{t_0}^{t_f} \tau^T \tau dt$	$\int_{t_0}^{t_f} \dot{\theta}^T \dot{\theta} dt$
0	0.000	53.75	166.67	33.38
1	0.125	5.85	8.34	14.55
2	0.250	2.49	2.62	5.90
3	0.375	2.32	2.98	3.99
4	0.500	2.15	3.30	3.10
5	0.625	2.09	3.72	2.58
6	0.750	2.10	4.24	2.35
7	0.875	2.16	4.84	2.05
8	1.000	2.25	5.49	1.92

Table 14: The performance measures for three redundancy resolution methods to trace a straight line at 45° with initial posture $(75°, -120°, 150°)$ and base located at (0.0,0.0)

trajectory	control scheme	max $\|\tau\|$	$\int_{t_0}^{t_f} \tau^T \tau dt$	$\int_{t_0}^{t_f} \dot{\theta}^T \dot{\theta} dt$
1	minimum torque	1.57	2.57	3.65
2	minimum acceleration	2.26	2.83	5.27
3	damped least squares	1.60	2.52	3.67

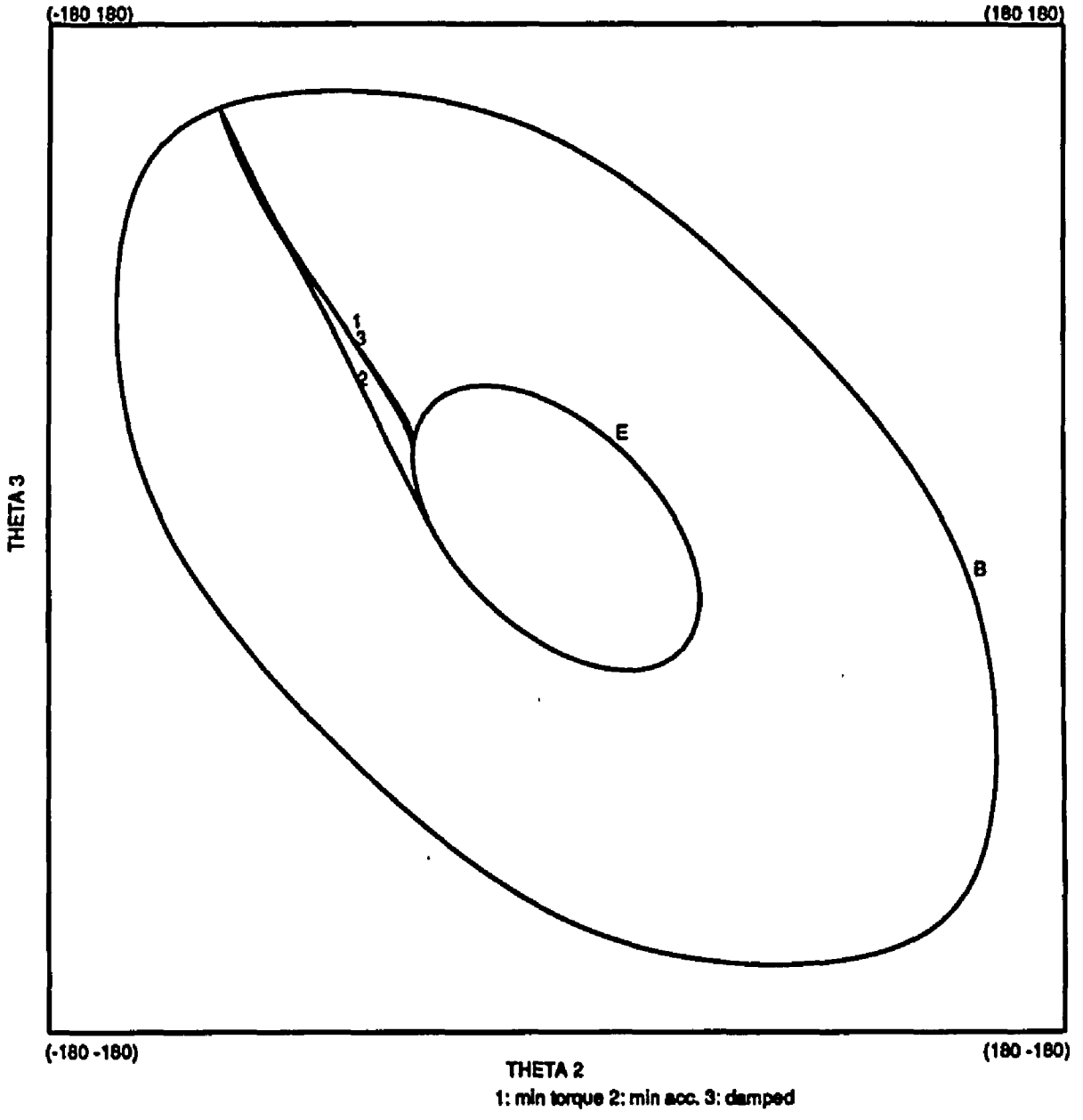

Figure 47: Projections of the joint angle space trajectories on the $\theta_1 = 0$ plane for minimum torque, minimum acceleration and damped least-squares algorithms to trace a straight line at 45° with initial posture $(-45°, 135°, -135°)$ and base located at (0.0,0.0)

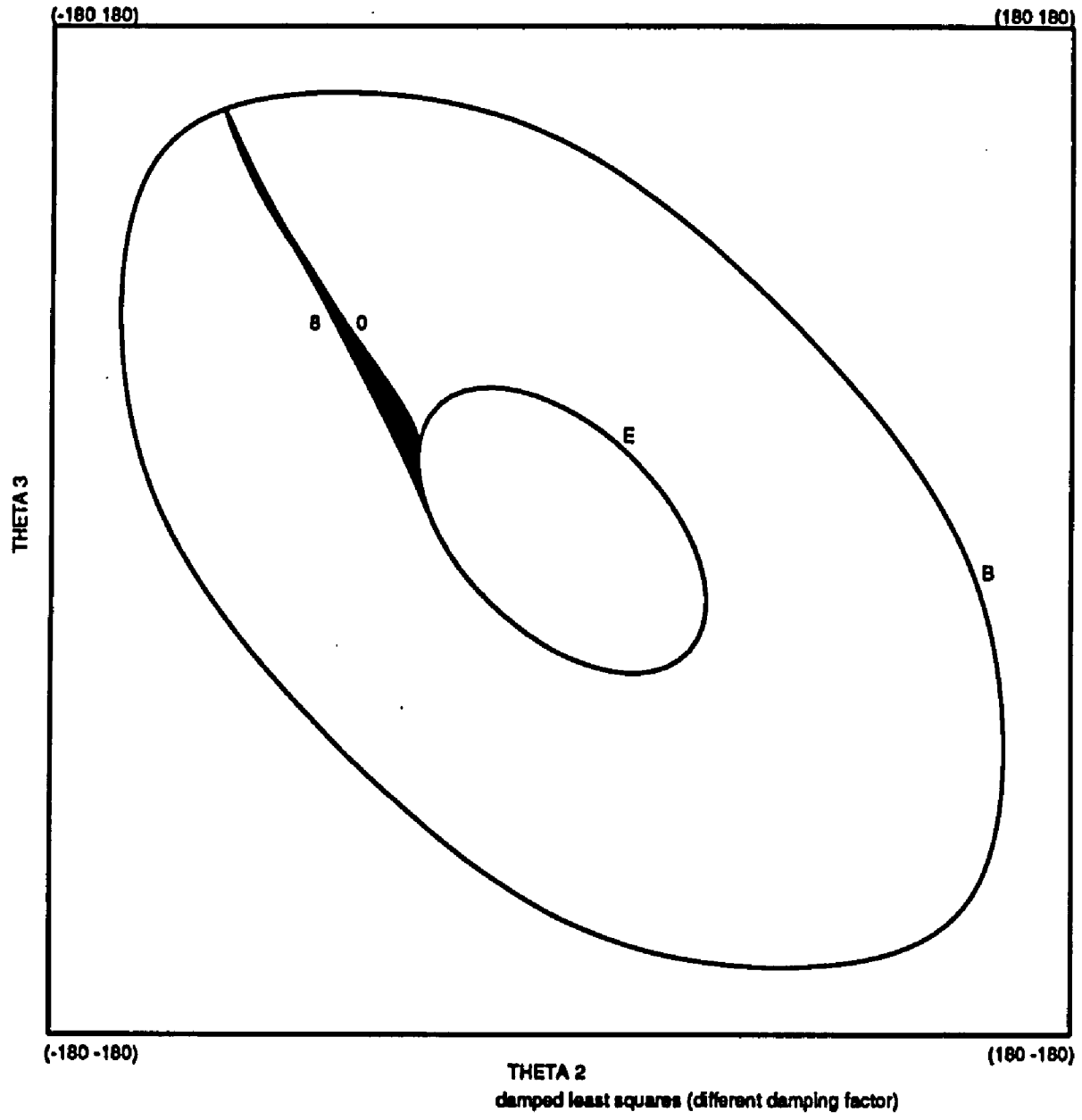

Figure 48: Projections of the joint angle space trajectories on the $\theta_1 = 0$ plane for minimum torque, minimum acceleration and damped least-squares algorithms to trace a straight line at 45° with initial posture $(75°, -120°, 150°)$ and base located at (0.0,0.0)

Table 15: Effects of damping factor on the performance measures for damped least-squares torque optimization method to trace a straight line at 45° with initial posture (75°, −120°, 150°) and base located at (0.0,0.0)

trajectory	damping factor	max $\|\tau\|$	$\int_{t_0}^{t_f} \tau^T \tau dt$	$\int_{t_0}^{t_f} \dot{\theta}^T \dot{\theta} dt$
0	0.000	1.58	2.57	3.65
1	0.125	1.60	2.56	3.70
2	0.250	1.64	2.56	3.76
3	0.375	1.69	2.59	3.86
4	0.500	1.77	2.68	4.00
5	0.625	1.86	2.80	4.18
6	0.750	1.98	2.92	4.45
7	0.875	2.11	2.89	4.81
8	1.000	2.26	2.83	5.27

5.5 Choice of a Proper Initial State

Another possible solution for resolving the instability problem in local torque optimization algorithm is to choose a proper initial state for starting the job. The required torques depend both on the initial state and the end effector's motion. For a particular trajectory, an optimal configuration and joint rate should be sought. Using this optimal configuration with proper joint rate for starting the given job, an optimal performance measure can be achieved. How the initial state affects the torque optimization algorithm is discussed below.

It is known that the state $(\theta, \dot{\theta})$ plays an important role in the optimization of a performance measure. An initial state, either initial posture or joint rate can be chosen to achieve a better performance measure. Two parts are included: one is to choose a proper initial configuration, and the other is to choose a proper amount of initial joint rate (in null space).

5.5.1 A Proper Initial Configuration

A straight-forward method for finding the best initial configuration is by taking all the possible configurations in the joint angle space which are associated with the specified end effector's position in the cartesian space as initial postures for starting the job and comparing their performance measures. The procedure used to generate this set of configurations was described in chapter two. A stable program for generating the possible joint configurations has been written by Chirco [5]. An example of finding the best posture for global torque performance measure can be searched by starting with each of these configurations to trace a given trajectory and comparing the required torques.

A list of performance measures, τ_{max}, I_τ and $I_{\dot{\theta}}$ for minimum norm of torque, damped least-squares and minimum norm of acceleration controls to trace the

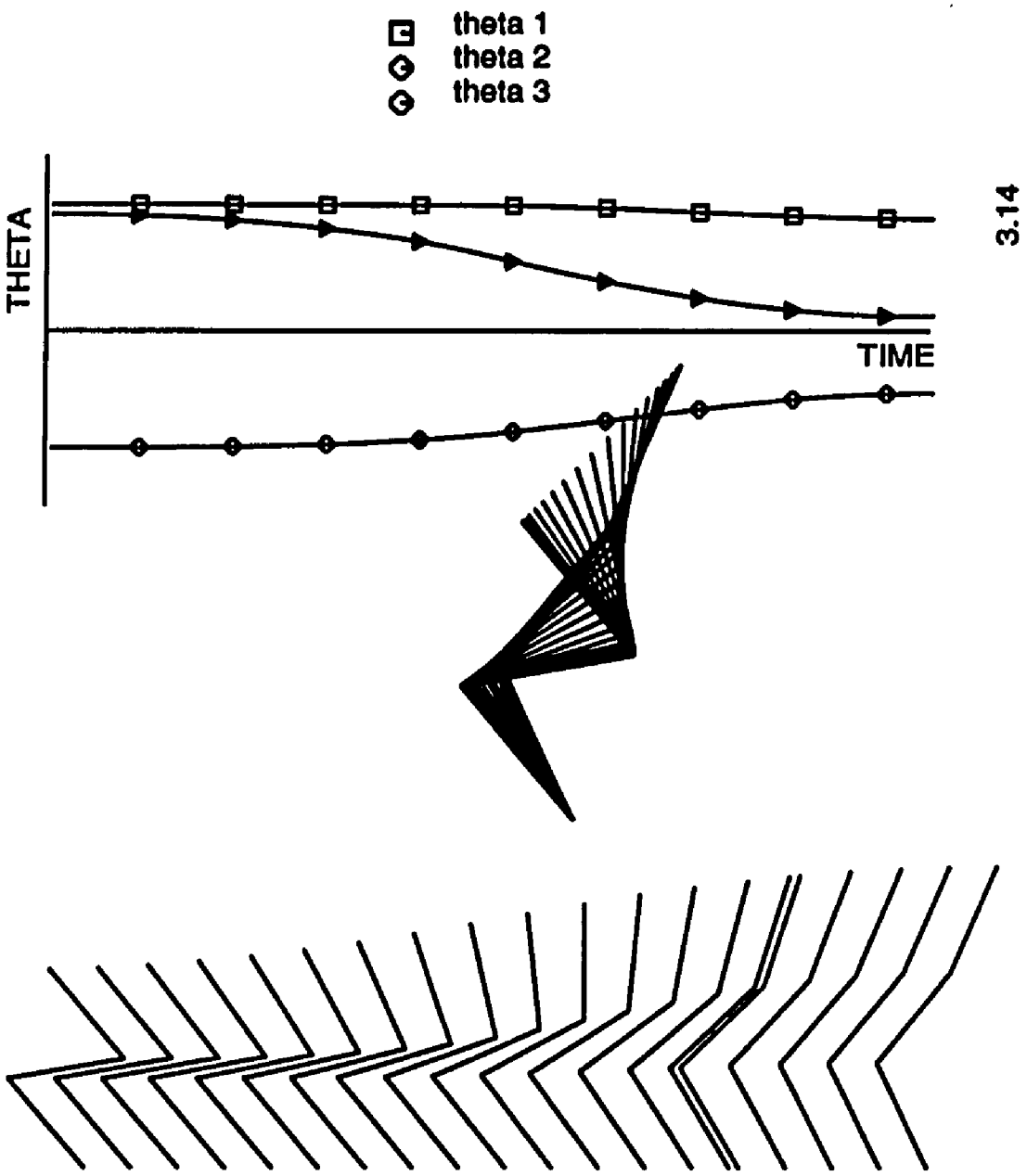

Figure 49: The joint angles and geometries of the manipulator for tracing a straight line at 45° with starting posture (130°, −120°, 120°) and base located at (0.0,0,0) for damped least-squares method

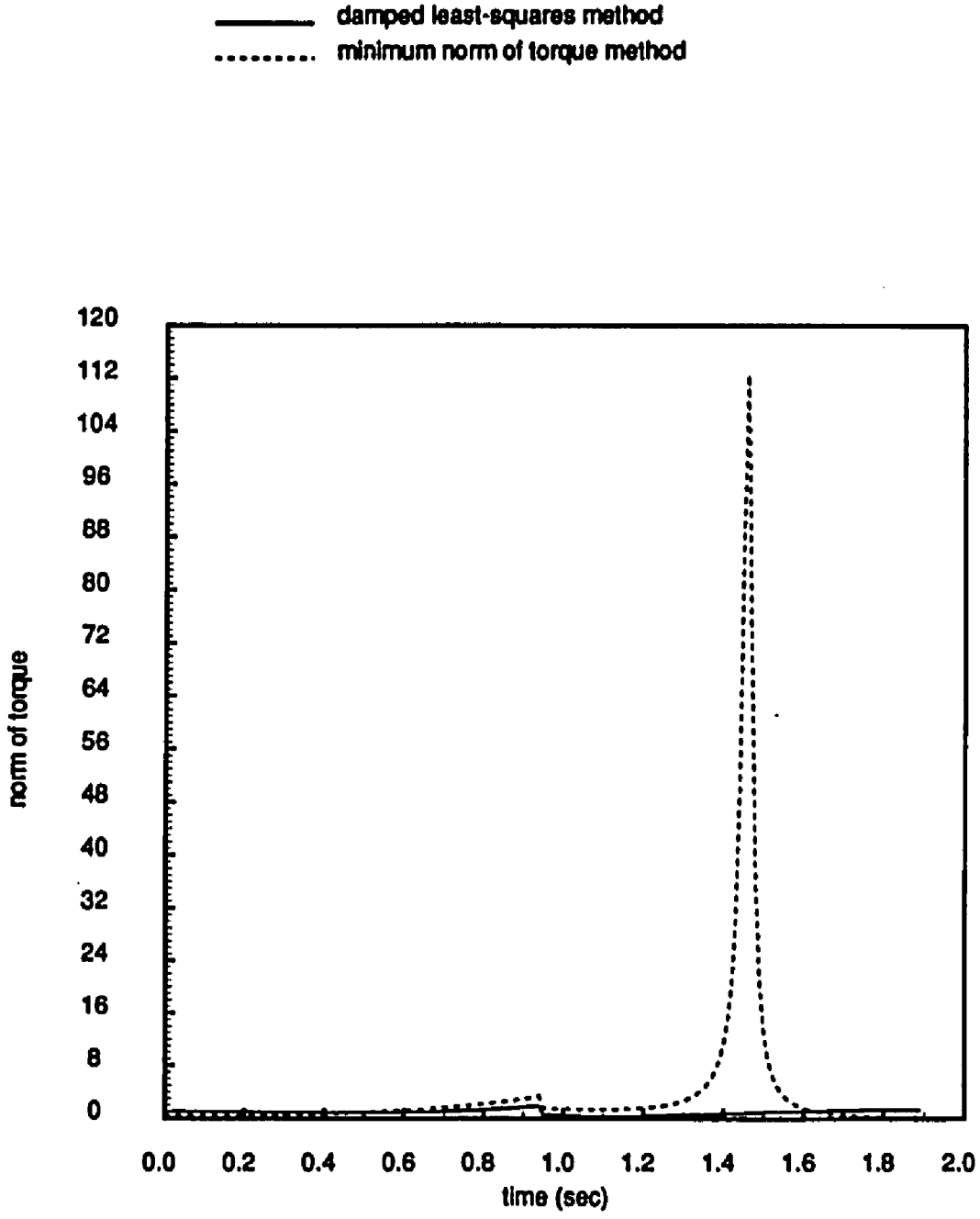

Figure 50: The norm of torques for tracing a straight line at 45° with starting posture (130°, −120°, 120°) and base located at (0.0,0.0) for minimum torque and damped least-squares methods

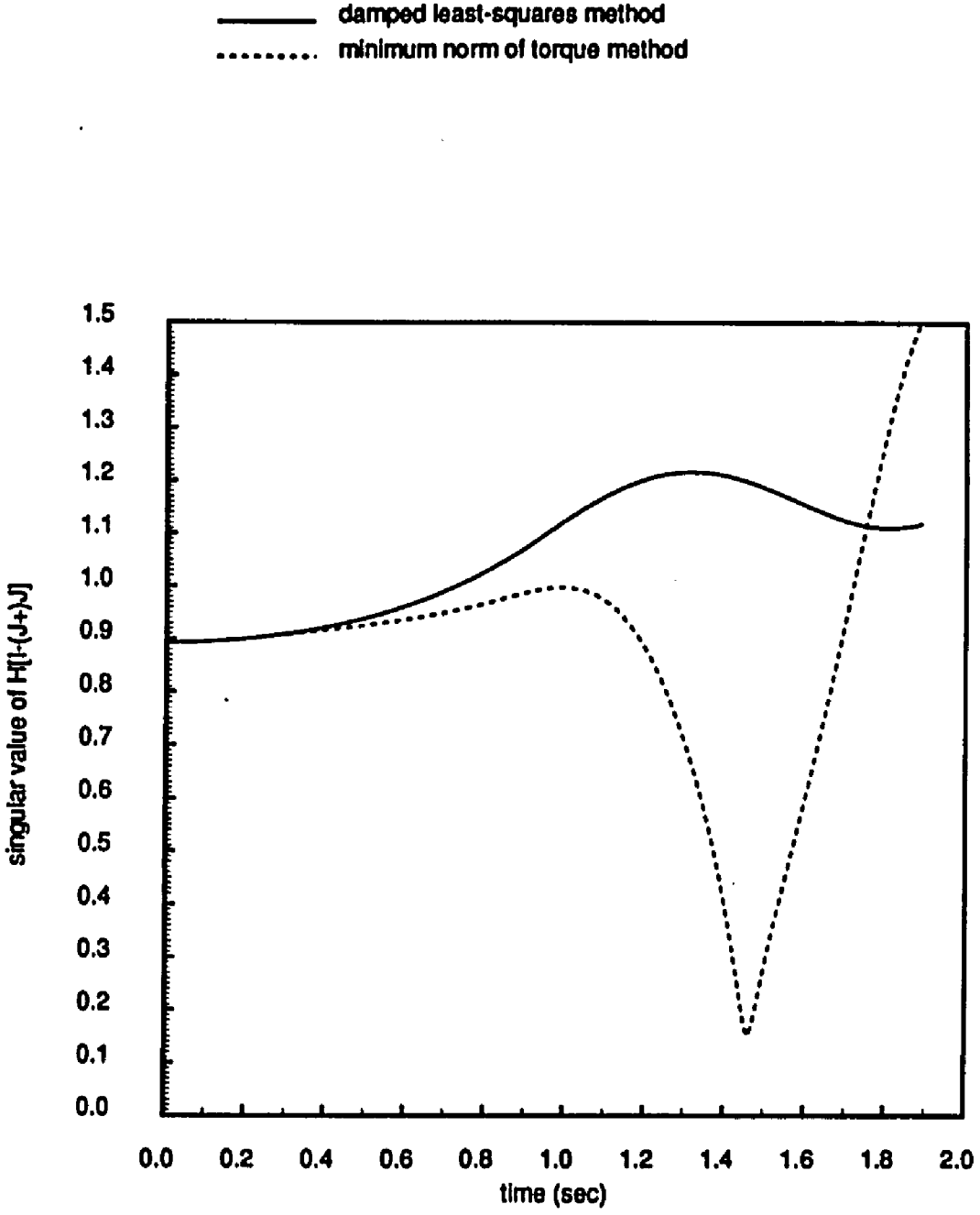

Figure 51: The singular value of $H(I - J^{+}J)$ for a straight line at 45° with starting posture (130°, −120°, 120°) and base located at (0.0,0.0) for minimum torque and damped least-squares methods

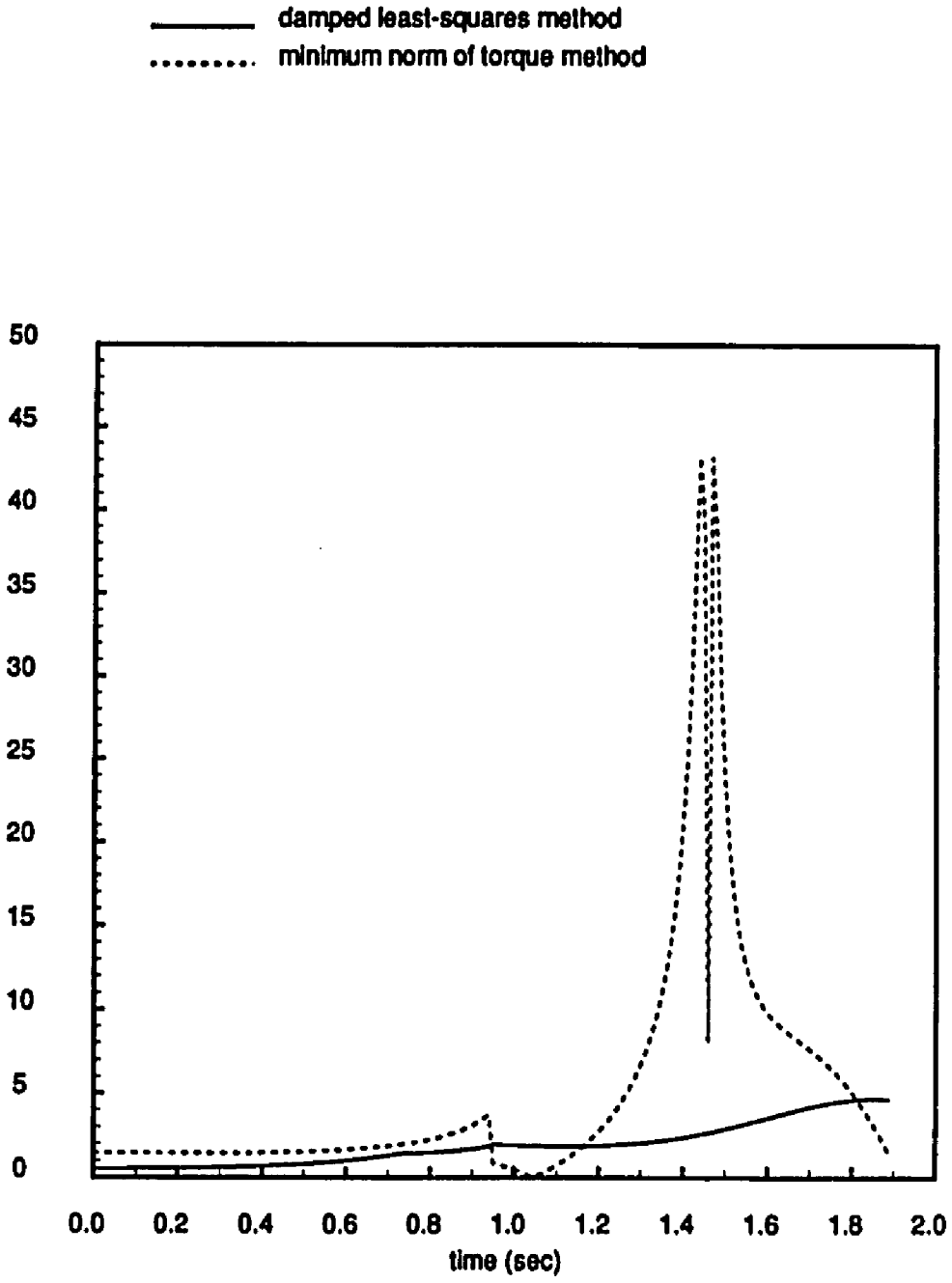

Figure 52: The product of the singular value of $H(I - J^{+}J)$ and $\| - \tau_p \|$ for a straight line at 45° with starting posture $(130°, -120°, 120°)$ and base located at (0.0,0.0) for minimum torque and damped least-squares methods

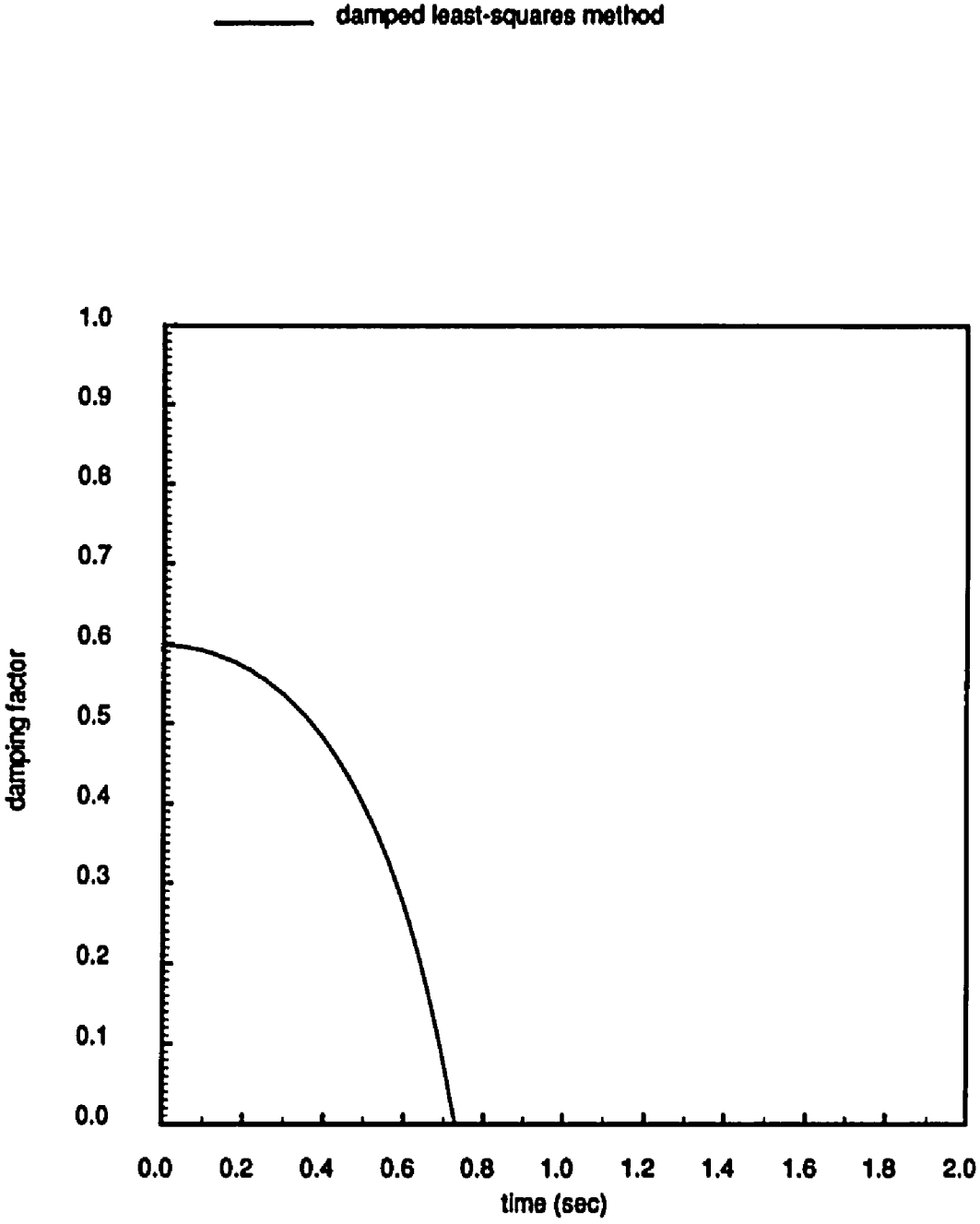

Figure 53: The damping factors for tracing a straight line at 45° with starting posture (130°, −120°, 120°) and base located at (0.0,0,0) for damped least-squares method

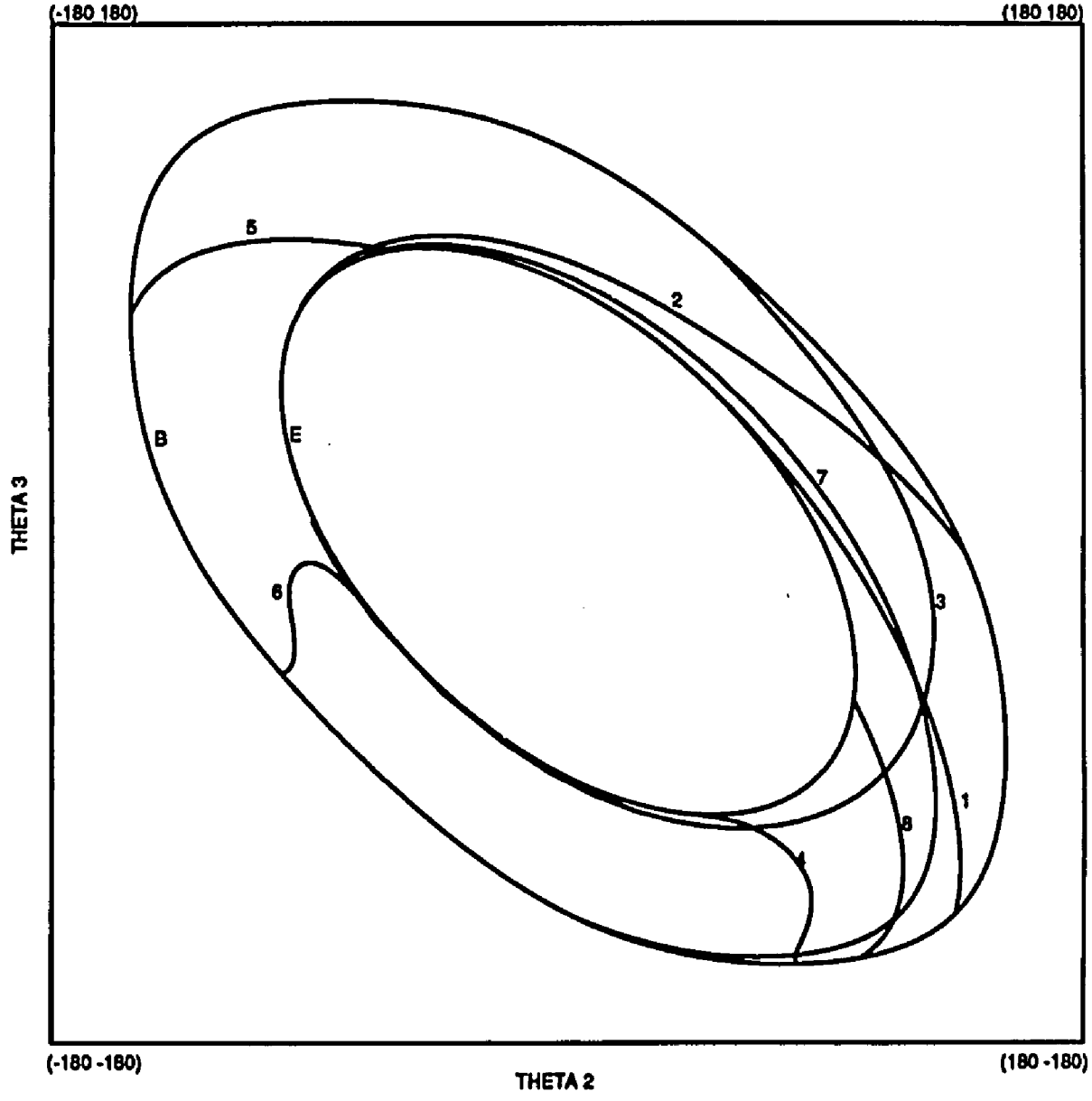

Figure 54: The projections of joint angle space trajectories on $\theta_1 = 0$ plane for a straight line at 45^o with initial postures given in Table 16, trajectories 3 and 7 pass through the small singular value region shown in Fig. 38

Table 16: The performance measures for minimum norm of torque control to trace a straight line at 45° with base located at (0.0,0.0) and $t_f = 1.822$ sec for 8 different starting postures

Trajectory	Initial θ			Cost functions		
	θ_1	θ_2	θ_3	$\max \|\tau\|$	$\int_{t_0}^{t_f} \tau^T \tau dt$	$\int_{t_0}^{t_f} \dot{\theta}^T \dot{\theta} dt$
1 (1)	−45.00°	135.00°	−135.00°	5.15	4.62	10.96
2 (39)	−122.32°	138.42°	−7.26°	8.23	26.91	23.33
3 (76)	−75.32°	50.82°	99.97°	238.99	1846.07	72.60
4 (114)	−17.32°	79.40°	−152.60°	2.95	4.01	1.62
5 (157)	59.68°	−152.60°	76.7°	3.30	6.03	2.52
6 (189)	75.68°	−100.32°	−50.41°	4.94	5.51	1.74
7 (228)	10.68°	3.40°	−136.65°	59.69	332.75	53.56
8 (254)	−25.32°	102.04°	−150.42°	1.92	2.02	2.13

straight line at 45° with base located at (0.0, 0.0) for 8 different initial postures are given in Tables 16 to 18, respectively. The projections of corresponding joint angle space trajectories on $\theta_1 = 0$ plane are shown in Fig. 54. The same performance measures by using minimum norm of torque control to trace the circular trajectory with base located at (0.0, 0.0) for 6 different initial postures are given in Table 19. The projections of those corresponding joint angle space trajectories on $\theta_1 = 0$ plane are shown in Fig. 63.

These figures and tables show that some starting configurations go through small singular value of $[H(I - J^+J)]^+$ region with high joint velocities while others do not. It is seen that for the same algorithm and the same starting end effector's position and motion in the cartesian space, some configurations becomes unstable and others give stable results. They illustrate the importance of the choice of starting postures. Fig. 55 gives all the possible configurations which correspond to the same end effector position, (1.414, −0.414). Fig. 56 shows the possible

Table 17: The performance measures for damped least-squares control to trace a straight line at 45° with base located at (0.0,0.0) and $t_f = 1.822$ sec for 8 different starting postures

Trajectory	Initial θ			Cost functions		
	θ_1	θ_2	θ_3	$\max \|\tau\|$	$\int_{t_0}^{t_f} \tau^T \tau dt$	$\int_{t_0}^{t_f} \dot{\theta}^T \dot{\theta} dt$
1 (1)	−45.00°	135.00°	−135.00°	1.77	1.72	1.77
2 (39)	−122.32°	138.42°	−7.26°	3.91	15.48	1.58
3 (76)	−75.32°	50.82°	99.97°	5.50	15.68	2.65
4 (114)	−17.32°	79.40°	−152.60°	3.75	5.02	1.17
5 (157)	59.68°	−152.60°	76.7°	2.56	6.16	1.11
6 (189)	75.68°	−100.32°	−50.41°	3.27	6.74	0.71
7 (228)	10.68°	3.40°	−136.65°	7.80	23.75	0.91
8 (254)	−25.32°	102.04°	−150.42°	1.90	1.86	1.27

Table 18: The performance measures for minimum acceleration control to trace a straight line at 45° with base located at (0.0,0.0) and $t_f = 1.822$ sec for 8 different starting postures

Trajectory	Initial θ			Cost functions		
	θ_1	θ_2	θ_3	$\max \|\tau\|$	$\int_{t_0}^{t_f} \tau^T \tau dt$	$\int_{t_0}^{t_f} \dot{\theta}^T \dot{\theta} dt$
1 (1)	−45.00°	135.00°	−135.00°	1.80	4.42	1.32
2 (39)	−122.32°	138.42°	−7.26°	4.14	17.84	1.53
3 (76)	−75.32°	50.82°	99.97°	4.43	31.87	1.03
4 (114)	−17.32°	79.40°	−152.60°	4.20	7.00	1.12
5 (157)	59.68°	−152.60°	76.7°	2.60	7.89	1.03
6 (189)	75.68°	−100.32°	−50.41°	3.24	6.80	0.71
7 (228)	10.68°	3.40°	−136.65°	7.76	24.57	0.88
8 (254)	−25.32°	102.04°	−150.42°	2.67	2.67	1.26

initial joint rates in null space, i.e., contributing no movement to the end effector. These two figures provide all the feasible initial postures and initial joint rates for performing the job.

The performance measure I_T for the 3–link manipulator to trace a straight line trajectory by using minimum norm of joint acceleration, minimum norm of joint torque and damped least-squares controls as a function of initial postures corresponding to homogeneous configurations of the end effector position $(1.414, -0.414)$ are given in Figs. 57 and 58. These figures indicate that proper initial postures are important for achieving a good performance measure for all of these control schemes.

The joint angles and the manipulator geometries as functions of time for the trajectories 3 and 8 in Table 16 are shown in Figs. 59 and 61. The torque required at each joint and the corresponding norm of joint torque for the above trajectories are also shown in Figs. 60 and 62.

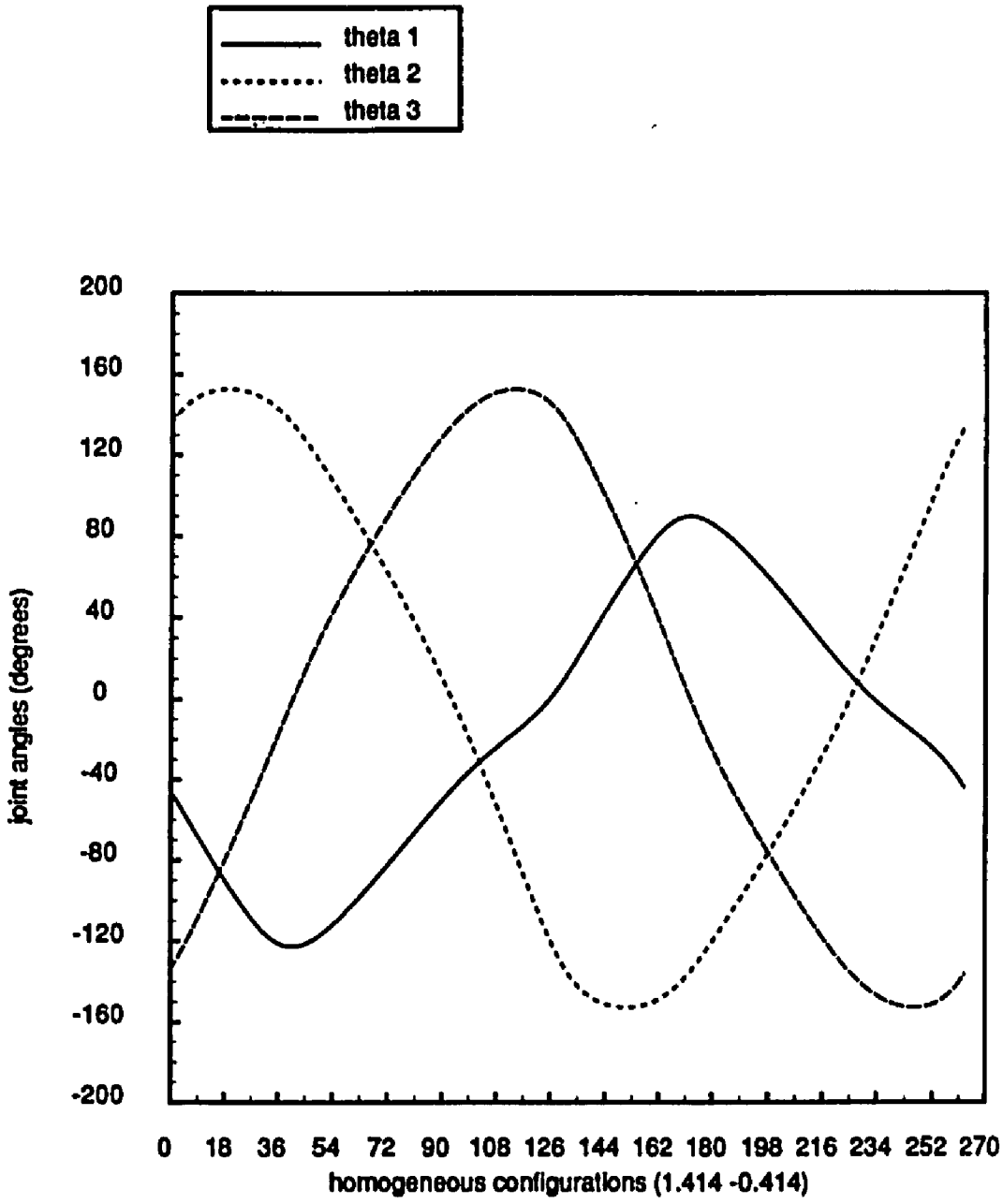

Figure 55: The homogeneous configurations of the starting end effector's position $(1.414, -0.414)$ with base located at (0.0,0.0)

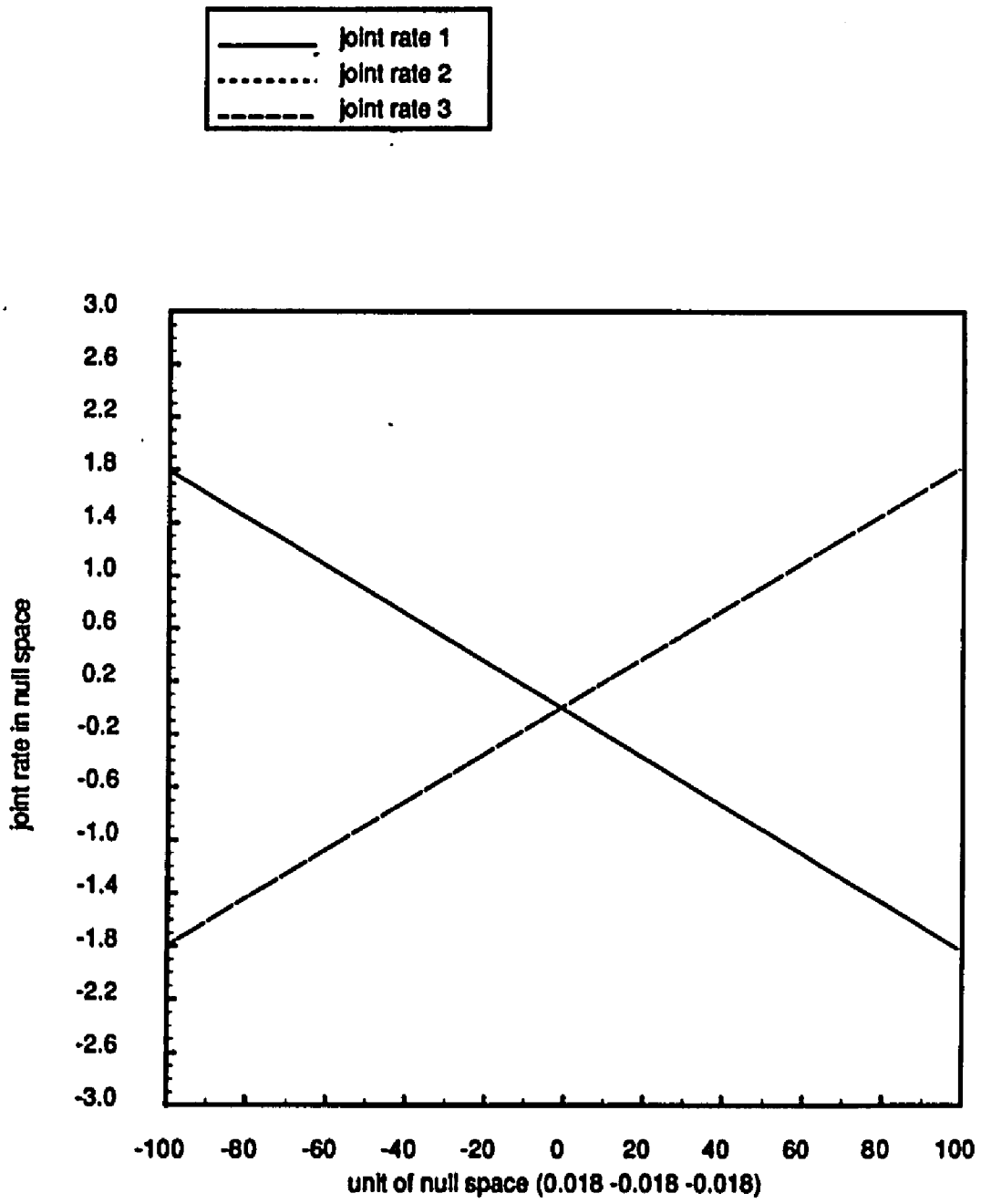

Figure 56: The initial joint rates in the null space for an given initial posture $(-45.0°, 135.0°, -135.0°)$ and base located at (0.0,0.0)

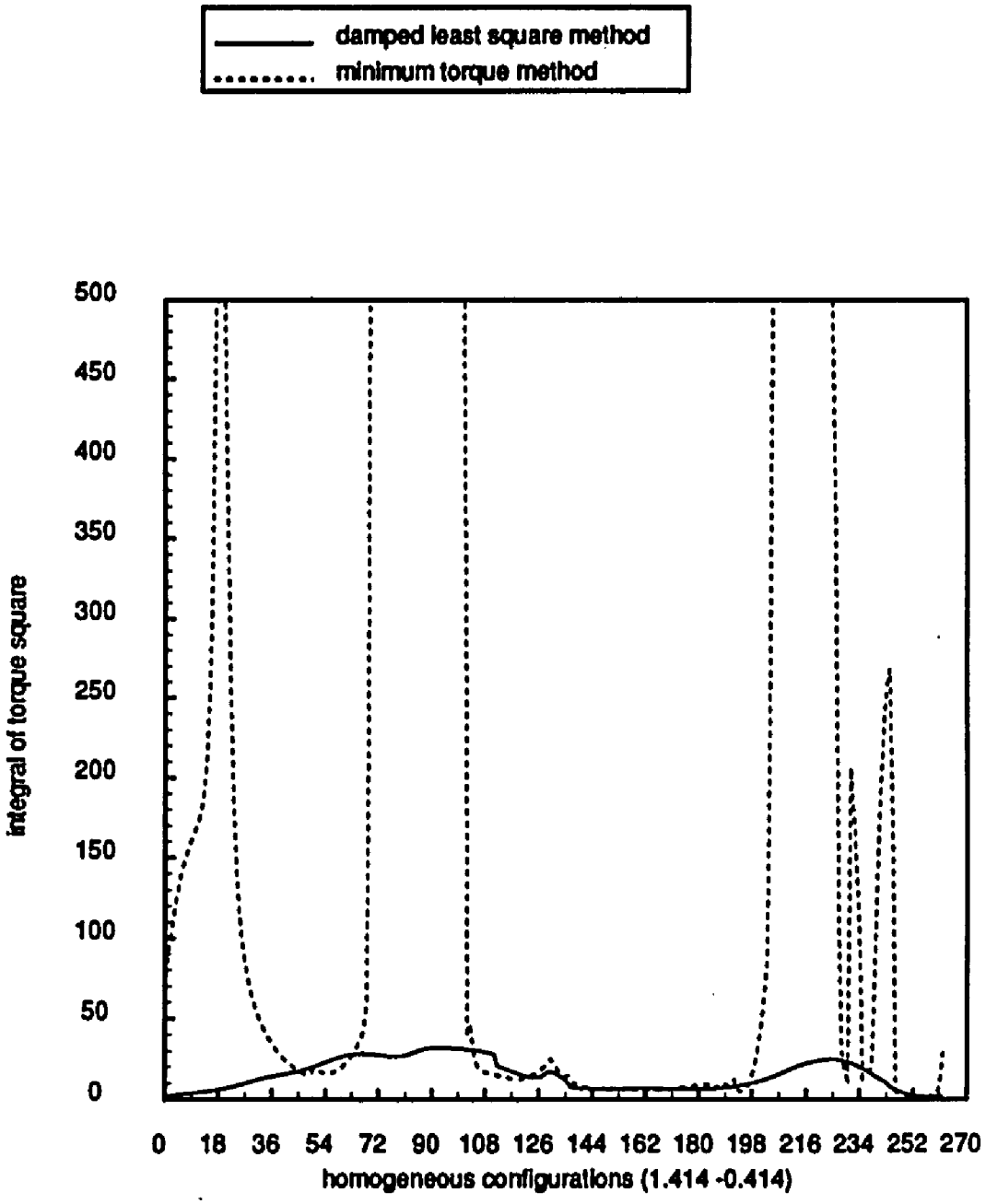

Figure 57: The performance measure, I_T, for minimum norm of torque and damped least-squares methods to trace a straight line at 45° with base located at (0.0,0.0) and $t_f = 1.9$ sec as a function of initial postures corresponding to homogeneous configurations of the end effector position $(1.414, -0.414)$

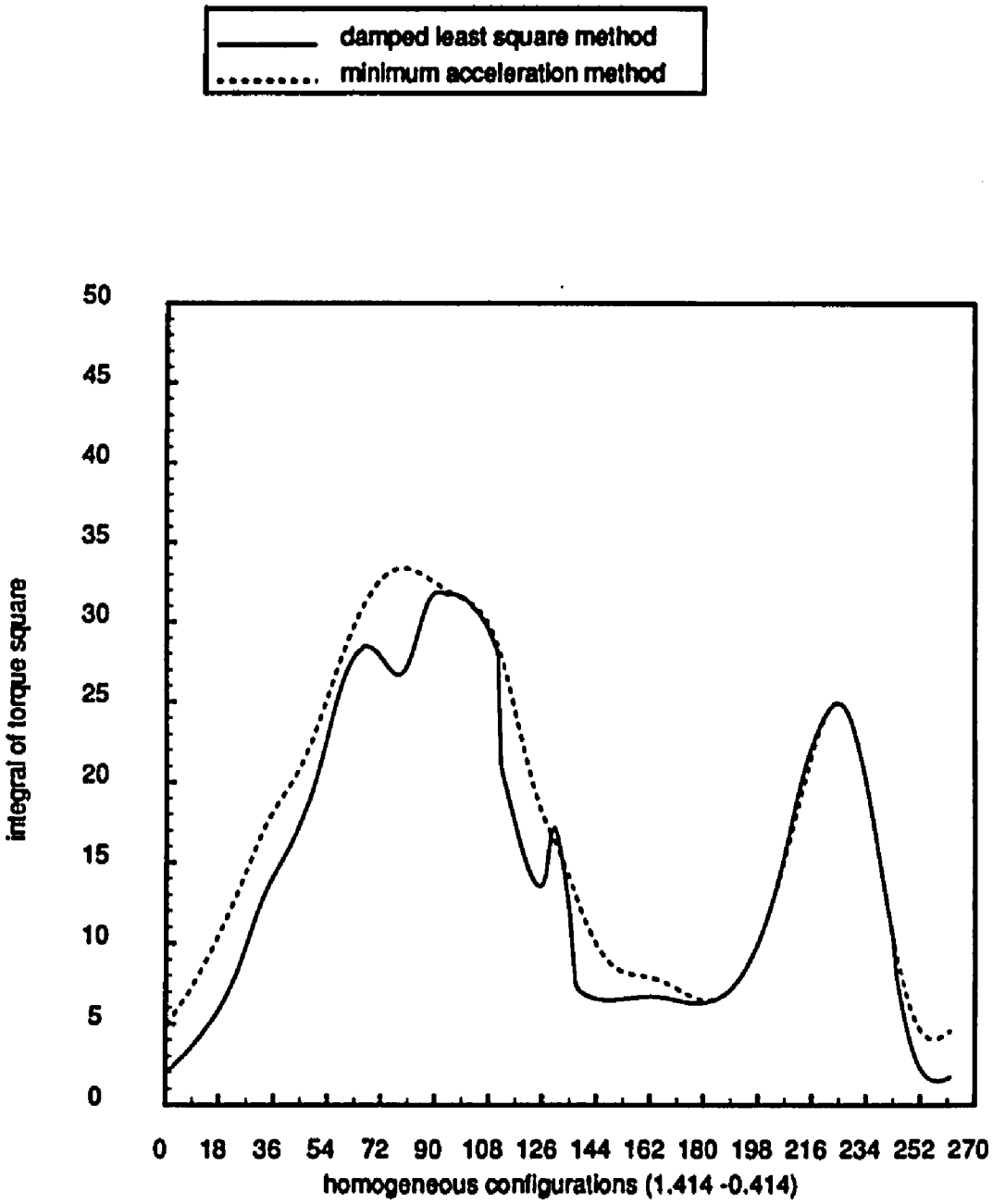

Figure 58: The performance measure, I_T, for minimum norm of joint acceleration and damped least-squares methods to trace a straight line at 45° with base located at (0.0,0.0) and $t_f = 1.9$ sec as a function of initial postures corresponding to homogeneous configurations of the end effector position $(1.414, -0.414)$

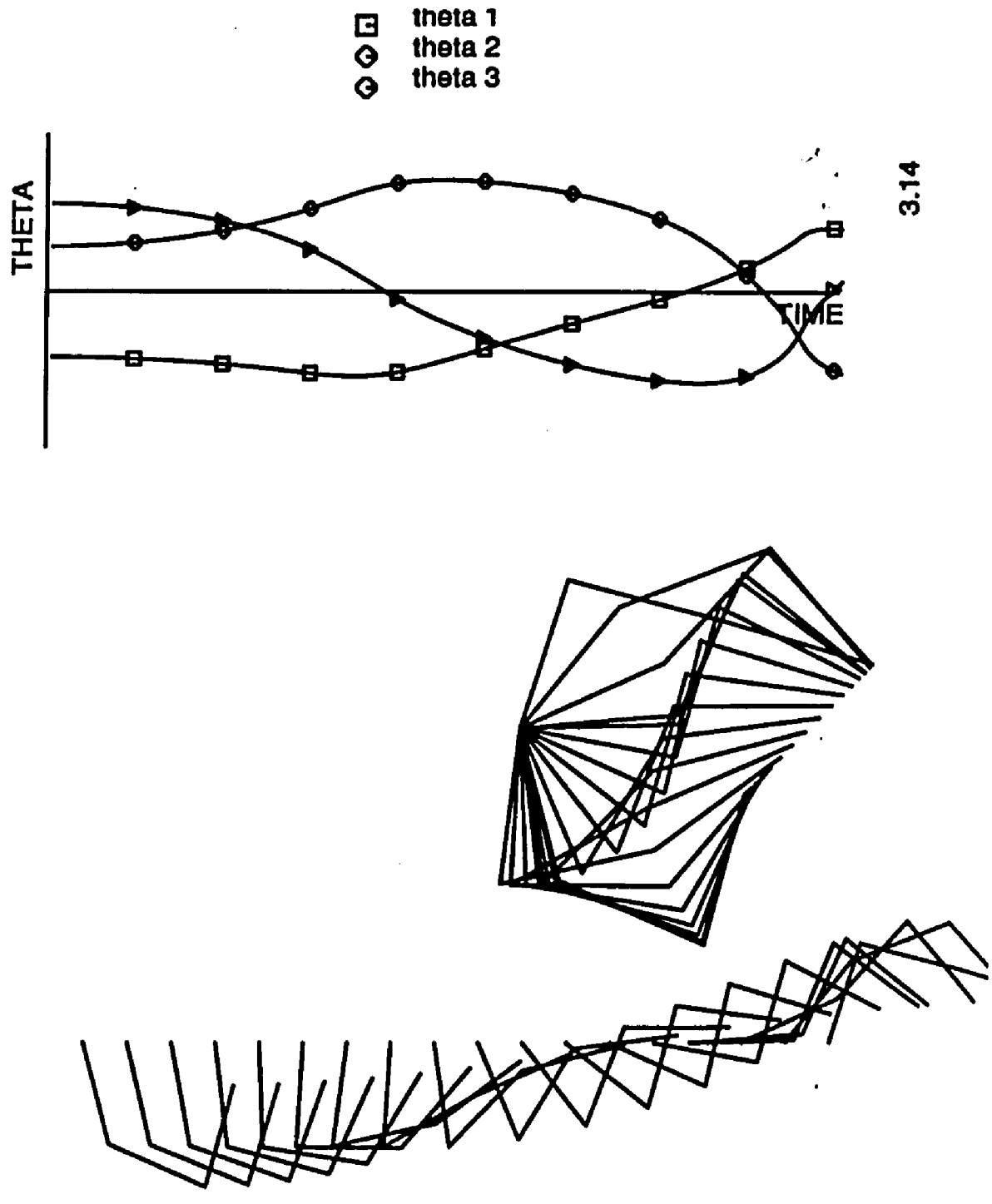

Figure 59: The joint angles and geometries as functions of time, tracing a straight line trajectory with initial posture $(-75.32°, 50.82°, 99.97°)$ corresponding to trajectory no. 3 (T=1.822 sec) in Table 16

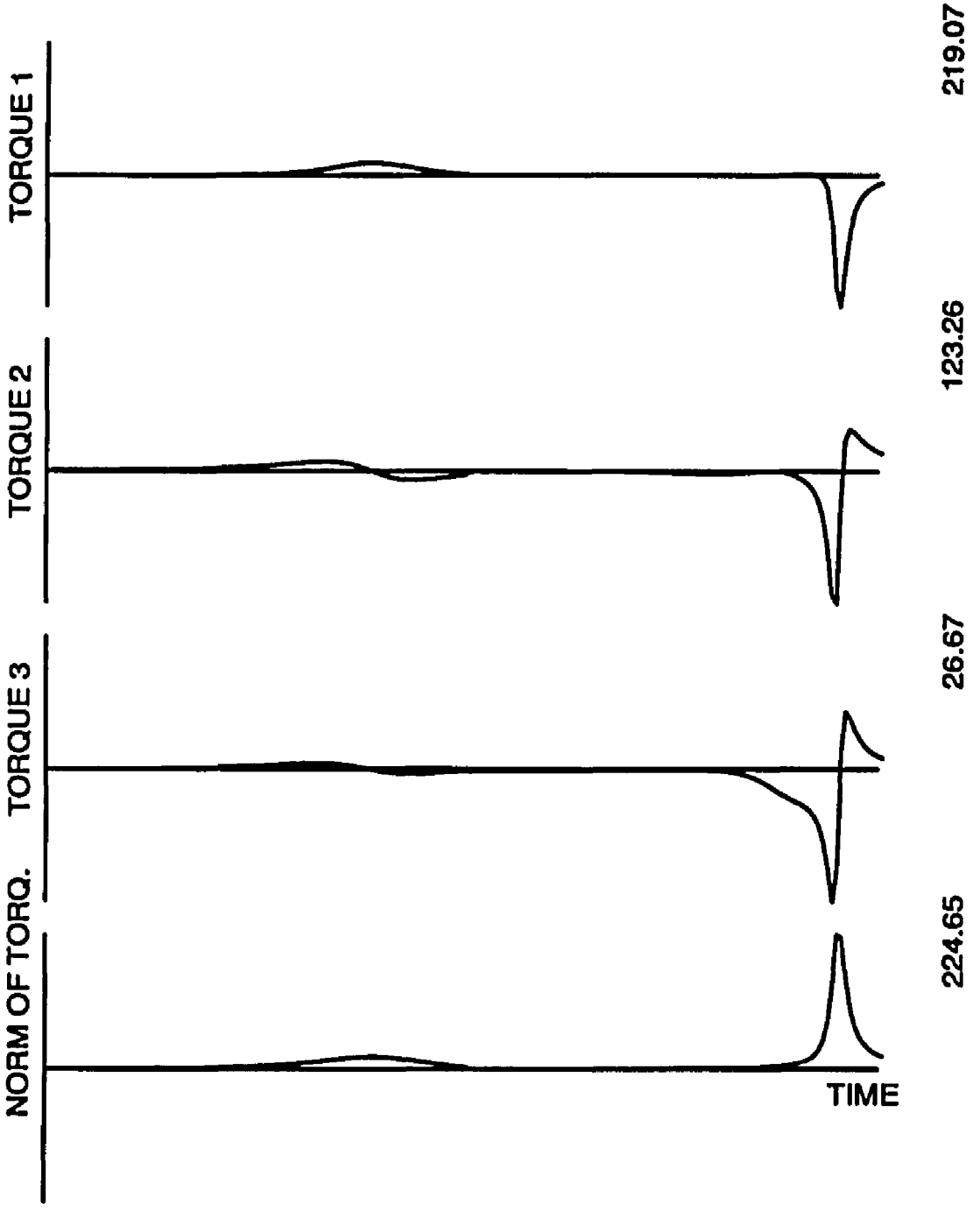

Figure 60: The joint torques and the norm of the torque as functions of time, tracing a straight line trajectory (T=1.822 sec) with initial posture $(-75.32^{\circ}, 50.82^{\circ}, 99.97^{\circ})$ corresponding to trajectory no. 3 in Table 16

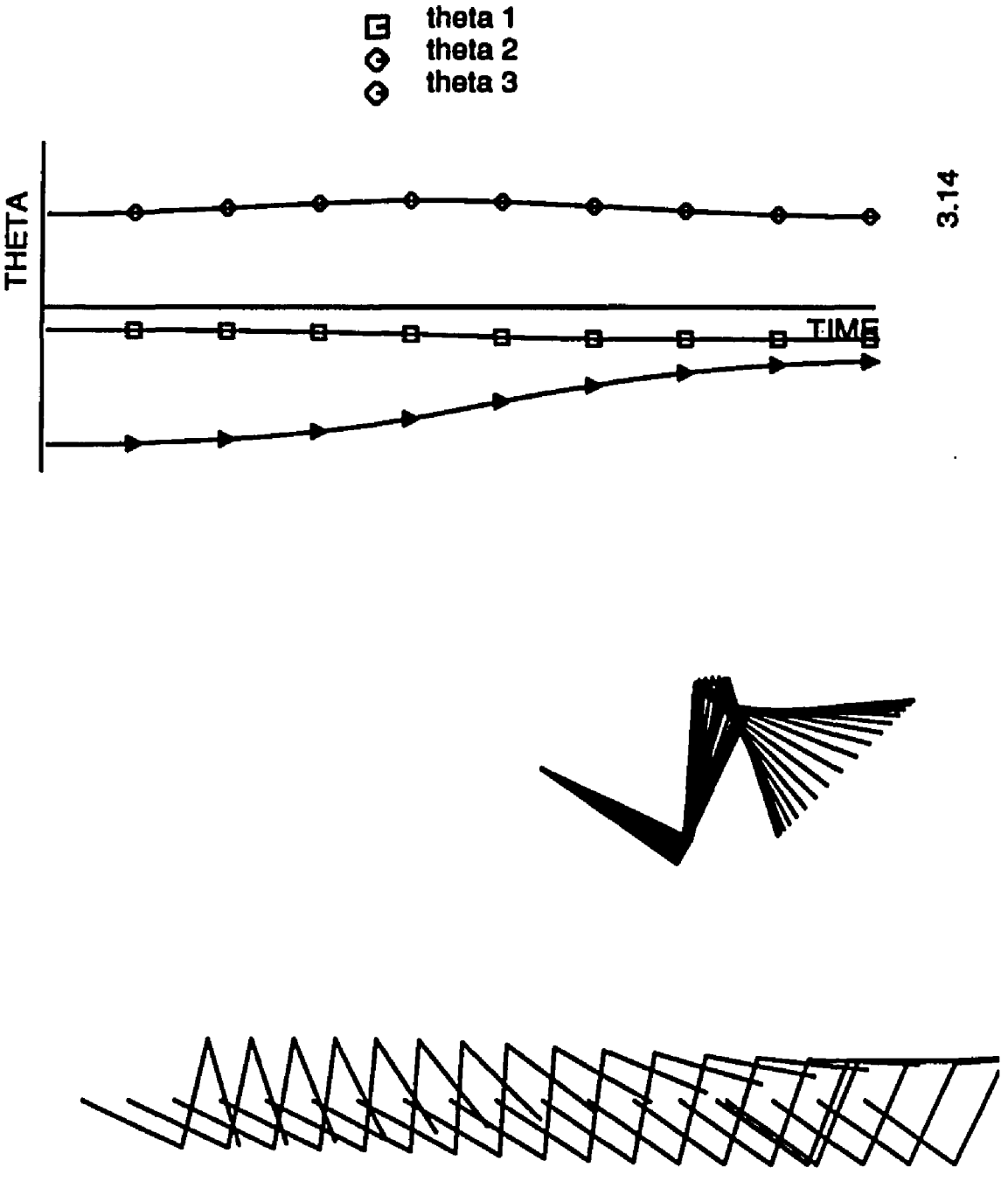

Figure 61: The joint angles and geometries as functions of time, tracing a straight line trajectory with initial posture $(-25.32°, 102.04°, -150.42°)$ corresponding to trajectory no. 8 (T=1.822 sec) in Table 16

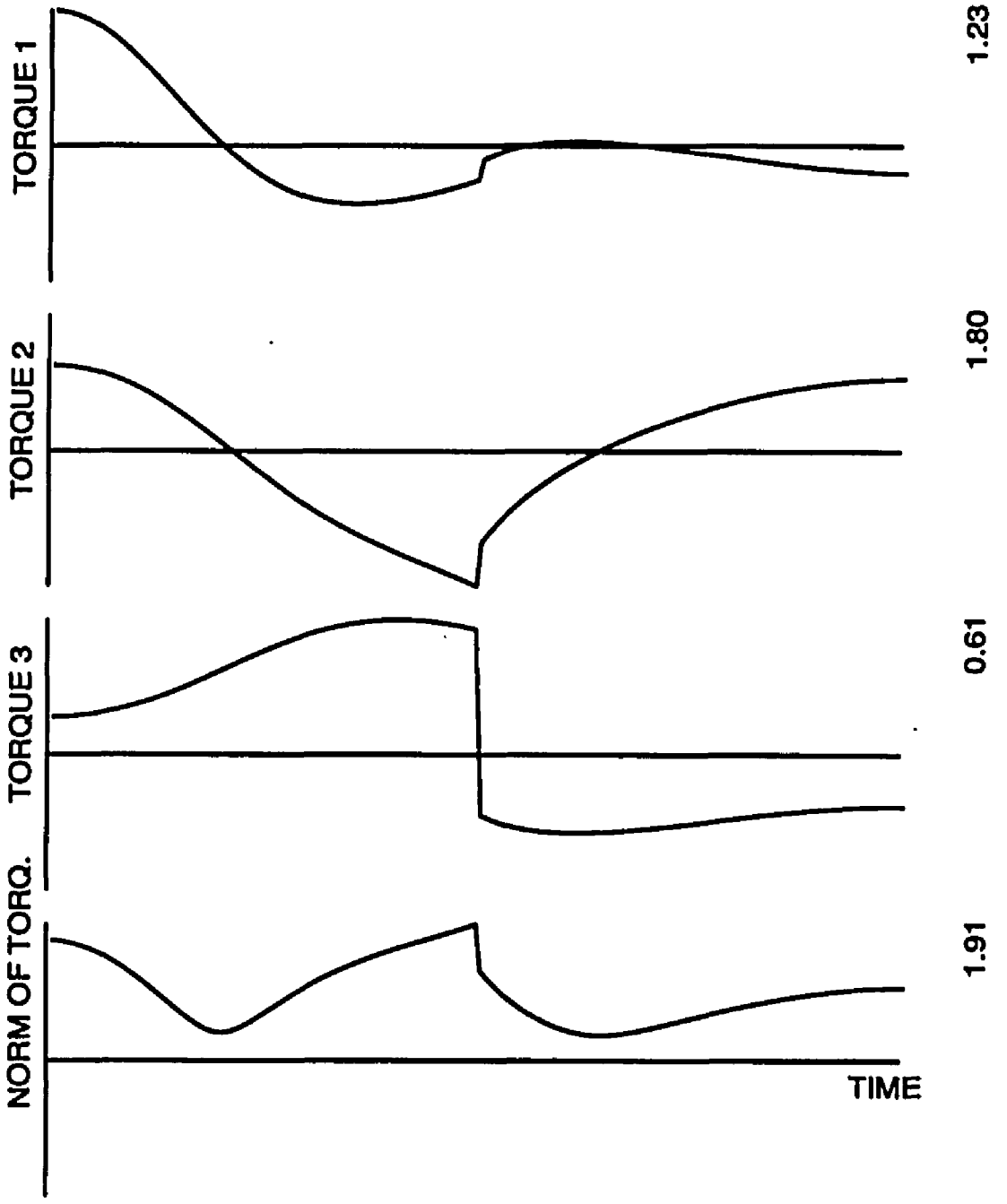

Figure 62: The joint torques and the norm of the torque as functions of time, tracing a straight line trajectory (T=1.822 sec) with initial posture $(-25.32°, 102.04°, -150.42°)$ corresponding to trajectory no. 8 in Table 16

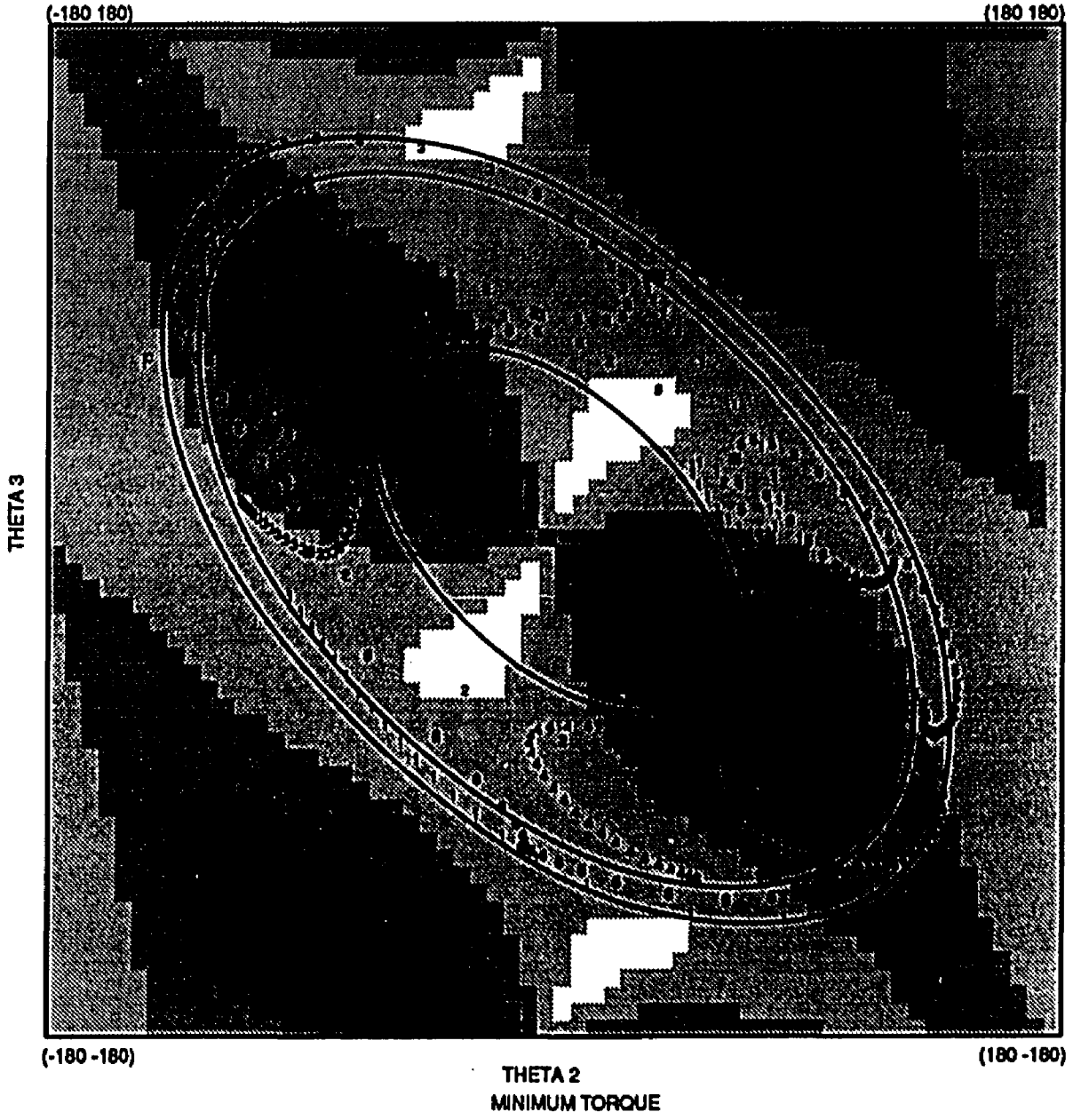

Figure 63: The projection of the joint angle space trajectories on the $\theta_1 = 0$ plane for minimum norm of torque control tracing a circle trajectory with zero initial joint rates and different initial postures as given in Table 19, trajectories 2 and 6 pass through the small singular value region shown in Fig. 38

Table 19: The performance measures for minimum norm of torque control to trace a circular trajectory with base located at (0.0,0.0) and zero initial joint rate for 6 different initial postures

Trajectory	Initial θ			Cost functions		
	θ_{1_0}	θ_{2_0}	θ_{3_0}	$\int_{t_0}^{t_f} \tau^T \tau dt$	$\int_{t_0}^{t_f} \dot{\theta}^T \dot{\theta} dt$	$\int_{t_0}^{t_f} \ddot{\theta}^T \ddot{\theta} dt$
1	73.8	35.3	88.7	2116.30	97.85	20424.98
2	136.5	-91.2	123.2	35455.50	183.50	269889.21
3	203.2	-115.0	8.3	374.24	49.02	509.90
4	129.0	48.6	-126.4	104.88	95.9	121.4
5	104.6	95.9	-121.4	226.32	24.15	1160.03
6	41.4	117.4	-14.0	12696.98	139.76	60919.75

The joint angles and the manipulator geometries as functions of time for the trajectories 1 and 5 in Table 19 are shown in Figs. 64 and 66. The torque required at each joint and the norm of joint torque for the above trajectories are also shown in Figs. 65 and 67.

5.5.2 A Proper Initial Joint Rate for Some Specific Initial Posture

The effect of initial postures on the torque optimization algorithm has been shown in the previous section. That is, some starting configurations (θ_0) perform the optimization of the required torques better than others. While the choice of this proper initial configuration is effective for the torque optimization, the other state variable, joint rate, also has a similar influence on the performance of the torque optimization algorithm.

The proper initial joint rate ($\dot{\theta}_0$) can be searched along the direction of the null-space vector for optimizing the required torques with respect to some specific initial posture (θ_0). As can be seen, the proper choice of both the initial joint rate $\dot{\theta}$ and the initial joint angle (θ) are important in the optimization of the torque.

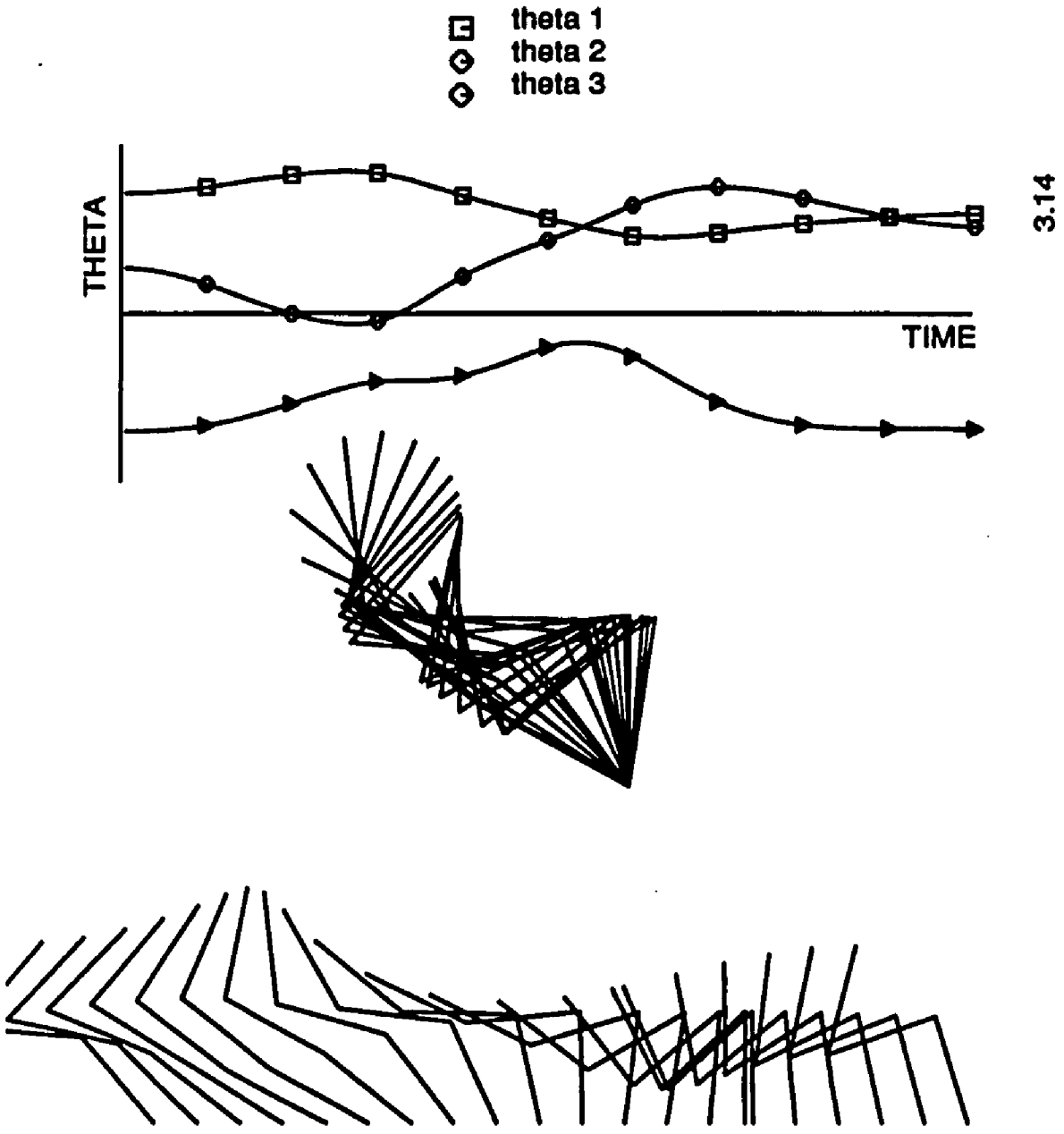

Figure 64: The joint angles and geometries as functions of time, tracing a circle trajectory with initial posture $(129.0°, 48.6°, -126.4°)$ corresponding to trajectory no. 4 in Table 19

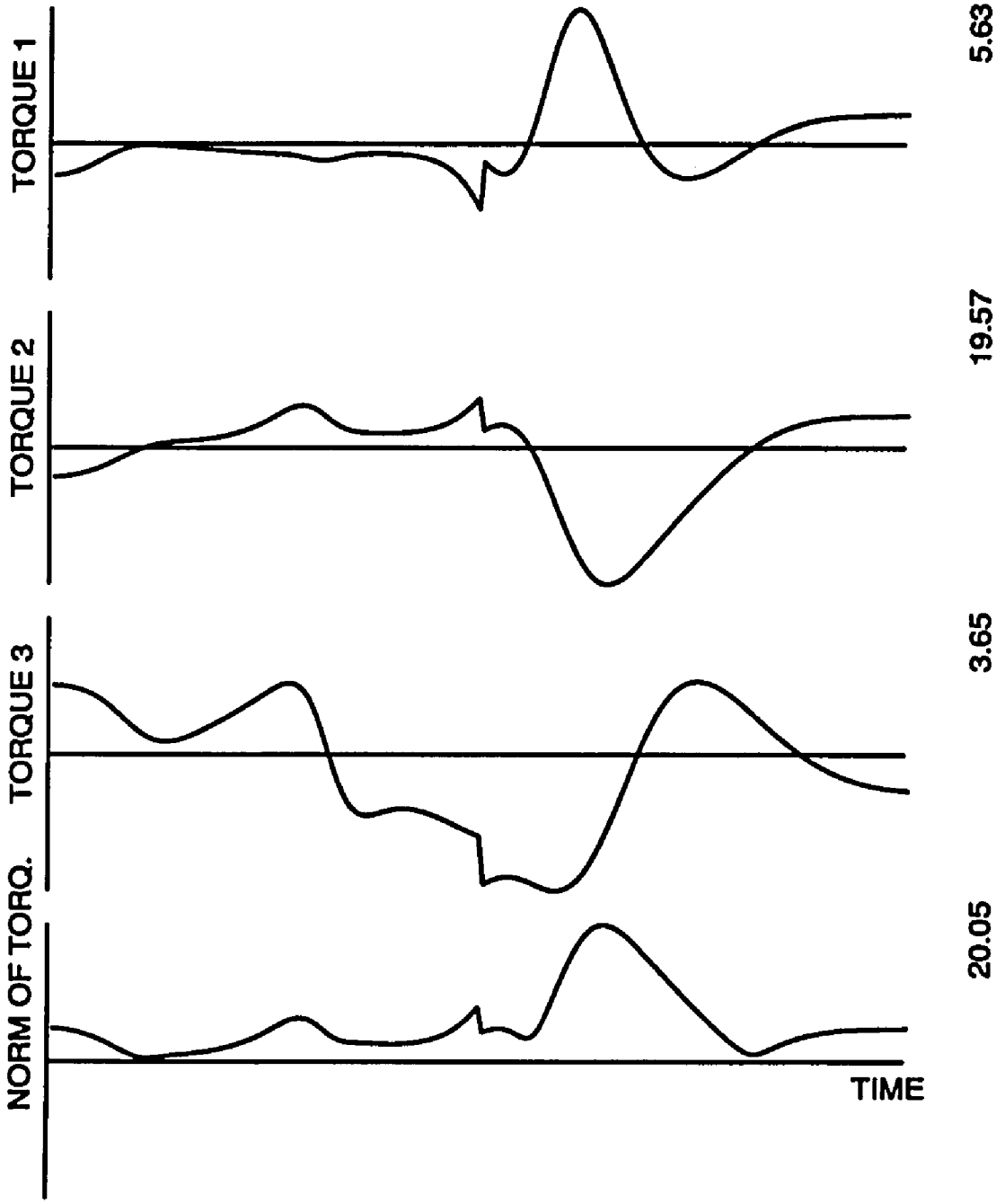

Figure 65: The joint torques and the norm of the torque as functions of time, tracing a circle trajectory with initial posture $(129.0°, 48.6°, -126.4°)$ corresponding to trajectory no. 4 in Table 19

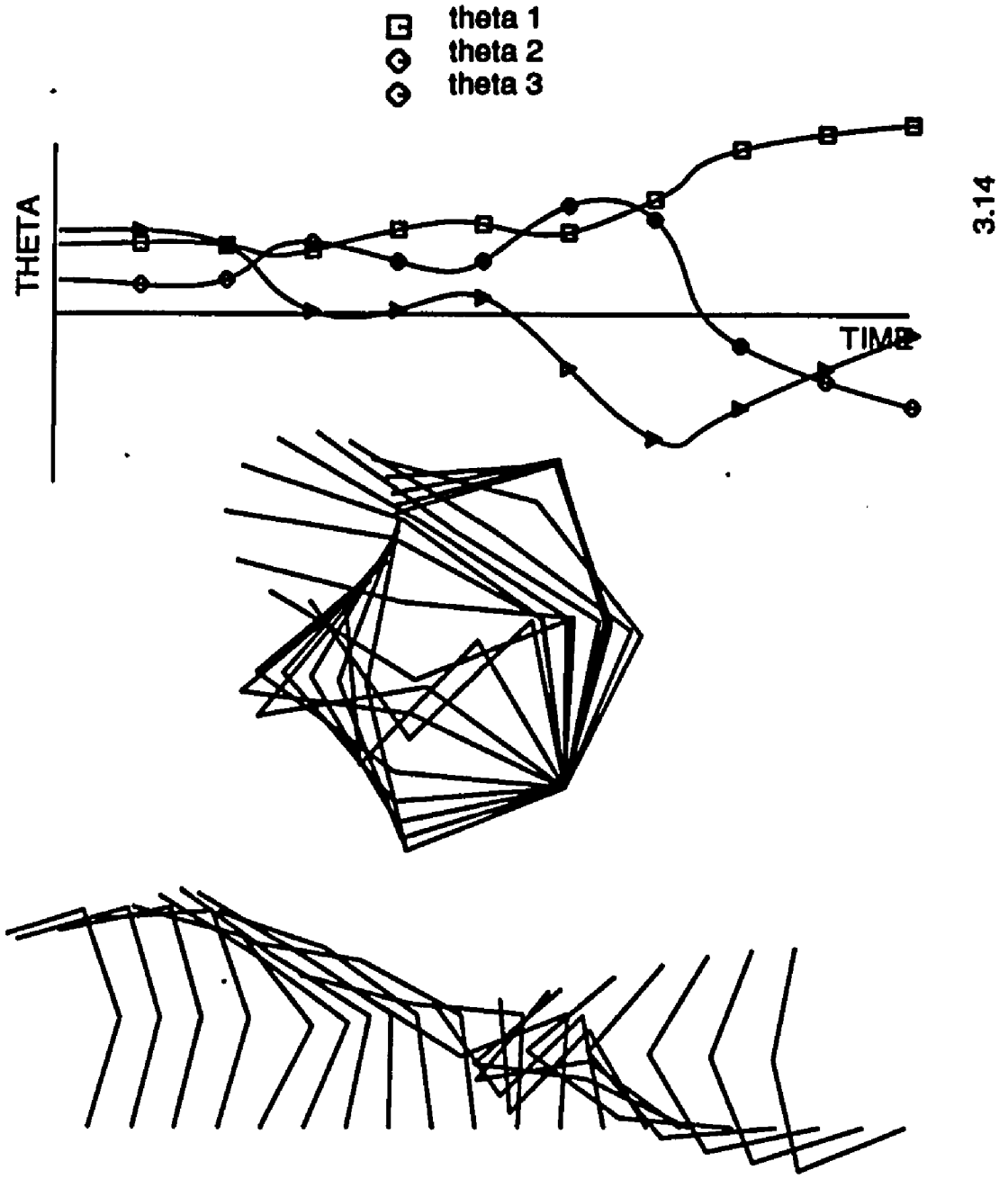

Figure 66: The joint angles and geometries as functions of time, tracing a circle trajectory with initial posture (73.8°, 35.3°, 88.7°) corresponding to the trajectory no. 1 in Table 19

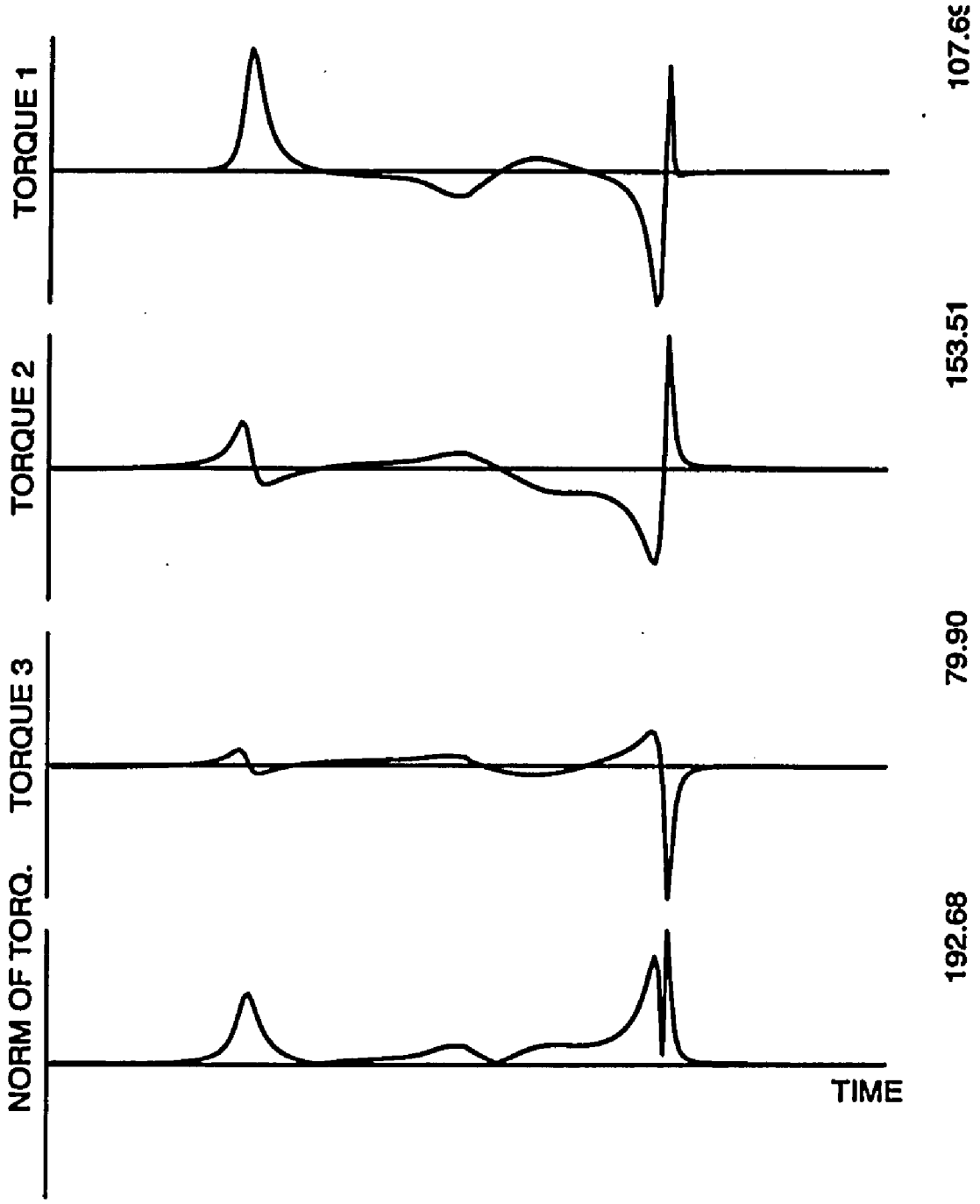

Figure 67: The joint torques and the norm of the torque as functions of time, tracing a circle trajectory with initial posture $(-73.8°, 35.3°, 88.7°)$ corresponding to trajectory no. 1 in Table 19

The following figures and tables show the effects of the initial joint rates on the torque optimization algorithm. Several configurations are chosen for demonstrating the effects of the initial joint rates.

The projections of the joint angle space trajectories on $\theta_1 = 0$ plane for minimum norm of torque control the end effector tracing a straight line with an initial posture $(-45°, 135°, -135°)$ and 8 different initial joint rates are shown in Fig. 68. The associated cost functions $\max \|\tau\|$, $\int_{t_0}^{t_f} \tau^T \tau dt$ and $\int_{t_0}^{t_f} \dot{\theta}^T \dot{\theta} dt$ by using minimum norm of torque, damped least-squares and minimum norm of acceleration controls are given in Tables 20 to 22. The joint angles and the manipulator geometries as functions of time for the trajectories 3 and 6 in Table 20 are shown in Figs. 69 and 71. The torque required at each joint and the norm of joint torques for the above trajectories are also shown in Figs. 70 and 72.

The projections of the joint angle space trajectories on $\theta_1 = 0$ plane for minimum norm of torque control the end effector tracing a circle with an initial posture $(104.6°, 95.9°, -121.4°)$ and 6 different initial joint rates are shown in Fig. 73. The joint angles and the manipulator geometries as functions of time for the trajectories 1 and 4 in Table 23 are shown in Figs. 74 and 76. The torque required at each joint and the norm of joint torques for the above trajectories are also shown in Figs. 75 and 77.

It can be seen that it is possible for a specific starting configuration to find an initial joint rate which stabilizes the torque optimization algorithm. That is, an initial joint rate is picked up in order to avoid passing the small singular value region of $[H(I - J^+J)]^+$ with its high joint rates. Therefore, choosing an appropriate starting joints' configuration as well as the initial joint rates is effective and important for the stability of the torque optimization.

Table 20: The performance measures for minimum norm of torque control to trace a straight line at 45° with initial posture $(-45°, 135°, -135°)$, base located at (0.0,0.0) and $t_f = 1.822$ sec for 8 different initial joint rates

Trajectory	Initial $\dot{\theta}$			Cost functions		
	$\dot{\theta}_{1_0}$	$\dot{\theta}_{2_0}$	$\dot{\theta}_{3_0}$	$\max \|\tau\|$	$\int_{t_0}^{t_f} \tau^T \tau dt$	$\int_{t_0}^{t_f} \dot{\theta}^T \dot{\theta} dt$
1	1.47	-1.47	-1.47	64.64	301.70	32.09
2	0.98	-0.98	-0.98	1.76	1.16	5.76
3	0.74	-0.74	-0.74	0.90	0.53	2.00
4	0.37	-0.37	-0.37	1.49	0.98	1.68
5	0.0	0.0	0.0	5.15	4.62	10.96
6	-0.37	0.37	0.37	43.93	209.66	49.45
7	-0.74	0.74	0.74	346.86	3383.91	116.84
8	-1.11	1.11	1.11	343.14	3503.37	129.28

Table 21: The performance measures for damped least-squares torque optimization control to trace a straight line at 45° with initial posture $(-45°, 135°, -135°)$, base located at (0.0,0.0) and $t_f = 1.822$ sec for 8 different initial joint rates

Trajectory	Initial $\dot{\theta}$			Cost functions		
	$\dot{\theta}_{1_0}$	$\dot{\theta}_{2_0}$	$\dot{\theta}_{3_0}$	$\max \|\tau\|$	$\int_{t_0}^{t_f} \tau^T \tau dt$	$\int_{t_0}^{t_f} \dot{\theta}^T \dot{\theta} dt$
1	1.47	-1.47	-1.47	6.69	40.60	5.27
2	0.98	-0.98	-0.98	2.20	4.82	3.33
3	0.74	-0.74	-0.74	1.48	1.78	2.45
4	0.37	-0.37	-0.37	1.02	0.78	1.52
5	0.0	0.0	0.0	1.77	1.72	1.77
6	-0.37	0.37	0.37	2.27	4.11	2.97
7	-0.74	0.74	0.74	4.50	6.59	4.40
8	-1.11	1.11	1.11	7.97	19.44	5.81

Table 22: The performance measures for minimum norm of acceleration control to trace a straight line at 45° with initial posture $(-45°, 135°, -135°)$, base located at (0.0,0.0) and $t_f = 1.822$ sec for 8 different initial joint rates

Trajectory	Initial $\dot{\theta}$			Cost functions		
	$\dot{\theta}_{1_0}$	$\dot{\theta}_{2_0}$	$\dot{\theta}_{3_0}$	$\max \|\tau\|$	$\int_{t_0}^{t_f} \tau^T \tau dt$	$\int_{t_0}^{t_f} \dot{\theta}^T \dot{\theta} dt$
1 (19)	1.47	-1.47	-1.47	6.74	41.70	5.30
2 (45)	0.98	-0.98	-0.98	2.58	7.48	3.71
3 (59)	0.74	-0.74	-0.74	1.99	4.08	2.96
4 (80)	0.37	-0.37	-0.37	1.52	2.52	1.88
5 (100)	0.0	0.0	0.0	1.80	4.42	1.32
6 (120)	-0.37	0.37	0.37	2.41	6.78	2.30
7 (141)	-0.74	0.74	0.74	3.73	5.99	3.67
8 (162)	-1.11	1.11	1.11	6.35	13.10	5.11

Table 23: The performance measures for minimum norm of torques control to trace a circular trajectory with an initial posture (104.6°, 95.9°, −121.4°), base located at (0.0,0.0) and $t_f = 2.0sec$ for 6 different initial joint rates

Trajectory	Initial $\dot{\theta}$			Cost functions		
	$\dot{\theta}_{1_0}$	$\dot{\theta}_{2_0}$	$\dot{\theta}_{3_0}$	$\int_{t_0}^{t_f} \tau^T \tau dt$	$\int_{t_0}^{t_f} \dot{\theta}^T \dot{\theta} dt$	$\int_{t_0}^{t_f} \ddot{\theta}^T \ddot{\theta} dt$
1	0.985	-1.481	-0.651	25423.26	464.87	182625.02
2	0.746	-1.122	-0.493	174.69	39.83	1661.59
3	0.468	-0.703	-0.309	118.45	21.70	647.08
4	0.199	-0.299	-0.131	134.60	19.43	696.24
5	0.0	0.0	0.0	226.33	24.10	1151.05
6	-0.099	0.150	0.066	3606.01	195.44	28503.68

5.5.3 Effects of the Base Location

The effects on the local torque optimization algorithm by changing the base location are studied in this section. A 3-link planar manipulator was used in the computer simulation to trace a straight line 45° with constant acceleration in the first half of the path and constant deceleration in the second half. Fig. 78 is the result of the simulation which gives a relative performance measure I_τ for different base positions with the numbers 0 and f representing the smallest and the largest value respectively.

5.6 Summary

In this chapter the two questions of why the system becomes unstable and how to get rid of the instability mentioned in the beginning, have been answered. A manipulator passing through the small singular value region of the matrix $[H(I - J^+J)]$ with high joint rates is the source of instability. There exists two approaches for stabilizing the local toque optimization algorithm: one is to choose a

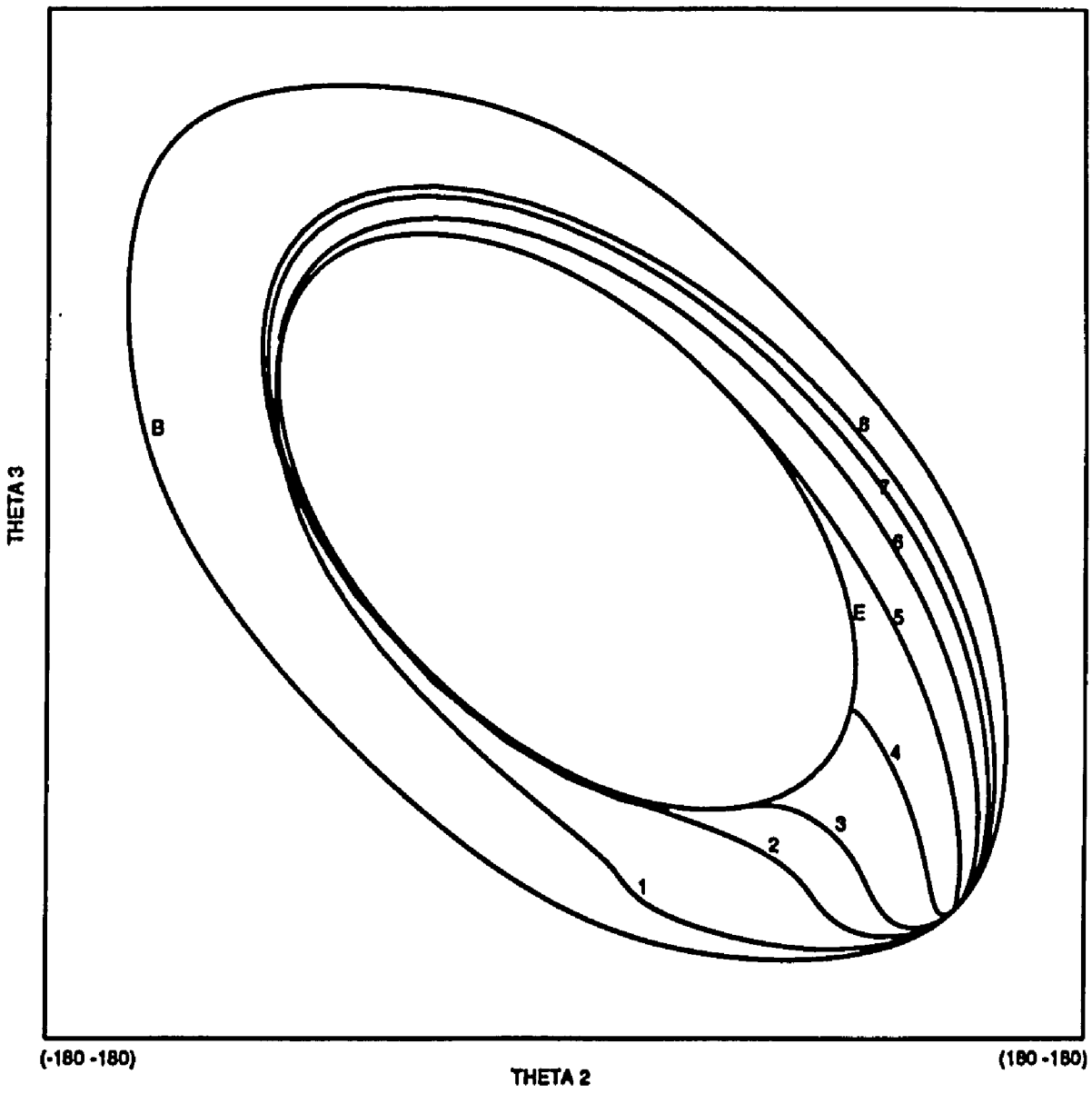

Figure 68: The projection of the joint angle space trajectories on the $\theta_1 = 0$ plane tracing a straight line with initial posture $(-45^\circ, 135^\circ, -135^\circ)$ and the initial joint rates as given in Table 20, trajectories 1, 6, 7 and 8 pass through small singular value region shown in Fig. 38

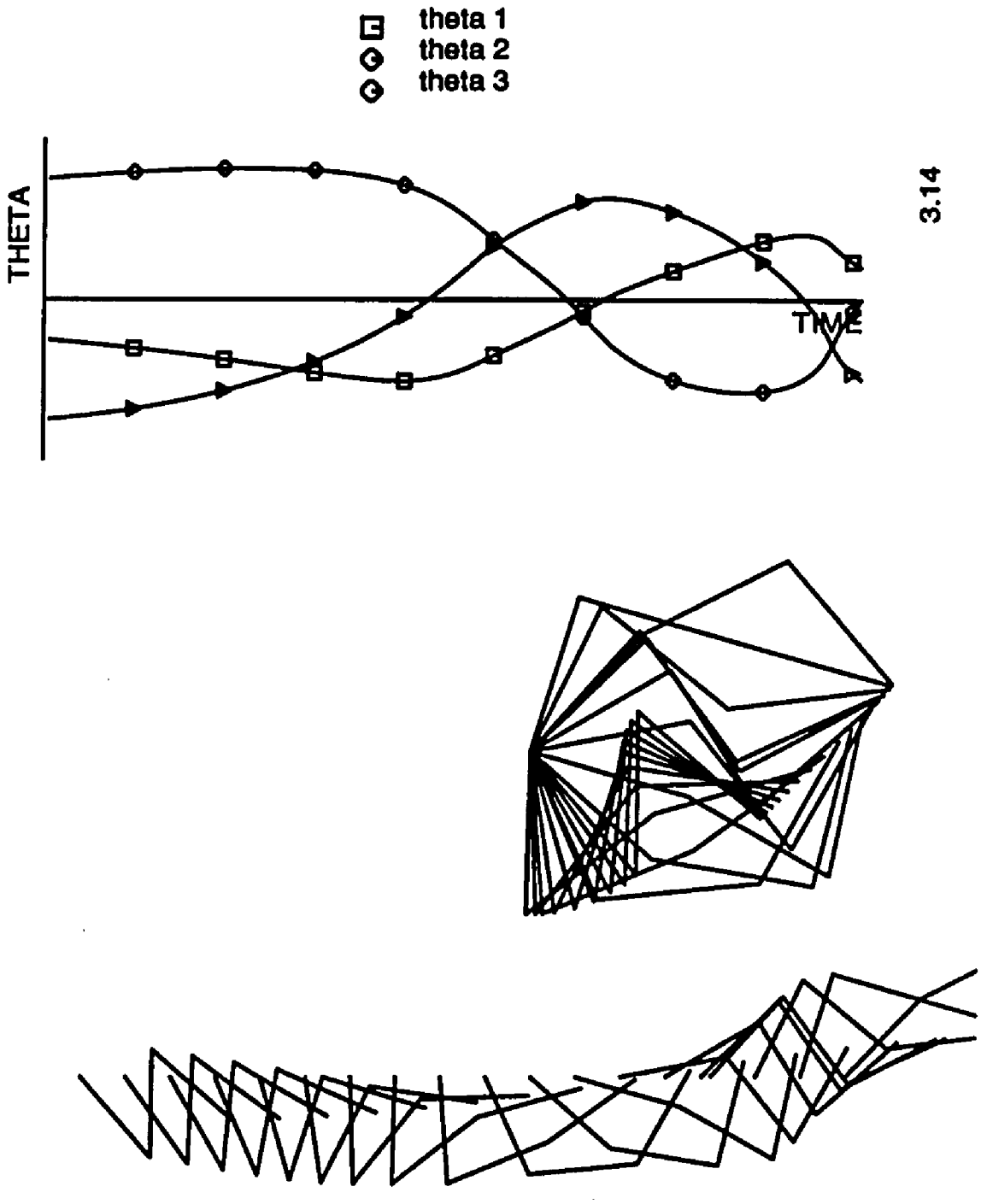

Figure 69: The joint angles and geometries as functions of time, tracing a straight line trajectory with initial posture $(-45°, 135°, -135°)$ and initial joint rates (-0.74,0.74,0.74) corresponding to trajectory no. 7 (T=1.822 sec) in Table 20

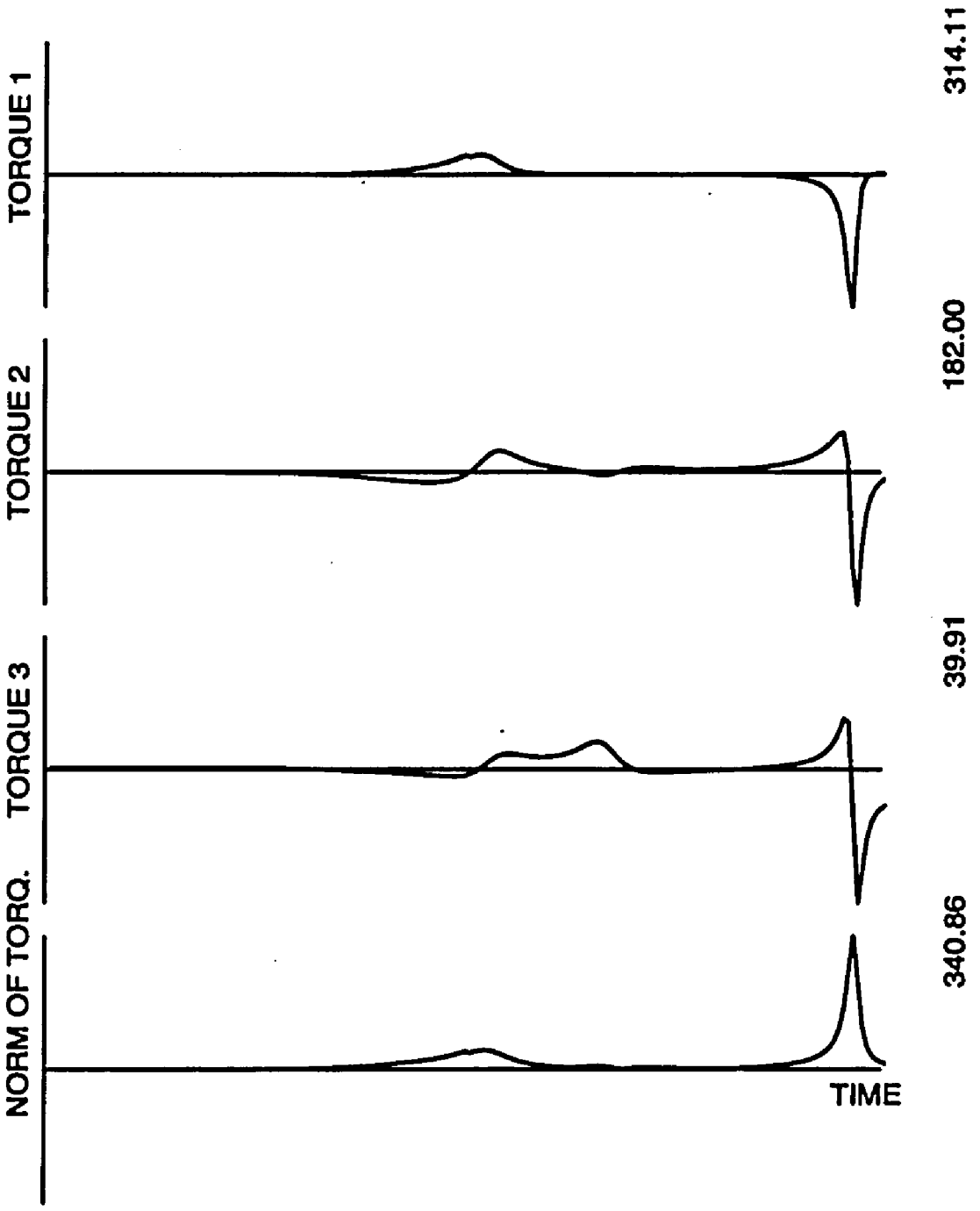

Figure 70: The joint torques and the norm of joint torques along the straight line trajectory (T=1.822 sec) as functions of time with initial posture $(-45°, 135°, -135°)$ and initial joint rates (-0.74,0.74,0.74) corresponding to trajectory no. 7 in Table 20

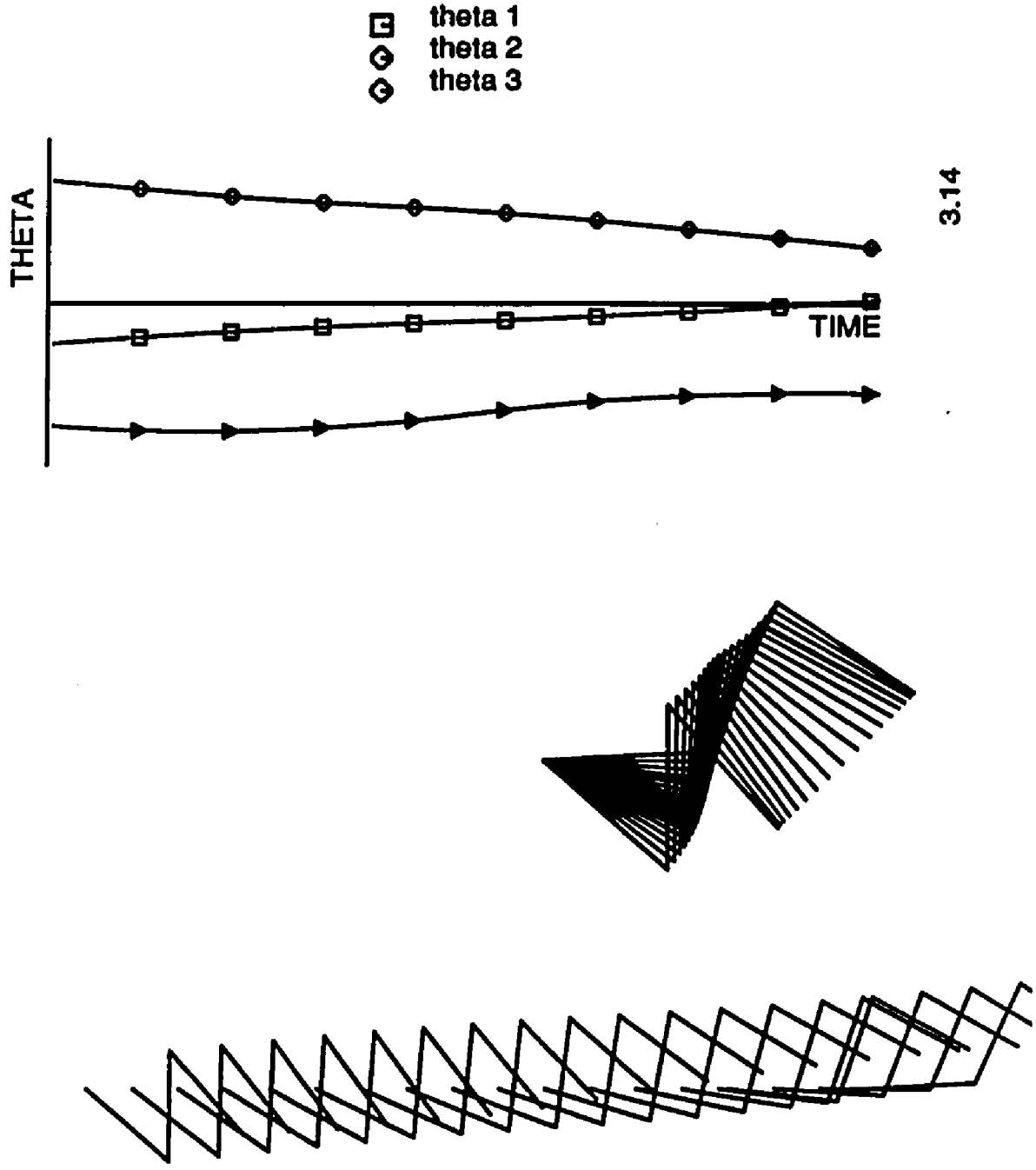

Figure 71: The joint angles and geometries as functions of time, tracing a straight line trajectory with initial posture $(-45°, 135°, -135°)$ and initial joint rates (0.74,-0.74,-0.74) corresponding to trajectory no. 3 (T=1.822 sec) in Table 20

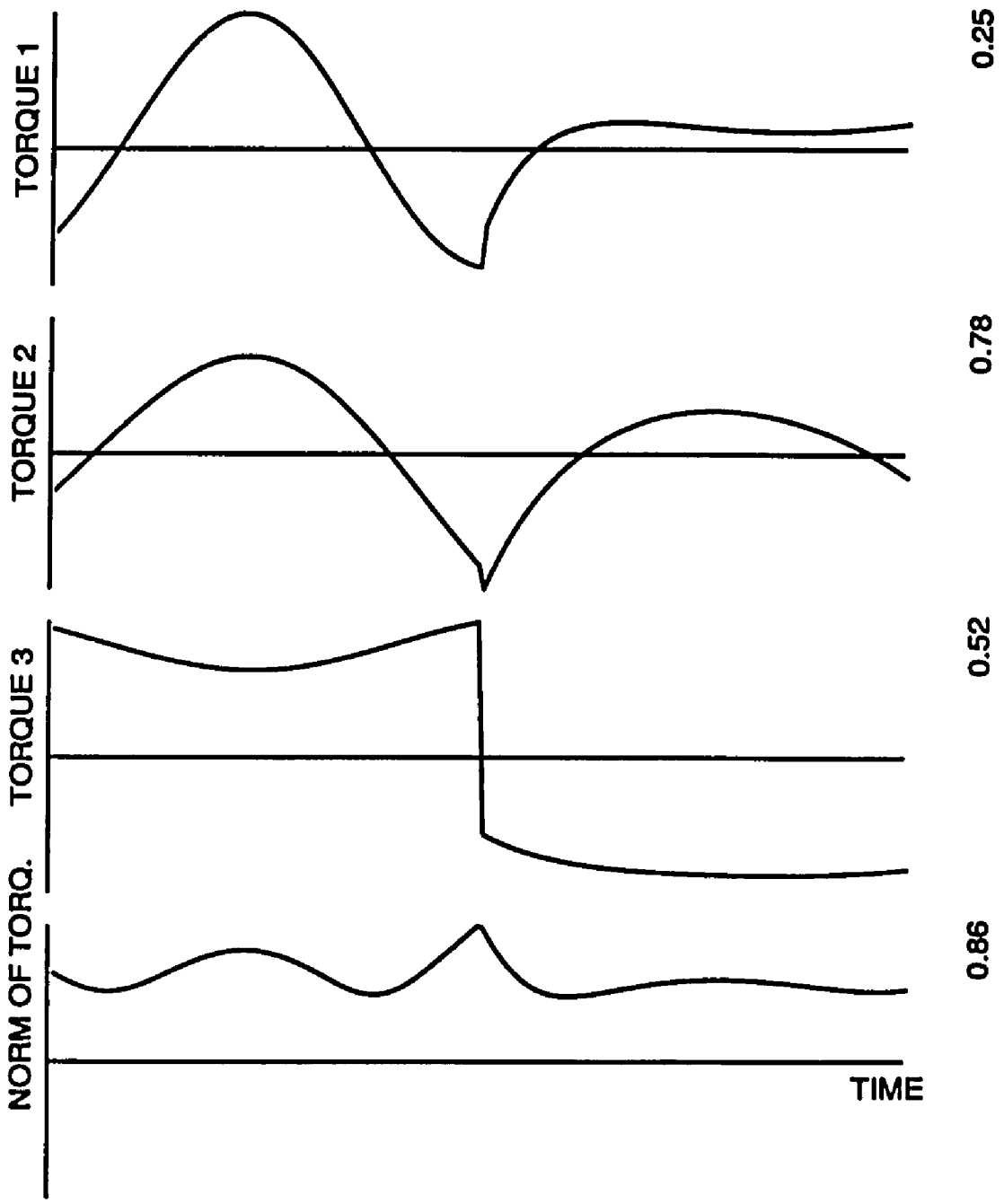

Figure 72: The joint torques and the norm of joint torques along the straight line trajectory (T=1.822 sec) as functions of time with initial posture $(-45°, 135°, -135°)$ and initial joint rates (0.74,-0.74,-0.74) corresponding to trajectory 3 in Table 20

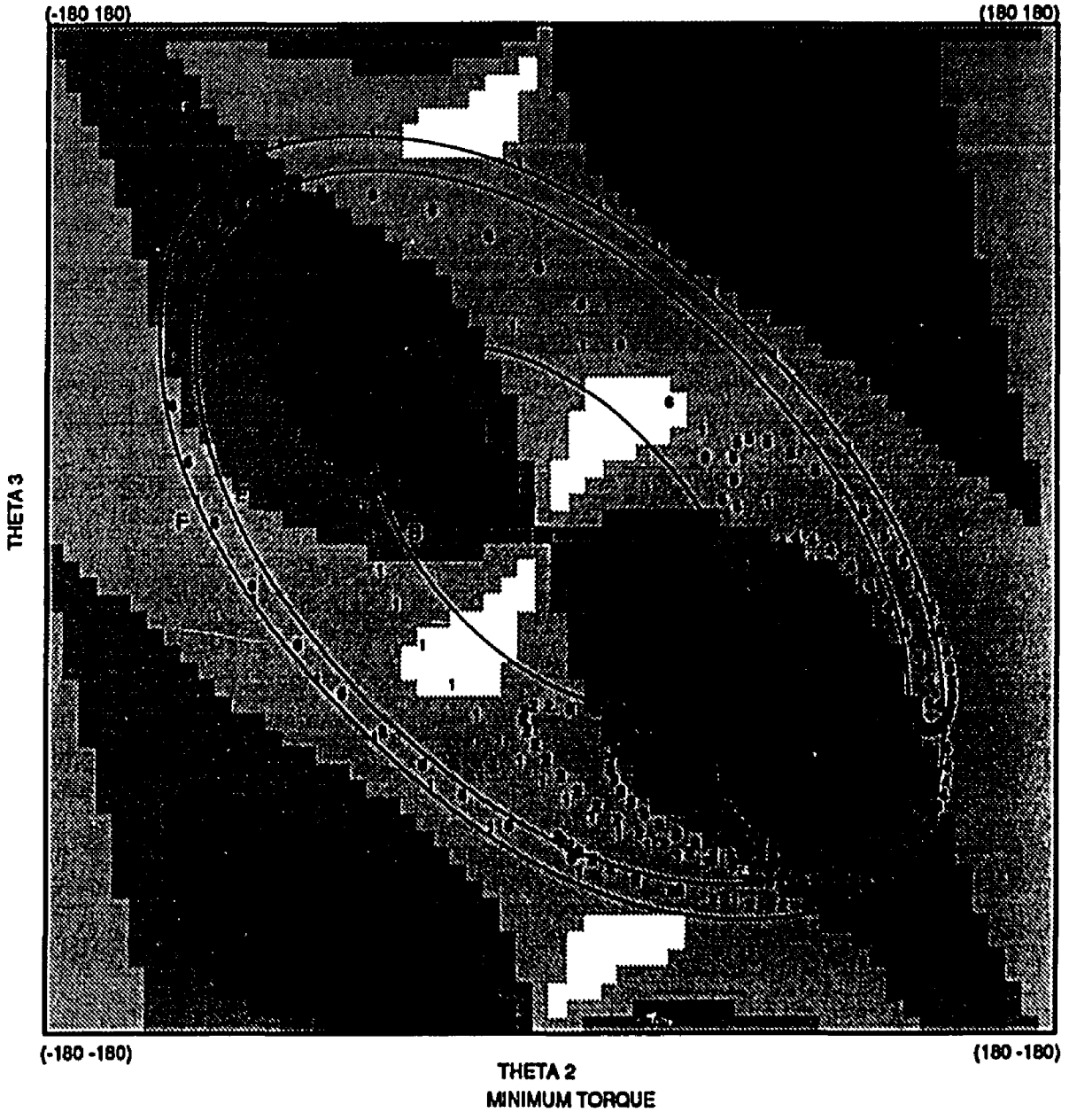

Figure 73: The projection of the joint angle space trajectories on $\theta_1 = 0$ plane to trace a circle trajectory with initial posture $(104.6°, 95.9°, -121.4°)$ for 8 different initial joint rates as given in Table 23, trajectories 1 and 6 pass through small singular value region shown in Fig. 38

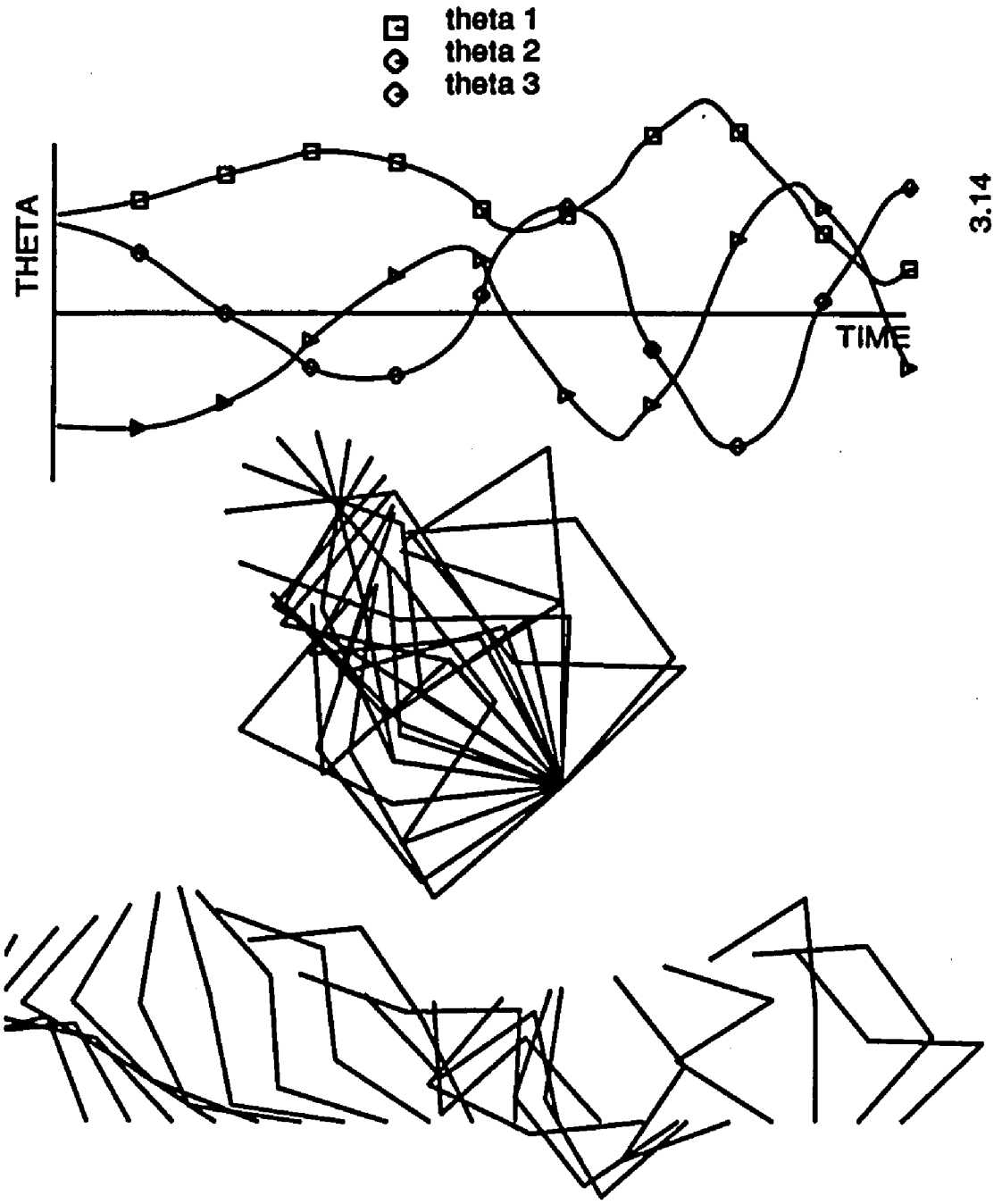

Figure 74: The joint angles and geometries as functions of time, tracing a circle trajectory with initial posture (104.6°, 95.9°, −121.4°) and initial joint rates (0.985,-1.481,-0.651) corresponding to trajectory 1 in Table 23

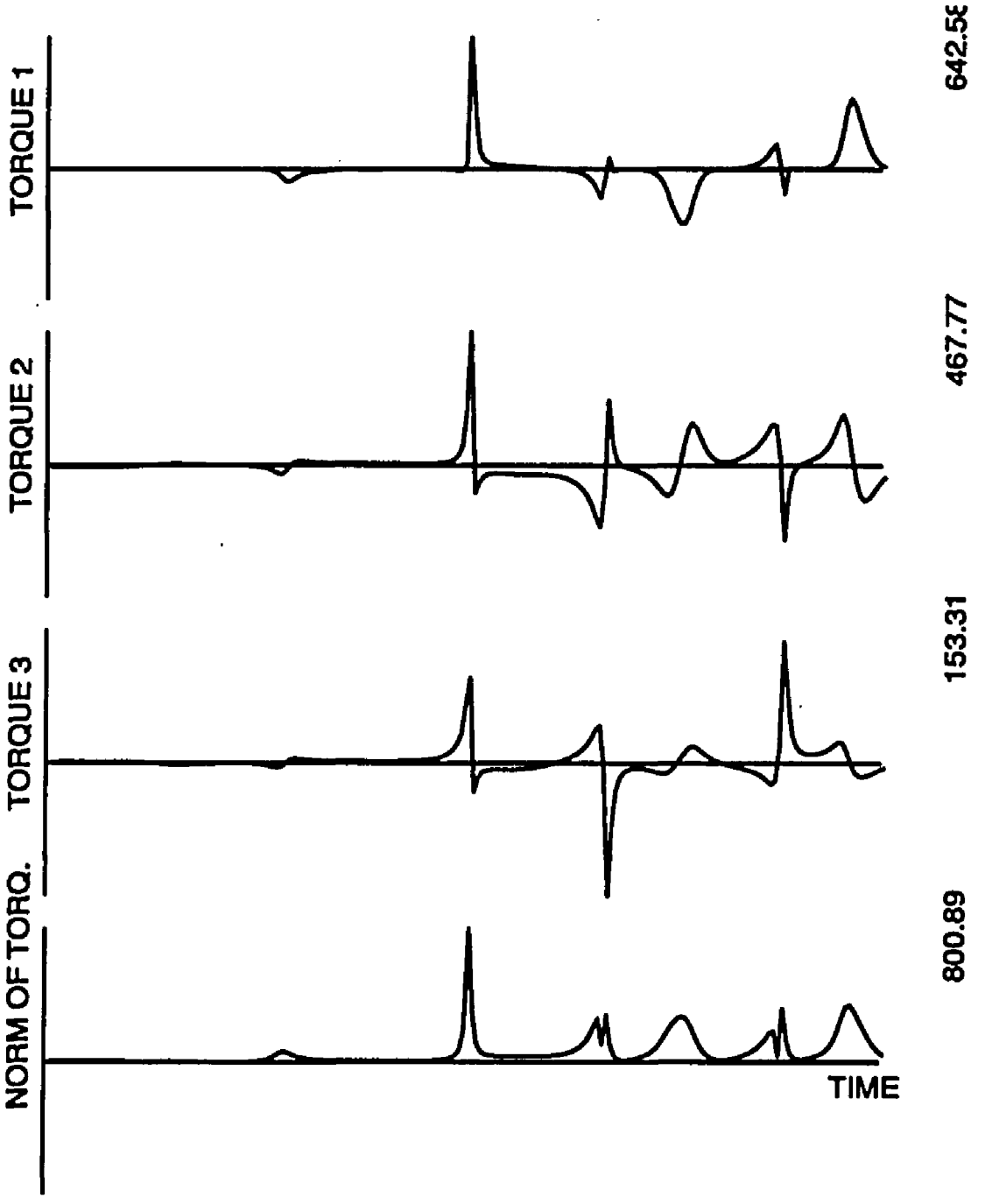

Figure 75: The joint torques and the norm of joint torques along a circle trajectory as a function of time with initial posture $(104.6°, 95.9°, -121.4°)$ and initial joint rates (0.985,-1.481,-0.651) corresponding to trajectory 1 in Table 23

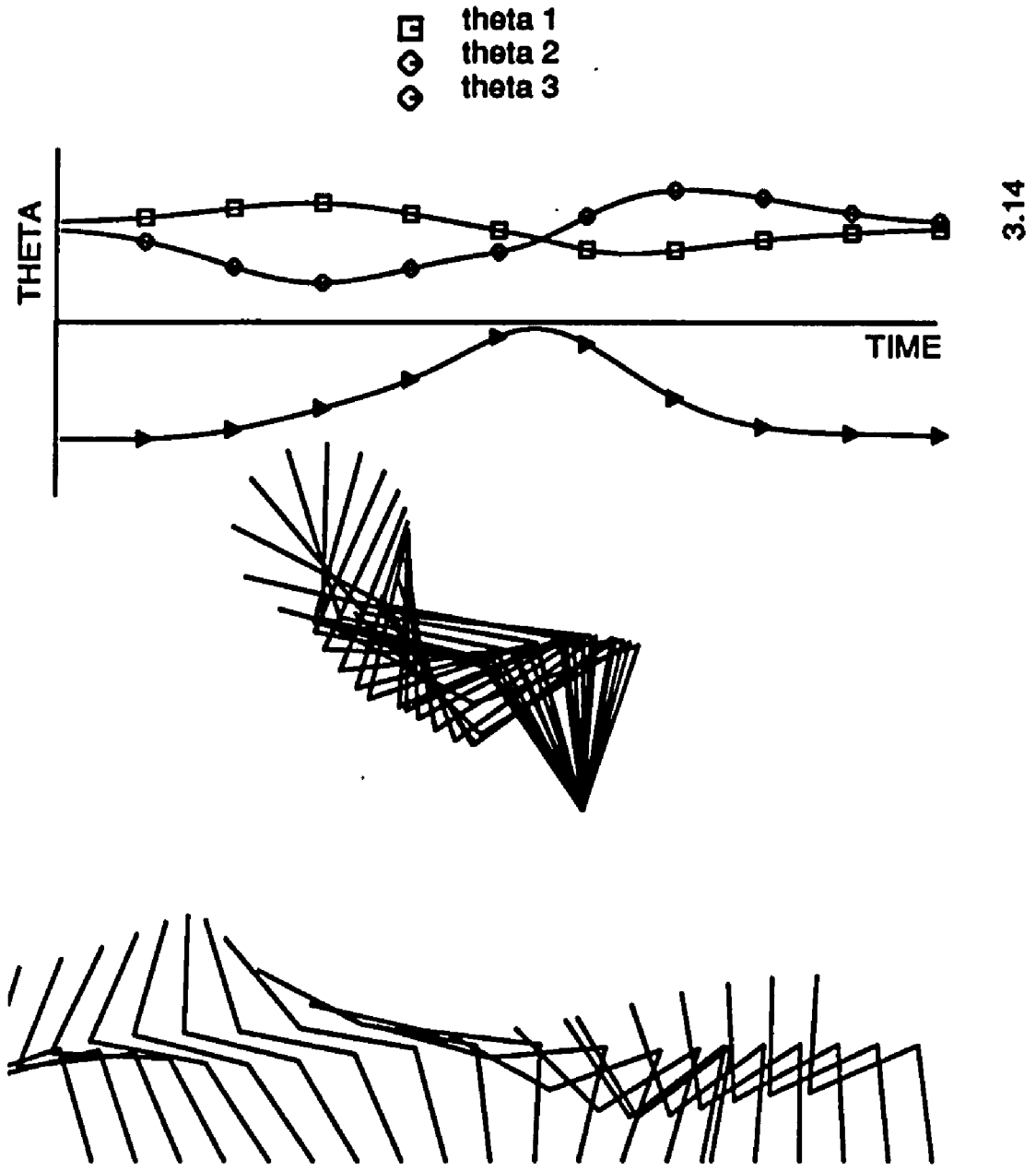

Figure 76: The joint angles and geometries as functions of time, tracing a circle trajectory with initial posture $(104.6°, 95.9°, -121.4°)$ and initial joint rates (0.199,-0.299,-0.131) corresponding to trajectory no. 4 in Table 23

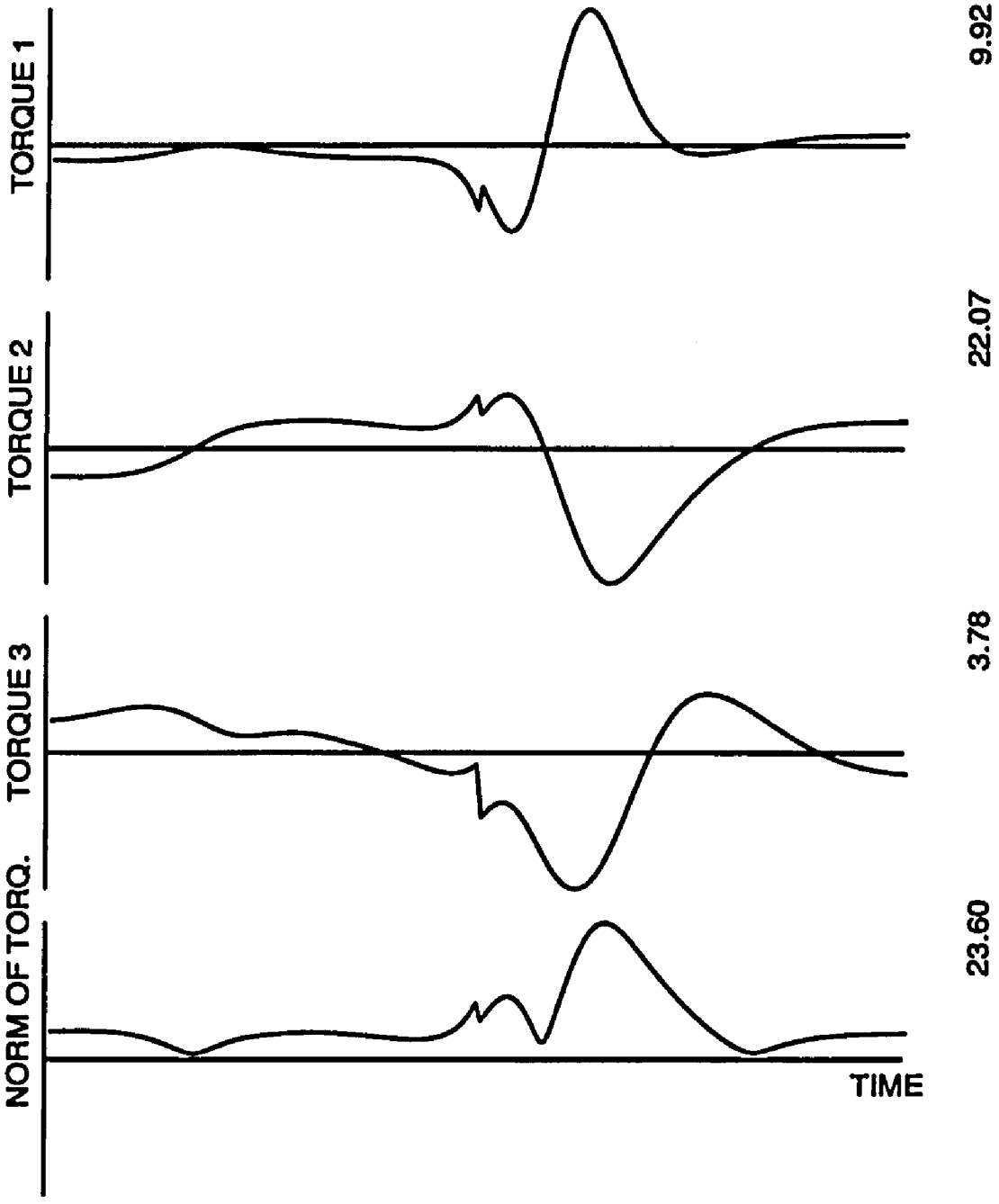

Figure 77: The joint torques and the norm of joint torques along a circle trajectory as a function of time with initial posture $(104.6^{\circ}, 95.9^{\circ}, -121.4^{\circ})$ and initial joint rates (0.199,-0.299,-0.131) corresponding to trajectory 4 in Table 23

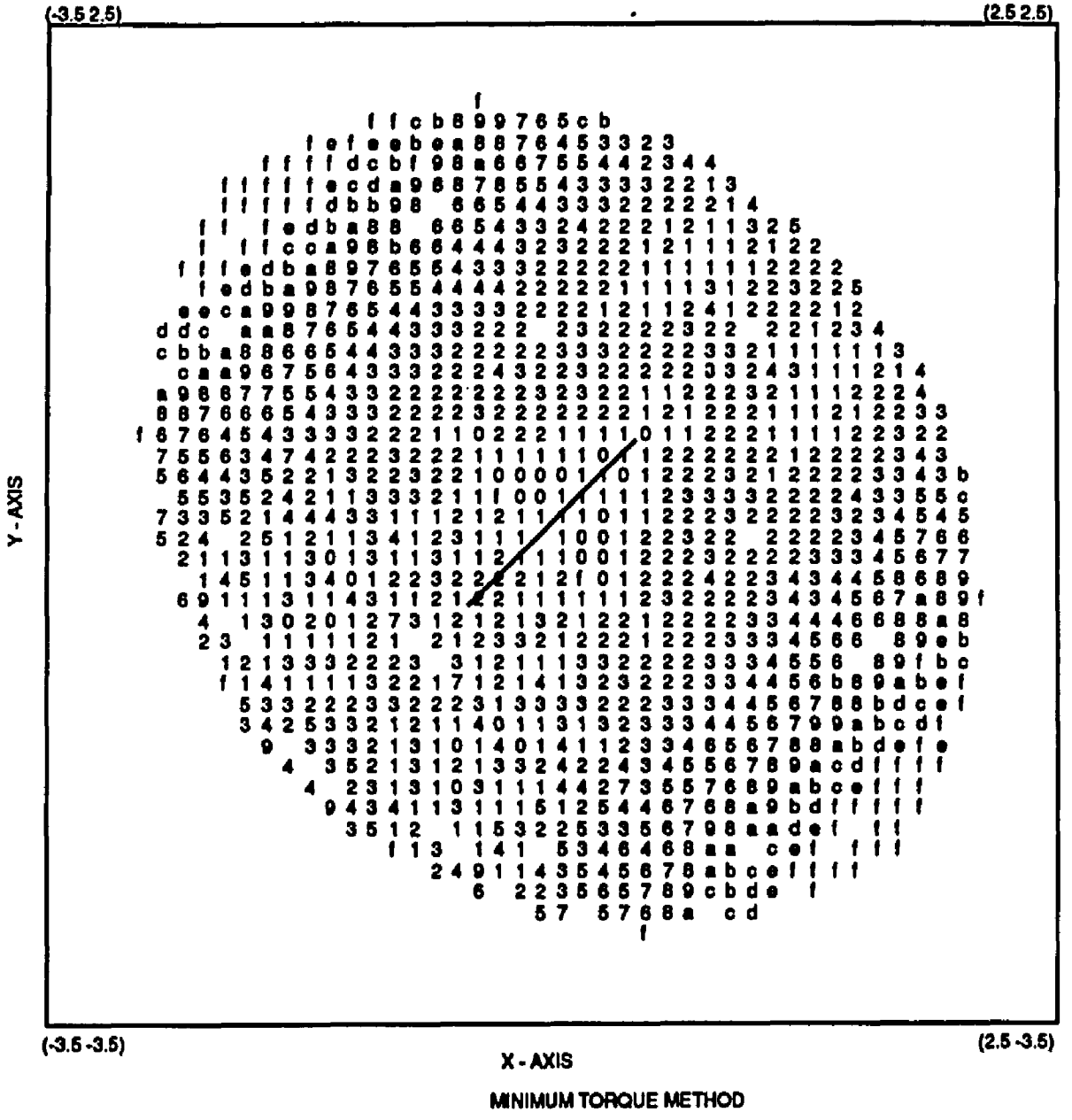

Figure 78: The relative performance measure I_T for different base locations with symbols 0 to f designate values from 1.45 to 25.0

proper initial condition $(\theta_0, \dot{\theta}_0)$, and the other is to properly utilize the null-space component (different control schemes). The computer simulations have shown that both approaches are capable of reaching a satisfactory result. Simulation results also demonstrate the effects of choosing initial postures, initial joint rates and base locations for local torque optimization algorithm on the performance measure I_τ. Both fixed and adaptive damping factor are used in the damped least-squares pseudoinverse method and a comparison has been made. Due to the complicated process of searching appropriate initial conditions, the first approach is suitable for off-line planning. An automatic regulating formula has been designed for adjusting the damping factor which responds for the proper usage of the available null-space component. Moreover, the computation of second approach is less complicated and can be used for real-time application.

CHAPTER VI

RESOLUTION OF KINEMATIC REDUNDANCY THROUGH GLOBAL OPTIMIZATION

Two main approaches for the optimization of a global cost function are calculus of variation and dynamic programming [27]. The variational approach of Pontryagin maximum principle leads to a non-linear two-points split boundary value problem that must be solved to obtain the optimal control. The dynamic programming first developed by Bellman [27] is based on the principle of optimality and results in a set of iterative formulas which are used for finding the optimal solutions.

Although the calculus of variation provides a sound theoretical basis for achieving global optimization, the difficulty in solving a non-linear two-points boundary value problem makes the variational approach not very effective for practical applications. On the other hand, the physical constraint equations can be used to reduce the number of feasible solutions. The dynamic programming technique may be more suitable for resolving the kinematic redundancy through globally optimizing some objective function. The principle of optimality can be applied to simplify the procedure of redundancy resolution through global optimization, that is, instead of solving a two-point boundary value problem, searches over the feasible solutions are used to obtain the optimal global solutions.

The Principle of Optimality originally stated by Bellman, is applicable to all

the multistage decision processes. It states: "An optimal policy has the property that, whatever the initial state c and the optimal first decision $u(1)$ may be, the remaining decisions constitute an optimal policy with regard to the state resulting from the first decision" [27]. This principle of optimality can be used for the proof of the following statement: "A trajectory optimizes the norm of torques globally only if it optimizes them locally ". In other words, the trajectory which globally optimizes the required torques is one of the trajectories which optimize the required torques locally. This statement is useful for obtaining the trajectory in the joint angle space which both follows the cartesian space end effector's trajectory and optimizes the required torques globally. The possible initial states $(\theta_0, \dot{\theta}_0)$ for starting a job can be sought from those which satisfy the kinematic constraint equations. Therefore, to find the global torque optimal trajectory becomes simpler and can be achieved by applying the local torque optimization algorithm and searching for the proper initial conditions (state) from the possible initial postures and joint rates. According to this argument, a global optimum can be found by sampling the entire feasible set of initial states and following the local optimization control strategy.

Two cases are considered for finding a trajectory to optimize the required torque globally. The first case is to start a job with fixed (zero) initial joint rate and a varied initial configuration. In this case, the best posture to minimize the torque can be searched among the possible configurations which has the same starting end effector position. The second case is to start a job with fixed initial posture and a varied initial joint rate. In this case, a suitable initial joint rate can be searched along the direction of null space and a local optimum with respect to this posture can be found. A comparison of the results between the proposed local optimization algorithm and the global algorithm proposed by Hollerbach and Suh

[13] will be given in a later section.

Resolution of the kinematic redundancy for optimizing the global performance measure is an important issue for controlling a redundant manipulator. The questions of how the algorithms work and how they are related to the optimization of the local performance measures are studied in this chapter. Several important performance measures such as joint rates' norm, kinetic energy consumption, joint accelerations' norm and actuators' torques are considered. General formulas of resolving the redundancy through global optimization of these performance measures are derived. The global and local optimization algorithms are related by the principle of optimality, so that the resolution of the redundancy through optimization of a global performance measure can be obtained by the resolution of the redundancy through optimization of a local performance measure with starting at a proper initial state.

6.1 Review of Global Optimization Methods

Much research has been done on the topic of the resolution of redundancy through global optimization [11,13,19,28,29]. Those that are related to this research are reviewed in this section.

6.1.1 Nakamura and Hanafusa Method

Nakamura and Hanafusa [19] have applied Pontryagin's maximum principle [27] to formulate the redundancy resolution problem as an optimal control problem where the null-space components treated as the control input. The optimal control of redundancy for the performance measure $I_{\dot{\theta}}$ was represented as follows:

$$\dot{\theta} = J^{+}\dot{\mathbf{x}} + (I - J^{+}J)\mathbf{y} \tag{6.1}$$

$$I_{\dot{\theta}} = \int_{t_0}^{t_f} \dot{\theta}^T \dot{\theta} dt \tag{6.2}$$

By applying the Pontryagin principle, the Hamiltonian for this problem is

$$H(\psi, \theta, t, y) = -\dot{\theta}^T \dot{\theta} + \psi[J^+ \dot{\mathbf{x}} + (I - J^+ J)\mathbf{y}] \tag{6.3}$$

where ψ is an adjoint vector. The optimal $\mathbf{y}(t)$ that maximizes the Hamiltonian Eq. (6.3) at every moment t, and the optimal trajectory θ are found by solving the following two-points split boundary value problem:

$$\begin{aligned} \dot{\theta} &= \frac{\partial H}{\partial \psi}, \\ \dot{\psi} &= -(\frac{\partial H}{\partial \theta}), \end{aligned} \tag{6.4}$$

with boundary conditions:

$$\begin{aligned} &\text{left end boundary} && \mathbf{x}(t_0) = \mathbf{f}(\theta(t_0)), \\ & && [I - J^+(\dot{\theta}(t_0))J(\theta(t_0))]\psi(t_0) = \mathbf{0} \\ &\text{right end boundary} && \psi(t_f) = \mathbf{0} \end{aligned} \tag{6.5}$$

An initial value adjusting method [30] was proposed and this two-points boundary value problem was solved conversely from t_f to t_0 then the original optimal problem was converted to a minimum value search problem.

6.1.2 Hollerbach and Suh Method

The local torque optimization technique developed by Hollerbach and Suh [12] encounters a stability problem when the end effector movement gets larger. It is

undesirable for requiring a big amount of torque to go through some specific configurations, while the algorithm is designed and expected to optimize the torques. A globally optimization technique was proposed by Hollerbach and Suh [13] to solve this problem. They used calculus of variation techniques and redundancy parameterization to achieve a global optimal solution. But the special way of redundancy parameterization restricts their algorithm so that it is valid for a special manipulator. And the complicated computations also make their global optimal solution not practical for real-time applications.

Hollerbach and Suh [13] parameterized the redundancy by having $\phi = \theta_1 + \theta_2 + \theta_3$ and applied calculus of variation to derive a 4th order differential equation for ϕ that is the Euler-Lagrange equation for resolving the redundancy through optimization of the norm of torque globally. They set the initial posture to an arbitrary configuration and the initial joint rates to 0 and search over the second and third order derivatives ($\ddot{\phi}(0)$ and $\frac{\partial^3 \phi}{\partial t_3}(0)$) to arrive at an optimal trajectory which minimized the global measure, i.e., the integration of the torque square along the specified trajectory. This method has several disadvantages: first, the parameterization of the redundancy is valid only for the 3−link planar manipulator, a special case. For other cases, it is very difficult to use this kind of parameterization. That is, this kind of parameterization is very difficult to extend and to apply to other manipulators. Second, the initial configuration and initial joint rate should be allowed to change during the optimization search so that a real optimal solution can be reached, that is, a four-dimensional instead of a two-dimensional search should be conducted. Finally, a fourth-order differential equation should be solved with split boundary conditions split at the initial and final time instants, that is, a two-point boundary value problem should be solved for finding the optimal solution.

On the other hand, if the local optimization algorithm is used for updating the corresponding state $(\theta, \dot{\theta})$, and a two-dimensional search is carried over the possible initial states which satisfy both the constraint equations $\mathbf{x} = f(\theta)$ and $\dot{\mathbf{x}} = J\dot{\theta}$, then there is no need for parameterization for the redundancy, and only a second order differential equation needs to be satisfied.

A general formula for globally optimizing the required torques is derived in the next section. The redundancies in the derived formula are expressed in terms of the jacobian matrix, and no special parameterizations has been introduced. In conclusion,

- By using the local torque optimization technique, an optimal trajectory which optimizes the torque globally may not exist. The main reason for the instability is that the algorithm may pass through a state which is dynamically singular. In order to solve this problem, either a partial amount of null-space component should be applied to optimize the required torque or a proper initial state value $(\theta, \dot{\theta})$ should be chosen to start a job.

- For a given end effector position and some reachable point in the cartesian space, a stable joint space trajectory which follows the local torque optimization algorithm can be found, by searching either over all the possible initial configuration or joint rate or both of them.

- The principle of optimality relates the redundancy resolution algorithms for local and global optimization of torques. That is, the global optimization of torque can be achieved by sampling all the feasible local torque optimization solutions

6.2 Derivation of the Formulas for Resolving Redundancy Globally at the Velocity Level

The Euler-Lagrange equation and boundary conditions for resolving the kinematic redundancy at the velocity level and globally optimizing the joint rate or energy consumption are derived in this section.

6.2.1 Redundancy Resolution through Global Joint Rate Square Optimization

Before deriving the formula for optimizing the energy consumption globally, the global optimization of joint rate is first derived. The problem of globally optimizing the norm of joint rate is defined as: derive the Euler-Lagrange equation and the required boundary conditions for optimizing the following cost function

$$I_{\dot{\theta}} = \int_{t_0}^{t_f} \dot{\theta}^T \dot{\theta} dt \tag{6.6}$$

with the following coordinate transformation equations as their equality constraints.

$$f_k(\theta, \mathbf{x}) = 0. \tag{6.7}$$

The theory of calculus of variation gives the Euler-Lagrange equation to optimize the cost function of Eq. (6.6) with constraint equation Eq. (6.7) as:

$$\frac{\partial g_a}{\partial \theta} - \frac{d}{dt}\frac{\partial g_a}{\partial \dot{\theta}} = 0 \tag{6.8}$$

where

$$g_a = \dot{\theta}^T \dot{\theta} + \sum_k \lambda_k f_k(\theta, \mathbf{x}) \tag{6.9}$$

is the augmented cost function. Each term of the Eq. (6.8) is calculated as follows:

$$\frac{\partial g_a}{\partial \theta} = \sum_k \lambda_k \frac{\partial f_k(\theta, \mathbf{x})}{\partial \theta} = J^T \boldsymbol{\lambda} \tag{6.10}$$

and

$$\frac{\partial g_a}{\partial \dot{\theta}} = 2\ddot{\theta}. \tag{6.11}$$

By substituting Eqs. (6.10) and (6.11) into Eq. (6.8)

$$\ddot{\theta} = -0.5 J^T \lambda. \tag{6.12}$$

The constraint equation at the acceleration level for a redundant manipulator is

$$\ddot{\mathbf{x}} = J\ddot{\theta} + \dot{J}\dot{\theta}. \tag{6.13}$$

By substituting Eq. (6.13) into Eq. (6.12) and solving for λ

$$\lambda = -2(JJ^T)^{-1}(\ddot{\mathbf{x}} - \dot{J}\dot{\theta}) \tag{6.14}$$

is obtained. By substituting Eq. (6.14) back into Eq. (6.12), the Euler-Lagrange equation for global optimization of the cost function (6.6) is obtained.

$$\begin{aligned} \ddot{\theta} &= J^T(JJ^T)^{-1}(\ddot{\mathbf{x}} - \dot{J}\dot{\theta}) \\ &= J^+(\ddot{\mathbf{x}} - \dot{J}\dot{\theta}). \end{aligned} \tag{6.15}$$

As far as the boundary conditions are concerned, the following equations must be satisfied both at the initial time, $t = t_0$ and at the final time, $t = t_f$ are

$$\begin{aligned} \mathbf{x} &= f(\theta) \\ \dot{\theta} &= J^+\dot{\mathbf{x}}. \end{aligned} \tag{6.16}$$

6.2.2 Resolving Kinematic Redundancy through Global Kinematic Energy Optimization

By considering the integration of the kinematic energy squared as an objective function, the Euler-Lagrange equation and the associated boundary conditions for globally optimizing the energy consumption are derived as follows: The cost function is:

$$I_{H\dot{\theta}} = \int_{t_0}^{t_f} (H\dot{\theta})^T (H\dot{\theta}) dt. \tag{6.17}$$

and the kinematic constraint equation is:

$$f_k(\theta, \mathbf{x}) = 0. \tag{6.18}$$

From the theory of calculus of variation, the Euler-Lagrange equation is

$$\frac{\partial g_a}{\partial \theta} - \frac{d}{dt}\frac{\partial g_a}{\partial \dot{\theta}} = 0 \tag{6.19}$$

$$\begin{aligned} g_a &= \dot{\theta}^T H^T H \dot{\theta} + \sum_k \lambda_k f_k(\theta, \mathbf{x}) \\ &= \dot{\theta}^T A \dot{\theta} + \sum_k \lambda_k f_k(\theta, \mathbf{x}) \end{aligned} \tag{6.20}$$

is the augmented cost function with $A = H^T H$. Each term of the Eq. (6.7) is calculated as follows:

$$\begin{aligned} \frac{\partial g_a}{\partial \theta} &= \frac{\partial(\dot{\theta}^T A \dot{\theta})}{\partial \theta} + \sum_k \lambda_k \frac{\partial f_k(\theta, \mathbf{x})}{\partial \theta} \\ &= \frac{\partial(\dot{\theta}^T A \dot{\theta})}{\partial \theta} + J^T \lambda \end{aligned} \tag{6.21}$$

$$\frac{d}{dt}\frac{\partial g_a}{\partial \dot{\theta}} = 2(A\ddot{\theta} + \dot{A}\dot{\theta}). \tag{6.22}$$

By substituting Eqs. (6.21) and (6.22) into Eq. (6.19) then

$$\ddot{\theta} = -0.5A^{-1}J^T\lambda + \mathbf{b} \tag{6.23}$$

where

$$\mathbf{b} = -A^{-1}[0.5\frac{\partial(\dot{\theta}^T A\dot{\theta})}{\partial\theta} + \dot{A}\dot{\theta}]. \tag{6.24}$$

The constraint equations at the acceleration level for a redundant manipulator is:

$$\ddot{\mathbf{x}} = J\ddot{\theta} + \dot{J}\dot{\theta}. \tag{6.25}$$

By substituting Eq. (6.23) into Eq. (6.25) and solve for λ

$$\lambda = -2(JA^{-1}J^T)^{-1}[(\ddot{\mathbf{x}} - \dot{J}\dot{\theta}) - J\mathbf{b}] \tag{6.26}$$

By substituting Eq. (6.26) back into Eq. (6.23) and the Euler-Lagrange equation for global optimization of the cost function (6.69) gives

$$\ddot{\theta} = J_A^{\dagger}(\ddot{\mathbf{x}} - \dot{J}\dot{\theta}) + [I - J_A^{\dagger}J]\mathbf{b} \tag{6.27}$$

where $J_A{}^{+} = A^{-1}J^T(JA^{-1}J^T)^{-1}$ and b is given by Eq. (6.24)

As far as the boundary conditions are concerned, the following equations must be satisfied both at the initial time $t = t_0$ and at the final time $t = t_f$.

$$\begin{aligned} \mathbf{x} &= f(\theta) \\ \dot{\theta} &= J_A^{\dagger}\dot{\mathbf{x}}. \end{aligned} \tag{6.28}$$

6.3 Derivation of the Formulas for Resolving Redundancy Globally at the Acceleration Level

Similarly the Euler-Lagrange equation and the boundary conditions for resolving the kinematic redundancy at the acceleration level by globally optimizing the norm of joint acceleration or the norm of the required torques can be derived.

6.3.1 Redundancy Resolution through Global Joint Acceleration Square Optimization

In order to find the formula for optimization of the required torques globally, the global optimization of norm of accelerations is first derived. The problem is defined as finding the Euler-Lagrange equation and the required boundary conditions for optimizing the following cost function

$$I_{\ddot{\theta}} = \int_{t_0}^{t_f} \ddot{\theta}^T \ddot{\theta} dt \tag{6.29}$$

with the following coordinate transformation equations as their equality constraint.

$$f_k(\theta, \mathbf{x}) = 0. \tag{6.30}$$

The calculus of variation theory gives the required Euler-Lagrange equation to optimize the cost function of Eq. (6.29) with constraint Eq. (6.30) to be

$$\frac{\partial g_a}{\partial \theta} - \frac{d}{dt}\frac{\partial g_a}{\partial \dot{\theta}} + \frac{d^2}{dt^2}\frac{\partial g_a}{\partial \ddot{\theta}} = 0 \tag{6.31}$$

where

$$g_a = \ddot{\theta}^T \ddot{\theta} + \sum_k \lambda_k f_k(\theta, \mathbf{x}) \tag{6.32}$$

is the augmented cost function. Each term of Eq. (6.31) is calculated as follows:

$$\frac{\partial g_a}{\partial \theta} = \sum_k \lambda_k \frac{\partial f_k(\theta, \mathbf{x})}{\partial \theta} = J^T \boldsymbol{\lambda} \tag{6.33}$$

where

$$J = \frac{\partial f_k(\theta, \mathbf{x})}{\partial \theta} \tag{6.34}$$

is the Jacobian of the manipulator, and $\boldsymbol{\lambda} = [\lambda_1, \lambda_2, \cdots, \lambda_m]^T$ is the Lagrange multiplier for the m constraint equations.

$$\frac{\partial g_a}{\partial \dot{\theta}} = 0 \tag{6.35}$$

$$\frac{d^2}{dt^2}(\frac{\partial g_a}{\partial \ddot{\theta}}) = \frac{d^2}{dt^2}(2\ddot{\theta}) = 2\frac{d^4\theta}{dt^4}. \tag{6.36}$$

By substituting Eqs. (6.33),(6.35) and (6.36) into Eq. (6.31)

$$\frac{d^4\theta}{dt^4} = -0.5 J^T \boldsymbol{\lambda} \tag{6.37}$$

is obtained.

From the previous chapter Eq. (4.5), the 4th order constraint equations for a redundant manipulator expressed as

$$\frac{d^4\mathbf{x}}{dt^4} = J\frac{d^4\theta}{dt^4} + 3(\dot{J}\frac{d^3\theta}{dt^3} + \ddot{J}\ddot{\theta}) + \frac{d^3J}{dt^3}\dot{\theta}. \tag{6.38}$$

By substituting Eq. (6.37) into Eq. (6.38) and solving for $\boldsymbol{\lambda}$

$$\boldsymbol{\lambda} = -2(JJ^T)^{-1}[\frac{d^4\mathbf{x}}{dt^4} - 3(\dot{J}\frac{d^3\theta}{dt^3} + \ddot{J}\ddot{\theta}) - \frac{d^3J}{dt^3}\dot{\theta}] \tag{6.39}$$

is obtained.

By substituting Eq. (6.39) back into Eq. (6.37) then the Euler-Lagrange equation for global optimization of the cost function Eq. (6.29)

$$\begin{aligned} \frac{d^4\theta}{dt^4} &= J^T(JJ^T)^{-1}[\frac{d^4\mathbf{x}}{dt^4} - 3(\dot{J}\frac{d^3\theta}{dt^3} + \ddot{J}\ddot{\theta}) - \frac{d^3J}{dt^3}\dot{\theta}] \\ &= J^+[\frac{d^4\mathbf{x}}{dt^4} - 3(\dot{J}\frac{d^3\theta}{dt^3} + \ddot{J}\ddot{\theta}) - \frac{d^3J}{dt^3}\dot{\theta}] \end{aligned} \tag{6.40}$$

is obtained.

As far as the boundary conditions are concerned, the following equations must be satisfied both at the initial time $t = t_0$ and at the final time $t = t_f$.

$$\begin{aligned} \mathbf{x} &= f(\theta) \\ \dot{\mathbf{x}} &= J\dot{\theta} \\ \ddot{\theta} &= J^{+}(\ddot{\mathbf{x}} - \dot{J}\dot{\theta}) \\ \frac{d^3\mathbf{x}}{dt^3} &= J\frac{d^3\theta}{dt^3} + 2\dot{J}\ddot{\theta} + \ddot{J}\dot{\theta}. \end{aligned} \tag{6.41}$$

6.3.2 Redundancy Resolution through Global Optimization of Joint Torques

Before deriving the Euler-Lagrange equation for global optimization of the required torque the following problem is first solved. This problem is defined as finding the Euler-Lagrange equation and the required boundary conditions so that the following cost function is optimized:

$$I_{H\ddot{\theta}} = \int_{t_0}^{t_f} (H\ddot{\theta})^T (H\ddot{\theta}) dt \tag{6.42}$$

subject to the constrains

$$f_k(\theta, \mathbf{x}) = 0 \tag{6.43}$$

From the theory of calculus of variation, the Euler-Larange equation is

$$\frac{\partial g_a}{\partial \theta} - \frac{d}{dt}\frac{\partial g_a}{\partial \dot{\theta}} + \frac{d^2}{dt^2}\frac{\partial g_a}{\partial \ddot{\theta}} = 0 \tag{6.44}$$

where

$$\begin{aligned} g_a &= \ddot{\theta}^T H^T H\, \ddot{\theta} + \sum_k \lambda_k f_k(\theta, \mathbf{x}) \\ &= \ddot{\theta}^T A \ddot{\theta} + \sum_k \lambda_k f_k(\theta, \mathbf{x}) \end{aligned} \tag{6.45}$$

is the augmented cost function and $A = H^T H$.

Each term of Eq. (6.44) is calculated as follows:

$$\begin{aligned} \frac{\partial g_a}{\partial \theta} &= \frac{\partial(\ddot{\theta} A\, \ddot{\theta})}{\partial \theta} + \sum_k \lambda_k \frac{\partial f_k(\theta, \mathbf{x})}{\partial \theta} \\ &= \frac{\partial(\ddot{\theta} A\, \ddot{\theta})}{\partial \theta} + J^T \boldsymbol{\lambda} \end{aligned} \tag{6.46}$$

$$\frac{\partial g_a}{\partial \dot{\theta}} = 0 \tag{6.47}$$

$$\frac{d^2}{dt^2} \frac{\partial g_a}{\partial \ddot{\theta}} = \frac{d^2}{dt^2}(2A\ddot{\theta}) = 2(A\frac{d^4\theta}{dt^4} + 2\dot{A}\frac{d^3\theta}{dt^3} + \ddot{A}\, \ddot{\theta}). \tag{6.48}$$

By substituting Eqs. (6.46),(6.47) and (6.48) into Eq. (6.44)

$$\frac{d^4\theta}{dt^4} = -0.5A^{-1}J^T\boldsymbol{\lambda} + \mathbf{c} \tag{6.49}$$

is obtained where

$$\mathbf{c} = -A^{-1}[0.5\frac{\partial(\ddot{\theta}^T A\ddot{\theta})}{\partial \theta} + 2\dot{A}\frac{d^3\theta}{dt^3} + \ddot{A}\ddot{\theta}]. \tag{6.50}$$

By substituting Eq. (6.49) into Eq. (6.38) and solving for $\boldsymbol{\lambda}$

$$\boldsymbol{\lambda} = -2(JA^{-1}J^T)^{-1}[\frac{d^4\mathbf{x}}{dt^4} - 3(\dot{J}\frac{d^3\theta}{dt^3} + \ddot{J}\theta) - \frac{d^3J}{dt^3}\dot{\theta} - J\mathbf{c}] \tag{6.51}$$

is obtained.

By substituting Eq. (6.51) back into Eq. (6.49) then the Euler-Lagrange equation for global optimization of the cost function (6.42) is

$$\begin{aligned}
\frac{d^4\theta}{dt^4} &= -0.5A^{-1}J^T\lambda + \mathbf{c} \\
&= A^{-1}J^T(JA^{-1}J^T)^{-1}[\frac{d^4\mathbf{x}}{dt^4} - 3(\dot{J}\frac{d^3\theta}{dt^3} + J\ddot{\theta}) - \frac{d^3J}{dt^3}\dot{\theta}]\mathbf{c} \\
&\quad -[A^{-1}J^T(JA^{-1}J^T)^{-1}J - I]\mathbf{b} \\
&= J_A{}^+[\frac{d^4\mathbf{x}}{dt^4} - 3(\dot{J}\frac{d^3\theta}{dt^3} + \ddot{J}\ddot{\theta}) - \frac{d^3J}{dt^3}\dot{\theta}] - [J_A{}^+J - I]\mathbf{c} \qquad (6.52)
\end{aligned}$$

where $J_A{}^+ = A^{-1}J^T(JA^{-1}J^T)^{-1}$ and $\mathbf{c}$ is given by Eq. (6.50).

As far as the boundary conditions are concerned, the following equations are satisfied both at the initial time $t = t_0$ and at the final time $t = t_f$.

$$\begin{aligned}
\mathbf{x} &= f(\theta) \\
\dot{\mathbf{x}} &= J\dot{\theta} \\
\ddot{\theta} &= J_A^{\dagger}(\ddot{\mathbf{x}} - \dot{J}\dot{\theta}) \\
\frac{d^3\mathbf{x}}{dt^3} &= J\frac{d^3\theta}{dt^3} + 2\dot{J}\ddot{\theta} + \ddot{J}\,\dot{\theta}. \qquad (6.53)
\end{aligned}$$

The Euler-Lagrange equation and the associated boundary conditions for global optimization of the joint torques will now be derived:

This problem is defined as finding the Euler-Lagrange equation and the required boundary conditions so that the following cost function is optimized.

$$I_\tau = \int_{t_0}^{t_f} \tau^T\tau dt \qquad (6.54)$$

which subject to the constraints

$$f_k(\theta, \mathbf{x}) = 0 \tag{6.55}$$

and with

$$\tau = H\ddot{\theta} + \mathbf{C}(\dot{\theta}, \theta) + \mathbf{g}(\theta) \tag{6.56}$$

where $H\ddot{\theta}$ is the component due to the joint accelerations, $\mathbf{C}(\dot{\theta}, \theta)$ is the coriolis and centrifugal torque and $\mathbf{g}(\theta)$ is torque generated by gravity. Then the term $\tau^T\tau$ becomes

$$\begin{aligned}
\tau^T\tau &= [H\ddot{\theta} + \mathbf{C}(\dot{\theta}, \theta) + \mathbf{g}(\theta)]^T[H\ddot{\theta} + \mathbf{C}(\theta, \theta) + \mathbf{g}(\theta)] \\
&= \ddot{\theta}^T H^T H\ddot{\theta} + \ddot{\theta}^T H^T(\mathbf{C} + \mathbf{g}) + (\mathbf{C} + \mathbf{g})^T H\ddot{\theta} + (\mathbf{C} + \mathbf{g})^T(\mathbf{C} + \mathbf{g}) \\
&= \ddot{\theta}^T A\ddot{\theta} + \ddot{\theta}^T \mathbf{P}(\dot{\theta}, \theta) + \mathbf{P}^T(\dot{\theta}, \theta)\ddot{\theta} + \mathbf{Q}^T(\dot{\theta}, \theta)\mathbf{Q}(\dot{\theta}, \theta)
\end{aligned} \tag{6.57}$$

where

$$\begin{aligned}
H(\theta)^T H(\theta) &= A(\theta) \\
H(\theta)^T[C(\dot{\theta}, \theta) + \mathbf{g}(\theta)] &= \mathbf{P}(\dot{\theta}, \theta) \\
C(\dot{\theta}, \theta) + \mathbf{g}(\theta) &= \mathbf{Q}(\dot{\theta}, \theta)
\end{aligned} \tag{6.58}$$

From the theory of calculus of variation, the Euler-Lagrange equation is:

$$\frac{\partial g_a}{\partial \theta} - \frac{d}{dt}\frac{\partial g_a}{\partial \dot{\theta}} + \frac{d^2}{dt^2}\frac{\partial g_a}{\partial \ddot{\theta}} = 0 \tag{6.59}$$

where

$$g_a = \tau^T\tau + \sum_k \lambda_k f_k(\theta, \mathbf{x}) \tag{6.60}$$

is the augmented cost function. From equation (6.57)

$$g_a = \ddot{\theta}^T A\ddot{\theta} + \ddot{\theta}^T \mathbf{P}(\dot{\theta},\theta) + \mathbf{P}^T(\dot{\theta},\theta)\ddot{\theta} + \mathbf{Q}^T(\dot{\theta},\theta)\mathbf{Q}(\dot{\theta},\theta) + \sum_k \lambda_k f_k(\theta,\mathbf{x}) \quad (6.61)$$

is obtained.

Each term of Eq. (6.59) is calculated as follows:

$$\begin{aligned}\frac{\partial g_a}{\partial \theta} &= \frac{\partial}{\partial \theta}(\ddot{\theta}^T A\ddot{\theta} + \ddot{\theta}^T \mathbf{P} + \mathbf{P}^T\ddot{\theta} + \mathbf{Q}^T\mathbf{Q}) + \sum_k \lambda_k f_k(\theta,\mathbf{x})) \\ &= \frac{\partial}{\partial \theta}(\ddot{\theta}^T A\ddot{\theta} + \ddot{\theta}^T \mathbf{P} + \mathbf{P}^T\ddot{\theta} + \mathbf{Q}^T\mathbf{Q}) + J^T\boldsymbol{\lambda} \quad (6.62)\end{aligned}$$

$$\frac{\partial g_a}{\partial \dot{\theta}} = \frac{\partial}{\partial \dot{\theta}}(\ddot{\theta}^T \mathbf{P} + \mathbf{P}^T\ddot{\theta} + \mathbf{Q}^T\mathbf{Q}) \quad (6.63)$$

$$\begin{aligned}\frac{d^2}{dt^2}\frac{\partial g_a}{\partial \ddot{\theta}} &= \frac{d^2}{dt^2}[2(A\ddot{\theta} + \mathbf{P})] \\ &= 2(A\frac{d^4\theta}{dt^4} + 2\dot{A}\frac{d^3\theta}{dt^3} + \ddot{A}\ddot{\theta} + \ddot{\mathbf{P}}). \quad (6.64)\end{aligned}$$

By substituting Eqs. (6.62),(6.63) ands (6.64) into equation (6.59)

$$\frac{d^4\theta}{dt^4} = -0.5A^{-1}J^T\boldsymbol{\lambda} + \mathbf{d} \quad (6.65)$$

where

$$\begin{aligned}\mathbf{d} &= A^{-1}[-0.5\frac{\partial}{\partial \theta}(\ddot{\theta}^T A\ddot{\theta} + \ddot{\theta}^T \mathbf{P} + \mathbf{P}^T\ddot{\theta} + \mathbf{Q}^T\mathbf{Q}) + 0.5\frac{d}{dt}\frac{\partial}{\partial \dot{\theta}}(\ddot{\theta}\mathbf{P}^T \\ &\quad + \mathbf{P}^T\ddot{\theta} + \mathbf{Q}^T\mathbf{Q}) - (2\dot{A}\frac{d^3\theta}{dt^3} + \ddot{A}\ddot{\theta} + \ddot{\mathbf{P}})] \quad (6.66)\end{aligned}$$

is obtained.

By substituting Eq. (6.65) into Eq. (6.38) and solving for $\boldsymbol{\lambda}$

$$\boldsymbol{\lambda} = -2(JA^{-1}J^T)^{-1}[\frac{d^4\mathbf{x}}{dt^4} - 3(\dot{J}\frac{d^3\theta}{dt^3} + \ddot{J}\ddot{\theta}) - \frac{d^3J}{dt^3}\dot{\theta} - J\mathbf{d}] \quad (6.67)$$

is obtained.

By substituting Eq. (6.67) back into Eq. (6.65) then the Euler-Lagrange equation for global optimization of the cost function (6.54), i.e., I_T

$$\begin{aligned}
\frac{d^4\theta}{dt^4} &= -0.5A^{-1}J^T\lambda + A^{-1}\mathbf{d} \\
&= A^{-1}J^T(JA^{-1}J^T)^{-1}[\frac{d^4\mathbf{x}}{dt^4} - 3(\dot{J}\frac{d^3\theta}{dt^3} + \ddot{J}\ddot{\theta}) - \frac{d^3J}{dt^3}\dot{\theta}] \\
&\quad -[A^{-1}J^T(JA^{-1}J^T)^{-1}J - I]A^{-1}\mathbf{d} \\
&= J_A{}^+[\frac{d^4\mathbf{x}}{dt^4} - 3(\dot{J}\frac{d^3\theta}{dt^3} + \ddot{J}\ddot{\theta}) - \frac{d^3J}{dt^3}\dot{\theta}] - [J_A{}^+J - I]\mathbf{d} \qquad (6.68)
\end{aligned}$$

is obtained.

As far as the boundary conditions are concerned, the following equations must be satisfied both at the initial time $t = t_0$ and at the final time $t = t_f$.

$$\begin{aligned}
\mathbf{x} &= f(\theta) \\
\dot{\mathbf{x}} &= J\dot{\theta} \\
\ddot{\theta} = J^+(\ddot{\mathbf{x}} - \dot{J}\dot{\theta}) + [H(I - J^+J)]^+(-\tau_p) \\
\frac{d^3\mathbf{x}}{dt^3} &= J\frac{d^3\theta}{dt^3} + 2\dot{J}\ddot{\theta} + \ddot{J}\dot{\theta}. \qquad (6.69)
\end{aligned}$$

The problems of joint rate, joint acceleration and required torque optimization have the common feature that the possible initial state $(\theta, \dot{\theta})$ is not random. They belong to a special set which depends on the end effector's position. This feature makes the global search easier and simpler. The optimal solution can be obtained by carrying the search over this special set. It is not necessary to solve a complicated two-point boundary value problem.

6.4 Summary

Resolution of the kinematic redundancy for optimizing the global performance measure is an important issue for controlling a redundant manipulator. The questions of how the algorithms work and how they are related to the optimization of the local performance measures have been studied in this chapter. Several important performance measures such as joint rates' norm, kinetic energy consumption, joint accelerations' norm and actuators' torques are considered. General formulas of resolving the redundancy through global optimization of these performance measures are derived. The global and local optimization algorithms are related by the principle of optimality, so that the resolution of the redundancy through optimization of a global performance measure can be obtained by the resolution of the redundancy through optimization of a local performance measure with starting at a proper initial state.

A local optimization technique does not take the initial state into account and therefore it may not get an optimal global trajectory. Partial utilization of the redundancy can be applied to control a redundant manipulator and achieve an acceptable global performance measure. At optimal initial states, the optimal trajectories satisfy both local and global optimization criteria. Therefore, global optimization can be implemented by sampling all the feasible trajectories which satisfy the local optimization criteria.

CHAPTER VII

CONCLUSION AND SUGGESTION OF FUTURE WORK

7.1 Conclusion

The redundancy introduced to a manipulator has been shown to be useful for improving the system performance. The performance is improved either by increasing the flexibility or reducing the required efforts through the proper usage of the null space components. The kinematic redundancy of a manipulator can be resolved through either local or global optimization of different objective functions. Several approaches have been developed for resolving the kinematic redundancy. Due to the complicated physical structure and control schemes needed for controlling the redundant manipulator, developing proper algorithms for redundancy utilization is important for facilitating the control of a redundant manipulator.

In this work, two popular schemes for redundancy resolution, minimum norm of joint rate and minimum norm of joint acceleration methods are investigated and compared. Moreover, the resolution of the redundancy is extended to the minimization of the norm of high-order derivatives. These resolution schemes and the relationships between them are obtained. The effects of using the null space are demonstrated through the optimization of different performance measures. An important property that has been found is that initial postures which minimize the global measure of joint rate's norm are conservative.

The instability problem of the local torque optimization technique has been

studied. The dynamic singularities which cause stability problem of local torque optimization are introduced and two possible solutions to avoid the manipulator falling into these undesirable situations are proposed. Global optimization together with best location of the base are determined. The relationship between the methods of resolving kinematic redundancy through local and global optimizations are obtained.

The results which are obtained from this work are summarized as follows:

- The homogeneous sets of initial postures and joint rates are useful test bases for evaluating the performance for different redundancy resolving methods

- The choice of proper initial posture, initial joint rate and base location are useful for a redundant manipulator to achieve better performance measures.

- At the optimal configuration, the solution is conservative and the trajectories satisfy both local and global optimization criteria.

- As the redundancy is resolved at the higher-derivative level, the cost function become more sensitive to the initial postures.

- A local optimization technique which starts to perform a job at an arbitrary initial state may not arrive at an optimal trajectory. Therefore, partial utilization of the redundancy for controlling a redundant manipulator in choicing an initial state can achieve an acceptable global performance measure.

- A general formula of resolution of kinematic redundancy through global optimization of torques, which is not restricted to a planar 3–link manipulator, has been derived.

- The principle of optimality makes it possible to obtain global optimization by searching among the possible initial states.

7.2 Extended Research

Redundancy resolution techniques are very important for the control of a kinematic redundant manipulator. Stable and effective algorithms are required for resolving the redundancy so that the undesirable situations can be avoided and the performance can be improved. In this work, a three-link planar manipulator model and simple performance measures are used for computer simulation. In this model only the position in the x-y plane is considered. For a real manipulator, both position and orientation should be considered, that is, using a multi-criteria objective function and three-dimensional model including both position and orientation is the next stage of research.

Computation time is another factor to be considered in future research. The computation for resolving the kinematic redundancy is time consuming, therefore, either efficient computation algorithms or powerful machines can be used to improve the processing speed so that the optimization process can be achieved in a resonable time.

APPENDIX A

FORMULAS FOR CALCULATING TORQUES FOR A 3-LINK PLANAR MANIPULATOR

The recursive Newton-Euler's dynamic equations for the required torques of a 3−link planar manipulator are derived in the following sections. First, the coordinate transformation is introduced, then the corresponding recursive equations for calculating the required torques are derived.

A.1 Coordinate Transformation

The link coordinate is defined according to Denavit-Hartenberg notation [31]. With this notation, the joints of a manipulator which start from the base are called the 1st joint, the 2nd joint,$\cdots$ etc. and end with the end effector, the $(n+1)$th joint. The ith link connects the ith joint with the $(i+1)$th joint. There are n joint coordinate frames assigned for a n−link manipulator with the origin of the ith coordinate located at the $(i+1)$th joint. The link parameters α_i, d_i, a_i and θ_i are shown in Fig. 79 [31]. In order to simplify the computation, the manipulators which are composed of only simple rotational joints are considered. That is, α_i, d_i, and a_i are constants, and only θ_i is a variable.

Let ${}^jA_i$ be the coordinate transformation matrix which transform the quantities from the ith coordinate to the jth coordinate. The column vectors of ${}^jA_i$ represents unit vectors in the directions of $\hat{x}_i$, $\hat{y}_i$, $\hat{z}_i$ with reference to the jth

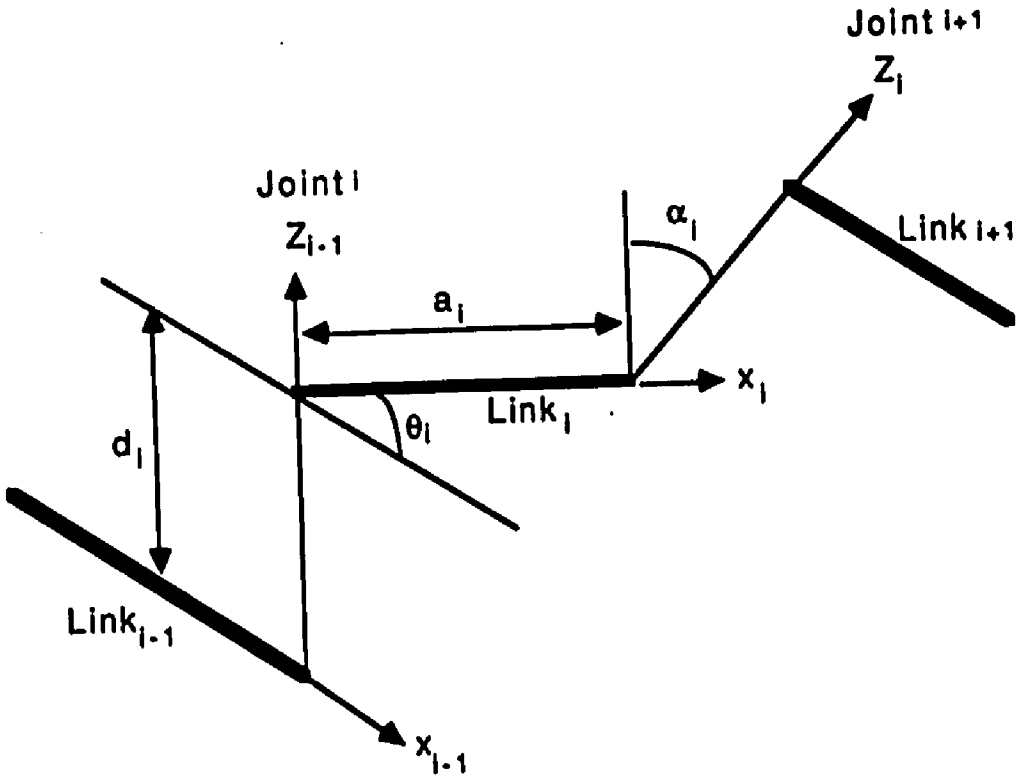

Figure 79: The Denavit-Hartenberg notation for a manipulator [31]

coordinate. That is,

$$\begin{bmatrix} {}^{j}x & {}^{j}y & {}^{j}z \end{bmatrix}^T = {}^{j}A_i \begin{bmatrix} {}^{i}x & {}^{i}y & {}^{i}z \end{bmatrix}^T. \tag{A.1}$$

The matrix ${}^{j}A_i$ can also be decomposed into the product of succeeding coordinate transformation matrices, i.e.,

$${}^{j}A_i = {}^{j}A_k \, {}^{k}A_l \cdots {}^{p}A_i. \tag{A.2}$$

If only the revolute joints are considered, the Denavit-Hartenberg parameters [1] are $a = 0$, $d = 0$, and θ is the independent variable. The forward and backward rotational transformation matrix between coordinate i and $i+1$ are as follows:
1) the forward transformation, i.e., expressing the quantities in ith coordinate with respect to the $i+1$th coordinate is

$$\begin{bmatrix} x_{i+1} \\ y_{i+1} \\ z_{i+1} \end{bmatrix} = {}^{i+1}\mathbf{R}_i \begin{bmatrix} x_i \\ y_i \\ z_i \end{bmatrix}, \tag{A.3}$$

with the forward transformation matrix

$${}^{i+1}\mathbf{R}_i = \begin{bmatrix} C_{i+1} & S_{i+1} & 0 \\ -S_{i+1} & C_{i+1} & 0 \\ 0 & 0 & 1 \end{bmatrix}. \tag{A.4}$$

2) Backward transformation, i.e., expressing the quantities in $i+1$th coordinate with respect to ith coordinate is:

$$\begin{bmatrix} x_i \\ y_i \\ z_i \end{bmatrix} = {}^{i}\mathbf{R}_{i+1} \begin{bmatrix} x_{i+1} \\ y_{i+1} \\ z_{i+1} \end{bmatrix}, \tag{A.5}$$

with the backward transformation matrix

$$ {}^{i}\mathbf{R}_{i+1} = \begin{bmatrix} C_{i+1} & -S_{i+1} & 0 \\ S_{i+1} & C_{i+1} & 0 \\ 0 & 0 & 1 \end{bmatrix}, \qquad (A.6) $$

where $C_i = \cos\theta_i$ and $S_i = \sin\theta_i$.

A.2 Derivation of Recursive Equations for Calculating the Required Torques for a 3–link Manipulator

An efficient recursive formula for calculating the required forces and torques was developed by Orin and Schrader [23,32]. It was also summarized by Nakamura [24]. The derivation of the iterative torque equations has three steps: first using forward iterative equations to calculate the accelerations associated with the ith link from that of the $(i-1)$th link. Second, applying backward iterative equations to calculate the torque and force exerted on the ith link from that of $(i+1)$th link. Third, using Newton-Euler equations and force balance equation to link these two sets of equations, and the results give the torque iterative equations at the ith joint.

The inertia matrix of link i with respect to its own center of mass is

$$ {}^{c_i}I_i = \begin{bmatrix} 0 & 0 & 0 \\ 0 & I_{yy_i} & 0 \\ 0 & 0 & I_{zz_i} \end{bmatrix}. \qquad (A.7) $$

The forward recursive equations for calculating the acceleration associated with $(i+1)$th link are:

$$ {}^{i+1}\omega_{i+1} = {}^{i+1}R_i\,{}^{i}\omega_i + \dot{\theta}_{i+1}\,{}^{i+1}\hat{z}_{i+1} \qquad (A.8) $$

$$
\begin{aligned}
{}^{i+1}\dot{\omega}_{i+1} &= {}^{i+1}R_i\,{}^{i}\dot{\omega}_i + {}^{i+1}R_i\,{}^{i}\omega_i \times \dot{\theta}_{i+1}\,{}^{i+1}\hat{z}_{i+1} + \ddot{\theta}_{i+1}\,{}^{i+1}\hat{z}_{i+1} && \text{(A.9)}\\
{}^{i+1}\dot{v}_{i+1} &= {}^{i+1}R_i[{}^{i}\dot{\omega}_i \times {}^{i}P_{i+1} + {}^{i}\omega_i \times ({}^{i}\omega_i \times {}^{i}P_{i+1}) + {}^{i}\dot{v}_i] && \text{(A.10)}\\
{}^{i+1}\dot{v}_{c_{i+1}} &= {}^{i+1}\dot{\omega}_i \times {}^{i+1}P_{c_{i+1}} + {}^{i+1}\omega_{i+1} \times ({}^{i+1}\omega_{i+1} \times {}^{i}P_{i+1}) \\
&\quad + {}^{i+1}\dot{v}_{i+1}. && \text{(A.11)}
\end{aligned}
$$

The backward recursive equations for calculating the torque and force asserted on each link are:

$$
\begin{aligned}
{}^{i}f_i &= {}^{i}R_{i+1}\,{}^{i+1}f_{i+1} + {}^{i}F_i && \text{(A.12)}\\
{}^{i}n_i &= {}^{i}R_{i+1}\,{}^{i+1}n_{i+1} + {}^{i}P_{c_i} \times {}^{i}F_i + {}^{i}P_{i+1} \times {}^{i}R_{i+1}\,{}^{i+1}f_{i+1}. && \text{(A.13)}
\end{aligned}
$$

The forward and backward recursive equations are linked together through the relationship provided by Newton and Euler equations and the balance equations of force or torque at each link. That is, Newton's equation

$$
{}^{i}F_i = m_i\,{}^{i}\dot{v}_i \qquad \text{(A.14)}
$$

and Euler's equation

$$
{}^{i}N_i = {}^{c_i}I_i\,{}^{i}\dot{\omega}_i + {}^{i}\omega_i \times {}^{c_i}I_i\,{}^{i}\omega_i. \qquad \text{(A.15)}
$$

And the balance equations of force and torque for link i are

$$
\begin{aligned}
{}^{i}F_i &= {}^{i}f_i - {}^{i}f_{i-1}\\
{}^{i}N_i &= {}^{i}n_i - {}^{i}n_{i-1}, && \text{(A.16)}
\end{aligned}
$$

where ${}^i\mathbf{F}_i$: Force i acting on the center of mass for link i.

${}^i\mathbf{N}_i$: Torque i acting on the center of mass for link i.

${}^i\mathbf{f}_i$: Force i exerted on link i by link i-1.

${}^i\mathbf{n}_i$: Torque exerted on link i by link i-1.

l_i : the length of link i,

m_i : the mass of link i,

${}^i\mathbf{P}_{c_i}$: the position vector of the center of mass.

Assume there are no forces acting on the end effector, i.e., the forces $\mathbf{f}_{n+1}$, and the torques $\mathbf{n}_{n+1}$, acting on the end effector are zero. The base of the manipulator is assumed not moving, so that $\dot{\omega}_0 = 0$, $\omega_0 = 0$ and ${}^0\dot{\mathbf{v}}_0 = g\hat{y}_0$.

Since each link of a manipulator is considered as a rigid body, the location of the center of mass and the inertia matrix can be calculated if the mass distribution is given. In order to perform a task, each link should be accelerated or decelerated. The forces required for the desired motion are functions of the desired acceleration and deceleration, the mass distribution of each link and the specific task. Newton's equation and Euler's equation give the relations among the required forces and torques, inertias, and accelerations. The torque needed on each link to perform the job is

$$ {}^i\tau_i = {}^i\mathbf{n}_i^T \, {}^i\hat{z}_i, \tag{A.17} $$

The required torques on each link in closed form for a 3−link manipulator are derived as follows:

Assume there are no forces acting on the far end, i.e., $\mathbf{f}_4 = 0$ and $\mathbf{n}_4 = 0$. The base of the manipulator is not moving so, $\dot{\omega}_0 = 0$, $\omega_0 = 0$ and ${}^0\dot{\mathbf{v}}_0 = g\hat{y}_0$. For uniformly distributed mass, the position vector of the center of mass for link

i is ${}^{i}\mathbf{P}_{c_i} = 0.5l_i\hat{\mathbf{x}}_i$. The inertia matrix of this link with respect to its own center of mass is

$$ {}^{c_i}\mathbf{I}_i = \begin{bmatrix} 0 & 0 & 0 \\ 0 & I_{yy_1} & 0 \\ 0 & 0 & I_{zz_1} \end{bmatrix}. \tag{A.18} $$

The derivation starts by carrying the forward iteration. First the angular velocity ω and angular acceleration $\dot{\omega}$, with respect to the origin of ith coordinate, are calculated as follows:

$$ {}^{1}\omega_1 = \dot{\theta}_1\, {}^{1}\hat{\mathbf{z}}_1 = \begin{bmatrix} 0 \\ 0 \\ \dot{\theta}_1 \end{bmatrix}, \tag{A.19} $$

$$ {}^{2}\omega_2 = {}^{2}\mathbf{R}_1 \begin{bmatrix} 0 \\ 0 \\ \dot{\theta}_1 \end{bmatrix} + \dot{\theta}_2\, {}^{2}\hat{\mathbf{z}}_2 = \begin{bmatrix} 0 \\ 0 \\ \dot{\theta}_1 + \dot{\theta}_2 \end{bmatrix}, \tag{A.20} $$

$$ {}^{3}\omega_3 = \begin{bmatrix} 0 \\ 0 \\ \dot{\theta}_1 + \dot{\theta}_2 + \dot{\theta}_3 \end{bmatrix}, \tag{A.21} $$

$$ \dot{\omega}_1 = 0 + {}^{1}\mathbf{R}_0\, {}^{0}\omega_0 \times \dot{\theta}_1\, {}^{1}\hat{\mathbf{z}}_1 + \ddot{\theta}_1\, {}^{i+1}\hat{\mathbf{z}}_{i+1} = \begin{bmatrix} 0 \\ 0 \\ \ddot{\theta}_1 \end{bmatrix}, \tag{A.22} $$

$$ {}^{2}\dot{\omega}_2 = \begin{bmatrix} 0 \\ 0 \\ \ddot{\theta}_1 + \ddot{\theta}_2 \end{bmatrix}, \tag{A.23} $$

$$^3\dot{\omega}_3 = \begin{bmatrix} 0 \\ 0 \\ \ddot{\theta}_1 + \ddot{\theta}_2 + \ddot{\theta}_3 \end{bmatrix}, \tag{A.24}$$

Then the accelerations of the end point with respect to the origin of its coordinate, $\dot{\mathbf{v}}$ and with respect to its center of mass, $\dot{\mathbf{v}}_c$ can be calculated.

The acceleration for the end point of each link with respect to the origin of each coordinate are:

$$^0\dot{\mathbf{v}}_0 = \begin{bmatrix} 0 \\ g \\ 0 \end{bmatrix}, \tag{A.25}$$

$$^1\dot{\mathbf{v}}_1 = {}^1\mathbf{R}_0 \left\{ {}^0\dot{\omega}_0 \times {}^0\mathbf{P}_1 + {}^0\omega_0 \times ({}^0\omega_0 \times {}^0\mathbf{P}_1) + \begin{bmatrix} 0 \\ g \\ 0 \end{bmatrix} \right\} = \begin{bmatrix} gS_1 \\ gC_1 \\ 0 \end{bmatrix}, \tag{A.26}$$

$$^2\dot{\mathbf{v}}_2 = \begin{bmatrix} l_1\ddot{\theta}_1 S_2 - l_1\dot{\theta}_1^2 C_2 + gS_{12} \\ l_1\ddot{\theta}_1 C_2 + l_1\dot{\theta}_1^2 S_2 + gC_{12} \\ 0 \end{bmatrix}, \tag{A.27}$$

$$^3\dot{\mathbf{v}}_3 = \begin{bmatrix} l_2(\ddot{\theta}_1 + \ddot{\theta}_2)S_3 - l_2(\dot{\theta}_1 + \dot{\theta}_2)^2 C_3 - l_1\ddot{\theta}_1 S_{23} - l_1\dot{\theta}_1^2 C_{23} + gS_{123} \\ l_2(\ddot{\theta}_1 + \ddot{\theta}_2)C_3 + l_2(\dot{\theta}_1 + \dot{\theta}_2)^2 S_3 + l_1\ddot{\theta}_1 C_{23} + l_1\dot{\theta}_1^2 S_{23} + gC_{123} \\ 0 \end{bmatrix}. \tag{A.28}$$

The accelerations for the end point of each link with respect to its center of mass are:

$$^1\dot{\mathbf{v}}_{c_1} = {}^1\dot{\omega}_1 \times {}^1\mathbf{P}_{c-1} + {}^1\omega_1 \times ({}^1\omega_1 \times {}^1\mathbf{P}_1) + {}^1\dot{\mathbf{v}}_1 = \begin{bmatrix} -l_1\dot{\theta}_1^2 + gS_1 \\ l_1\dot{\theta}_1^2 + gC_1 \\ 0 \end{bmatrix}, \tag{A.29}$$

$$
{}^2\dot{\mathbf{v}}_{c_2} = \begin{bmatrix} -l_2(\dot{\theta}_1+\dot{\theta}_2)^2 + l_1\ddot{\theta}_1 S_2 - l_1\dot{\theta}_1^2 C_2 + gS_{12} \\ l_2(\ddot{\theta}_1+\ddot{\theta}_2) + l_1\ddot{\theta}_1 C_2 + l_1\dot{\theta}_1^2 S_2 + gC_{12} \\ 0 \end{bmatrix}. \tag{A.30}
$$

The elements of ${}^3\dot{\mathbf{v}}_{c_3}$ are

$$
\begin{aligned}
{}^3\dot{v}_{c_{3_1}} &= -l_3(\dot{\theta}_1+\dot{\theta}_2\dot{\theta}_3)^2 + l_2(\ddot{\theta}_1+\ddot{\theta}_2)S_3 - l_2(\dot{\theta}_1+\dot{\theta}_2)^2 C_3 \\
&\quad -l_1\ddot{\theta}_1 S_{23} - l_1\dot{\theta}_1^2 C_{23} + gS_{123} \\
{}^3\dot{v}_{c_{3_2}} &= l_3(\ddot{\theta}_1+\ddot{\theta}_2+\ddot{\theta}_3) + l_2(\ddot{\theta}_1+\ddot{\theta}_2)C_3 + l_2(\dot{\theta}_1+\dot{\theta}_2)^2 S_3 \\
&\quad +l_1\ddot{\theta}_1 C_{23} + l_1\dot{\theta}_1^2 S_{23} + +gC_{123} \\
{}^3\dot{v}_{c_{3_3}} &= 0.
\end{aligned} \tag{A.31}
$$

From the above derivations, the quantities for linear and angular accelerations have been determined. Therefore Newton's and Euler's equations are used to find the force and moment at the center of gravity. The applied force and generated moment at each joint are as follows:

$$
{}^1\mathbf{F}_1 = m_1\,\dot{\mathbf{v}}_{c_1} = \begin{bmatrix} -m_1 P_{c_1}\dot{\theta}_1^2 + m_1 g S_1 \\ m_1 P_{c_1}\ddot{\theta}_1 + m_1 g C_1 \\ 0 \end{bmatrix}, \tag{A.32}
$$

$$
\begin{aligned}
{}^2\mathbf{F}_2 &= m_2\,\dot{\mathbf{v}}_{c_2} \\
&= \begin{bmatrix} -m_2 P_{c_2}(\dot{\theta}_1+\dot{\theta}_2)^2 + m_2 l_1\ddot{\theta}_1 S_2 - m_2 l_1\dot{\theta}_1^2 C_2 + m_2 g S_{12} \\ m_2 P_{c_2}(\ddot{\theta}_1+\ddot{\theta}_2) + m_2 l_1\ddot{\theta}_1 C_2 - m_2 l_1\dot{\theta}_1^2 S_2 + m_2 g C_{12} \end{bmatrix},
\end{aligned} \tag{A.33}
$$

$$
{}^3\mathbf{F}_3 = m_3\,{}^3\ddot{\mathbf{v}}_{c_3} = \begin{bmatrix} F_{3_1} & F_{3_2} & F_{3_3} \end{bmatrix} \tag{A.34}
$$

where

$$
\begin{aligned}
F_{3_1} &= -m_3 P_{c_3}(\dot{\theta}_1+\dot{\theta}_2+\dot{\theta}_3)^2 + m_3 l_2(\ddot{\theta}_1+\ddot{\theta}_2)S_3 \\
&\quad -m_3 l_2(\dot{\theta}_1+\dot{\theta}_2)^2 C_3 + m_3 l_1 \ddot{\theta}_1 S_{23} - m_3 l_1 \dot{\theta}_1^2 C_{23} + m_3 g S_{123} \\
F_{3_2} &= m_3 P_{c_3}(\ddot{\theta}_1+\ddot{\theta}_2+\ddot{\theta}_3) + m_3 l_2(\ddot{\theta}_1+\ddot{\theta}_2)C_3 \\
&\quad -m_3 l_2(\dot{\theta}_1+\dot{\theta}_2)^2 S_3 + m_3 l_1 \ddot{\theta}_1 C_{23} - m_3 l_1 \dot{\theta}_1^2 S_{23} + m_3 g C_{123} \\
F_{3_3} &= 0, \qquad\qquad (A.35)
\end{aligned}
$$

and

$$
{}^1\mathbf{N}_1 = {}^{c_1}\mathbf{I}_1\,{}^1\dot{\omega}_1 + {}^1\omega_1 \times {}^{c_1}\mathbf{I}_1\,{}^1\omega_1 = \begin{bmatrix} 0 \\ 0 \\ I_{zz_1}\ddot{\theta}_1 \end{bmatrix}, \qquad (A.36)
$$

$$
{}^2\mathbf{N}_2 = {}^{c_2}\mathbf{I}_2\,{}^2\dot{\omega}_2 + {}^2\omega_2 \times {}^{c_2}\mathbf{I}_2\,{}^2\omega_2 = \begin{bmatrix} 0 \\ 0 \\ I_{zz_2}\ddot{\theta}_2 \end{bmatrix}, \qquad (A.37)
$$

$$
{}^3\mathbf{N}_3 = {}^{c_3}\mathbf{I}_3\,{}^3\dot{\omega}_3 + {}^3\omega_3 \times {}^{c_3}\mathbf{I}_3\,{}^3\omega_3 = \begin{bmatrix} 0 \\ 0 \\ I_{zz_3}\ddot{\theta}_3 \end{bmatrix}. \qquad (A.38)
$$

Knowing the applied forces and moments at joints, the backward iteration equations are used to obtain the required torque and force at each joint. Given that there are no loads on the end effector, the boundary conditions of end effector are ${}^4\mathbf{f}_4 = \mathbf{0}$ and ${}^4\mathbf{n}_4 = \mathbf{0}$

$$
{}^3\mathbf{f}_3 = {}^3\mathbf{R}_4\,{}^4\mathbf{f}_4 + {}^3\mathbf{F}_{\bar{3}} = \mathbf{0} + {}^3\mathbf{F}_3 = {}^3\mathbf{F}_3, \qquad (A.39)
$$

$$^3\mathbf{n}_3 = {}^3\mathbf{N}_3 + {}^3\mathbf{R}_4\,{}^4\mathbf{n}_4 + {}^3\mathbf{P}_{c_3} \times {}^3\mathbf{F}_3 + {}^3\mathbf{P}_4 \times {}^3\mathbf{R}_4\,{}^4\mathbf{f}_4. \tag{A.40}$$

The components of $^3\mathbf{n}_3$ are $^3n_{3_1} = 0$, $^3n_{3_2} = 0$, and

$$\begin{aligned} {}^3n_{3_3} &= (I_{zz_3} + m_3 P_{c_3}^2)(\ddot{\theta}_1 + \ddot{\theta}_2 + \ddot{\theta}_3) + m_3 P_{c_3} l_2 (\ddot{\theta}_1 + \ddot{\theta}_2) C_3 \\ &\quad + m_3 P_{c_3} l_2 (\dot{\theta}_1 + \dot{\theta}_1)^2 S_3 + m_3 P_{c_3} l_1 \ddot{\theta}_1 C_{23} \\ &\quad + m_3 P_{c_3} l_1 \dot{\theta}_2 S_{23} + m_3 P_{c_3} g C_{123}, \end{aligned} \tag{A.41}$$

and

$$^2\mathbf{f}_2 = {}^2\mathbf{R}_3\,{}^3\mathbf{f}_3 + {}^2\mathbf{F}_2 = \begin{bmatrix} {}^2f_{2_1} & {}^2f_{2_2} & {}^2f_{2_3} \end{bmatrix}^T, \tag{A.42}$$

$$\begin{aligned} {}^2f_{2_1} &= -m_3 P_{c_3} (\dot{\theta}_1 + \dot{\theta}_2 + \dot{\theta}_3)^2 C_3 - m_3 P_{c_3} (\ddot{\theta}_1 + \ddot{\theta}_2 + \ddot{\theta}_3) S_3 \\ &\quad - (m_3 l_2 + m_2 P_{c_3})(\dot{\theta}_1 + \dot{\theta}_2)_2 + (m_2 + m_3) l_1 \ddot{\theta}_1 S_2 \\ &\quad - (m_2 + m_3) l_1 \dot{\theta}_1^2 C_2 + (m_2 + m_3) g S_{12} \end{aligned}$$

$$\begin{aligned} {}^2f_{2_2} &= -m_3 P_{c_2} (\dot{\theta}_1 + \dot{\theta}_2 + \dot{\theta}_3)^2 S_3 + m_3 P_{c_3} (\ddot{\theta}_1 + \ddot{\theta}_2 + \ddot{\theta}_3) C_3 \\ &\quad + (m_3 l_2 + m_2 P_{c_2})(\dot{\theta}_1 + \dot{\theta}_2)_2 + (m_2 + m_3) l_1 \ddot{\theta}_1 C_2 \\ &\quad + (m_2 + m_3) l_1 \dot{\theta}_1^2 S_2 + (m_2 + m_3) g C_{12} \end{aligned}$$

$$^2f_{2_3} = 0, \tag{A.43}$$

$$^2\mathbf{n}_2 = {}^2\mathbf{N}_2 + {}^2\mathbf{R}_3\,{}^3\mathbf{n}_3 + {}^2\mathbf{P}_{c_2} \times {}^2\mathbf{F}_2 + {}^2\mathbf{P}_3 \times {}^2\mathbf{R}_3\,{}^3\mathbf{f}_3, \tag{A.44}$$

The components of ${}^2\mathbf{n}_2$ are ${}^2n_{2_1} = 0$, ${}^2n_{2_2} = 0$ and

$$\begin{aligned}
{}^2n_{2_3} &= I_{zz_2}(\ddot{\theta}_1 + \ddot{\theta}_2)\,{}^3n_{3_3} \\
&\quad + m_2 P_{c_2}^2(\ddot{\theta}_1 + \ddot{\theta}_2) + m_2 P_{c_2} l_1 \ddot{\theta}_1 C_2 + m_2 P_{c_2} l_1 \dot{\theta}_1^2 S_2 + m_2 P_{c_2} g C_{12} \\
&\quad - m_3 P_{c_3} l_2(\ddot{\theta}_1 + \ddot{\theta}_2 + \ddot{\theta}_3) S_3 + m_3 P_{c_3} l_2(\ddot{\theta}_1 + \ddot{\theta}_2 + \ddot{\theta}_3) C_3 \\
&\quad + m_3 l_2^2(\ddot{\theta}_1 + \ddot{\theta}_2) + m_3 l_1 l_2 \ddot{\theta}_1 C_2 + m_3 l_1 l_2 \dot{\theta}_1^2 S_2 + m_3 l_2 g C_{12}, \qquad \text{(A.45)}
\end{aligned}$$

$${}^1\mathbf{f}_1 = {}^1\mathbf{R}_2\,{}^2\mathbf{f}_2 + {}^1\mathbf{F}_1 = \begin{bmatrix} {}^1f_{1_1} & {}^1f_{1_2} & {}^1f_{1_3} \end{bmatrix}^T, \qquad \text{(A.46)}$$

where

$$\begin{aligned}
{}^1f_{1_1} &= -m_3 P_{c_3}(\dot{\theta}_1 + \dot{\theta}_2 + \dot{\theta}_3)^2 C_{23} - m_3 P_{c_3}(\ddot{\theta}_1 + \ddot{\theta}_2 + \ddot{\theta}_3) S_{23} \\
&\quad - (m_3 l_2 + m_2 P_{c_3})(\dot{\theta}_1 + \dot{\theta}_2)_2 C_2 - (m_2 P_{c_2} + m_3 l_2)(\ddot{\theta}_1 + \ddot{\theta}_2) S_2 \\
&\quad - (m_1 P_{c_1} + m_2 l_1 + m_3 l_1)\dot{\theta}_1^2 + m_1 + (m_2 + m_3) g S_1
\end{aligned}$$

$$\begin{aligned}
{}^1f_{1_2} &= -m_3 P_{c_3}(\dot{\theta}_1 + \dot{\theta}_2 + \dot{\theta}_3)^2 S_{23} - m_3 P_{c_3}(\ddot{\theta}_1 + \ddot{\theta}_2 + \ddot{\theta}_3) C_{23} \\
&\quad - (m_3 l_2 + m_2 P_{c_3})(\dot{\theta}_1 + \dot{\theta}_2)_2 S_2 - (m_2 P_{c_2} + m_3 l_2)(\ddot{\theta}_1 + \ddot{\theta}_2) C_2 \\
&\quad - (m_1 P_{c_1} + m_2 l_1 + m_3 l_1)\dot{\theta}_1^2 + (m_1 + m_2 + m_3) g C_1 \\
{}^1f_{1_3} &= 0, \qquad \text{(A.47)}
\end{aligned}$$

$${}^1\mathbf{n}_1 = {}^1\mathbf{N}_1 + {}^1\mathbf{R}_2\,{}^2\mathbf{n}_2 + {}^1\mathbf{P}_{c_1} \times {}^1\mathbf{F}_1 + {}^1\mathbf{P}_2 \times {}^1\mathbf{R}_2\,{}^2\mathbf{f}_2, \qquad \text{(A.48)}$$

with the components: ${}^1n_{1_1} = 0$, ${}^1n_{1_2} = 0$ and

$$\begin{aligned}
{}^1n_{1_3} &= I_{zz_2}\ddot{\theta}_1 + {}^2n_{2_2} + m_1 P_{c_1}^2 \ddot{\theta}_1 + m_1 P_{c_1} g C_1 \\
&\quad - m_3 P_{c_3} l_1(\ddot{\theta}_1 + \ddot{\theta}_2 + \ddot{\theta}_3) S_{23} + m_3 P_{c_3} l_1(\ddot{\theta}_1 + \ddot{\theta}_2 + \ddot{\theta}_3) C_{23}
\end{aligned}$$

$$+(m_3l_2+m_2P_{c_2})l_1(\ddot{\theta}_1+\ddot{\theta}_2)C_2-(m_3l_2+m_2P_{c_2})l_1(\dot{\theta}_1+\dot{\theta}_2)^2S_2$$
$$+(m_3+m_2)l_1^2\ddot{\theta}_1+(m_3+m_2)l_1gC_1. \qquad \text{(A.49)}$$

The torque on joint i, $\tau_i = {}^i\mathbf{n}_i^T \cdot {}^i\hat{\mathbf{z}}_i$. By substituting the values of ${}^i\mathbf{n}_i$ into this equation, the torque on each joint is obtained.

$$\begin{aligned}\tau_1 &= I_{zz_1}\ddot{\theta}_1+m_1P_{c_1}^2\ddot{\theta}_1+m_1P_{c_1}gC_1\\
&\quad -m_3P_{c_3}l_1(\ddot{\theta}_1+\ddot{\theta}_2+\ddot{\theta}_3)S_{23}+m_3P_{c_3}l_1(\ddot{\theta}_1+\ddot{\theta}_2+\ddot{\theta}_3)C_{23}\\
&\quad +(m_3l_2+m_2P_{c_2})l_1(\ddot{\theta}_1+\ddot{\theta}_2)C_2-(m_3l_2+m_2P_{c_2})l_1(\dot{\theta}_1+\dot{\theta}_2)^2S_2\\
&\quad +(m_3+m_2)l_1^2\ddot{\theta}_1+(m_3+m_2)l_1gC_1+\tau_2, \qquad \text{(A.50)}\end{aligned}$$

$$\begin{aligned}\tau_2 &= I_{zz_2}(\ddot{\theta}_1+\ddot{\theta}_2)+m_2P_{c_2}^2(\ddot{\theta}_1+\ddot{\theta}_2)+m_2P_{c_2}l_1\ddot{\theta}_1C_2\\
&\quad +m_2P_{c_2}l_1\dot{\theta}_1^2S_2+m_2P_{c_2}gC_{12}-m_3P_{c_3}l_2(\ddot{\theta}_1+\ddot{\theta}_2+\ddot{\theta}_3)S_3\\
&\quad +m_3P_{c_3}l_2(\ddot{\theta}_1+\ddot{\theta}_2+\ddot{\theta}_3)C_3+m_3l_2^2(\ddot{\theta}_1+\ddot{\theta}_2)+m_3l_1l_2\ddot{\theta}_1C_2\\
&\quad +m_3l_1l_2\dot{\theta}_1^2S_2+m_3l_2gC_{12}+\tau_3, \qquad \text{(A.51)}\end{aligned}$$

$$\begin{aligned}\tau_3 &= (I_{zz_3}+m_3P_{c_3}^2)(\ddot{\theta}_1+\ddot{\theta}_2+\ddot{\theta}_3)+m_3P_{c_3}l_2(\ddot{\theta}_1+\ddot{\theta}_2)C_3\\
&\quad +m_3P_{c_3}l_2(\dot{\theta}_1+\dot{\theta}_1)^2S_3+m_3P_{c_3}l_1\ddot{\theta}_1C_{23}\\
&\quad +m_3P_{c_3}l_1\dot{\theta}_2S_{23}+m_3P_{c_3}gC_{123}. \qquad \text{(A.52)}\end{aligned}$$

If the torque equations are written in the form as follow

$$\tau = \mathbf{H}(\theta)\ddot{\theta}+\mathbf{B}(\theta)[\dot{\theta}\dot{\theta}]+\mathbf{C}(\theta)[\dot{\theta}^2]+\mathbf{g}(\theta) \qquad \text{(A.53)}$$

with

$$[\dot{\theta}\dot{\theta}] \stackrel{\text{def}}{=} \begin{bmatrix} \dot{\theta}_1\dot{\theta}_2 \\ \dot{\theta}_2\dot{\theta}_3 \\ \dot{\theta}_3\dot{\theta}_1 \end{bmatrix}, \qquad \text{and} \qquad [\dot{\theta}^2] \stackrel{\text{def}}{=} \begin{bmatrix} \dot{\theta}_1{}^2 \\ \dot{\theta}_2{}^2 \\ \dot{\theta}_3{}^2 \end{bmatrix},$$

then the inertia matrix is

$$H(\theta) = \begin{bmatrix} h_{11} & h_{12} & h_{13} \\ h_{21} & h_{22} & h_{23} \\ h_{31} & h_{32} & h_{33} \end{bmatrix}, \tag{A.54}$$

where

$$\begin{aligned}
h_{11} &= \sum_{i=1}^{3} I_{zz_i} + \sum_{i=1}^{3} m_i P_{c_i} + m_3 l_2^2 + (m_2 + m_3) l_1^2 + 2m_3 P_{c_3} l_2 C_3 \\
&\quad + 2m_3 P_{c_3} l_1 C_{23} + 2m_2 P_{c_2} l_1 C_2 + 2m_3 l_1 l_2 C_2 \\
h_{12} &= \sum_{i=2}^{3} I_{zz_i} + \sum_{i=2}^{3} m_i P_{c_i}^2 + 2m_3 P_{c_3} l_2 C_3 + m_3 l_2 l_1 C_2 \\
&\quad + m_2 P_{c_2} l_1 C_2 + m_3 P_{c_3} l_1 C_{23} \qquad \text{(A.55)} \\
h_{13} &= I_{zz_3} + m_3 P_{c_3}^2 + m_3 P_{c_3} l_2 C_3 + m_3 P_{c_3} l_1 C_{23} \\
h_{21} &= h_{12} \\
h_{22} &= \sum_{i=2}^{3} I_{zz_i} + \sum_{i=2}^{3} m_i P_{c_i}^2 + m_3 l_2^2 + 2m_3 P_{c_3} l_2 C_3 \\
h_{23} &= I_{zz_3} + m_3 P_{c_3}^2 + M_3 P_{c_3} l_2 C_3 \\
h_{31} &= h_{13} \\
h_{32} &= h_{23} \\
h_{33} &= I_{zz_3} + M_3 P_{c_3}^2. \qquad \text{(A.56)}
\end{aligned}$$

The components of the B matrix are

$$
\begin{aligned}
b_{11} &= -2(m_3 l_1 + m_2 P_{c_2}) l_1 S_2 - 2 m_3 P_{c_3} S_{23} \\
b_{12} &= -2 m_3 P_{c_3} (l_2 S_3 - l_1 S_{23}) \\
b_{13} &= -2 m_3 P_{c_3} (l_2 S_3 - l_1 S_{23}) \\
b_{21} &= 0 \\
b_{22} &= -2 m_3 P_{c_3} l_2 S_3 \\
b_{23} &= -2 m_3 P_{c_3} l_2 S_3 \\
b_{31} &= 2 m_3 P_{c_3} l_2 S_3 \\
b_{32} &= 0 \\
b_{33} &= 0.
\end{aligned}
\tag{A.57}
$$

The components of the C matrix are

$$
\begin{aligned}
c_{11} &= 0 \\
c_{12} &= -(m_3 l_2 + m_2 P_{c_2}) l_1 S_2 - m_3 P_{c_3} l_1 S_{23} \\
c_{13} &= -m_3 P_{c_3} (l_2 S_3 + l_1 S_{23}) \\
c_{21} &= (m_3 l_2 + m_2 P_{c_2}) l_1 S_2 + m_3 P_{c_3} l_1 S_{23} \\
c_{22} &= 0 \\
c_{23} &= -m_3 P_{c_3} l_2 S_3 \\
c_{31} &= m_3 P_{c_3} (l_2 S_3 + l_1 S_{23}) \\
c_{32} &= m_3 P_{c_3} l_2 S_3 \\
c_{33} &= 0.
\end{aligned}
\tag{A.58}
$$

The gravity vector, g is

$$\begin{bmatrix} m_3 P_{c_3} g C_{123} + (m_2 P_{c_2} + m_3 l_2) g C_{12} + (m_1 P_{c_1} + m_2 l_1 + m_3 l_1) g C_1 \\ m_3 P_{c_3} g C_{123} + (m_2 P_{c_2} + m_3 l_2) g C_{12} \\ m_3 P_{c_3} g C_{123} \end{bmatrix} \quad (A.59)$$

APPENDIX B

CALCULATION OF THE JACOBIAN AND ITS DERIVATIVES FOR A 3-LINK PLANAR MANIPULATOR

The jacobian matrix J and its higher-order derivatives are derived in this section. These equations have some iterative properties and are useful for the formulation of computer simulation. The jacobian J is

$$
\begin{aligned}
J &= \begin{bmatrix} J_{11} & J_{12} & J_{13} \\ J_{21} & J_{22} & J_{23} \end{bmatrix} \\
&= \begin{bmatrix} -l_1 S_1 - l_2 S_{12} - l_3 S_{123} & -l_2 S_{12} - l_3 S_{123} & -l_3 S_{123} \\ l_1 C_1 + l_2 C_{12} + l_3 C_{123} & l_2 C_{12} + l_3 C_{123} & l_3 C_{123} \end{bmatrix}
\end{aligned} \tag{B.1}
$$

Differentiating equation (B.2), the first derivative of jacobian J is

$$
\begin{aligned}
\dot{J} &= \begin{bmatrix} \dot{J}_{11} & \dot{J}_{12} & \dot{J}_{13} \\ \dot{J}_{21} & \dot{J}_{22} & \dot{J}_{23} \end{bmatrix} \\
&= \begin{bmatrix} -(J_{21} - J_{22})\dot{\theta}_1 + \dot{J}_{12} & (J_{11} - J_{12})\dot{\theta}_1 + \dot{J}_{22} \\ -(J_{22} - J_{23})(\dot{\theta}_1 + \dot{\theta}_2) + \dot{J}_{13} & (J_{12} - J_{13})(\dot{\theta}_1 + \dot{\theta}_2) + \dot{J}_{23} \\ -J_{23}(\dot{\theta}_1 + \dot{\theta}_2 + \dot{\theta}_3) & J_{13}(\dot{\theta}_1 + \dot{\theta}_2 + \dot{\theta}_3) \end{bmatrix}^T
\end{aligned} \tag{B.2}
$$

Differentiating the equation (B.3), the second derivative of the jacobian J is

$$\ddot{J} = \begin{bmatrix} \ddot{J}_{11} & \ddot{J}_{12} & \ddot{J}_{13} \\ \ddot{J}_{21} & \ddot{J}_{22} & \ddot{J}_{23} \end{bmatrix} \tag{B.3}$$

The elements of this matrix are

$$\begin{aligned}
\ddot{J}_{11} &= -(\dot{J}_{21} - \dot{J}_{22})\dot{\theta}_1 - (J_{21} - J_{22})\ddot{\theta}_1 + \ddot{J}_{12} \\
\ddot{J}_{12} &= -(\dot{J}_{22} - \dot{J}_{23})(\dot{\theta}_1 + \dot{\theta}_2) - (J_{22} - J_{23})(\ddot{\theta}_1 + \ddot{\theta}_2) + \ddot{J}_{13} \\
\ddot{J}_{13} &= -\dot{J}_{23}(\dot{\theta}_1 + \dot{\theta}_2 + \dot{\theta}_3) - J_{23}(\ddot{\theta}_1 + \ddot{\theta}_2 + \ddot{\theta}_3) \\
\ddot{J}_{21} &= (\dot{J}_{11} - \dot{J}_{12})\dot{\theta}_1 + (J_{11} - J_{12})\ddot{\theta}_1 + \ddot{J}_{22} \\
\ddot{J}_{22} &= (\dot{J}_{12} - \dot{J}_{13})(\dot{\theta}_1 + \dot{\theta}_2) + (J_{12} - J_{13})(\ddot{\theta}_1 + \ddot{\theta}_2) + \ddot{J}_{23} \\
\ddot{J}_{23} &= \dot{J}_{13}(\dot{\theta}_1 + \dot{\theta}_2 + \dot{\theta}_3) + J_{13}(\ddot{\theta}_1 + \ddot{\theta}_2 + \ddot{\theta}_3)
\end{aligned} \tag{B.4}$$

Differentiating the equation (B.4), the third derivative of the jacobian J is

$$\frac{d^3J}{dt^3} = \begin{bmatrix} \frac{d^3J_{11}}{d^3t} & \frac{d^3J_{12}}{d^3t} & \frac{d^3J_{13}}{d^3t} \\ \frac{d^3J_{21}}{d^3t} & \frac{d^3J_{22}}{d^3t} & \frac{d^3J_{23}}{d^3t} \end{bmatrix} \tag{B.5}$$

The elements of the matrix $\frac{d^3J}{dt^3}$ are

$$\begin{aligned}
\frac{d^3J_{11}}{dt^3} &= -(\dddot{J}_{21} - \dddot{J}_{22})\dot{\theta}_1 - 2(\ddot{J}_{21} - \ddot{J}_{22})\ddot{\theta}_1 - (\dot{J}_{21} - \dot{J}_{22})\frac{d^3\theta_1}{dt^3} + \frac{d^3J_{12}}{dt^3} \\
\frac{d^3J_{12}}{dt^3} &= (\dddot{J}_{22} - \dddot{J}_{23})(\dot{\theta}_1 + \dot{\theta}_2) - 2(\ddot{J}_{22} - \ddot{J}_{23})(\ddot{\theta}_1 + \ddot{\theta}_2) \\
&\quad -(\dot{J}_{22} - \dot{J}_{23})(\frac{d^3\theta_1}{dt^3} + \frac{d^3\theta_2}{dt^3}) + \frac{d^3J_{13}}{dt^3} \\
\frac{d^3J_{13}}{dt^3} &= -\dddot{J}_{23}(\dot{\theta}_1 + \dot{\theta}_2 + \dot{\theta}_3) - 2\ddot{J}_{23}(\ddot{\theta}_1 + \ddot{\theta}_2 + \ddot{\theta}_3) \\
&\quad -\dot{J}_{23}(\frac{d^3\theta_1}{dt^3} + \frac{d^3\theta_2}{dt^3} + \frac{d^3\theta_3}{dt^3}) \\
\frac{d^3J_{21}}{dt^3} &= (\dddot{J}_1 - \dddot{J}_{12})\dot{\theta}_1 + 2(\ddot{J}_{11} - \ddot{J}_{12})\ddot{\theta}_1 + (\dot{J}_{11} - \dot{J}_{12})\frac{d^3\theta_1}{dt^3} + \frac{d^3J_{22}}{dt^3}
\end{aligned}$$

$$
\begin{aligned}
\frac{d^3 J_{22}}{dt^3} &= (\dddot{J}_{12} - \dddot{J}_{13})(\dot{\theta}_1 + \dot{\theta}_2) + 2(\ddot{J}_{12} - \ddot{J}_{13})(\ddot{\theta}_1 + \ddot{\theta}_2) \\
&\quad + (J_{12} - J_{13})\left(\frac{d^3\theta_1}{dt^3} + \frac{d^3\theta_2}{dt^3}\right) + \frac{d^3 J_{23}}{dt^3} \\
\frac{d^3 J_{23}}{dt^3} &= \dddot{J}_{13}(\dot{\theta}_1 + \dot{\theta}_2 + \dot{\theta}_3) + 2\ddot{J}_{13}(\ddot{\theta}_1 + \ddot{\theta}_2 + \ddot{\theta}_3) \\
&\quad - J_{13}\left(\frac{d^3\theta_1}{dt^3} + \frac{d^3\theta_2}{dt^3} + \frac{d^3\theta_3}{dt^3}\right)
\end{aligned}
\tag{B.6}
$$

BIBLIOGRAPHY

[1] R. P. Paul, *Robot Manipulators: Mathematics, Programming and Control.* MIT Press, 1981.

[2] J. P. Trevelyan, P. D. Kovesi, and M. C. H. Ong, "Motion control for a sheep shearing robot," in *Robotics Research: The First International Symposium*, M. Brady and R. Paul, Eds., pp. 175–190, MIT Press, 1984.

[3] J. Baillieul, "A constraint oriented approach to inverse problems for kinematically redundant manipulators," in *1987 IEEE International Conference on Robotics and Automation*, pp. 1827–1833, Raleigh, N.C., March-April 1987.

[4] S. L. Chiu, "Control of redundant manipulators for task compatibility," *IEEE Proc. 1987 International Conference on Robotics and Automation*, pp. 1718–1724, March 31 - April 3 1987. Raleigh, NC.

[5] C. Klein and B. Blaho, "Dexterity measures for the design and control of kinematically redundant manipulators," *The International Journal of Robotics Research*, vol. 6 ,No. 2, pp. 72–84, Summer 1987.

[6] A. A. Maciejewski and C. A. Klein, "Obstacle avoidance for kinematically redundant manipulators in dynamically varying environments," *The International Journal of Robotics Research*, vol. 4, no. 3, pp. 109–117, Fall 1985.

[7] A. Liegeois, "Automatic supervisory control of the configuration and behavior of multibody mechanisms," *IEEE Trans. Systems, Man, Cybern.*, vol. SMC-7, no. 12, pp. 868–871, December 1977.

[8] T. Yoshikawa, "Manipulability of robotic mechanisms," *Robotics Research, the Second International Symposium*, pp. 439–446, 1985. The MIT Press, Cambridge, Massachusetts.

[9] R. Dubey and J. Y. S. Luh, "Redundant robot control for higher flexibility," *IEEE Proc. 1987 International Conference on Robotics and Automation*, pp. 1066–1072, March 31 - April 3 1987. Raleigh, NC.

[10] K. Kee, "The nature of drift in pseudoinverse control of kinematically redundant manipulators," M.S. Thesis, The Ohio State University, 1987.

[11] D. E. Whitney, "Resolved motion rate control of manipulators and human prostheses," *IEEE Transactions on Man Machine System*, vol. MMS-10, pp. 47–53, 1969.

[12] J. M. Hollerbach and K. C. Suh, "Redundancy resolution of manipulators through torque optimization," *IEEE Proc. 1985 International Conference on Robotics and Automation*, pp. 1016–1021, March 1985. St. Louis, Mo.

[13] K. C. Suh and J. M. Hollerbach, "Local versus global torque optimization of redundant manipulators," *IEEE Proc. 1987 International Conference on Robotics and Automation*, pp. 619–624, March 31 - April 3 1987. Raleigh, NC.

[14] R. V. Mayorga and A. K. C. Wong, "A singularities avoidance method for the trajectory planing of redundant and nonredundant robot manipula-

tors," *IEEE Proc. 1987 International Conference on Robotics and Automation*, pp. 1707–1712, March 31 - April 3 1987. Raleigh, NC.

[15] J. Baillieul, "Avoiding obstacles and resolving kinematic redundancy," *IEEE 1986 International Conferance on Robotics and Automation*, vol. 3, , April 7-10 1986. San Francisco, CA.

[16] C. Klein and C. Huang, "Review of pseudo-inverse control for use with kinematically redundant manipulators," *IEEE Trans. on System, Man and Cybernetics*, vol. SCM-13, pp. 245–250, 1983.

[17] L. Sciavicco and B. Siciliano, "A dynamic solution to the inverse kinematic problem for redundant manipulators," *IEEE Proc. 1987 International Conference on Robotics and Automation*, pp. 1081–1087, March 31 - April 3 1987. Raleigh, NC.

[18] V. V. Pavlov and A. N. Voronin, "Multicriterion synthesis of exterior space infrastructure in an intelligent robot," *Soviet Automatic Control*, vol. 17, pp. 45–49, Jan./Feb. 1984.

[19] Y. Nakamura, "Optimal redundancy control of robot manipulators," *The International Journal of Robotics Research*, vol. 6, no. 1, pp. 32–42, Spring 1987. The MIT Press, Cambridge, Massachusetts.

[20] P. H. Chang, "A closed-form solution for the control of manipulators with kinematic redundancy," *IEEE 1986 International Conference on Robotics and Automation*, vol. 1, pp. 9–14, April 7-10 1986. San Francisco CA.

[22] V. C. Klema and A. J. Laub, "The singular value decomposition: Its computation and some applications," *IEEE Transactions on Automatic Control*, vol. AC-25, no. 2, pp. 164–176, April 1980.

[23] D. E. Orin and M. W. Walker, "Efficient computation of the jacobian for robot manipulators.," *International Journal of Robotic Research*, vol. 3, no. 4, pp. 66–75, 1984.

[24] Y. Nakamura, H. Hanafusa, Y. Yokokohji, and T. Yoshikawa, "Efficient computation and kinematic representation for robot manipulator simulation," *15th International Symposium on Industrial Robots*, September 1985. Tokyo, Japan.

[25] A. A. Maciejewski, "The analysis and control of robotic manipulators operating at or near kinematically singular configurations," Ph.D. Thesis, The Ohio State University, 1987.

[26] Y. Nakamura and H. Hanafusa, "Inverse kinematic solutions with singularity robustness for robot manipulator control," *IEEE Journal of Dynamic System, Measurement, and Control*, vol. 108, pp. 163–171, September 1986.

[27] D. E. Kirk, *Optimal Control Theory*. Englewood Cliffs, New Jersey: Prentice Hall, Electrical Engineering Series, 1972.

[28] D. E. Whitney, "The mathematics of coordinated control of prostheses and manipulators," *ASME Journal of Dynamic Systems, Measurement, Control*, vol. 94, no. 4, pp. 303-309, 1972.

[29] M. Uchiyama, K. Shimizu, and K. Hakomori, "Performance evaluation of manipulators using the jacobian and its application to trajectory planning,"

Robotics Research, the Second International Symposium, pp. 447–454, 1985. The MIT Press, Cambridge, Massachusetts.

[30] T. Ojika and Y. Kasue, "Initial-value adjusting method for the solution of nonlinear multipoint boundary-value problems," *Journal of Mathematical Analysis and Application*, vol. 69, pp. 359–371, 1979.

[31] J. Denavit and R. B. Hartenberg, "A kinematic notation for lower-pair mechanisms basis on matrices," *ASME Journal of Dynamic Systems, Measurement, Control*, vol. 23, pp. 215–221, 1955.

[32] D. E. Orin and W. W. Schrader, "Efficient jacobian determination for robot manipulators," in *Robotics Research: The First International Symposium*, M. Brady and R. Paul, Eds., pp. 727–734, MIT Press, 1984.